A Compact Radio Beacon and Antenna Deployer Design

Indirect HF/VHF Ionospheric Characterisation from a Nanosatellite Platform

Alessandro Battegazzore

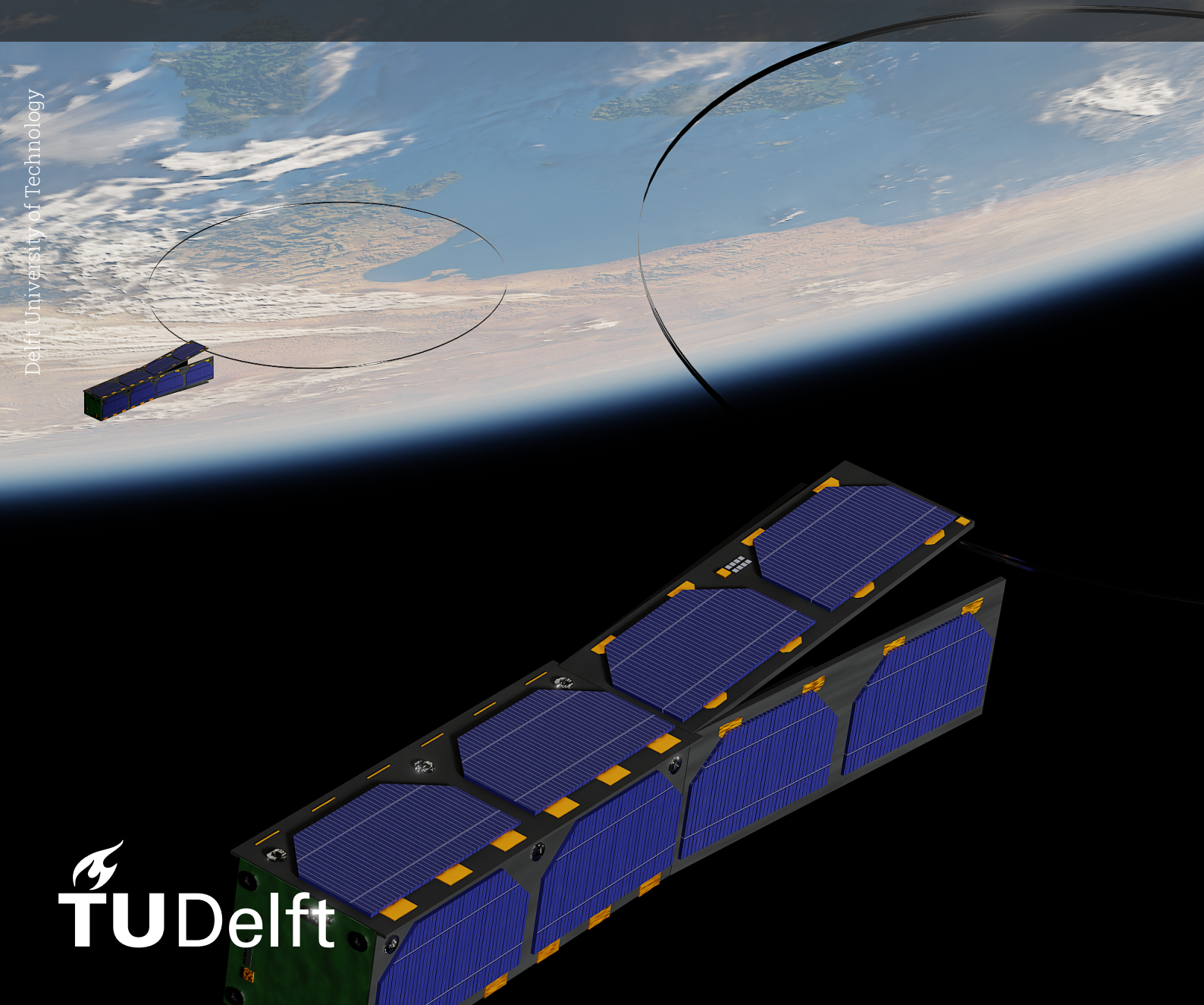

Delft University of Technology

TU Delft

This page is intentionally left blank

TU Delft

A Compact Radio Beacon and Antenna Deployer Design

Indirect HF/VHF Ionospheric Characterisation from a Nanosatellite Platform

by

Alessandro Battegazzore

to obtain the degree of Master of Science in Aerospace Engineering
at Delft University of Technology.

Student number:	4994221
Project duration:	February, 2025 – December, 2025
Thesis supervision:	Jurgen Vanhamel Delft University of Technology

Cover: Own work, Delfi-Twin satellites fitted with the RABSII instrument orbiting the Earth

An electronic version of this thesis is available at `https://repository.tudelft.nl/`.

TU Delft

Preface

This thesis is the culmination of almost a year of work, and between the Bachelor and the Master, of more than six years here in Delft. That's a long time. But at the same time, not at all. First things first, I want to thank Jurgen for first proposing, and supervising my work this past year. Your help and expertise throughout the whole process have been extremely valuable and has helped me learn a lot about the (sometimes magic) world of antennas.

From TU Delft, thank you Ines for all the sanity checks on the deployer design, it made a big difference in feeling less doubtful in some of the *unconventional* design choices presented. Thank you Stefano for always making time for my questions even when perhaps too busy already. And lastly, thank you also to Walter, and the rest of the RABSII team, for the SimNEC tutorials and access to all the data required for my work.

To my friends, thank you for all the climbing sessions, which helped me stay sane during the dark days of the Dutch winter. Getting through the writing would have not been possible otherwise. And last but not least, thank you Kim, Austin and Lucas for always being there for me. Kim and Austin specifically, for having to read through a book and a half worth of dry technical reports to get me over the finish line. Couldn't have done it without you.

Looking back at the past year, there have been some high, and there have been some lows. While working alone for so long may be something I won't miss, I surely will miss the flexibility to work remotely whenever needed. It gave me the wonderful chance to live in Paris with my partner Kim, which I will treasure very much. Thank you again Kim for listening to me talk about antennas (probably) way too much, and for bringing a bit of much needed sunshine.

And now, finally, I can call this done. I hope you will enjoy the read as much as I'll enjoy the unburdened Christmas holidays with my family, who's unwavering support got me through the Master.

Alessandro Battegazzore
Delft, December 2025

Summary

The ionosphere is a layer of the upper atmosphere characterized by a high density of charged ions. Within the ionosphere itself, a few distinct layers can be identified: the D layer, the E layer, and the F layer (subdivided into the F1 and F2 layers). Of particular interest for this thesis project, is the E layer. While other ionospheric layers display significant day/night and seasonal variations, the E layer is constantly present. Within the E layer a particularly variable phenomena occurs: the so-called 'sporadic E phenomena'. Sporadic E describes highly localized ionospheric regions with high ion densities, sometimes also referred to as 'Sporadic E clouds'. These clouds are often responsible for scattering, reflecting, and overall disrupting radio signals on the HF/VHF bands. Given the unpredictability, and high spatial and temporal variability of Sporadic E clouds, ground-based measurement techniques often struggle to meaningfully image their structure. Indirect measurement by a space-based LEO radio beacon is proposed through the RABSII instrument, scheduled to fly aboard the upcoming TU Delft mission: Delfi-Twin.

The Delfi-Twin mission consists of a pair of 3P PocketQube nanosatellites flying in formation, each about 15x5x5 cm in size. The RABSII instrument would consist of two individual radio beacon antennas, each beacon flying on one of the two spacecrafts. One beacon will broadcast at a frequency of 28 MHz and one at 50 MHz. Some concepts for the RABSII instrument have already been investigated, with the current design option considered being a 5 m long SMA actuated resonant dipole antenna. While potentially feasible, the large size of a resonant antenna transmitting in the HF/VHF band poses significant deployment risks given the small size of the host platform. This work focusses on exploring alternative options, and, based on the known science objectives, investigate how small the radio beacon can be made. As most constraining in terms of required performance, the choice was made to only investigate the 28 MHz instrument for the design and analysis process. This work presents a feasible design for the 28 MHz beacon antenna as well as a deployer capable of stowing and deploying the antenna from the Delfi-Twin satellite platform.

Beginning from the science case and satellite platform, several system constraints have been identified. Most constraining for the RABSII instrument design is the available space aboard Delfi-Twin: only 80x40x4 mm^3 per instrument. Based on these constraints, the radio link from the beacon to ground has been modelled. Two noise sources have been identified as dominant: man-made terrestrial noise, and galactic extra-terrestrial noise. Regarding losses, the link is dominated by significant free-space losses. Polarisation losses have also been modelled. Due to the interactions between HF/VHF signals and the Earth's magnetic field, their polarisation was determined to be effectively randomised by the time they reach ground. Stochastic modelling of the polarisation orientation yielded estimates for expected mismatch losses which were validated against literature data. While preliminary, the link model was deemed to be detailed enough to yield sufficient results on the required beacon's RF performance. A minimum required EIRP of -19.2 dB W was identified for the 28 MHz beacon's antenna.

Based on the identified required RF performance, an antenna design was then investigated. Ansys Electronics and SimNEC (based on the NEC-2 engine) were used to simulate various antenna designs. The following design dimensions were identified:

- Antenna conductor shape
- Antenna conductor size
- Antenna conductor cross-section
- Antenna conductor material
- Matching network topology

Possessing the greatest influence on RF performance, the conductor shape (or antenna type) was investigated first. Two options were identified as potentially viable: a loop antenna, and a dipole antenna. Considering the small size of the Delfi-Twin spacecraft, and studying commercially available antenna deployers, the antenna size was constrained to a maximum of 1.5 m (length for the dipole, and diameter for the loop). Based on the observed RF performance within the defined size constraints, the loop antenna was identified as more promising for the RABSII radio beacon. Looking at the remaining design dimensions, cross-section, material, and matching network topology were investigated as a function of loop diameter. Comparing the measured performance against the defined system requirements resulted in the following antenna configuration for the 28 MHz instrument:

- Antenna conductor shape: **Loop**
- Antenna conductor size: **Loop diameter between 0.75 m and 1.25 m**
- Antenna conductor cross-section: **Rectangular, with dimensions 3x0.1 mm**
- Antenna conductor material: **1.4310 Spring Steel**
- Matching network topology: **L-Network**

Lastly, based on the presented antenna design, a deployer concept was defined. The approach devised can be conceptually compared to a VHS tape cassette, where the antenna strip is wound up on two spring loaded spools for storage. Upon release from its stowed configuration, the two spools actuate, powered by the torsion springs at their cores to unwind the strip into the final loop shape. To investigate the feasibility of this concept, the design was refined using CAD, and then physically prototyped. A representative demonstrator was made out of a combination of commercially available components and SLA printed resin parts. Qualitative testing of the demonstrator showed that the design is promising, as it is able to fulfil many of the design objectives. A reduced-scale antenna strip was successfully stowed and deployed. While some areas still require further design work and testing, the mechanical deployment approach seems capable of fulfilling the deployment requirements of the antenna while remaining within the constraints imposed by the host satellite platform.

To conclude, this thesis project investigated the science case of the proposed RABSII instrument. The radio link was modelled, and an antenna design was investigated, characterised, and shown to meet the defined system requirements. A novel deployer design was conceptualised, prototyped, and tested to investigate how to integrate this antenna onto the Delfi-Twin platform. In addition to the work done for the RABSII instrument, the analysis presented provides relevant data on the performance of electrically short antennas in the HF radio transmission band. These types of antennas are rarely used for space applications, and the relation between their performance and size is often unclear and undefined in literature. The data presented provides relevant insights in how electrically short antennas may be used to reduce the footprint of telecommunication systems aboard modern small satellites. Furthermore, the novel deployer design could also serve as a useful starting point for other antenna systems by providing preliminary insights into the operations of a new antenna deployment approach.

Contents

Preface i

Summary ii

Nomenclature xi

1 Introduction 1
- 1.1 Project Scope . . . 1
- 1.2 How to Read . . . 2

I Project Background 3

2 Project Objectives 4
- 2.1 RABSII Instrument and Science Case . . . 4
  - 2.1.1 Science Case . . . 4
  - 2.1.2 Current Development Status . . . 6
- 2.2 Delfi Twin Mission . . . 7
- 2.3 Research Questions . . . 8

3 Relevant Literature 10
- 3.1 RA-1: Theory of Link Budget Analyses . . . 11
  - 3.1.1 Radiated Signal Power . . . 11
  - 3.1.2 Attenuation Sources . . . 12
  - 3.1.3 Noise Power . . . 14
- 3.2 RA-2: Theory of Radio Antennas . . . 16
  - 3.2.1 Impedance and Admittance of Ideal Components . . . 16
  - 3.2.2 Antenna Resonance and Anti-Resonance . . . 17
  - 3.2.3 Antenna Quality factor and Bandwidth . . . 18
  - 3.2.4 Electrical Length . . . 19
  - 3.2.5 Skin Effect . . . 23
- 3.3 RA-3: Practical Considerations of Real Antenna Systems . . . 24
  - 3.3.1 Impedance Matching . . . 24
  - 3.3.2 Ideal versus Real Components . . . 29
  - 3.3.3 Balanced versus Unbalanced Systems . . . 30
- 3.4 RA-4: Deployment Mechanisms and Technologies . . . 31
  - 3.4.1 Shape Memory Alloys (SMAs) . . . 31
  - 3.4.2 Inflatables . . . 32
  - 3.4.3 Strain-Based Systems: Tape Springs and STEMs . . . 32
  - 3.4.4 Electric Motors . . . 32
  - 3.4.5 Magnetic Actuators . . . 33
  - 3.4.6 Burn Wires . . . 33

4 Requirements Definition 34
- 4.1 Mission Constraints . . . 34
  - 4.1.1 Science Case . . . 34
  - 4.1.2 Satellite Platform . . . 35
- 4.2 Link Budget Analysis . . . 36
  - 4.2.1 Assumptions . . . 36
  - 4.2.2 Noise Power . . . 37
  - 4.2.3 Polarisation Mismatch Loss . . . 38
  - 4.2.4 Outcomes . . . 42

4.3 System Requirements . . . 43

5 Summary of Key Outcomes and Decisions 45

II Antenna Conceptual Design 46

6 Antenna Design Space 47
6.1 Conductor Shape . . . 47
6.1.1 Dipole Antennas . . . 47
6.1.2 Loop Antennas . . . 48
6.1.3 Other Antennas . . . 49
6.1.4 Summary . . . 49
6.2 Conductor Size . . . 50
6.3 Conductor Cross-section . . . 50
6.4 Conductor Material . . . 50
6.4.1 Uniform Materials . . . 51
6.4.2 Composite Materials . . . 51
6.5 Matching Network Topology . . . 52

7 Antenna Performance Analysis Approach 54
7.1 Objectives . . . 54
7.2 Approach . . . 55
7.3 Simulation Software Used . . . 55

8 Design Choices 57
8.1 Conductor Shape Choice . . . 57
8.1.1 Maximum Allowable Antenna Size . . . 57
8.1.2 Loop vs Dipole: Bandwidth . . . 60
8.1.3 Loop vs Dipole: Directivity . . . 62
8.1.4 Loop vs Dipole: Radiated Power . . . 64
8.1.5 Final Choice . . . 66
8.2 Remaining Design Choices . . . 67
8.2.1 Conductor Cross-section . . . 67
8.2.2 Conductor Material . . . 69
8.2.3 Matching Network Topology . . . 69

9 Design Characterisation 70
9.1 Directivity . . . 71
9.1.1 Antenna Directivity Pattern . . . 71
9.1.2 Satellite Attitude and Antenna Orientation . . . 73
9.1.3 Spacecraft-to-Ground-Station Relative Orientation . . . 74
9.2 Radiated Power . . . 75
9.3 Matching Network Efficiency . . . 76
9.4 Available Bandwidth . . . 77
9.4.1 Real Components Availability Limitations . . . 77
9.4.2 Real Components Manufacturing and Thermal Tolerances . . . 78
9.4.3 Bandwidth Limitations Mitigation Strategies . . . 80
9.5 Size Decision . . . 81
9.6 SimNEC and Ansys Electronics Validation . . . 81

10 Summary of Key Outcomes and Decisions 84

III Demonstrator Construction and Testing 85

11 Antenna Deployment Conceptual Design 86
11.1 Deployment Constraints . . . 86
11.2 Available Interface to Delfi-Twin . . . 87
11.3 Design Options . . . 88

11.3.1 Delfi-Twin RABSII Mounting Interface . . . 88
11.3.2 Antenna Deployment Approach . . . 90
11.4 Design Choices . . . 92
11.5 Conceptual Design Summary . . . 94

12 Antenna Deployer Design **95**
12.1 Design Overview . . . 95
12.2 Rotor Assembly . . . 96
12.3 Deployer Case Assembly . . . 100
12.4 HDRM Assembly . . . 101
12.5 Packing and Deployment Sequence . . . 102

13 Deployer Functional Demonstration **104**
13.1 Demonstrator Objectives . . . 104
13.2 Assumptions and Design Simplifications . . . 105
13.3 Components Acquisition . . . 106
13.4 Demonstrator Assembly . . . 108
13.5 Performance and Lessons Learned . . . 111
13.6 Mechanical Testing Recommendations . . . 120

14 Summary of Key Outcomes and Decisions **122**

IV Project Outcomes **123**

15 Results Overview **124**
15.1 Link Budget Results . . . 124
15.2 RF Design Results . . . 125
15.2.1 Design Choices . . . 125
15.2.2 Final Design Characterisation . . . 128
15.3 Mechanical Design Results . . . 130

16 Conclusion **132**
16.1 Closing Remarks . . . 135

17 Recommendation and Future Work **137**

References **139**

A Composite Capacitors Code **143**

List of Figures

2.1 Ionospheric layers [80] . . . 5
2.2 Sporadic E detection approach [80] . . . 6
2.3 RABSII instrument SMA; courtesy of the RABSII team . . . 6
2.4 Flown Delfi-family cubesats and PocketQube satellites from TU Delft . . . 7
2.5 Delfi-Twin spacecraft in both its low drag (left) and high drag (right) configurations [78] 7

3.1 Signal and noise power along transmission path [74] . . . 11
3.2 Radiation patterns of a few common antennas . . . 12
3.3 Specific atmospheric attenuation as a function of signal frequency [40] (page 27) . . . 13
3.4 Specific rain attenuation as a function of signal frequency [40] (page 43) . . . 14
3.5 Minimum expected noise temperature from terrestrial and extra-terrestrial sources [40] (page 124) . . . 15
3.6 Impedance of a 5-meter-long dipole antenna centered around the first resonant mode . 18
3.7 Impedance of a 5-meter-long dipole antenna between 20 and 200 MHz . . . 19
3.8 Impedance of a 5-meter-long dipole, left of the graph are frequencies at which the antenna operates as electrically short . . . 20
3.9 Capacitive hat added to a monopole antenna [49] (page 183) . . . 22
3.10 Linearly loaded loop antenna [49] (page 187) . . . 23
3.11 Increasingly loaded dipole, f/f_0 is the ratio of measured resonant frequency over resonant frequency of a standard dipole of same length, R is the radiation resistance [49] (page 187) . . . 23
3.12 Load impedance, $Z_{load} = 1.61 + 926j$ at 28 MHz . . . 25
3.13 Matching network topology, source on the left, load on the right . . . 26
3.14 Example matching network matching path, load in blue, source in yellow normalised to 1 at the centre . . . 26
3.15 Generalised 2-port system connecting a source and a load, arrows are energy flows, a refers to inputs, b to output, subscript 1 to port 1, and subscript 2 to port 2 . . . 27
3.16 S_{11} and S_{21} for an example tuned matching network around a centre frequency of f_c =28 MHz . . . 28

4.1 Galactic temperature map measured at $f_m = 408$ MHz [64] . . . 38
4.2 Distribution of the absolute value of polarisation loss $L_{p,\,dB}$ . . . 40
4.3 SNR in reception for two perpendicular dipoles for two different transmitting stations, in blue and red; the difference between the two is plotted in black [79] . . . 41

6.1 Dipole antenna of length L. For resonance, $L \approx \lambda/2$ . . . 47
6.2 Circular loop antenna of diameter D . . . 48
6.3 Considered conductor cross-section schematics . . . 51
6.4 Common **unbalanced** matching network topologies; capacitors with capacitance of C and inductors with inductance of L; source on the right, antenna on the left . . . 52
6.5 Common **balanced** matching network topologies; capacitors with capacitance of C and inductors with inductance of L; sources on the right, antenna on the left . . . 53

8.1 Resonant antenna sizes to scale next to Delfi-Twin (conductor thickness not to scale) . 59
8.2 Maximum allowed antenna sizes to scale next to Delfi-Twin (conductor thickness not to scale) . . . 59
8.3 Antenna coupling within the range ± 250 kHz around the central transmitting frequency of 28 MHz; $VSWR = 1.00 : 1$ at 28 MHz . . . 60
8.4 Bandwidth in kHz vs antenna size for both a loop and a dipole . . . 61

8.5 Radiation pattern shape at 28 MHz for the 1.5 m sized antennas . . . 62
8.6 Directivity gain across the azimuth and elevation planes . . . 62
8.7 Loop antenna directivity gain as a function of antenna size . . . 63
8.8 Dipole antenna directivity gain as a function of antenna size . . . 63
8.9 Feed reactance versus antenna size for both a loop and a dipole . . . 64
8.10 Matching network resistive losses as a fraction of the total supplied RF power . . . 65
8.11 Loop antenna radiated power as a function of antenna size . . . 65
8.12 Dipole antenna radiated power as a function of antenna size . . . 66
8.13 Parametric cross-sections definitions . . . 67
8.14 Radiation efficiency against loop diameter for various cross-sections . . . 68
8.15 Radiation efficiency against loop diameter for various conductor materials . . . 69

9.1 Loop antenna directivity on polar plots as a function of antenna size . . . 71
9.2 Loop antenna directivity on Cartesian plots as a function of antenna size . . . 72
9.3 Maximum variation in directivity gain as a function of antenna size for both the azimuth and elevation directions . . . 72
9.4 Attitude motion of the Delfi-Twin satellite; velocity vector v; Delfi-Twin long axis vector a 73
9.5 Angle range between the satellite and the ground station, link in blue . . . 74
9.6 Loop antenna radiated power on polar plots as a function of antenna size . . . 75
9.7 Loop antenna radiated power on Cartesian plots as a function of antenna size . . . 75
9.8 Matching network resistive losses as a fraction of the total supplied RF power . . . 76
9.9 Feed impedance of the loop antenna as a function of diameter . . . 76
9.10 Bandwidth as a function of loop diameter for various return loss thresholds . . . 77
9.11 Ideal required matching network; $C_1 = 4.8185$ pF; $C_2 = 302$ pF . . . 78
9.12 Matched impedance (blue) and expected impedance at the edged of the matching network capacitor tolerance range (red crosses) . . . 79
9.13 Return loss as a function of frequency for a perfectly matched system (blue), and for a system with matching network capacitance variation equal to the maximum tolerance range (red) . . . 80
9.14 Loop feed impedance comparison between Ansys and SimNEC . . . 82
9.15 Radiation efficiency comparison between Ansys and SimNEC . . . 82
9.16 Directivity gain comparison between Ansys and SimNEC . . . 83

11.1 Delfi-Twin spacecraft various wing configurations . . . 87
11.2 Delfi-Twin spacecraft solar cells placement . . . 87
11.3 RABSII payload available volume (red box) in relation to Delfi-Twin . . . 88
11.4 Mounting option 1: wing mounted; available deployer volume in red . . . 89
11.5 Mounting option 2: bus mounted; available deployer volume in red . . . 89
11.6 Hinge deployer mounted on the top of the Delfi main bus, work from Aboubakr el Jouhri [43] . . . 90
11.7 Pop-up tent loop antenna folding steps; deployer footprint in red (80x40 mm); antenna terminals in black . . . 91
11.8 Cassette loop stowage approach; deployer footprint in red (80x40 mm); spools in gray; torsion springs as spirals . . . 92
11.9 Bus-mounted Delfi-Twin interface . . . 93
11.10 Wing-mounted Delfi-Twin interface . . . 93

12.1 Overview of the complete deployer design . . . 95
12.2 Deployer design with the top PCB removed . . . 96
12.3 Rotor assembly components coloured; rigid rotors in red; torsion springs in blue; antenna conductor strip in green . . . 97
12.4 Required loop deployment orientations; deployer footprint in red; Delfi-Twin wing panel in green . . . 97
12.5 Loop conductor deployment steps; antenna conductor (green) thickness exaggerated for clarity . . . 98
12.6 Deployer case assembly components coloured; case bottom in red; case top PCB in green; bushings in blue . . . 100

12.7 Deployer case bottom part . . . 100
12.8 HDRM assembly components coloured; burn wire(s) in red; locking fingers in green; retaining M2.5 bolts in blue . . . 101
12.9 Locking fingers in their rest position . . . 102

13.1 Case bottom . . . 108
13.2 Bushings integrated into the case bottom . . . 108
13.3 Rotors and springs added to the case bottom . . . 109
13.4 Springs connected to the inner surface of the rotors . . . 109
13.5 Locking fingers component added to the assembly . . . 109
13.6 Antenna conductor added to the assembly; clamps used to prevent the rotors from deploying prematurely . . . 110
13.7 Transparent top plate added to complete the assembly . . . 110
13.8 Bent (left) and straight (right) locking fingers . . . 111
13.9 Contact point between deployed antenna conductor and deployer case bottom marked in red . . . 112
13.10 Various material options for the bushings shafts . . . 113
13.11 Shaft diameter resin calibration block . . . 113
13.12 Aluminium antenna strip plastically deformed after being integrated into the deployer . 114
13.13 Joint location of two antenna steel strips; Join thickness: 0.47 mm; Nominal strip thickness: 0.07 mm . . . 115
13.14 Antenna strip configuration around one of the rotors . . . 116
13.15 PTFE tubing used to reduce potential contact between antenna strip and . . . 116
13.16 Various degrees of twisting in the coiled antenna strips . . . 117
13.17 Stable scaled loop made with a perfectly straight (untwisted) aluminium strip . . . 117
13.18 Single spring per rotor configuration . . . 118
13.19 Double spring per rotor configuration . . . 118
13.20 Quad spring per rotor configuration . . . 119
13.21 3D printed demonstrator bottom case under the microscope . . . 120

15.1 Bandwidth as a function of antenna size for both a loop and a dipole . . . 126
15.2 Resistive power losses in the matching network as a fraction of total supplied RF power, and as a function of antenna size for both a loop and a dipole . . . 126
15.3 Loop antenna radiated power as a function of antenna size . . . 127
15.4 Dipole antenna radiated power as a function of antenna size . . . 127
15.5 Maximum variation in directivity gain as a function of antenna size for for both the azimuth and elevation directions . . . 128
15.6 Loop antenna radiated power on Cartesian plots as a function of antenna size . . . 129
15.7 Return loss as a function of frequency for a perfectly matched system (blue), and for a system with matching network capacitance variation equal to the maximum tolerance range (red) . . . 130
15.8 Overview of the deployer design . . . 131

List of Tables

3.1 Ideal impedance of RLC components . . . 29
3.2 Real impedance of RLC components . . . 29

4.1 Median man-made noise temperature at the RABSII instrument transmitter frequencies 37
4.2 Galactic noise temperature range at the RABSII instrument transmitter frequencies . . . 38
4.3 Full rotations of the signal polarisation due to Faraday Rotation for low, medium, and high estimates of the TEC . . . 39
4.4 Link budget for the 28 MHz instrument. Parameters in order of calculation/usage, together with their computed value and unit. Each row is coloured according to whether the parameter is an input (red), a intermediate result (green), or a output (blue). Assumptions and mission constraints are considered as inputs. . . . 42
4.5 Link budget for the 50 MHz instrument. Parameters in order of calculation/usage, together with their computed value and unit. Each row is coloured according to whether the parameter is an input (red), a intermediate result (green), or a output (blue). Assumptions and mission constraints are considered as inputs. . . . 43
4.6 28 MHz RABSII instrument system requirements . . . 44

6.1 Considered antenna types and relevant RF properties . . . 49
6.2 Uniform material options and relevant properties [39, 38] . . . 51
6.3 Conductive coating options over a structural steel substrate [39, 38] . . . 52

8.1 Existing tape-deployed dipole antenna systems; aspect ratio is defined by the tape length divided by the tape width . . . 58
8.2 Loop versus dipole parameters for comparative analysis . . . 60
8.3 Loop and Dipole antenna bandwidths . . . 61
8.4 Cross-sections geometrical parameters . . . 68

9.1 Chosen antenna properties summary . . . 70

13.1 Deployer demonstrator components . . . 107

15.1 Frequency-dependent link budget figures . . . 124
15.2 Minimum required characteristics of the two transmitting antennas . . . 125

16.1 Minimum required antenna gain and radiated power for the two RABSII instruments . . . 133
16.2 Qualitative sensitivity of various antenna RF performance metrics with respect to changes in design parameters; Ranging from *Significant* (black), *Moderate* (gray), and *Negligible* (white) . . . 134

Nomenclature

Abbreviations

Abbreviation	Definition
AC	Alternating Current
BALUN	Balanced-Unbalanced Transformer
CAD	Computer Aided Design
CDF	Cumulative Distrubution Function
CW	Continuous Wave (analog radio transmission mode)
EIRP	Equivalent Isotropic Radiated Power
EM	Electromagnetic
FDM	Fused Deposition Modelling
FT4	Fast Telegraphy 4-tone (digital radio mode)
GUI	Graphical User Interface
HDRM	Hold Down and Release Mechanism
HF	High Frequency
HFSS	High Frequency Structure Simulator
ITU	International Telecommunication Union
LEO	Low Earth Orbit
NEC	Numerical Electromagnetic Code
P	PocketQube Unit (5x5x5 cm)
PCB	Printed Circuit Board
PDF	Probability Density Function
PEC	Perfect Electric Conductor
PEEK	PolyEther Ether Ketone
PLA	PolyLactic Acid
PQ	PocketQube
PTFE	Polytetrafluoroethylene
RA	Research Area
RABSII	Radio Amateur Beacons aboard a nanoSatellite for the Investigation of the Ionosphere
REQ	Requirement
RF	Radio Frequency
RQ	Research Question
SLA	Stereolithography
SMA	Shape Memory Alloy
SNR	Signal-to-Noise Ratio
SWR	Standing Wave Ratio
TEC	Total Electron Content
U	CubeSat Unit (10x10x10 cm)
UHF	Ultra High Frequency
UNUN	Unbalanced-Unbalanced Transformer
UV	Ultraviolet
VHF	Very High Frequency
VHS	Video Homes System
VSWR	Voltage Standing Wave Ratio

Symbols

Symbol	Definition	Unit
A	Area	[m^2]
AR	Axial ratio	[-]
B	Bandwidth	[Hz]
B	Susceptance	[S]
B	Magnetic field strength	[T]
C	Capacitance	[F]
d	Distance (between transmitter and receiver)	[m]
d	Cross-section diameter	[m]
D	Loop antenna diameter	[m]
E	Young's modulus	[Pa]
F	Noise factor	[dB]
f	Frequency	[Hz]
G	Electrical length (ratio of antenna length to wavelength)	[-]
G	Gain	[dB]
G	Conductance	[S]
J	Current Density	[A/m^2]
k_b	Boltzmann constant	[J/K]
L	Length	[m]
L	Loss gain	[dB]
L	Inductance	[H]
N	Noise power	[W] or [dBW]
N_T	Total electron content	[el/m^2]
n_e	Local electron density	[el/m^3]
P	Power	[W]
Q	Quality factor	[-]
R	Resistance	[Ω]
R	Rotation rate	[$^\circ$/s]
R	Bend radius	[m]
RL	Return Loss	[dB]
S	Propagation path	[-]
S_{11}	Reflection coefficient (S-parameter)	[-]
S_{21}	Forward transmission coefficient (S-parameter)	[-]
T	Temperature	[K]
T	Torque	[Nm]
t	Thickness	[m]
V	Velocity	[m/s]
v	Delfi-Twin velocity vector	[-]
w	Width	[m]
X	Reactance	[Ω]
Y	Admittance	[S]
Z	Impedance	[Ω]
θ	Angle (polarisation, orientation, etc.)	[rad] or [deg]
δ	Skin depth	[m]
ε	Permittivity	[F/m]
λ	Wavelength	[m]
μ	Permeability	[H/m]
ρ	Density	[kg/m^3]
ρ	Resistivity	[Ωm]
σ	Stress	[Pa]
σ	Conductivity	[S/m]
ω	Angular frequency	[/s]

1

Introduction

The ionosphere is part of the upper atmosphere, and as the name suggests, it is a portion of the atmosphere with a high density of charged ions. The ionosphere, and its composition, plays a large role on High Frequency (HF) and Very High Frequency (VHF) radio communication by scattering and reflecting signals travelling through it. Given the high temporal and spatial variability in its structure, it is challenging to accurately and reliably characterise the ionospheric composition through direct earth-based measurements. Looking at space, an orbital platform could be used to regularly survey the ionosphere and provide updated global maps of the charged particle densities. There is hence a need for a small inexpensive instrument which can be used to facilitate both ground-based and space-based HF/VHF radio communication.

1.1. Project Scope

This thesis project slots within the current design and development of the RABSII payload, which stands for *Radio Amateur Beacons aboard a nanoSatellite for the Investigation of the Ionosphere*. The RABSII payload is to be flown aboard the PocketQube satellite Delfi-Twin, currently under development by the Aerospace Faculty at TU Delft.

The RABSII payload is a radio beacon to be used to globally measure and characterise the ionosphere on a recurring basis. While some work has already been done on the payload, a complete look at the mission, from the science case all the way to prototyping and integration is yet to be done.

This thesis aims to fill that gap by first investigating the implications of the RABSII science case on the system link budget. Based on the link budget outputs, a conceptual design for the radio beacon will be devised. The choice on the development path will be based on what has the most promising performance, but also on expanding the current concept scope of the RABSII project by considering innovative and perhaps unconventional design approaches.

Based on these overarching goals, the project will be divided into three key phases. The first phase of the project will work towards identifying the performance requirements for the RABSII instrument. Based on these requirements and constraints, the second phase of the project will focus on developing an antenna system capable of delivering sufficient RF performance to meet the system requirements. Lastly, the third project phase will take this antenna system and attempt to devise a solution to integrate, store, and deploy it from the host satellite platform. A design will be proposed for a deployer which meets the identified system requirements.

The project aims to produce the following key outcomes:

- A set of key requirements useful to delimitate the antenna and deployment design space.
- An antenna design with sufficient RF performance to meet the RABSII science case goals.
- A mechanical design of an antenna deployer capable of integrating the RABSII antenna onto the host satellite platform.

1.2. How to Read

The report is subdivided in parts according to the defined key project phases.

In order, the first report part discusses project phase one, spanning the project background, the science case, and the link budget. Essentially, everything from background knowledge to baseline analysis required to define a set of measurable system requirements from the overarching scientific objectives.

The second report part discusses project phase two. It presents the design space for the RABSII antenna and analyses the RF performance of various competing options. Based on the results obtained from analysis, the most promising option is selected for further development.

The third report part discusses project phase three. It takes as a starting point the antenna conceptual design from the previous part, and devises an approach to stow, deploy, and operate it aboard the host satellite. The expected outcome is a physical prototype to demonstrate the key features of the deployment approach.

Lastly, the fourth report part draws conclusions on what has been achieved with respect to the objectives and scope of the project as a whole. Lessons learned and recommendations for future steps will also be presented to guide potential future development on the RABSII payload.

To understand the driving requirements behind the system design, read part one. If the reader wants to understand the RF performance of the proposed beacon design, read part two. If instead the reader wants to understand the proposed deployer design and its mechanical performance, read part three. While for general conclusions on the outcomes of this project, read part four.

Each report part concludes with a short chapter, summarising the key takeaways from that part. Read these chapters (chapter 5, chapter 10, or chapter 14) if interested in the general outcomes of each project phase without delving into the technical details.

Part I:

Project Background

2

Project Objectives

In order to meaningfully define the questions this work attempts to answer, some relevant background must be provided. Firstly, the RABSII instrument is introduced in section 2.1 together with the underlying science case and current state of development. Following, in section 2.2, a brief introduction to the Delfi Twin platform which will host the RABSII payload is provided. Based on these two key elements, the objectives of this project and the relevant research questions are presented in section 2.3.

2.1. RABSII Instrument and Science Case

RABSII, short for *Radio Amateur Beacons aboard a nanoSatellite for the Investigation of the Ionosphere*, is a scientific instrument currently under development. The goal of the RABSII instrument is to provide global coverage for measurement and characterisation of the sporadic E ionospheric phenomena. As earlier introduced, sporadic E is a localised highly variable concentration of ions in the ionospheric E-layer, sometimes also referred to as sporadic E clouds. As described in the paper by Vanhamel et al [80], measurements will be done by placing a pair of HF/VHF radio beacons on two different spacecrafts flying in coordinated formation. Each beacon will broadcast a beacon signal on a separate frequency. At ground, a network of radio stations will listen for the emitted signals from the passing satellites and be able to infer the presence and density of sporadic E clouds between the transmitter (space) and receiver (ground). This space-based approach aims to tackle the key issue with current sporadic E detection approaches, namely, the lack of up-to-date global coverage.

The two beacons will operate on the 28 MHz and 50 MHz frequency bands. In vacuum, this corresponds to wavelengths of approximately 10.7 m and 6 m respectively. Radio antenna sizes are generally directly proportional to the transmitted wavelength. Resonant dipoles for example (commonly used on small satellites) are generally half the length of the transmitted wavelength [68]. This poses major challenges when it comes to integrating a potentially sizeable antenna on board a satellite the size of Delfi-Twin, only 3P in volume (15x5x5 cm^3). Regardless of the final design, trade-offs between RF and deployment performance must be performed to deliver a sufficiently strong radio signal in a form factor compatible with the Delfi-Twin satellites.

2.1.1. Science Case

While not the primary focus for this work, understanding the science goals of the RABSII instrument is still important to the development of the system. As compromises will have to be made between the various performance metrics, understanding where compromises can and cannot be made depends mainly on whether the final product can still fulfil its scientific objectives.

As previously mentioned, the RABSII instrument aims at providing a space-based solution for measuring the sporadic E phenomena. Sporadic E is an atmospheric phenomenon occurring within the ionosphere. The ionosphere is a layer of the atmosphere rich in ions ranging between 60 and 1600 km. Primarily responsible for the generation of these ions are cosmic rays and the Sun's activity, specifically ultraviolet (UV) light and X-rays. Within the ionosphere itself, multiple distinct layers can be identified based on both height and electron density. Figure 2.1 presents an overview of these layers according to their height above the Earth. As the Sun has a strong influence on the electron density and composition of these atmospheric layers, their intensity is highly dependent on both the local height, as well as the day/night cycle and Sun's activity.

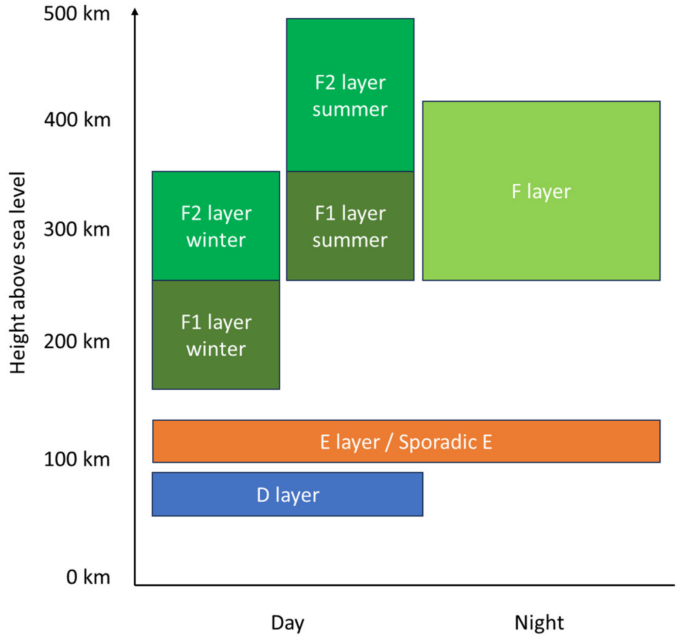

Figure 2.1: Ionospheric layers [80]

The E-layer specifically is a relatively thin layer, between 5 and 10 km thick, generally present between a height of 100 and 125 km. The E-layer is constantly present, during both daytime and nighttime. Of particular interest for this work and for the RABSII instrument, the E-layer of the ionosphere is where the sporadic E phenomena takes place. Sporadic E is a localized variable phenomena of high densities of charged particles, or clouds, which are particularly reflective towards signals in the HF (3-30 MHz) and VHF (30-300 MHz) radio bands. Without delving into the complex processes responsible for sporadic E, it is important to note that the mechanisms responsible for these ions are numerous and hard to accurately model. Namely, high atmosphere wind shear, magnetic field disturbances (especially in polar regions), and meteoric ablation can contribute to the formation of sporadic E clouds. This unpredictable nature means that long-range radio communication in these bands often significantly deviates from predictive models in unexpected ways.

To regularly detect the occurrence of sporadic E at a global scale, the RABSII instrument is proposed in the original paper published by Vanhamel et al [80]. To do so, the radio beacon in space will work in tandem with a network of radio-amateur receiving stations. Based on the location of the satellite, the individual radio station, and the strength of the received signal, presence of sporadic E between the transmitter and receiver can be inferred. Figure 2.2 shows this detection mechanism. To detect sporadic E occurrence in relevant transmission bands, beacon signals will be transmitted on both 28 and 50 MHz. This necessitates two separate antenna payloads, each transmitting on its own frequency band.

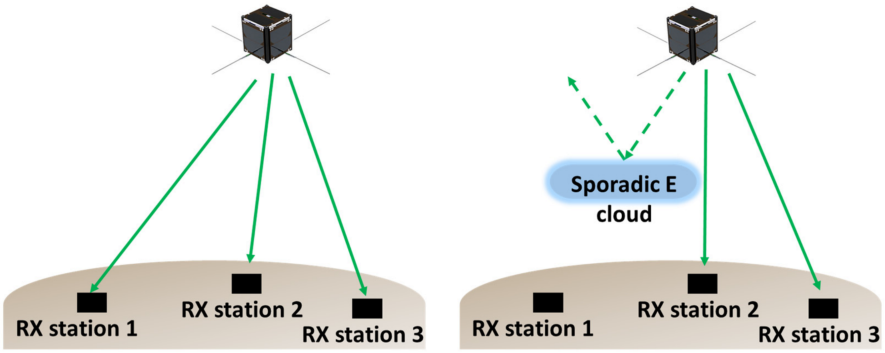

Figure 2.2: Sporadic E detection approach [80]

2.1.2. Current Development Status

RABSII is an ongoing project. Some work has already been done to investigate a viable strategy to meet the science objectives within the constraints of the satellite platform. The primary concern with the feasibility of the instrument is the combination of the limited available space aboard Delfi Twin, and the large required antenna size due to the low transmitting frequency of the beacon.

As of the writing of this thesis, a half-wave dipole is the main option considered for the beacon's antenna. Half-wave dipoles are resonant antennas generally characterised by adequate omnidirectional performance and radiation efficiency. Due to their simplicity and performance, dipoles are a common choice aboard modern cubesats, and small satellites in general [53, 2].

The current RABSII instrument concept features two thin metallic wires, around 0.3 mm in diameter and a quarter of the transmitting wavelength in length each. These two wires would come out of the satellite in opposing directions to form a single dipole antenna. On the two transmitting bands, this translates to antennas of roughly 3 and 5 m in length respectively. with Delfi Twin measuring only 15 cm in its largest dimension, integrating and deploying these antennas is a significant engineering challenge. The team working on the instrument is currently testing and evaluating whether shape-memory alloys (SMAs) could offer a viable solution to the deployment problem. With some prototypes made and work done on trying to demonstrate the deployment, this approach may be a possible solution. Figure 2.3 presents the SMA prototype.

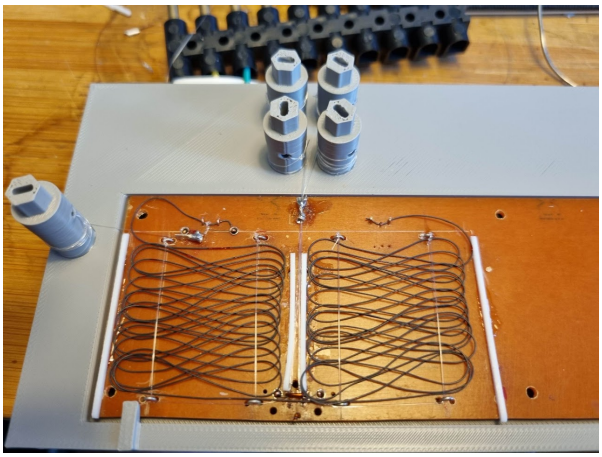

Figure 2.3: RABSII instrument SMA; courtesy of the RABSII team

While SMAs could provide sufficiently controlled actuation forces to deploy the antenna, the considerably long and thin wires are still a large unknown when it comes to reliable operations once in space.

2.2. Delfi Twin Mission

The upcoming Delfi Twin mission is the most recent in a line of small satellites developed by the Delft Space Laboratory at TU Delft. Being directly integrated within the Aerospace faculty at the university, the lab serves the dual purpose of technology development and demonstration, as well as education of Master and PhD students working in the field of small satellites. Starting all the way back in 2004, the lab has previously developed, launched and operated three distinct satellites: Delfi-C3, Delfi-n3Xt, and Delfi-PQ. The first two, Delfi-C3 and Delfi-n3Xt, being triple-unit (3U) CubeSats, with one unit (U) defined as a modular cube of $10\,\text{x}10\,\text{x}10\,\text{cm}^3$ in volume [25, 8]. The third, Delfi-PQ, a step down in size, being a triple-unit (3P) PocketQube satellite instead, with one unit defined as a modular cube of $5\,\text{x}5\,\text{x}5\,\text{cm}^3$ [63]. An image for each satellite can be found in Figure 2.4.

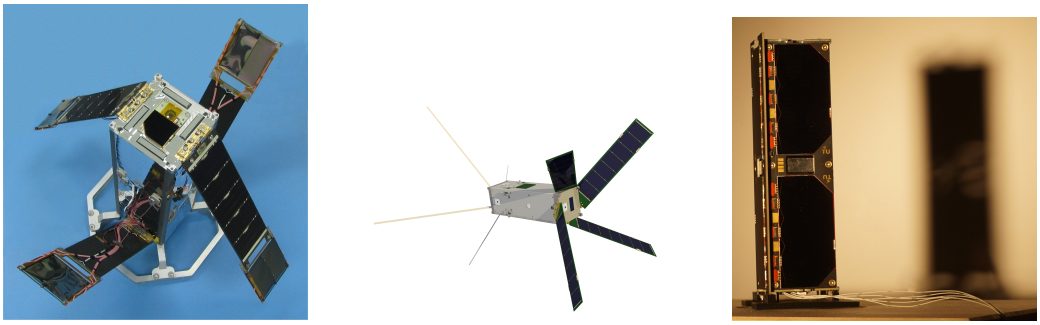

(a) Delfi-C^3 [27] **(b)** Delfi-n3Xt [17] **(c)** Delfi-PQ [78]

Figure 2.4: Flown Delfi-family cubesats and PocketQube satellites from TU Delft

Delfi Twin is the latest project developed by the Delfi Space Laboratory. Currently in its development phase, the mission's key objective is to demonstrate autonomous formation flight with a pair of PocketQube satellites [75]. Each satellite's design is an elaboration on the original Delfi-PQ satellite platform. As such, each Delfi Twin satellite measures $5\,\text{x}5\,\text{x}15\,\text{cm}^3$ in size. Movable wings will perform the dual function of both housing the solar cells, and changing the spacecraft's drag to remain in a controlled formation with each other. The latter will be achieved by actively altering the angle between the wings and the main satellite body. A render of the current Delfi Twin design can be found in Figure 2.5

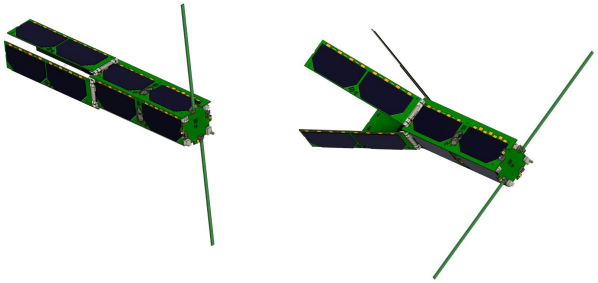

Figure 2.5: Delfi-Twin spacecraft in both its low drag (left) and high drag (right) configurations [78]

While the wings will be used to alter the spacecraft's trajectory, its attitude is not actively controlled. Based on its geometry, the satellite's long axis (vertical in Figure 2.5) is expected to remain roughly aligned with the velocity vector. This alignment will oscillate by roughly $\pm 20°$. Additionally, the satellite is expected to also rotate about its long axis continuously at a spin rate of about $5\text{-}10\,°\,\text{s}^{-1}$. These numbers are initial estimates, but should represent the expected satellite dynamics during flight. Complete dynamic modelling and simulation is currently under work to refine these estimates.

While the primary mission objective of Delfi Twin is to demonstrate controlled formation flying, it will also host RABSII as an active scientific payload. The exact approach to meet RABSII scientific objectives within the constraints of the Delfi Twin platform is yet to be finalised. The current deployment approach, presented in subsection 2.1.2, has advantages and disadvantages as a result of the engineering decisions made. On the one hand, the use of a well understood antenna design gives confidence that the beacon will have sufficient RF performance to complete the scientific objectives. On the other hand, the considerably long and thin wires making up the dipole are a significant deployment and operational risk which may not be easy to mitigate. Tangling of antenna lines, or the antenna's dynamic response to the combined oscillating spacecraft and disturbance torques may be problematic when it comes to stable and reliable operation.

2.3. Research Questions

The research gap that this thesis aims to fulfil slots right between the objectives of the RABSII instrument and the objectives of the Delfi Twin mission. While the overall RABSII instrument objectives are purely scientific in nature, their technical implementation is what is relevant for this work. In practice, the RABSII instrument must emit an omnidirectional radio beacon signal strong enough to be received and decoded by ground stations within the existing amateur-radio network. The Delfi Twin mission instead aims at demonstrating controlled formation flying of a pair of identical 3P PocketQube satellites. Additionally, and if possible, Delfi Twin aims at giving space to additional scientific payloads compatible with the mission parameters.

In order to maximise the chances of mission success for the RABSII instrument, this thesis focusses on investigating options when it comes to the design of both the antenna and the deployer for the payload. Looking at both elements, the antenna and the deployer design, is considered crucial to ensure the solution(s) proposed is actually viable. The research objective of this thesis can hence be defined as follows.

Research Objective

To design an HF antenna beacon payload compatible with the Delfi Twin satellite platform, and demonstrate its stowage and deployment.

In order to address this project objective, a few relevant research questions can be identified. ***RQ-X*** identifies research questions whereas ***RQ-X.X*** identifies the corresponding sub-questions.

Research Questions

RQ-1: What antenna gain and radiated power is required to close the science case's link budget with sufficient margin?

- **RQ-1.1:** What are the relevant noise sources to consider in the instrument link budget?
- **RQ-1.2:** What are the relevant attenuation sources to consider in the instrument link budget?

RQ-2: To what extent can the antenna be downscaled compared to the currently proposed half-wave dipole while still meeting the RF requirements of the science case?

- **RQ-2.1:** What key antenna design parameters effect its RF performance?
- **RQ-2.2:** How sensitive is the antenna RF performance to the identified design parameters?
- **RQ-2.3:** What combination of materials/geometry/drive electronics is sufficient to meet the identified requirements?

RQ-3: How can the RABSII antenna be effectively packaged to be compatible with integration aboard the Delfi-Twin satellite platform?

- **RQ-3.1:** What system requirements are driving when it comes to the mechanical design of the antenna deployer?
- **RQ-3.2:** How can the designed RABSII antenna be stored and deployed?
- **RQ-3.3:** How can the devised deployment approach be demonstrated within the resource and time constraints of this project?
- **RQ-3.4:** What aspects of the deployment are critical and must be further investigated?

3

Relevant Literature

The first step towards tackling the research questions was to identify and explore the relevant research areas. The knowledge acquired during this process will serve as a starting point for the design, analysis, and implementation of the antenna payload.

Based on the research questions, the following areas are identified as relevant to the project:

Background Research Areas

- **RA-1:** Theory of link budget analyses
- **RA-2:** Theory of radio antennas
- **RA-3:** Practical considerations of real antenna systems
- **RA-4:** Deployment mechanisms and technologies

Starting with research area one (**RA-1**), link budgets are a type of analysis commonly used to determine the feasibility and performance of a radio transmission and reception path. Specifically for space, any satellite using radio communication to transfer and receive commands and data relies on a stable working downlink/uplink connection with ground. To determine the feasibility, performance, and characteristics of this connection, a link budget analysis is used. For the RABSII instrument, this type of analysis will be used to determine the required antenna performance to close the link with the ground segment of the mission. As such, it is important to investigate and categorise sources of loss, attenuation, and noise that will be relevant for this specific mission scenario.

Areas two and three (**RA-2** & **RA-3**) deal with the theory, design, implementation, and operation of radio antenna systems. Given the elementary knowledge on this subject prior to the completion of this project, both of these areas are of key importance if any useful results are to be obtained. Within **RA-2**, the ground theory behind the design and performance of antennas is investigated. **RA-3** instead aims at gathering information on how these antenna systems can be implemented, considering a more practical aspect.

Lastly, the fourth research area (**RA-4**) aims at providing a general overview at what options exists when it comes to storing and actuating a deployable structure in space. While the final design of the antenna deployer will need to include some degree of creative thinking, it is necessary to have a good overview of what technologies and approaches have worked before.

3.1. RA-1: Theory of Link Budget Analyses

This chapter presents the general theory behind the link budget analysis to be carried out to further investigate the exact required antenna performance. After a general introduction to link budgets, a few key aspects are touched upon. Firstly, power of the radiated signal in subsection 3.1.1, secondly, the sources of losses and hence signal attenuation in subsection 3.1.2, and lastly the sources of noise in subsection 3.1.3. For all the information provided, the RABSII use-case is considered, meaning a downlink-only budget with a space-based transmitter operating at either 28 or 50 MHz.

A link budget is a way to size a communication system based on its foreseen operation. A general transmission case to be analysed is defined as follows. Starting from the system input, some power is provided by the spacecraft to the transmitter and antenna system. Within the transmitter, the signal is first generated and then amplified before being fed to the antenna through a cable. At the antenna, the signal will be first passed through an impedance matching network, or matching transformer, before being radiated into free space as radio waves. As it travels through free space, the signal will experience a certain degree of attenuation, varying depending on the medium and signal frequency. Upon reaching the receiver, the signal will be picked up by the ground station antenna and converted from radio waves into electric signals. From there, the signal travels through some length of cable to the amplifier. After being amplified, it is decoded and processed accordingly. A general illustration of the signal and noise power levels along the signal's journey can be found in Figure 3.1.

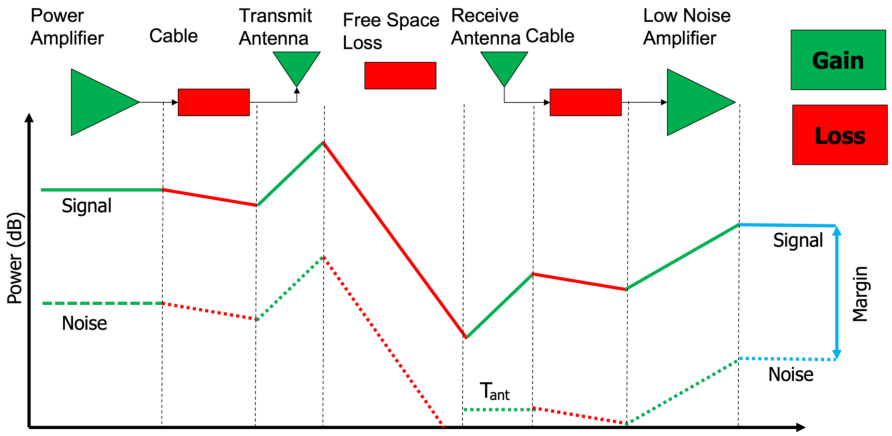

Figure 3.1: Signal and noise power along transmission path [74]

Once both the noise and signal power have been quantified, a margin can be defined as the ratio between the two. This margin, or signal-to-noise ratio (SNR) is the driving parameter to verify that the signal indeed has sufficient power at reception to be correctly decoded. [74, 40]

3.1.1. Radiated Signal Power

Looking at the radiated power first, there are a few aspects to be considered. Both the raw input power and the antenna characteristic play a large role in determining how effectively the system radiates the signal. Regarding the input power, quite intuitively, the higher the input power, the higher the radiated power. Within a limited operating range, a change in input power is generally linearly correlated to a change in radiated power.

Regarding the antenna itself, more must be known about the system to determine the radiated power. Power leaving an antenna as EM-waves expands in all directions, but depending on the shape of the conductor, this emitted power is almost never uniformly radiated. One key antenna property is hence its radiation pattern. An antenna radiation pattern is the relation between radiated power density and direction. Radiation patterns are normally visualised as a surface in 3D space centred at the origin. The relative distance of this surface from the origin indicates the relative intensity of the power signal in any direction. A perfectly isentropic antenna, hence radiating equally in all directions, will have a radiation pattern represented by a perfect sphere. The radiation pattern of a few common antennas as examples are presented in Figure 3.2.

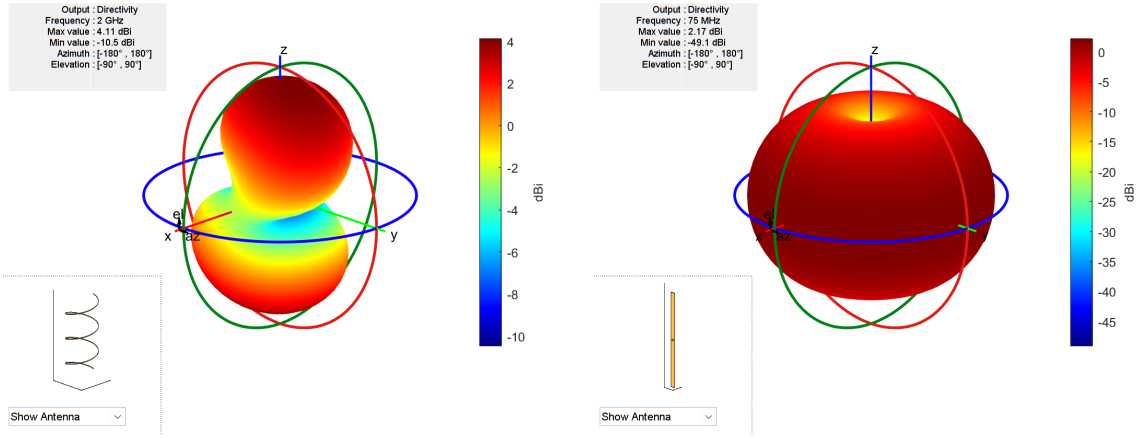

(a) Helix **(b)** Dipole

Figure 3.2: Radiation patterns of a few common antennas

Note the unit for the surfaces in Figure 3.2. The magnitude of the field intensity in any direction is measured in dBi, or decibel isentropic. This is simply a ratio between the radiation intensity over the intensity of an ideal isentropic radiator (perfectly spherical radiation pattern).

Returning to the link budget, depending on the operational mode and situation, an appropriate gain is selected to represent the antenna's performance. If a highly directional antenna is used, the gain may be estimated as the dBi within a few to a few tens of degrees from the optimal pointing. With omnidirectional antennas, a statistical analysis may be carried out to identify the expected gain throughout all mission phases.

Once the antenna gain is determined, it can be used to compute the Equivalent Isentropic Radiated Power, or EIRP. This is the equivalent power an ideal isentropic radiator would need to output to match the antenna's power in the chosen direction. EIRP in dB W can be computed as follows:

$$EIRP_{dBW} = 10 \cdot log_{10}(P) + G_{antenna} - L_{system} \tag{3.1}$$

Where P is the power fed to the antenna in Watts, G is the gain, and L are the system losses.

3.1.2. Attenuation Sources

Returning to Figure 3.1, the most significant signal losses occur between the transmitting and receiving antenna. While the distance travelled significantly affects this signal attenuation, there are also other factors to consider.

Free Space Loss

Free space loss simply refers to the decrease in signal power density as the emitted EM-waves expand in all directions from the antenna. The magnitude of the loss hence directly depends on the distance between the transmitter and the receiver. In addition, this loss depends on the frequency of the carrier wave, with lower frequencies experiencing less losses, and higher ones more losses due to free space. The equation to compute the free space losses for a signal is as follows: [40]

$$L_{FS,dB} = 20 \cdot log_{10}\left(\frac{4\pi d}{\lambda}\right) \tag{3.2}$$

Where $L_{FS,dB}$ is the free space loss in decibels, d is the actual distance between transmitter and receiver, and λ is the wavelength of the signal. For communication around LEO, losses in the range of around 150 dB can be expected, depending on the frequency band used.

Atmospheric Gasses Attenuation

For space-to-ground or ground-to-space communication, the signal must travel through the atmosphere. Radio propagation through a medium adds additional losses and attenuation highly dependent on wave and medium properties. When it comes to the atmosphere, the chemical composition of the gasses in the air determines the attenuation of the signal. The gasses with the highest effect on attenuation are generally diatomic oxygen (O_2) and water vapour (H_2O). Figure 3.3 presents the specific attenuation as a function of signal frequency.

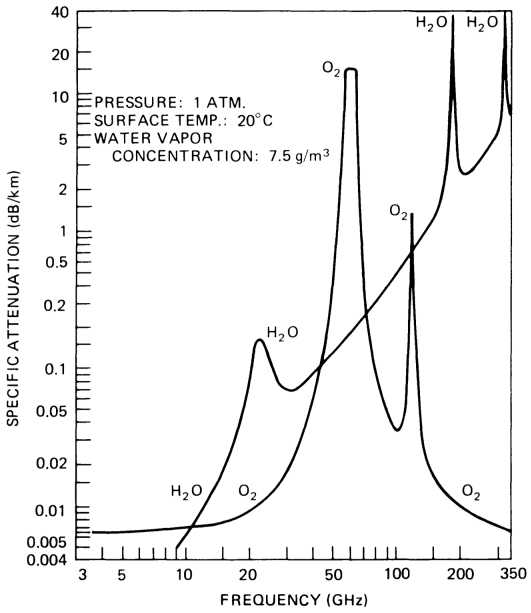

Figure 3.3: Specific atmospheric attenuation as a function of signal frequency [40] (page 27)

As can be seen, the signal frequency has a huge affect on the attenuation, and for waves below the GHz range, almost no atmospheric attenuation is expected. For the instrument to be designed, operating below 50 MHz means atmospheric attenuation is negligible. [40]

Rain Attenuation

While water vapour dissolved in the atmosphere attenuates radio signals, actual rain, hence liquid water particles, also contribute to signal attenuation. Figure 3.4 presents the specific attenuation due to rain depending on the rain rate R in mm h^{-1}.

Similarly to atmospheric attenuation, it can be clearly seen how for anything below the GHz range, attenuation is essentially negligible for the scope of this project. [23]

Ionospheric Attenuation

The last attenuation source to be considered is due to the ionosphere, a layer of the upper atmosphere with regions rich in charged particles. As such, it is effective at reflecting incoming signals at the great expense of signal strength. While this would otherwise be an issue to be taken into account, as the whole purpose of this mission is studying this layer of the atmosphere, it can essentially be ignored. Ionospheric reflections in the transmitted signal is the very thing the mission concept is attempting to measure, and is hence not only acceptable, but the desired outcome. [40]

Polarisation Mismatch Losses

While technically still a source of signal attenuation, polarisation mismatch losses are more a product of the signal itself rather than the environment. Polarisation of a signal refers to the phase relation between the magnetic and electric component of the RF signal. Polarisation describes how the resultant of the combined electric and magnetic fields oscillates. Furthermore, polarisation is also a property of a transmitter/receiver antenna, depending on the polarisation of the signal it generates. A signal/antenna can be linearly, elliptically, or circularly polarised.

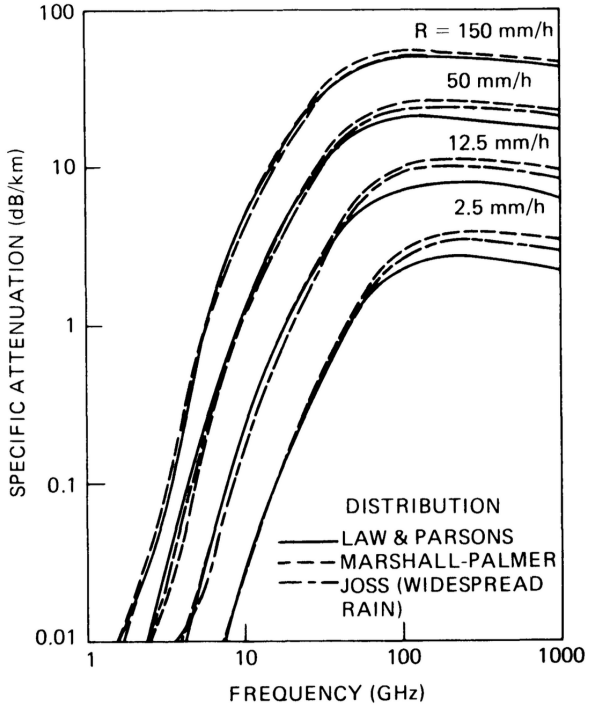

Figure 3.4: Specific rain attenuation as a function of signal frequency [40] (page 43)

Mismatch losses arise when the receiving antenna has a different polarisation than the incoming signal. This can be seen as the receiver being poorly 'tuned' to resonate with the incoming EM wave. This poor 'tuning' results in a poor efficiency when converting the incoming signal power into oscillating currents and voltages in the conductor. In practical terms, imagine a wave oscillating vertically trying to go through a narrow horizontal slot. Most of the energy will not make it through. This is the case of a vertically polarised signal being received by a horizontally polarised antenna.

In the generalised case, the following equation describes the loss in dB due to polarisation mismatch [61]. Do note that both the signal and antenna are assumed to have an elliptical polarisation with a certain axial ratio between the major and the minor axis. A perfectly circularly polarised signal will have an axial ratio of one, while a linearly polarised signal will have an axial ratio approaching infinity.

$$L_{p,dB} = -10 \cdot log_{10}\left[\frac{1}{2} + \frac{1}{2}\left(\frac{4AR_S AR_R + (1 - AR_S^2)(1 - AR_R^2) \cdot cos(2\theta)}{(1 + AR_S^2)(1 + AR_R^2)}\right)\right] \tag{3.3}$$

Where AR_S and AR_R are the signal's and receiver's polarisation axial ratios respectively (both expressed as a fraction, not in dB). θ is the angle between the major axes of the signal's and transmitter's polarisation ellipses.

3.1.3. Noise Power

The last aspect when it comes to determining a link budget, is estimating the noise power. Referring to Figure 3.1, sources of noise can be identified. While some noise is introduced to the signal before transmission, the attenuation experienced by this noise in free space before reaching the receiver antenna makes it negligible to the link margin. The dominant noise source to be investigated is the noise at signal reception at the ground station antenna. Determining the link margin is hence a matter of estimating the noise power at ground.

Two key noise sources must be considered at ground, terrestrial noise, and extraterrestrial noise. The first originates from sources on Earth, and is mostly a product of human activity. The latter originates from other extra-terrestrial sources, such as the Sun, or cosmic background radiation. Each noise source is discussed below in the appropriate section.

Before discussing noise sources in more detail, the concept of noise must be better defined. Noise is power distributed over a certain frequency range which does not carry any information. When the power of the noise is too high compared to the power of the actual signal, the signal itself is 'drowned out' and cannot be accurately recovered. The noise power over a certain band of frequencies depends on the noise temperature, and the width of the band itself. It can be defined as follows: [40]

$$N_{dBW} = 10 \cdot log_{10}(k_b B T) \tag{3.4}$$

Where N_{dBW} is the noise power in decibels Watt, k_b is the Boltzmann constant (with a value of $k_b = 1.380649 \times 10^{-23} J/K$), B is the bandwidth in Hertz, and T is the noise temperature in Kelvin. While this may seem simple, the issues with estimating noise power stems from the difficulty in accurately determining the temperature of the noise. Estimating noise power means estimating noise temperature.

Based on historical data and observations, noise can be categorised according to its source. What noise source dominates the link budget depends on the frequency at which the system operates. A breakdown of estimated minimum noise power according to its source can be found in Figure 3.5.

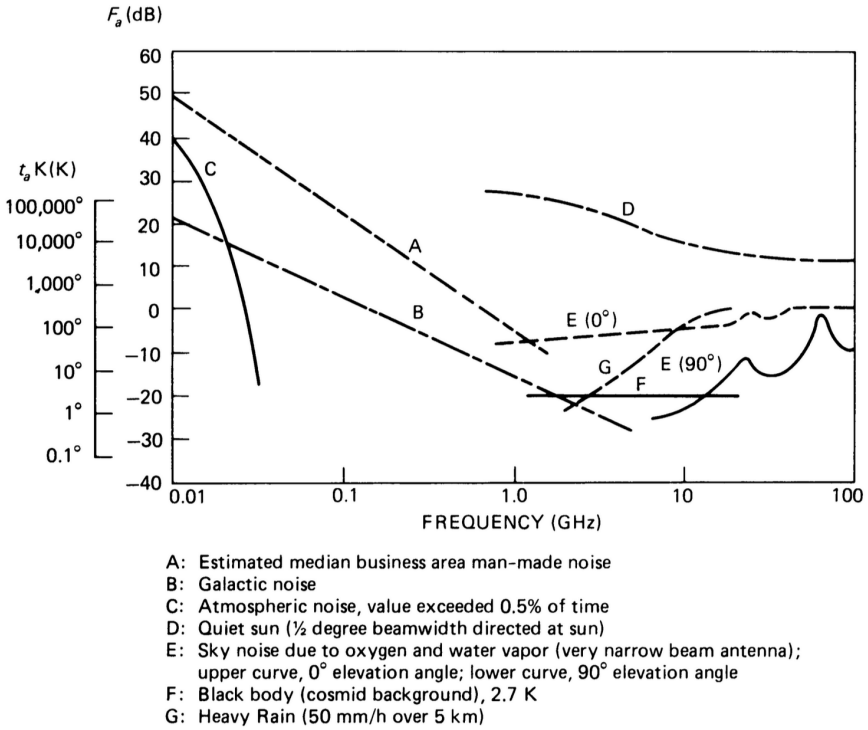

Figure 3.5: Minimum expected noise temperature from terrestrial and extra-terrestrial sources [40] (page 124)

Of particular importance to the instrument to be designed, noise power above around 30 MHz is dominated by galactic noise (curve B) with atmospheric noise (curve C) quickly fading to negligible. Careful consideration must be made to check whether this is indeed the case for the exact signal frequency which will be used before ignoring atmospheric noise sources.

Terrestrial Noise

Terrestrial noise is considerably challenging to accurately quantify or estimate. As heavily influenced by human activity, it greatly differs from location to location. In real missions, to accurately determine the link budget, it is common to directly measure the noise power at a range of frequencies at the relevant ground station. For the RABSII instrument, many ground stations will be used, relying on a number of non-commercial, amateur stations. This means that getting an exact figure for the noise power at ground is difficult. A better approach is to attempt to generate a realistic estimate for the noise temperature and add a significant link margin when closing the budget.

As can be seen in Figure 3.5, while man-made noise sources are by far dominant near cities and human activity, they are much lower in isolated plots of land. Depending on the physical location of the ground stations in the network, noise can be estimated based on recommendations and data from various international associations, such as the ITU. While this needs to be verified numerically, for now, it cannot be determined whether terrestrial noise will be greater than or smaller than extra-terrestrial noise. [40, 74]

Extra-Terrestrial Noise

Besides man-made noise, galactic noise is the next largest source of noise power in the operating frequency band of the instrument to be designed (28-50 MHz). While more predictable than man-made noise, a significant range of values is still expected depending on the exact configuration. The orientation of the receiving antenna for example plays a large role, depending on whether it is pointing towards the galactic plane or not, or depending on whether the sun is near the signal source in the sky.

To obtain values for the estimated galactic noise temperature, real temperature maps of the sky can be used. While these are specific to a certain measurement frequency, the results obtained can be scaled to the desired frequency with the equation below. [40]

$$T_G(f) = T_G(f_m) \times \left(\frac{f}{f_m}\right)^{-2.75} + 2.7 \tag{3.5}$$

Where T_G is the galactic noise temperature, $T_G(f_m)$ is the noise temperature at certain measurement frequency f_m, and f is the desired frequency. Note the small factor of 2.7 added to account for the contribution of the cosmic background radiation.

Regardless of exact value, galactic noise temperature can be expected to range roughly between $30\,000$ and $150\,000$ K. [29]

3.2. RA-2: Theory of Radio Antennas

Regarding the theoretical background of radio antennas, the following topics are presented in order. First, a brief introduction to impedance and admittance is provided in subsection 3.2.1. This is coupled with how ideal components in RLC circuits contribute to the impedance of a system. Next, the resonant and anti-resonant behaviour of antennas is discussed in subsection 3.2.2. subsection 3.2.3 presents the theoretical and practical definition of antenna quality factors and their relation to bandwidth. subsection 3.2.4 presents relevant information regarding antenna electrical length, the limitation of short antennas, and approaches to lengthened antennas electrically. Lastly, subsection 3.2.5 presents an overview to the skin effect, particularly relevant for antennas in the HF band.

3.2.1. Impedance and Admittance of Ideal Components

While resistance is generally sufficient to describe components in a DC circuit, things get more complex when looking at AC circuits. The relation between the time dependent currents and voltages, and components is described by their impedance. Impedance is a complex number measured in Ohms (Ω) which describes the properties of any component in an RLC circuit, being resistors, inductors, capacitors, or a combination of the three (such as in real components). Impedance is defined as follows:

$$Z = R + jX \tag{3.6}$$

Where Z is the impedance, R is resistance, X is the reactance (imaginary component of impedance), and j is the imaginary unit. Admittance instead is defined as the reciprocal of impedance.

$$Y = \frac{1}{Z} = G + jB \tag{3.7}$$

Where Y is the admittance measured in Siemens ($\mho$), G is the conductance, and B is the susceptance. In practice, impedances in RLC circuits are added together for components in series, and admittances are added together for components in parallel.

Besides the mathematical definitions, understanding impedance is relevant to working with real antenna systems. While resistance affects the relation between voltage and current in steady state conditions, reactance relates the phase between alternating voltages and currents. Depending on whether reactance is positive or negative, this phase difference will change. In the case the reactance is positive, the circuit will resist changes in current, hence voltage changes will lead current changes. The opposite is true, with negative reactance resisting changes in voltage, and hence current changes leading voltage changes.

This behaviour can be linked to real components. Ideal components are considered for now: ideal resistors, ideal capacitors, and ideal inductors. Ideal resistors have a purely real impedance, hence with some resistance and no reactance. As will later be discussed, this is what an ideal tuned antenna should look like. Ideal capacitors instead have no resistance and only a negative reactance, while ideal inductors have no resistance but a positive reactance. Depending on whether the reactance is positive or negative, it is referred to as inductive or capacitive reactance respectively.

$$X > 0 \rightarrow abs(X) = X_L \tag{3.8}$$

$$X < 0 \rightarrow abs(X) = X_C \tag{3.9}$$

The equations to go from capacitors and inductors properties to their reactance are as follows:

$$X_L = 2\pi f L \tag{3.10}$$

$$X_C = \frac{1}{2\pi f C} \tag{3.11}$$

Where f is the signal frequency, L is the inductance of an inductor, and C is the capacitance of a capacitor. Their admittance (in ideal conditions when $R = 0$) is computed by simply taking the reciprocal of reactance. It is important to note that reactance (and susceptance) is a frequency dependent property of a component. A capacitor, for example, will have a constant capacitance C measured in Farads F, but its capacitive reactance in Ohms Ω will change in response to the frequency of the signal it is exposed to. The same is true for inductors. This is relevant to antennas as when matching source to load impedance, efficient energy transfer can be achieved at the design frequency only. The way reactance of an untuned antenna changes will directly influence the achievable bandwidth. See subsection 3.3.1 for more details. [24]

3.2.2. Antenna Resonance and Anti-Resonance

Resonance in it of itself is not necessarily a required property for an antenna. The goal is not strictly to have a resonant antenna, but rather to have an efficient radiator with impedance as close as possible to that of the transmitter. With this in mind, resonance is still quite relevant when it comes to efficiently feeding an antenna.

As earlier discussed, antennas, just like other RLC circuits, have properties which are highly dependent on the frequency of the voltage (and current) which is applied. It is common practice to plot the impedance of an antenna against the signal frequency to see how the two are related. Figure 3.6 presents the real and imaginary components (resistance and reactance) of a sample antenna as a function of signal frequency. A half-wave dipole is used as an example.

With the resistance in blue and reactance in red, resonance is defined as the frequency at which the reactance is equal to zero. In this case, this occurs at roughly $27\,\text{MHz}$ where the impedance of the antenna is purely resistive. The frequency at which an antenna will be resonant depends on a few factors, but most relevant is its length. Radiation of RF waves in antennas occurs due to alternating electric and magnetic fields. These fields are generated by oscillating voltage and current within the antenna. To radiate most effectively, and to have no reactance, the antenna should have a length capable of maintaining a standing wave in its internal current distribution. This translates to resonant behaviour only at regular multiples of the signal's wavelength.

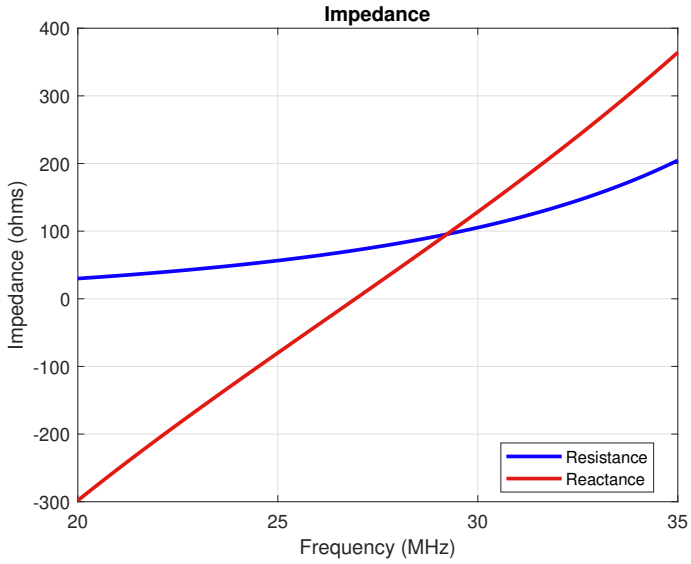

Figure 3.6: Impedance of a 5-meter-long dipole antenna centered around the first resonant mode

Returning to a simple dipole, its impedance can be again plotted for a wider frequency range, see Figure 3.7.

Marked in black are the frequencies at which the antenna's reactance becomes zero, hence the frequencies at which the antenna is called resonant. With the lowest resonant frequency still at $27\,\text{MHz}$, the antenna now clearly shows many other resonant points at regular intervals. These points are at the frequencies with wavelengths equal to higher octave standing waves within the same antenna length ($5\,\text{m}$ in this case). [26, 24]

Although all marked points have an equal reactance of zero, not all points have the same resistance. Half the points have a resistance roughly around $100\,\Omega$, while the other half have a resistance an order of magnitude higher, above $1\,\text{k}\Omega$. With a reasonable input signal voltage, a useful current can be achieved at points with lower resistance, while an almost negligible one can be achieved when the resistance is high. Points with zero reactance and high resistance are called anti-resonant. In practice, this translates to the antenna essentially operating as a filter at frequencies at which it is anti-resonant. Depending on the type of antenna and configuration, the anti-resonant peaks in resistance may be in the order of tens to hundreds of $k\Omega$. [54]

3.2.3. Antenna Quality factor and Bandwidth

As discussed in the previous section, when it comes to the reactance of an antenna, its behaviour as a function of frequency is also relevant. To quantify the behaviour and changes in reactance around the operating frequency of an antenna, a quality factor Q is defined. The mathematical definition of the quality factor for an antenna is as follows:

$$Q = \frac{f_0}{2R_0} \times \frac{\Delta X}{\Delta f} \tag{3.12}$$

Where f_0 is the relevant signal frequency, R_0 is the resistance of the circuit at frequency f_0, and $\Delta X/\Delta f$ is the change in reactance over the change in frequency. The last term is essentially the gradient of the reactance curve measured at the relevant frequency f_0. It must be noted that this definition is applicable to RLC circuits in general, and is not limited to antennas alone. In the case of antennas specifically, this quality factor is essentially an indication of the achievable bandwidth. A lower quality factor translates to a larger achievable bandwidth, and inversely a higher quality factor translates into a smaller achievable bandwidth.

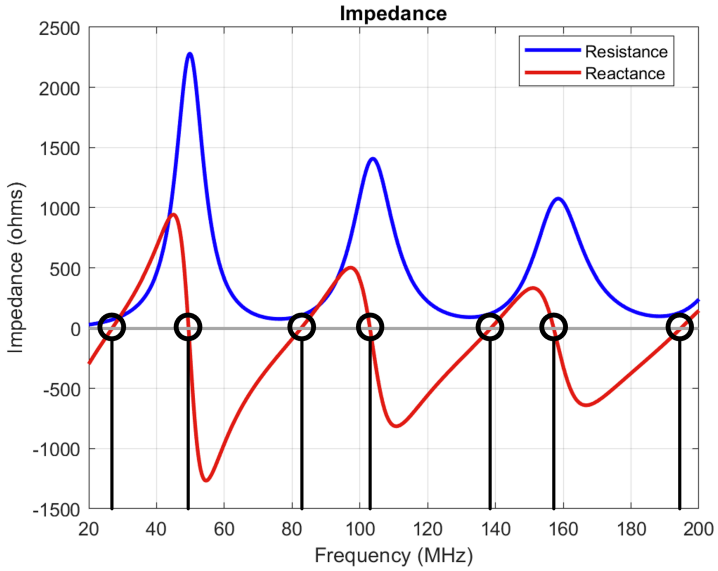

Figure 3.7: Impedance of a 5-meter-long dipole antenna between 20 and 200 MHz

The relation between quality factor and bandwidth can be explained by looking at the coupling efficiency between the source (transmitter) and the load (antenna). As earlier described, power is transferred from the source to the load most effectively when the impedance of the two is identical. Let's consider a perfectly resonant antenna with an impedance identical to that of the source at a specific transmitting frequency equal to the resonant frequency ($f = f_0$). As the transmitting frequency f either increases or decreases, the antenna's reactance will change by a factor $(\Delta X/\Delta f) \times (f - f_0)$. At some point, this reactance will make the antenna's impedance too high to receive power from the transmitter. For larger values of the gradient $\Delta X/\Delta f$ (and hence larger quality factor Q), this mismatch threshold between load and source impedance will be reached with smaller changes in transmitting frequency f. Hence, a smaller bandwidth for a larger value of Q.

In the case of antennas specifically, for simplicity, the quality factor is often defined in terms of the bandwidth directly as follows:

$$Q = \frac{f_0}{f_{max} - f_{min}} = \frac{f_0}{B} \tag{3.13}$$

Where f_0 is the centre frequency of the antenna's bandwidth, f_{max} and f_{min} are the highest and lowest frequencies the antenna can broadcast respectively, and B is the bandwidth. [26, 24]

3.2.4. Electrical Length

As earlier alluded to, the length of an antenna is the most important parameter when determining the frequency at which it resonates. Generally, the length relevant to resonance is the length of the conductor used to construct the antenna, regardless of the shape. Naturally, the shape of the conductor does affect the performance of the antenna in other ways, but its length is directly related to the resonant frequency of the final antenna. Mathematically, the electrical length G of an antenna is defined as the ratio of physical length L over signal wavelength λ.

$$G = \frac{L}{\lambda} \tag{3.14}$$

Antennas with an electrical length G of less than 0.1 are considered electrically short. Nonetheless, antennas much larger than 0.1, but still smaller than 0.5 behave similarly to antennas categorized as electrically short. Antennas operated as electrically large are often resonant antennas. They are characterized by high radiation efficiencies and large bandwidths.

When it comes to communication in the HF band though, practical considerations related to the required physical size of resonant antennas makes them often impractical. With varying degrees of lower efficiency, non-resonant electrically short antennas can be a viable option depending on the exact application. Within the context of this project, the two required broadcasting frequencies of 28 and 50 MHz translate to wavelengths of roughly 10 m and 6 m respectively. This poses significant challenges with respect to integration with a compact space-based platform. Electrically short antennas must hence be investigated to later assess their feasibility. [49, 46]

Electrically Short Antennas

While the threshold is generally placed at $G < 0.1$, there is no exact threshold for an antenna to be electrically short. Regardless of the exact size, an electrically short antenna does not behave like a resonant antenna and is generally characterized by a much lower efficiency. From a practical perspective, operating an antenna as electrically short just means operating at a frequency lower than the lowest resonant mode. Returning to the example dipole used to explain resonance, this means operating it at a frequency below 27 MHz, as can be seen in Figure 3.8.

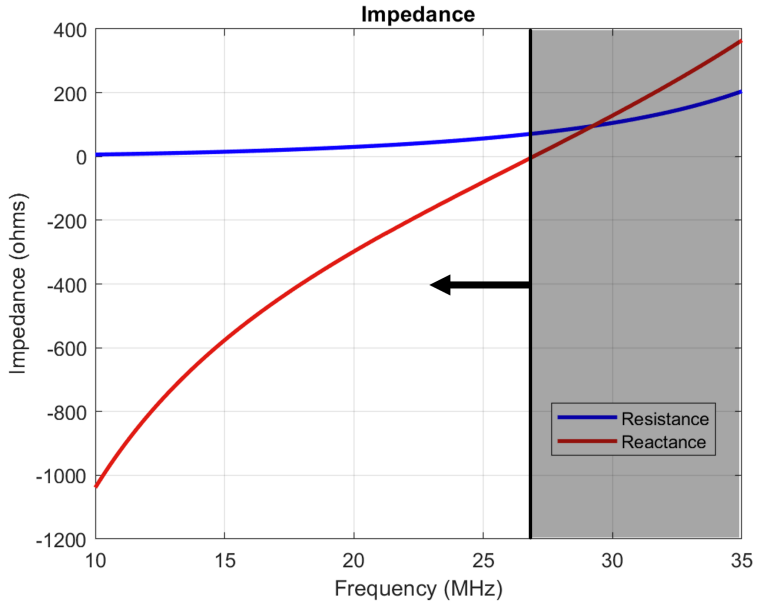

Figure 3.8: Impedance of a 5-meter-long dipole, left of the graph are frequencies at which the antenna operates as electrically short

Being non-resonant, the antenna will not have a reactance equal to zero by itself. It will require additional components (either a capacitor or an inductor) to cancel out the imaginary part of the impedance. While not a problem in it of itself, the additional components are a further source of loss in the system. Depending on the amount of reactance which must be cancelled out, and on whether it is inductive or capacitive, these losses can be significant. In real short antennas, resistive losses from matching components often exceed the radiation resistance of the antenna itself.

In addition to the undesirable large reactance, electrically short antennas have considerably small radiation resistance. Not only does this further reduce their efficiency, but it also adds further complications when it comes to impedance matching. An antenna with a low resistance, often below $1\,\Omega$, needs its impedance to be raised to $50\,\Omega$ (or whatever value the source impedance has). This is a further source of loss which must be accounted for when evaluating whether a short antenna may have sufficient performance for a specific mission. [46, 20, 11]

Electrical Lengthening of HF Antennas

While electrically short antennas may not have great overall performance, there are various ways they can be lengthened electrically while keeping their size physically the same. A combination of these techniques, together with clever antenna design, can allow for a significant reduction in footprint of a transmitting system while still transmitting at low frequencies relatively efficiently.

Just like any other RLC circuit, the resonant frequency of an antenna system is determined by many factors. Each of these factors can be modified to alter the frequency at which the system resonates. While the length of the conductor is of primary importance, other aspects contribute to determining where the circuit resonates. The following techniques from literature are approaches to keep the conductor length the same, while decreasing its resonant frequency. It must be noted that combinations of some, if not all, of the presented techniques are viable options for drastic shortening of a base antenna. The interactions between these various approaches must although be investigated practically. [49]

Reactive Elements

As resonance is defined as the frequency at which the reactance of an antenna is equal to zero, changing the reactance curve can alter the resonant frequency f_0. Adding capacitive or inductive elements to an antenna effectively shifts the reactance curve either up or down. The direction of the shift depends on the reactance of the component added: adding capacitive loading will shift the curve down, while adding inductive loading will shift it upwards. If done right, this effectively moves the point at which reactance is equal to zero. In practice, this results in the antenna-plus-load system having a different resonant frequency than the antenna alone. To lower the resonant frequency, the reactance added should have a positive value (inductive) if the gradient of the antenna's reactance is positive, and vice versa.

Besides the type of reactance loading to be added, there are various choices in terms of how this loading is applied to the antenna itself. The following options must be considered:

1. Base loading
2. Top loading
3. Distributed loading

Considering the first option, base loading means adding the reactive load to the base of the antenna. In contrast, top loading instead refers to the reactive load being added to the top of the antenna. These two types of loading are generally referred to as lumped loading, as the reactive component (be it a capacitor or inductor) is added at a single point along the antenna conductor. While base and top loading are viable options for a single ended antenna, double ended antennas, or antennas with a closed geometry such as loops, do not have a well-defined base or top. In such cases, the lumped reactive load can still be added along the length of the conductor. Generally, preserving symmetry is desired to avoid unpredictable radiation patterns.

While effective at reducing the resonant frequency of an antenna, lumped loads also have drawbacks when it comes to overall performance. Most notably, the addition of a lumped load increases the slope of the reactance curve. As discussed in subsection 3.2.3, this equates to an increase in the quality factor, and hence a reduction in the available bandwidth. Increases in the antenna's quality factor can be mitigated by shifting lumped loads to roughly the middle of the conductor, or alternatively, using a distributed reactive load. A distributed reactive load acts identically to a lumped one, but instead of being concentrated at one point, it is distributed across part, or the whole length, of the conductor. For example, a distributed inductive load can be achieved by coiling the main conductor onto itself with a coil diameter much smaller than its electrical length.

Lastly, in addition to increasing the antenna's quality factor, the addition of reactive loads also affects overall efficiency. As no added component can be ideal, there will be resistive losses for any element added onto the original bare antenna conductor. Depending on the configuration and size of the loads, these losses can range from negligible to significant. [49, 46, 65]

Top Hats or Radials

While geometrically different from lumped or distributed loads, top hats (sometimes referred to as capacitive hats) and radials are effectively also reactive loads. As such, they work on the same principle as lumped or distributed loads, shifting the antenna's original reactance curve and hence changing its resonant frequency.

Top hats effectively act as capacitive top loads. They can take many different shapes and sizes, but they all work on the same working principle. Thin conductive wires are connected stemming out from the top end of the antenna conductor. Their length, number, and distribution determines their effective capacitance, which will change the reactance curve of the overall antenna-plus-hat system. A basic example of a capacitive hat can be seen in Figure 3.9.

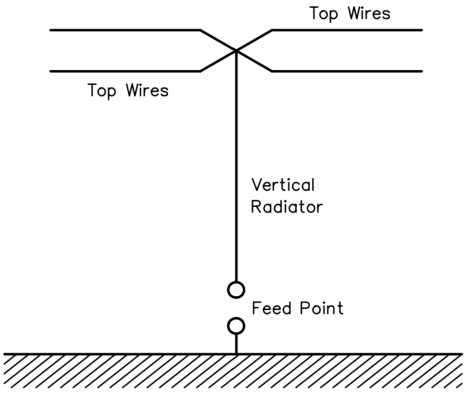

Figure 3.9: Capacitive hat added to a monopole antenna [49] (page 183)

A cross with all wires connected in the centre is the ideal shape for a top hat, but some trade-offs must be taken into account when deciding on the exact design.

Radials are in principle similar to top hats, with the key difference being that they are attached at the base of an antenna instead of on the top. They act as a reactive base load for the antenna they are installed on. For single ended antennas, base radials are often used as the conductive ground plane necessary to ground the antenna itself. [49, 46, 65]

Linear Loading

Differently from the previous option, linear loading is an approach which does not rely on the addition of RLC components to the bare antenna. Linear loading instead refers to changing the shape of the underlying conductor to alter the resonant frequency of the system. Put simply, linear loading on an antenna looks like the addition of switchbacks in the antenna conductor. A simple example of a linearly loaded loop antenna can be seen in Figure 3.10.

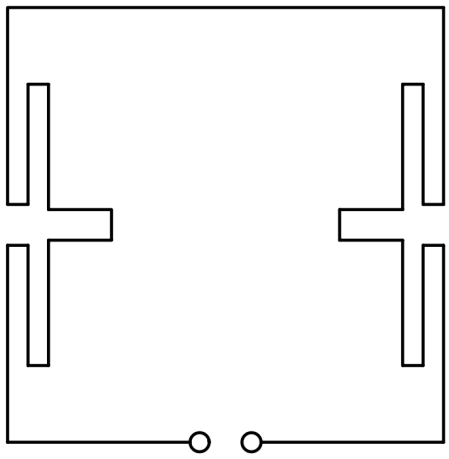

Figure 3.10: Linearly loaded loop antenna [49] (page 187)

Linear loading has a few advantages over reactive loading as it works on a different principle. The switchbacks in the antenna conductor lower the resonant frequency by means of self-resonance between different segments of the conductor. As such, it generally achieves little additional losses, does not alter or degrade the radiation pattern, and does not significantly affect the antenna's quality factor. The main drawback of linear loading is usually the decrease in radiation resistance for the overall loaded antenna system. An example of a linearly loaded dipole can be found in Figure 3.11.

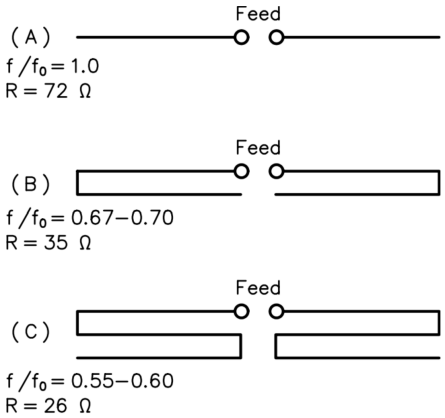

Figure 3.11: Increasingly loaded dipole, f/f_0 is the ratio of measured resonant frequency over resonant frequency of a standard dipole of same length, R is the radiation resistance [49] (page 187)

As can be seen, the resonant frequency in this specific case is lowered by almost 50% in case C at the expense of a reduced radiation resistance. Depending on the exact use case and scenario, this may be a desirable trade-off. [49, 46, 65]

3.2.5. Skin Effect

The skin effect affects all conductors carrying an alternating current (AC). It is defined as the tendency of AC currents to concentrate on the surface of a conductor. The primary factor influencing the current distribution is the frequency of the alternating current. The higher the frequency, the more the currents concentrate on the surface of the conductor. When considering radio antennas with signal frequencies in the million or billion of Hz, the vast majority of the currents are carried by the thin surface layer of the antenna conductor.

The current density J decreases exponentially across a conductor. Starting with a surface current density of J_S, the current density as a function of the depth d within the conductor can be defined as follows [44].

$$J(d) = J_S \cdot e^{-(1+j)d/\delta} \tag{3.15}$$

Where δ is defined as the skin depth: the depth at which the current is equal to $1/e$ of the current at the surface J_S. The imaginary component j defines the phase change of the current as depth within the conductor increases.

The skin depth δ is defined as a function of the conductor properties as well as the signal's frequency as follows [44].

$$\delta = \sqrt{\frac{2\rho}{\omega\mu}\left(\sqrt{1+(\rho\omega\varepsilon)^2}+\rho\omega\varepsilon\right)} \tag{3.16}$$

Where ρ is resistivity of the conductor, μ is its permeability, ε is its permittivity, and ω is the angular frequency of the alternating current, equal to $2\pi f$ for a frequency of f.

Relevant to the RABSII instrument, the skin depth for a good conductor (such as copper) is equal to 12.5 µm and 9.3 µm for 28 and 50 MHz respectively. For worse conductors, such as aluminium, this skin depth value is expected to increase. [44]

3.3. RA-3: Practical Considerations of Real Antenna Systems

This section presents information gathered regarding the practical aspects of real antenna systems. Impedance matching is first presented in subsection 3.3.1, followed by a comparison of ideal and real circuit components in subsection 3.3.2, and lastly, the distinction between balanced and unbalanced systems in subsection 3.3.3.

3.3.1. Impedance Matching

As described in subsection 3.2.1, impedance defines the time-dependent and time-independent relation between voltage and current of a electronics component. As a signal (an alternating wave of current and voltage) is passed from a transmitter (source) to an antenna (load), it is of paramount importance that the supplied energy is effectively transferred from one to the other. To ensure that is the case, the impedance of the source and the impedance of the load must be matched as closely as possible. This process of matching the load impedance to the fixed source impedance is called impedance matching. [69]

This section first presents the general approach to impedance matching in subsection 3.3.1, then followed by a practical simplified example to illustrate how this is done in practice in item 3.3.1. Lastly, a few parameters, namely the (voltage) Standing Wave Ratio and S-parameters, are introduced to measure the achieved efficiency of the matching in Figure 3.3.1.

Matching Approach

The first step for impedance matching is accurately determining the impedance of both the load and the source. Source impedance in standard radio frequency transmission is usually purely resistive and equal to $50\,\Omega$.

$$Z_{source} = 50 + 0j \tag{3.17}$$

The impedance of an antenna can instead be determined through either analysis and simulation, or through direct measurement. Simulation of antenna systems, especially for non-standard antennas, is challenging and often yields results with large uncertainties.

$$Z_{load} = R_{load} + X_{load}j \tag{3.18}$$

Depending on the type of antenna being constructed and the range of the measured impedance, a few options/steps for matching are required.

Firstly, depending on whether the antenna is resonant or not (see subsection 3.2.2) the remaining inductive or capacitive reactance must be cancelled out. This is because the source impedance is always purely resistive. This reactance is usually cancelled out by a single series capacitor or inductor, with reactance equal and opposite to that of the antenna.

Once the load has a purely real impedance, its resistance must be matched to that of the source. Depending on the difference between the two, two main options are available, both with advantages and disadvantages. These include:

1. Matching transformer
2. Matching network

Looking at option one, a matching transformer could be used to match the resistance. This would involve either a BALUN or UNUN transformer with some integer ratio of impedance between input and output. Matching transformers are simple transformers made of two internal inductive coils. The ratio between the loops in the coils on the input and output side translates to a ratio of resistance. Commercial options generally exist for transformers with simple ratios, such as 2:1, 3:1, 3:2, etc. Ratios up to around 5:1 do exist, but going any higher usually results in undesirable losses in the resistance conversion. Beyond ratios of roughly 5:1, or to have finer control over the matching process, matching networks are typically employed. As will later be discussed in subsection 3.3.3, a matching transformer's function is not limited to impedance matching, but actually extends to the conversion between balanced and unbalanced systems.

The second option for impedance matching is employing a custom matching network. This refers to a combination of capacitors and inductors placed in series and/or parallel (referred to as shunt) to match the load's resistive impedance to the source's. Matching networks can have different topologies, referring to the various arrangements possible for the individual electronic components. The simplest matching network is composed of a single capacitor and a single inductor, one in series, and one in shunt configuration. This simple matching network is called an L matching network. More complex topologies, such as the T and Pi topologies, give more control over the impedance profile over the bandwidth, but require more components (and hence more losses). [5, 46, 24]

A Matching Example

Now that the general approach towards matching the load to the source impedance has been discussed, a simple example is presented. This is to show how the theory is applied in practice.

As potentially relevant to the final design of the instrument, a quarter wavelength loop antenna is analysed. The antenna is a circular loop antenna with a conductor $\lambda/4$ in length. The target frequency is $28\,\text{MHz}$. The load impedance is simulated and presented in Figure 3.12.

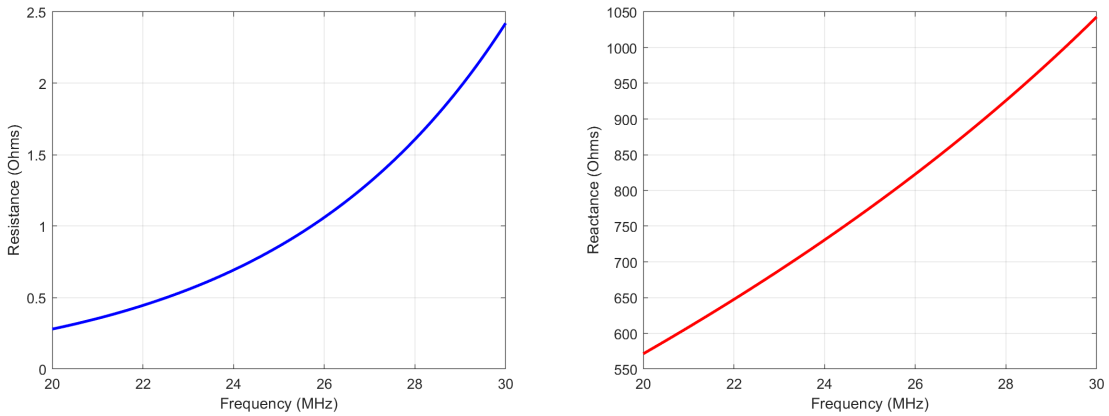

(a) Resistance **(b)** Reactance

Figure 3.12: Load impedance, $Z_{load} = 1.61 + 926j$ at $28\,\text{MHz}$

Being an electrically short antenna, the resistance is quite small, and the reactance is not equal to zero at the centre frequency (not resonant). As such, the first step is to make the load impedance fully resistive. The reactance is positive, hence inductive, so a capacitor in series provides the capacitive reactance required to cancel out the load reactance. At $28\,\text{MHz}$, the target centre frequency, the reactance is equal to $926\,\Omega$. Using the previous equations for capacitive reactance, a capacitor with a capacitance of $6.14\,\text{pF}$ is obtained to match the inductive reactance of the loop.

Regarding the matching network itself, an L-network is chosen. This includes an inductor in series, and a shunt capacitor together bringing the antenna resistance from around 1.6 to $50\,\Omega$ to match the source. This simple matching network can be seen in Figure 3.13.

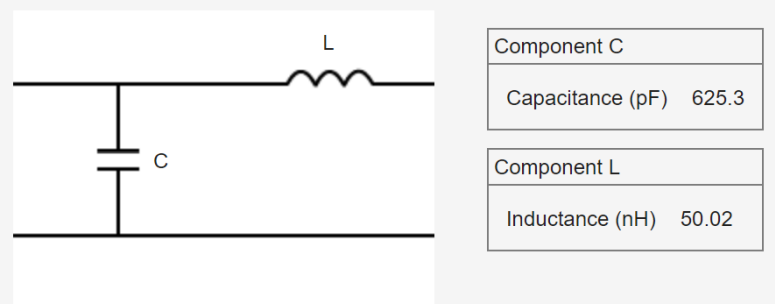

Figure 3.13: Matching network topology, source on the left, load on the right

Besides the exact values for the two components, it is relevant to understand that, even in an ideal case, two components with purely imaginary impedance can affect the load's real component of the impedance. The matching path of the impedance is visualised on a smith chart in Figure 3.14.

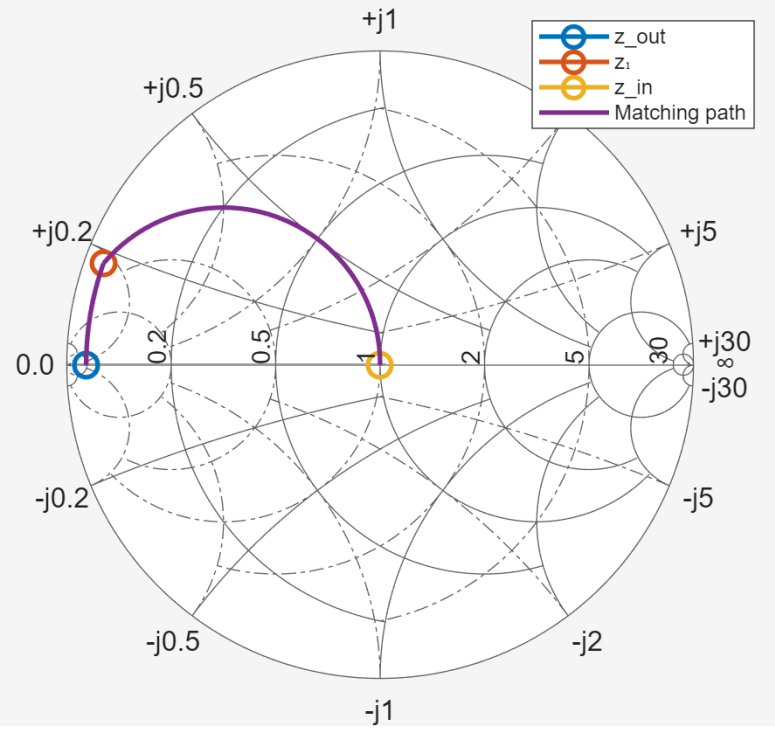

Figure 3.14: Example matching network matching path, load in blue, source in yellow normalised to 1 at the centre

It can be seen how the inductor adds a reactive component following the impedance lines on the chart from the blue point (load) to the red point. Next, the shunt capacitor eliminates the reactive component 'transforming' it into a resistive component following the admittance lines from the red point to the yellow point (the source).

Reflected Power: VSWR and S-Parameters

With the goal of a matching network being efficient coupling between source and load, it is important to quantify this efficiency. Two key parameters, essentially describing the same concept, are defined to understand how much of the source's power is transmitted onwards to the load, and how much is reflected. These two parameters are the S-parameter(s), and the (voltage) standing wave ratio (VSWR).

S-Parameters S-parameters define ratios between the power output and power input in a specific system. A system analysed can have any number of ports. These ports can be considered as points at which the power can enter and exit the system. A transmission line connecting a source to a load, such as for an antenna coupling system, is a two port system. One port is seen by the source, and one port is seen by the load. At each of these two ports energy can enter and exit. A generalised 2-port system is shown in Figure 3.15. Port 1 is connected to the source, port 2 to the load, and all possible energy flows are shown by the arrows. Green indicates the preferred path, from source to load, and red the undesired path, backwards from the load to the source.

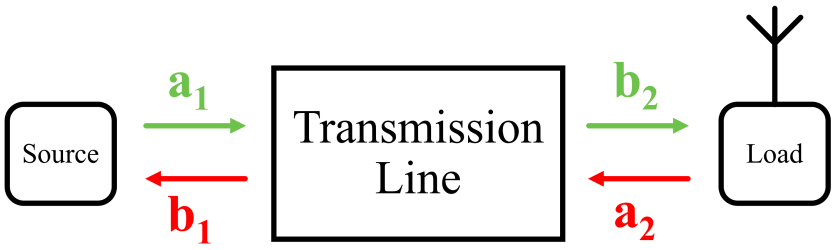

Figure 3.15: Generalised 2-port system connecting a source and a load, arrows are energy flows, a refers to inputs, b to output, subscript 1 to port 1, and subscript 2 to port 2

Based on this generalised 2-port definition, the vector equation relating inputs to outputs can be written as follows:

$$\vec{b} = \mathbf{S} \times \vec{a} \quad \Rightarrow \quad \begin{bmatrix} b_1 \\ b_2 \end{bmatrix} = \begin{bmatrix} S_{11} & S_{12} \\ S_{21} & S_{22} \end{bmatrix} \times \begin{bmatrix} a_1 \\ a_2 \end{bmatrix} \tag{3.19}$$

From a practical point of view, the parameters in the matrix **S** can be defined as ratios between the corresponding output and input powers.

$$S_{11} = \frac{b_1}{a_1} \quad (3.20) \qquad S_{21} = \frac{b_2}{a_1} \quad (3.21) \qquad S_{12} = \frac{b_1}{a_2} \quad (3.22) \qquad S_{22} = \frac{b_2}{a_2} \quad (3.23)$$

In a symmetric system, such as most antenna systems, the forward and backwards S-parameters are usually equal. This means that generally $S_{11} \approx S_{22}$ and $S_{21} \approx S_{12}$.

For a perfectly matched system, hence where the source and load impedances are equal ($Z_{load} = Z_{source}$), the forward transmission coefficient is equal to 1, and the reflection coefficient is equal to zero. This essentially means that all the power is transferred from the source to the load, and no power is reflected back to the source. Ideally:

$$S_{11,ideal} = 0 \quad \text{and} \quad S_{21,ideal} = 1 \tag{3.24}$$

Just like most other antenna parameters, these coefficients are not constant across the frequency domain. While a perfect matching network may ensure that the forward transmission coefficient is equal to 1, as the signal frequency either increases or decreases, it will inevitably decrease. The goal is to maintain the forward transmission efficiency sufficiently high across the entire bandwidth. Often measured in decibels (dB), a threshold is generally placed on the maximum value of the reflection coefficient (S_{11}) for acceptable coupling efficiency. This threshold to determine bandwidth is generally:

$$S_{11} \leq -10 \ \ dB \tag{3.25}$$

This translates to a reflection coefficient below 0.1, hence less than $10\,\%$ of the power reflected back to the source. Returning to the previously introduced example matching network (in item 3.3.1), a plot of the reflection and forward transmission coefficients (S_{11} and S_{21} respectively) can be seen in Figure 3.16. [46]

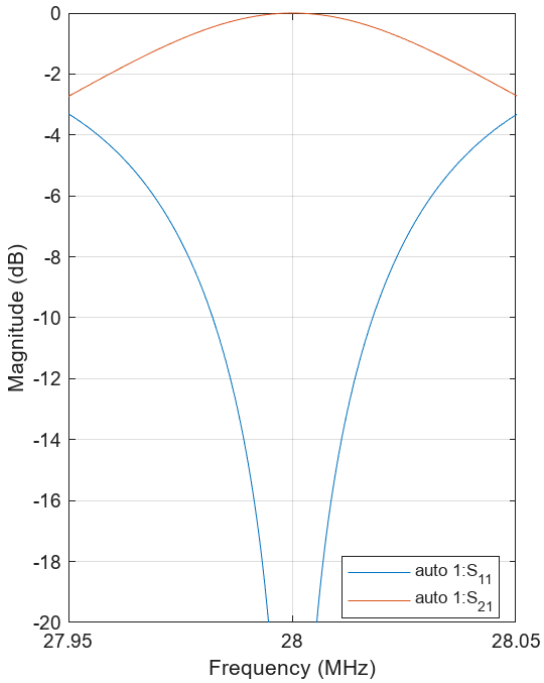

Figure 3.16: S_{11} and S_{21} for an example tuned matching network around a centre frequency of $f_c = 28\,$MHz

(Voltage) Standing Wave Ratio

Another parameter often used to describe how effectively a source is coupled to a load is the standing wave ratio (SWR), or voltage standing wave ratio (VSWR).

The standing wave ratio quantifies the magnitude of the standing wave created in the feed line connecting the source to the load due to power reflected at the interface between the two. In a real setup, as the impedance of the two cannot be exactly identical, some power leaving the source will be reflected from the interface with the load. This reflected power is identical to the transmitted signal, but smaller in magnitude (as hopefully most of the power is transferred forward to the load). The forward travelling signal, and backwards travelling reflected wave will interfere, creating a standing wave in the transmission line. Depending on the magnitude of the reflected power, this standing wave will be larger or smaller. The VSWR is the ratio of the highest voltage in this standing wave over the smallest voltage.

In the ideal case no power is reflected, no standing wave is created, and the VSWR will be equal to 1, its minimum possible value. As more and more power is reflected due to an impedance mismatch, the VSWR will increase, indicating a standing wave is now present in the transmission line. For example, a VSWR of 2:1 means that the ratio between magnitude of the peaks and troths of the standing wave is equal to 2. Practically, this means that the voltage in the transmission line oscillates between a maximum of $133\,\%$ and $66\,\%$ of the original signal voltage.

The VSWR and reflected power in percentage can be related directly by the following equation:

$$P_{\%,\,reflected} = 100 \cdot S_{11} = 100 \cdot \left(\frac{VSWR - 1}{VSWR + 1} \right)^2 \tag{3.26}$$

Besides transmission losses, minimising the reflected power is a matter of preserving the transmitter electronics. Typical values of VSWR for good coupling can be expected to be below 1.5 (less than 10 % reflected power). Starting from a value of VSWR of 2.5, damage to the transmission equipment may occur, and must hence be avoided at all cost. [55]

3.3.2. Ideal versus Real Components

Most of the theory presented up until now has been limited to ideal RLC components. This refers to components with impedance that is purely resistive or purely reactive. The impedance of an ideal resistor, ideal inductor, and ideal capacitor can be found in Table 3.1.

Table 3.1: Ideal impedance of RLC components

Component	Ideal Impedance
Resistor	$Z_R = R + 0j$
Inductor	$Z_L = 0 + X_L j$
Capacitor	$Z_C = 0 - X_C j$

While the resistance R is an intrinsic constant component property, inductive and capacitive reactance X_L and X_C are not, and depend on the signal's frequency. They are defined as follows:

$$X_L = 2\pi f \times L \tag{3.27}$$

$$X_C = \frac{1}{2\pi f \times C} \tag{3.28}$$

Where f is the signal's frequency, and L and C are the inductor's and capacitor's inductance and capacitance respectively (measured in Henrys and Farads).

Real components do not behave as ideal ones. Real resistors inevitably have some small reactive component, while real inductors and capacitors have some small parasitic resistive component. The magnitude of these unwanted reactive and resistive components to impedance depend on the physical construction of the various components, and are highly dependent on the signal frequency. As resistors are not directly used in matching networks, particular focus is placed on inductors and capacitors alone. Their real impedance is presented in Table 3.2.

Table 3.2: Real impedance of RLC components

Component	Real Impedance
Resistor	$Z_R = R + Xj$
Inductor	$Z_L = R_L + X_L j$
Capacitor	$Z_C = R_C - X_C j$

When considering inductors and capacitors in matching networks, their parasitic resistances (R_L and R_C) will contribute to losses in the system by dissipating part of the source's power as heat. This will decrease the efficiency of the antenna system. The magnitude of the parasitic resistance is generally correlated to the magnitude of the component's impedance. This means that an inductor or capacitor with larger reactance will dissipate (and hence waste) more power.

This behaviour is relevant when considering both matching networks losses, but also some of the techniques for increasing an antenna's electrical length. Reactive load will not only change the antenna's behaviour, but contribute to further reductions in radiation efficiency by introducing resistive loads. When considering electrically short antennas instead, if a large reactive component is present, its elimination might lead to a parasitic load significantly larger than the radiation resistance of the antenna itself.

Quality Factors

The parasitic resistance in an LC component and its reactance is related by a factor called a quality factor. The higher the quality factor, the more the component behaves like its ideal counterpart, hence with smaller resistance. Following are the mathematical definitions for the quality factors for an inductor and a capacitor respectively.

$$Q_L = \frac{X_L}{R_L} = \frac{2\pi f L}{R_L} \tag{3.29}$$

$$Q_C = \frac{X_C}{R_C} = \frac{1/(2\pi f C)}{R_C} \tag{3.30}$$

The exact values for these quality factors depend on many things, such as construction and operating frequency. For the relevant frequency range of 28 to 50 MHz (see Table 4.6), typical values can be obtained from literature to have an indication of the expected parasitic losses.

For real inductors, values of Q_L in the range of around 100 can be expected. This means that an inductor with reactance of $100\,\Omega$ will have a resistance of around $1\,\Omega$. For real capacitors instead, values of Q_C are about an order of magnitude higher, ranging around 1000. [81, 62]

This means that regardless of the matching network topology and antenna design, matching losses are usually dominated by inductors alone. For example, an electrically short antenna that has a large capacitive reactance will intrinsically have much higher matching losses than one with large inductive reactance. Hence, careful consideration must be placed on reducing as much as possible the number and reactance of inductors used in the system.

3.3.3. Balanced versus Unbalanced Systems

The last practical element discussed in this chapter is perhaps less intuitive, but nonetheless critical to efficient antenna performance. Depending on the configuration of the transmitter, transmission line, and antenna, a distinction can be made between balanced and unbalanced system.

Whether a system is balanced or unbalanced boils down to whether its connection to ground in the forward signal path, and the return path is equal. In practice, this refers to whether the impedance to ground of the system seen from the perspective of the load is equal in the forward and backwards path. Depending on the type of antenna used, this distinction may or may not be relevant in the first place. Whether it is or not, is related to what type of antenna is used.

An antenna can be either single ended or double ended. Examples of a single ended antenna is a monopole, while good examples of a double ended one is a dipole, or a loop. Current in a single ended antenna flows from a single feed point, through the conductor, and eventually to ground from the end of the antenna. Nearby structures, or a conductive ground plane, may be used to ground the antenna through a dielectric medium. A double ended antenna instead has two connection feed points, and current effectively flows from one feed point to the other. The signal at the two feed points in a double ended antenna is equal and opposite in magnitude. This is important to maintain an appropriate current distribution within the conductor, which is what allows the antenna to radiate in the first place.

As single ended antennas only have one feed point, it does not matter whether the line feeding it is balanced or not. The same is not true for double ended antennas. To maintain an equal and opposite signal on both feed lines, the impedance to ground on both must be the same. In summary, this means that a single ended antenna does not necessitate a balanced feed line, while a double ended antenna does for proper functioning.

The concept of balanced versus unbalanced systems is not limited to feed lines but extend to matching networks. If working with a double ended antenna, to keep the impedance to ground balanced, it is important to preserve symmetry in the matching network. [49, 46]

BALUN and UNUN Transformers

The signal output from a transmitter is almost always delivered through a coaxial cable. Being asymmetrical, coaxial cables are not balanced. As said, this means that they do not have identical impedance between the core conductor (carrying the signal), and the outer shield (carrying the return signal).

When feeding a double ended antenna, such as a dipole or a loop, this unbalanced feed line must be converted into a balanced input before feeding the antenna itself. This is usually done through the use of a Balanced-Unbalanced transformer, or BALUN. A BALUN internal configuration may vary, but in its most basic form, it only serves as a way to convert an unbalanced input into a balanced output. Often relying on transformers made up of inductors, the ratio of loops on the balanced and unbalanced side can be used to also transform the impedance of the load to match the source. Commercial BALUNs are generally available only with limited integer ratios of output to input impedance, so are not always a solution to perfectly match an antenna.

UNUNs, or Unbalanced-to-Unbalanced transformers, do not affect whether the system is balanced, but only serve as a way to match a moderate miss match between source and load impedance. They can be considered as less customizable alternatives to matching networks, and are hence often only used in amateur radio setups.

3.4. RA-4: Deployment Mechanisms and Technologies

This chapter presents a concise overview of technologies that could be relevant to the deployment of the instrument's antenna. The following are investigated:

- Shape Memory Alloys (SMAs)
- Inflatables
- Strain-based system: tape springs and STEMs
- Motors
- Magnetic actuators
- Burn wires

Given a previous personal background in mechanical design and mechanisms, this section of the report is kept short. Only the general characteristics of each technology are presented, enough to give a rough idea of the strengths and weaknesses to be further investigated later on, depending on the exact design direction chosen. The majority of the research work has been done on antennas and related fields, as much more unfamiliar when compared to deployment mechanisms. [10, 2]

3.4.1. Shape Memory Alloys (SMAs)

Shape memory alloys, or SMAs, are alloys generally based on Nickel. The key properties of shape memory alloys is their ability to 'memorize' a certain shape and return to it after plastic deformation once heat is applied. This process is based on the two-state crystalline structure of SMAs. In practice, depending on the temperature, shape memory alloys can be in either the cold martensite state, or in the hot austenite state. While in the cold martensite structure, they can be plastically deformed as any other malleable metal. As heat is applied and the temperature of the alloy surpasses a certain critical temperature, it returns to the predefined shape it 'memorised' during manufacturing. This behaviour is called one-way shape memory effect. Depending on the exact composition, this critical temperature can be altered to match the specific use case.

Under certain conditions, shape memory alloys can also be manufactured to memorise an additional shape in their cold state [34]. This translates to an alloy capable of switching between two different configurations depending on whether it is in its hot austenite state, or in the cold martensite state. [28, 19]

In space, shape memory alloys have often found application within hold down and release mechanisms, or HDRMs. Here they are used to hold down a preloaded element, usually under tension, until they are heated [60]. The change in shape is used to release the tensioned element and hence actuate the HDRM. In the field of mechanisms, they are increasingly interesting when integrated to provide actuation forces in complex systems. Either in conjunction with traditional or compliant mechanisms, they do not have any moving parts and can be scaled down considerably more than other actuation methods. [42]

3.4.2. Inflatables

Inflatable mechanisms, as the name suggests, revolve around using positive internal pressure to inflate, and hence enlarge, a bladder. This type of mechanism has often been used to deploy large structures requiring efficient packing form factors. They have been used to deploy airbags on NASA's Opportunity and Spirit rovers' Mars landings [57], but also antenna structures of various sizes [4, 13, 33], showcasing the versatility of the technology . There are numerous approaches to providing inflation gasses for actuation. For larger structures, pyrotechnics or chemical decomposition are sometimes employed to generate the inflation gasses. Compressed inert gasses are also viable options.

Differently from inflating structures on earth, the negligible pressure in the vacuum of space means that relatively low internal pressures are required to inflate space structures. These structures generally fall under two categories: boom deployed and integral structures. Boom deployed structures are composed of some (or many) connected booms, while integral structures are simply composed of a large bladder in the shape of the desired structure. [52]

Key considerations when it comes to inflatable mechanisms are the bladder composition and thickness, inflation pressure, inflating gas, and operating temperature/environment. Even with low inflation pressures, inflatables are generally not reliable when it comes to holding shape for extended periods of time. As such, they are often combined with other technologies to 'fix' the deployed configuration for the rest of the mission duration. Often, rigidisable resins are employed. These could be cured either using UV or heat. In a nutshell, they take over the load bearing role once the inflatable elements provide the required actuation force to bring the structure into its deployed configuration. [70, 51, 14]

3.4.3. Strain-Based Systems: Tape Springs and STEMs

Strain-based systems rely on internal elastic deformation to achieve actuation. Various approaches exist to constraining deployment motion, but most commonly, tape springs are employed. Given their simplicity and effectiveness, tape springs have become increasingly popular across small commercial CubeSats. From the name, tape springs behave almost identically to coiled measuring tapes. They are coiled for storage and release at deployment. Tape spring can have one, two, or multiple stable position (up to infinite for a continuously stable tape spring) based on their exact configuration, material, and geometry. These stable configurations are dictated by points of local minima in the internal energy of the system. In between these stable points (be it one, two, or more), are higher energy configurations. Often, additional mechanisms are employed to either restrain, or actuate the tape springs through those points of higher strain energy. Managing the release of internal strain is also crucial to avoid damage to the deployed tape spring. [71, 7]

STEM stands for Storable Tubular Extendible Member, and is a type of deployable boom based around tape springs. Coiled either along their short or long side, the tape springs coil onto themself forming a boom as they unfurl. [7]

3.4.4. Electric Motors

Electric motors are used extensively and generally well understood. They are a way to convert electric currents into highly constrained mechanical motion. They are not particularly relevant for the scope of this project, and as such, they are only briefly mentioned here for completeness sake.

Three main types of electric motors exist: brushed motors, brushless motors, and stepper motors. Brushed motors do not need an electronic speed controller and rely on contact brushes to generate the alternating electric fields necessary to drive them. They are often prone to failure due to the physical contact of the brushes. Brushless motors instead rely on external electronics to provide the alternating current necessary to drive them. They do not have moving or contacting parts. They are well-fitted for high RPM applications. Lastly, due to their internal configuration, stepper motors are made for high angular precision. They can reliably move by fractions of a degree with high repeatability and accuracy. While not suited for high speed applications, they possess high precision and moderate torque. [31, 35]

3.4.5. Magnetic Actuators

Magnetic actuators are most commonly employed in the domain of attitude control for LEO and MEO satellites. These actuators are known as magnetorquers. Magnetorquers interact with the Earth's magnetic field to impart torque onto the spacecraft for attitude control. More relevant to this project, are mechanism related magnetic actuators. Due to their generally heavy construction, magnetic actuators do not find great applicability aboard spacecrafts. They are generally restricted to applications requiring large forces to be applied over small distances, such as in the design of certain HDRMs. [32]

3.4.6. Burn Wires

Last in the list of relevant technologies are burn wires. Burn wires have significant flight heritage when it comes to space missions and space hardware due to their simplicity and versatility. Burn wire mechanisms are a type of single use mechanisms where a thin wire is destroyed via the application of an electric current. The action of destroying this wire, usually made of nickel-chromium (Nichrome), can be used in different ways to control the actuation of a mechanism. Namely, there are two ways in which this is usually done.

The first commonly employed method is by having the wire being responsible for holding down some sort of preloaded structure or appendage. The destruction of the wire then triggers the release of the tensioned element initiating the actuation. This sort of deployment actuation approach is generally reliable and has seen wide application.

The second common method to employ a burn wire is through the use of a so-called thermal knife. In this configuration, it is not the wire itself that breaks, but it is instead used as a heating element. Some sort of cord is used to restrain a loaded deployment, the burn wire is then wrapped around this restraining cord. When current is applied to the burn wire, it heats up melting through the cord and severing it. Cutting the cord releases what ever it was holding down. [77, 30]

4

Requirements Definition

To start tackling the research questions laid out in section 2.3, the requirements which will drive the system design are defined. This chapter provides an overview of the driving aspects that constrain the system in section 4.1, as well as a preliminary link budget analysis presented in section 4.2. The latter is the primary tool used to translate general mission specifications into measurable system requirements which can be used to actually guide the design process. The outcomes from both of these elements are used to define a non-comprehensive list of key system requirements, presented in section 4.3.

4.1. Mission Constraints

For the scope of this work, two main constraints are considered: the science case itself (described in section 2.1), and the satellite platform (described in section 2.2). While other factors also play a role in the development of the system, these two aspects were deemed driving with respect to the feasibility of the overall system. Given the early development stage of the RABSII instrument, aspects such as final cost and transport requirements are left as additional considerations once the project reaches a more mature stage.

4.1.1. Science Case

Starting from the science case, this section aims to translate the desired scientific output of the instrument into actionable requirements. In simple terms, the RABSII instrument is just a radio transmitter. All it needs to be able to do is repeatedly transmit a specific modulated beacon signal in all directions with sufficient strength for ground detection. In no particular order, the following aspects further characterise 'how' this must be achieved from a science-case point of view.

Operating Frequency

The operating frequency is perhaps the easiest aspect to define as explicitly dictated by the science case. The instrument must be able to transmit at a frequency of 28 and 50 MHz. In order to transmit on both frequencies at the same time, this function is to be achieved by two distinct transmitting antennas.

Signal Directionality

The emission radiation pattern of the transmitter should aim at being as omnidirectional as possible. While impossible to match a perfect isentropic emitter, directional antennas should be avoided as this would make transmitting to multiple ground stations at once impractical.

The key figure used to quantify whether the transmitter is sufficiently omnidirectional is the difference between the highest and the lowest power gain in the antenna's radiation pattern.

Signal Polarisation

Polarisation is an intrinsic property of electro-magnetic (EM) waves. For the RABSII instrument, signal polarisation is not relevant to the measurement of the sporadic E phenomena. As such, there are no requirements imposed on the emitted signal polarisation.

Transmitter Bandwidth

The required transmitter bandwidth is a potentially constraining requirement, especially when it comes to electrically short antennas. It is generally dictated by the chosen signal modulation scheme. For RABSII, beacon signals will be transmitted using the digital FT4 mode, and the analog CW mode. CW requires virtually no bandwidth as it simply comprises of on/off keying of the carrier signal, in practice, around 100 Hz of bandwidth is used for transmission. FT4 instead encodes data across four distinct tones within a 2500 Hz bandwidth. [80]

Considering that both modulation schemes will be used by both beacons (on 50 and 28 MHz respectively), a total bandwidth of 2500 Hz is required for the transmitter.

Signal-to-Noise Ratio

While not a signal property per se, the signal-to-noise ratio (SNR) of the signal at ground is relevant to determine whether the link is feasible. Based on the modulation techniques employed (FT4 and CW), a minimum SNR of -17.5 dB is required at reception on ground for data to be correctly decoded. In addition, the gain of the receiving antenna must also be considered. Inverted-V antennas or shortened dipoles are commonly used in the amateur radio network to receive in the HF band [48]. Data from chapter 6 in ARRL Antenna book [49], as well as chapter 9 and 10 from Rothammel's Antenna book [46] is used to estimate the expected ground station gain. Based on these sources, as well as discussions with experts on the topic from the RABSII team, a value of -2.5 dBi is chosen for the receiver's antenna gain.

Combining the two figures, the required SNR measured at ground needs to be equal to or greater than -15 dB. As this is not a requirement of the transmitter directly, it will be used as an input in the link budget analysis in section 4.2.

4.1.2. Satellite Platform

Similarly to the science case, the payload's host satellite platform also imposes constraints on the design of the RABSII instrument itself. It must be noted that both RABSII and Delfi Twin are ongoing projects still under heavy development. The estimates provided in this section must be considered as preliminary, as systems could, and will, be subject to change. Numbers presented in this section have been obtained through numerous discussions with the thesis supervisor, the team working on RABSII, and the team working on Delfi Twin.

In no particular order, the following are the system constraints originating from the design of the Delfi Twin satellite platform.

Available Power

Power available aboard Delfi Twin is rather limited. While the instrument will likely not operate continuously, a rough estimate of the power that can be allocated for RABSII has been made to be used as a starting point for the design. The satellite bus will be able to provide around 1 W of power, while the available RF power for the transmitter is estimated to be no greater than 500 mW. This is due to the inefficiencies of the DC to RF power conversion performed by the payload's modulator. The figures here presented are based on the hardware specifications currently used by the RABSII team. For the link budget performed in section 4.2, this input power of 500 mW is used.

Available Volume

Delfi Twin is small, which severely constrains the physical space that can be allocated to the RABSII payload. Based on the most up to date designs of the satellite, the total available volume for the instrument is 80x40x4 mm^3. While some of the power conversion and modulation electronics will fit inside the satellite bus, the entirety of the antenna storage and deployment system needs to fit within this bounding box.

Available Mass

While mass is generally a driving factor when it comes to space hardware, the tight volume constraints make it a secondary issue for the RABSII instrument. The available mass for the full beacon antenna and deployer system is 40 g. For reference, were the entire available volume to be filled with a solid block of aluminium (with a typical density of 2.7 g cm^{-3}), it would have a mass of just 34.5 g [56].

4.2. Link Budget Analysis

In order to translate the overarching constraints into system requirements, a link budget analysis is performed. This section documents the assumptions and estimates made, as well as the outcomes which are to be used to begin the design of the RABSII instrument.

Conventionally, a link budget analysis follows the propagation path: starting from the transmitter, then the signal propagation and potential attenuation, ending with the receiver. The outcome of such analysis is a link margin: a value, usually in dB, measuring how far above the noise floor the signal is at the end of the transmission chain. This sort of approach is used to assess the quality of the radio link once its characteristics are known. As the goal here is reversed, the approach towards the link budget will be opposite of the conventional approach.

The inputs for the analysis are to be the desired link margin, as well as the characteristics of the ground stations and satellite platform. The link is analysed going backwards along the transmission path, starting from the ground segment and ending in the transmitter, the beacon itself. This yields the gain and emitted power required from the RABSII transmitter for the ground link to be feasible.

According to the steps taken in the analysis, in order, this section covers the assumptions made (subsection 4.2.1), the noise power estimates (subsection 4.2.2), the expected polarisation mismatch losses (in subsection 4.2.3), and lastly the outcomes (subsection 4.2.4).

4.2.1. Assumptions

Given the early development stage of both RABSII and Delfi Twin, there is a lot about the system which is yet to be defined. To begin tackling these unknowns, some assumption have to be made regarding the system as a whole. Within the scope of the link budget analysis, the following assumptions are made.

Link Budget Analysis Assumptions

AS-LINK-1: Ground stations within the used network are not located in densely populated city areas

AS-LINK-2: Attenuation sources other than free-space loss are negligible

AS-LINK-3: A minimum elevation angle of 10° above the horizon is required to close the link

AS-LINK-4: Total losses before the transmitter antenna are equal to 3 dB

AS-LINK-5: A link margin of 6 dB is used as a starting point for the analysis

AS-LINK-1 is made based on information from the RABSII team regarding the type of ground station that will be used. While not all stations in the amateur network are in residential/rural areas, many are. Sizing the whole system to have sufficient power at ground for the signal to be decoded over the high power man-made noise expected in dense cities is unrealistic.

AS-LINK-2 is based on the literature presented in subsection 3.1.2. At the frequencies considered, 28 and 50 MHz, direct signal attenuation not due to free-space loss is negligible, hence not considered for this analysis.

Regarding **AS-LINK-3**, 5-10° is a common lower bound used to define link elevation above the horizon. This value is also used as starting point for the link budget of Delfi Twin itself, so it is deemed reasonable.

AS-LINK-4 describes the assumed losses between the modulator RF output and the antenna itself. This could be due to resistance of connectors/cables, or the matching network for the antenna itself. 3 dB is a value commonly used for preliminary link budgets.

Lastly, looking at **AS-LINK-5**, the desired link margin is a direct reflection of the maturity and confidence in the system. The novelty and experimental nature of the RABSII instrument carries more technical risk than a flight proven conventional radio transmitter. As such, While a value of 3 dB is generally used, a value of 6 dB, hence double, is chosen. This number was obtained after discussion with the RABSII team and thesis supervisor.

4.2.2. Noise Power

Meaningfully estimating the noise power at the receiver can be difficult, especially given the lack of specifics and the variety of locations of the ground stations. Regardless, the method used here is expected to provide reasonable first order estimates useful to begin design of the instrument.

Two main sources of noise have been identified in subsection 3.1.3: terrestrial and extra-terrestrial noise. Neither contribution was deemed negligible at the frequencies considered, hence both must be estimated individually and combined.

Terrestrial Noise

Terrestrial noise in the frequencies considered is primarily man-made. The power of this man-made terrestrial noise can vary significantly depending on the time of day and physical location. Given this variability, a statistical approach is the only viable option for estimating terrestrial noise power.

The method used to obtain realistic figures on expected noise power is based on the International Telecommunication Union (ITU) published recommendations. More specifically, recommendation ITU-R P.372-15 on '*Radio Noise*' [66]. Part six of the document presents median figures as well as expected variations for man-made noise in various locations: cities, cities' residential neighbourhoods, rural areas, and quiet (in radio) rural areas.

An additive Gaussian noise model is defined in the following form.

$$F_{am} = c - d \cdot log(f) \tag{4.1}$$

Where F_{am} is the man-made additive noise factor in dB, f is the frequency in MHz, and c and d are constants. Following **AS-LINK-1**, values for median man-made noise in rural areas are considered, which translates to $c = 67.2$ and $d = 27.7$. Using a reference temperature T_0 of 290 K, noise factors can be converted to an effective man-made noise temperature with the following relation.

$$T_m = T_0 + 10^{F_{am}/10} \tag{4.2}$$

At 28 and 50 MHz this translates into the median noise temperatures presented in Table 4.1. While variations are expected, this the maximum variability of these figures is computed to be within 2-5 dB W of noise power when considering the instrument's bandwidth. This is well within the system's link margin.

Table 4.1: Median man-made noise temperature at the RABSII instrument transmitter frequencies

Frequency (MHz)	**Median Man-Made Noise** (K)
28	150000
50	30000

Extra-Terrestrial Noise

Extra-terrestrial noise is noise which originates from in-space sources. At the relevant frequencies, this noise component is dominated by galactic noise (as presented in subsection 3.1.3). This is relatively easy to estimate. The model provided by Ippolito [40] is used. Galactic temperature maps, such as the one in Figure 4.1, are used to determine the variation in noise temperature at a certain reference frequency. These values for noise temperature are then scaled to the frequency of interest using the following equation.

$$T_G(f) = T_G(f_m) \times \left(\frac{f}{f_m}\right)^{-2.75} + 2.7 \tag{4.3}$$

Where T_G is the galactic noise temperature in kelvin, f_m is the measurement's frequency, and f is the frequency of interest. The constant 2.7 K added represents the cosmic background noise.

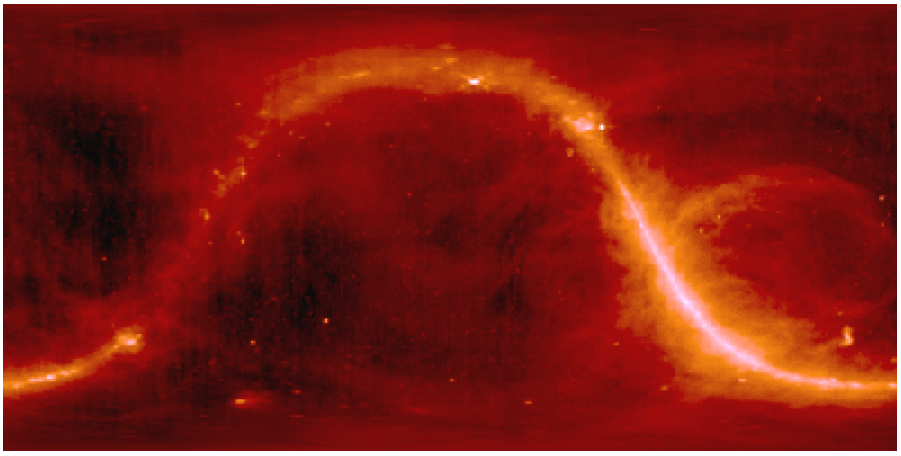

Figure 4.1: Galactic temperature map measured at $f_m = 408\,\text{MHz}$ [64]

Using the data presented by Ippolito [40], as well as reference data from NASA [58] and Oxford [59], a minimum and maximum value for galactic noise temperature is obtained in Table 4.2.

Table 4.2: Galactic noise temperature range at the RABSII instrument transmitter frequencies

Frequency (MHz)	**Galactic Noise Temperature**	
	Minimum (K)	***Maximum*** (K)
28	33000	156000
50	6700	32000

For man-made noise, a median approach was sensible as the variability is too uncertain to be meaningfully characterised. When looking at galactic noise instead, the maximum values will be used in the link budget, as they are only dependent on the position of the beacon with respect to the sky in the background.

4.2.3. Polarisation Mismatch Loss

The last aspect to be discussed before presenting the outcomes of the analysis, is the characterisation of polarisation mismatch losses. As introduced in Figure 3.1.2, the polarisation of the incoming signal and the receiving antenna must match for the two to be efficiently coupled. While this is always true regardless of the frequency, the behaviour with respect to polarisation of signals in the HF/low-VHF band is somewhat atypical.

The high charged ions concentration in the ionosphere has a significant effect on the signal properties. In addition to signal attenuation, discussed in Figure 3.1.2, the ionosphere distorts the signal itself. Namely, the charged particles cause *"rotation of the wave polarisation (Faraday rotation), time delay of the signal, and a change in the apparent direction of arrival due to refraction"* (from page 2 of ITU Recommendation ITU-R P.531-16 [67]). The highly variable composition of the ionosphere means that these effects can only be described with a stochastic approach.

Two approaches are presented to estimate the expected losses in the RABSII system. Firstly a general stochastic model based on the Faraday rotation phenomena is presented, followed by a more general literature-based approach.

Stochastic Faraday Rotation Model Estimates

The approach presented in Recommendation ITU-R P.531-16 [67] is followed and here presented. The magnitude of the faraday rotation of a signal's polarisation can be quantified with the following equation.

$$\theta = 2.36 \times 10^{-14} \cdot \frac{B_{av} N_T}{f^2} \tag{4.4}$$

Where B_{av} is the average Earth's magnetic field in T, N_T is the total electron content (or TEC) along the signal's path measured in el m^{-2}, and f is the signal's frequency in GHz. The Earth's magnetic field strength averages around $50\,\mu$T, while the TEC is a bit harder to estimate. TEC (N_T) is described by the following equation.

$$N_T = \int_S n_e(s)ds \tag{4.5}$$

Where S is the propagation path in m and $n_e(s)$ is the local electron concentration in el m^{-3}. As can be seen, the value for the TEC is the result of integrating the electron density over the propagation path of the signal. This means it is highly dependent on both the path geometry (and length), as well as the local charged particles concentrations. Without going into more complex atmospheric modelling, low, medium, and high values for the TEC can be defined: $N_{T,\,low} = 10^{16}$, $N_{T,\,med} = 10^{17}$, and $N_{T,\,high} = 10^{18}$ el m^{-2} respectively. Based on these estimates, as well as the transmitter frequency, the number of full rotations in the signal's polarisation is estimated, see Table 4.3.

Table 4.3: Full rotations of the signal polarisation due to Faraday Rotation for low, medium, and high estimates of the TEC

Frequency MHz	**Faraday Rotations** (-) **Low**	**Medium**	**High**
28	2.4	24	240
50	0.75	7.5	75

Being a heavily frequency dependent phenomena, Faraday rotations in signal polarisation are significant for the frequencies at which the RABSII instrument will operate at. Given the scale of the values presented in Table 4.3, as well as the known high variability of the phenomena, the following assumption is made about the signal polarisation, **AS-LINK-6**. Furthermore, as most commonly used antennas for space communication are linearly polarised, **AS-LINK-7** is also made.

Link Budget Analysis Assumptions - Continued

AS-LINK-6.: The beacon transmitter is linearly polarised.

AS-LINK-7.: Regardless of the polarisation orientation of the transmitter's antenna, the signal's polarisation angle at ground will be random.

In the, unlikely, case the beacon's antenna were to instead be circularly polarised, then Faraday rotation is not an effect which matters much in the link efficiency. If the beacon's antenna is linearly polarised instead, the perceived signal polarisation at ground will have a random orientation which is highly variable with respect to time (changes in the span of fractions of a second to a few seconds) [67]. This is due to the high rate of change in both the path length due to the satellite's high velocity, and the high localised TEC variability.

As dipoles/monopoles/loops are often used to receive on the 6 and $10\,$m bands [65], the following assumption is also made.

Link Budget Analysis Assumptions - Continued

AS-LINK-8.: The ground station(s) antenna(s) is linearly polarised.

Based on the assumptions made, the polarisation angle θ of the incoming signal can be modelled as a uniform distribution between the angle 0 and 2π rad as such $\theta \sim U(0, 2\pi)$. The probability density function (PDF) then becomes.

$$f_\theta(\theta) = \begin{cases} \frac{1}{2\pi} & \text{for } 0 \leq \theta < 2\pi \\ 0 & \text{elsewhere.} \end{cases} \tag{4.6}$$

Where f_θ is the PDF as a function of the continuous random variable θ. Returning to polarisation losses, simplifying Equation 3.3 with the assumptions made and taking the limit for both r_S and r_R going to infinity yields the following.

$$L_{p,\,dB} = 10 \cdot log_{10}(cos^2(\theta)) = g(\theta) \tag{4.7}$$

This defines the polarisation mismatch loss for a linearly polarised signal and receiver at an angle θ with respect to each other. Note that L can range from negative infinity up to zero. Using the definitions in the book by Dekking et al [16], the PDF f of this new continuous random variable $L_{p,\,dB}$ transformed by the function $g(\theta)$ (Equation 4.7) can be defined as follows.

$$f_{L_{p,\,dB}}(L_{p,\,dB}) = f_\theta(g^{-1}(L_{p,\,dB})) \cdot \left| \frac{d}{dL_{p,\,dB}} g^{-1}(L_{p,\,dB}) \right| \tag{4.8}$$

Solving for the PDF yields the following, the subscript for $L_{p,\,dB}$ is partially dropped for legibility.

$$f_L(L) = \begin{cases} \frac{1}{2\pi} \cdot \frac{ln(10) \cdot 10^{L/20}}{20 \cdot \sqrt{1 - 10^{L/10}}} & \text{for } -\infty < L_{p,\,dB} \leq 0 \\ 0 & \text{for } L_{p,\,dB} > 0 \end{cases} \tag{4.9}$$

Lastly, the cumulative distribution function (CDF) F, ca be obtained by integrating the PDF across the range of $L_{p,\,dB}$ to yield the following.

$$F_L(L) = \begin{cases} 0 & \text{for } -\infty < L_{p,\,dB} \leq 0 \\ \frac{arccos\left(\sqrt{10^{L/10}}\right)}{\pi/2} & \text{for } L_{p,\,dB} > 0 \end{cases} \tag{4.10}$$

Both the PDF and CDF of the polarisation loss are plotted in Figure 4.2.

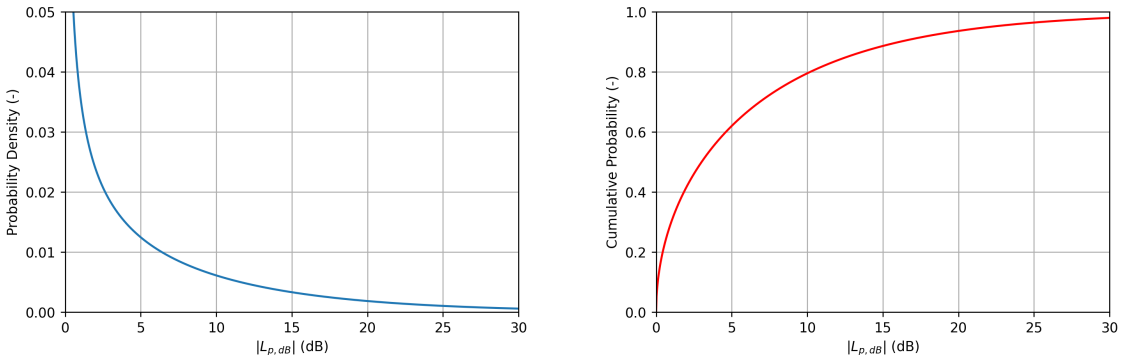

(a) Probability density function

(b) Cumulative distribution function

Figure 4.2: Distribution of the absolute value of polarisation loss $L_{p,\,dB}$

From the presented distribution it is clear how the majority of the polarisation orientation result in small polarisation losses. In fact, the expected median loss is just over -3 dB, which is almost the same as what would be expected if either the incoming signal or the receiving station was circularly polarised. This would intuitively make sense, as the randomly rotating signal polarisation would over time tend to approach the behaviour of a circularly polarised one. An expected loss due to polarisation mismatch of -3 dB is reasonable estimate, to be validated against relevant literature.

Literature-Based Estimates

To complement the simple model presented in the previous section, the obtained estimates are compared to what can be found in literature. While space-to-Earth radio communication in the HF/VHF band is rare, some experiments have been done on the performance of these bands.

Part of the paper by Vanhamel et al [79] presents a relevant analysis where reception of a linearly polarised signal on the 160 m-band is tested. More specifically, two perpendicularly mounted linearly polarised receiving antennas are used in combination to observe the relative difference in signal strength based on the receiver orientation. The findings can be seen in Figure 4.3.

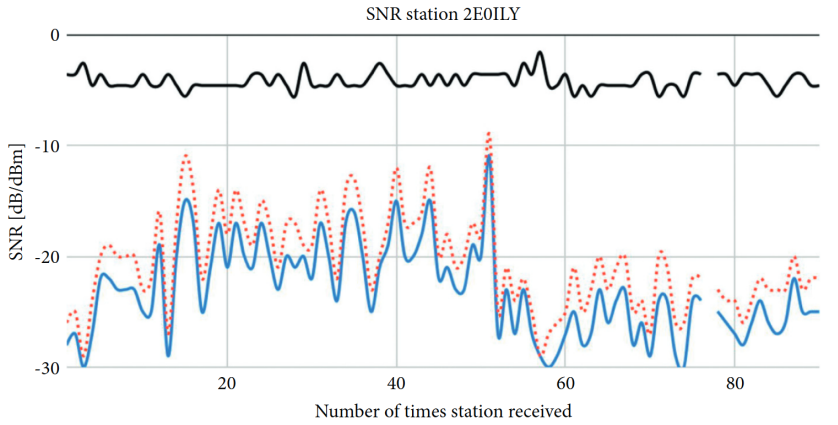

(a) Reception of the 2E0ILY transmitting station

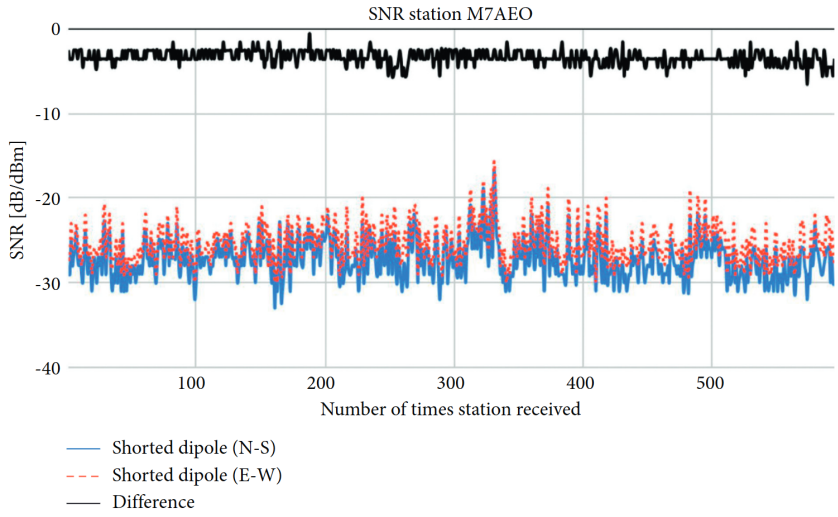

(b) Reception of the M7AEO transmitting station

Figure 4.3: SNR in reception for two perpendicular dipoles for two different transmitting stations, in blue and red; the difference between the two is plotted in black [79]

Looking at the black line for reception from both transmitting stations, the signal between the two antennas has a relatively constant difference of about 3 dB. While both the transmitters and receivers in this analysis are on ground, the signal propagation is still heavily affected by the same phenomena as for space-to-ground links. Furthermore, the difference in frequency band (about 2 MHz versus 28-50 MHz) does not significantly affect the expected observed behaviour. After all, the Faraday rotations may be in the range of thousands or a few tens, but the outcome on effectively randomising the perceived polarisation is the same.

Lastly, while not considered in this simple analysis, it is important to mention that other effects at the considered frequencies do still play a role on the observed signal. More specifically, atmospheric refraction and time delay of the signal effectively create multiple copies of the original signal which constructively and destructively combine on the way to the receiver. This has the practical effect of 'smoothing' out the perceived polarisation of the signal at reception. This is in line with the expectations coming from the model presented in the previous section.

To conclude, an expected polarisation mismatch loss of -3 dB is deemed reasonable. It should be possible to reduce this polarisation loss by better aligning the receiving/transmitting antenna pairs. However, given the uncontrolled attitude of Delfi Twin, not much control over this design aspect is expected.

4.2.4. Outcomes

In addition to the assumptions made, the analysis requires a few more input parameters to size the system. Based on the satellite platform and science case constraints, the following inputs are used.

1. Input RF Power: 500 mW
2. System Bandwidth: 2500 Hz
3. Satellite Orbital Height: 550 km

Based on a desired link margin of 6 dB. The link budget parameters are worked out starting from the reception at ground, all the way back to the beacon's transmission. While modelled from scratch for this analysis, the final link model was compared against AMSAT models (the same used by the Delfi-Twin team) to validate the outcomes [45].

Two separate tables present the results, Table 4.4 for the 28 MHz instrument, and Table 4.5 for the 50 MHz instrument. The *Type* column describes whether the parameter is an input, an output, or an intermediate result. The colour of the row is changed accordingly.

Table 4.4: Link budget for the 28 MHz instrument. Parameters in order of calculation/usage, together with their computed value and unit. Each row is coloured according to whether the parameter is an input (red), a intermediate result (green), or a output (blue). Assumptions and mission constraints are considered as inputs.

Parameter	Value	Unit	Type
Transmitter frequency	28	MHz	Input
Link Margin	6	dB	Input
SNR for decoding	-15	dB	Input
Effective noise temperature	$304\,000$	K	Intermediate result
Receiver bandwidth	2500	Hz	Input
Noise power	-139.8	dB W	Intermediate result
Signal power at ground	-148.8	dB W	Intermediate result
Polarisation losses	-3	dB	Intermediate result
Transmitter orbital height	550	km	Input
Minimum elevation angle	10	°	Input
Free-space losses	-126.6	dB	Intermediate result
Required EIRP	-19.2	dB W	Output
Total losses to antenna	-3	dB	Input
System input RF power	500	mW	Input
Minimum required transmitter gain	-13.2	dB	Output

Table 4.5: Link budget for the 50 MHz instrument. Parameters in order of calculation/usage, together with their computed value and unit. Each row is coloured according to whether the parameter is an input (red), a intermediate result (green), or a output (blue). Assumptions and mission constraints are considered as inputs.

Parameter	Value	Unit	Type
Transmitter frequency	50	MHz	Input
Link Margin	6	dB	Input
SNR for decoding	−15	dB	Input
Effective noise temperature	61 700	K	Intermediate result
Receiver bandwidth	2500	Hz	Input
Noise power	−146.7	dB W	Intermediate result
Signal power at ground	−155.7	dB W	Intermediate result
Polarisation losses	−3	dB	Intermediate result
Transmitter orbital height	550	km	Input
Minimum elevation angle	10	°	Input
Free-space losses	−131.6	dB	Intermediate result
Required EIRP	−21.1	dB W	Output
Total losses to antenna	−3	dB	Input
System input RF power	500	mW	Input
Minimum required transmitter gain	−15.1	dB	Output

Two key conclusions can be drawn from the numbers presented. The first key takeaway is that the design of the 28 MHz instrument is constraining over the 50 MHz instrument. Two key figures in the link budget are frequency dependent: the effective noise temperature (and hence noise power), and the free space loss. The former, noise power, is inversely proportional to frequency in this domain, hence we see a much lower value for the 50 MHz instrument over the 28 MHz one. The latter, free-space loss, is directly proportional to frequency, hence we see a larger loss for the 50 MHz instrument over the 28 MHz one. Combining the contributions of these two varying figures, the decrease in noise power is dominant over the increase in free-space loss. Overall, the transmitter for the 28 MHz instrument will need to have a higher total system gain than the 50 MHz in order to close the link to ground.

The second key takeaway is the output value itself. This chapter set out with the goal of obtaining concrete numerical system requirements for the RABSII instrument. The values for the *minimum required transmitter gain* are key to answer part of the first research question and provide a complete starting point for the conceptual design of the RABSII instrument.

4.3. System Requirements

Requirements presented in this chapter are strictly system requirements and are identified with a simple ID system. Each requirement ID has the following structure: ***REQ-XXX-00***. The first three-letter code (***REQ***) indicates it is indeed a requirement, and differentiate them from research areas (*RA*), research questions (*RQ*), assumptions (*AS*), etc. The second three-letter code can be either ***SCI***, ***SAT***, or ***LNK*** based on whether the requirement originates from the science case, the satellite platform, or the link budget analysis respectively. Regardless of the requirement source, the last number individually identifies each requirement incrementally.

The requirements for the 28 MHz instrument are presented in Table 4.6. From this point forward in the design and analysis process, the 28 MHz instrument is discussed exclusively. This is done as its design and performance is significantly more constraining than the 50 MHz one. If a feasible design can be devised for the 28 MHz instrument, one also exists for the 50 MHz instrument.

The most constraining and hence driving requirement for the RABSII payload is ***REQ-SAT-07***, defining the max available volume for the stowed system. This requirement is expected to shape most of the design choices to be made.

Table 4.6: 28 MHz RABSII instrument system requirements

ID	Requirement
REQ-SCI-01	The RABSII payload shall transmit the beacon signal at a frequency of 28 MHz
REQ-SCI-02	The RABSII payload shall transmit the beacon signal omni-directionally
REQ-SCI-03	The RABSII payload shall transmit the beacon signal with either a circular or a linear polarisation
REQ-SCI-04	The RABSII payload shall have a broadcasting bandwidth no less than 2.5 kHz
REQ-SCI-05	The SNR of the signal received at ground from the RABSII payload shall not be lower than -15 dB
REQ-SAT-06	The RABSII payload input RF power shall not exceed 500 mW
REQ-SAT-07	The total volume of the RABSII payload when stowed shall not exceed 80x40x4 mm^3
REQ-SAT-08	The total mass of the RABSII payload shall not exceed 40 g
REQ-SAT-09	The RABSII payload shall operate at an orbital altitude of 550 km
REQ-LNK-10	The RABSII payload EIRP shall not be lower than -19.2 dB W in any direction
REQ-LNK-11	The RABSII payload shall have a transmitter gain no less than -13.2 dB

5

Summary of Key Outcomes and Decisions

This first part of the report encompasses the first phase of the project and mainly deals with answering the first research question posed in section 2.3: ***What antenna gain and radiated power is required to close the science case's link budget with sufficient margin?***

The project objectives have first been presented in chapter 2. Literature relevant to the scope of this project was then discussed in chapter 3 divided into a few distinct research areas. Lastly, based on constraints originating from the science case, the satellite platform, and the radio link, system requirements have been defined in chapter 4.

Based on the work carried out throughout this first project phase, a few key findings and decisions have been made.

- The type of antenna (antenna conductor shape) seems to be the most relevant design aspect when it comes to influencing the expected RF performance. Deciding on what antenna type best suits RABSII will be important.
- Considering the low SNR of the digital modulation modes used, the required system gain appears not to high. Based on this, it does not seem like full size resonant antennas are necessary to close the link budget.
- Volume available for the instrument deployer will likely be the most constraining system requirements. Creative solutions will be required to fit a whole antenna deployer in the available volume of 80x40x$4\,\mathrm{mm}^3$.
- The performance requirements originating from the link budget are more stringent for the $28\,\mathrm{MHz}$ instrument than for the $50\,\mathrm{MHz}$ one. If a feasible design can be identified for the former, one will also exist for the latter. Hence, the decision is made to focus on developing an antenna and deployer only for the $28\,\mathrm{MHz}$ instrument for all subsequent project phases.

Part II:

Antenna Conceptual Design

6

Antenna Design Space

In order to begin designing the RABSII beacon antenna, its design space is here defined. A few distinct categories representing the key design decisions to be made are presented in this chapter. Namely, the shape of the antenna conductor in section 6.1, followed by its size (often relative to the transmission wavelength) in section 6.2, its cross-section in section 6.3, its material in section 6.4, and lastly the options and choices with respect to the matching network in section 6.5.

6.1. Conductor Shape

By far the most driving aspect in the design of the RABSII antenna is its shape. More specifically, the shape of the conductor making up the antenna itself. The shape of an antenna has significant consequences on the expected transmission characteristics. While virtually infinite number of options are available, a few well defined antenna shapes are commonly used for radio communication. Specifically looking at space-based radio communication, dipole antennas are most often the go-to antenna choice due to their versatility and good omnidirectional performance [15]. In addition to dipoles, when looking at transmission on the HF/VHF bands, loop antennas are often used by radio amateur due to their good overall performance and transmission omni-directionality [65]. These two antenna types, and their expected performance characteristics, are presented in subsection 6.1.1 and subsection 6.1.2. Less relevant antenna types for this project, such as helical antennas and monopoles are presented in subsection 6.1.3. Lastly, a brief summary of these antenna options for small satellite platforms is presented in subsection 6.1.4

6.1.1. Dipole Antennas

Dipole antennas are simple, they consist of two linear conductors equal in length extending in opposite directions. A simplified diagram for a generic dipole can be found in Figure 6.1. To achieve resonance, the length L of a dipole antenna must be equal to half the wavelength λ of the transmitting frequency [5].

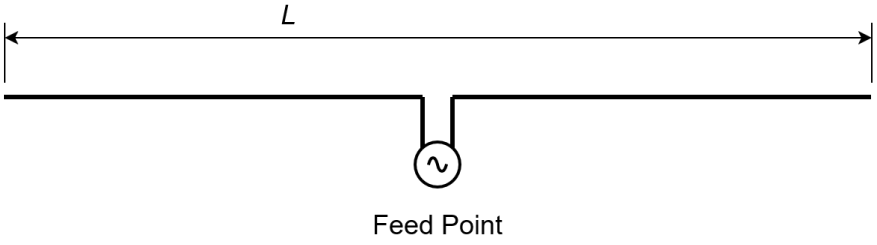

Figure 6.1: Dipole antenna of length L. For resonance, $L \approx \lambda/2$

Dipole antennas have the following characteristics.

- **Radiation Efficiency**: High efficiency at resonant length, efficiency drops considerably as the dipole get shortened.
- **Radiation Pattern**: Doughnut-shaped radiation pattern with nulls aligned axially with the feed point. Generally omnidirectional.
- **Bandwidth**: Wide bandwidth at resonance. Highly dependent on matching network design and antenna length.
- **Feed Type**: Double-ended antenna, hence unbalanced feed point. Requires a BALUN for proper functioning (if connected to an unbalanced source) and a balanced matching network (if present).
- **Polarisation**: Linearly polarised

These points generally hold for resonant dipoles, which are likely not feasible for RABSII given their large required size compared to the host satellite platform (roughly $5\,\mathrm{m}$ in length for the $28\,\mathrm{MHz}$ instrument). For electrically short dipoles, significant changes can be expected. Mainly, a significant decrease in both radiation efficiency and available bandwidth, and a mild reduction in the depth of radiation pattern nulls. [46, 49]

6.1.2. Loop Antennas

Loop antennas, as the name implies, are simply a conductor shaped in an open loop fed across the opening. This loop can take any different shape as long as it is continuous. Common designs employ round, square or triangular loops (delta loop), with the key defining feature being the length of the conductor used. For resonance, the length of the conductor must approach the wave length λ of the transmitting frequency. These resonant loops are also sometimes referred to as full wave loops. Figure 6.2 presents a schematic of a simple circular loop with diameter D. [22]

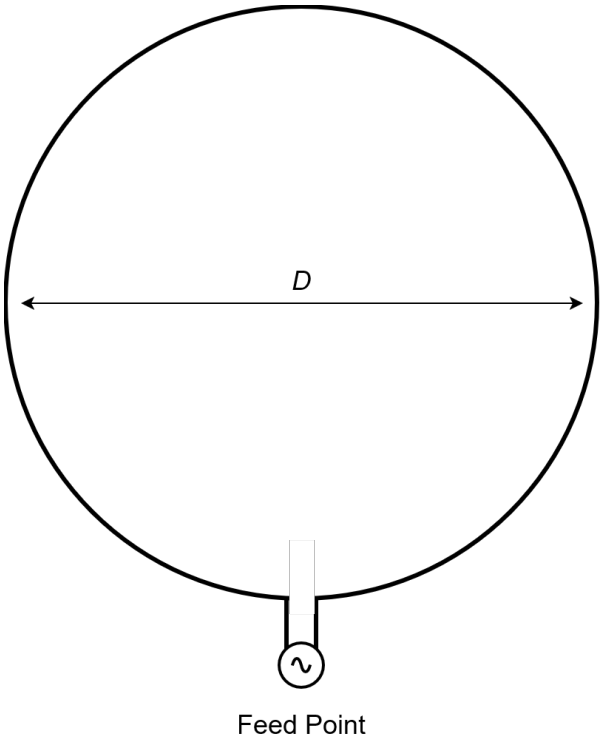

Figure 6.2: Circular loop antenna of diameter D

As presented for dipoles, the following characteristics can be expected from loop antennas.

- **Radiation Efficiency**: High efficiency at resonant length, efficiency drops considerably as the loop gets smaller.

- **Radiation Pattern**: Elongated doughnut-shaped pattern with nulls aligned with the loop's axis. Depending on the exact loop shape, this elongation may be signifiant resulting in a somewhat directional pattern. Otherwise, generally omnidirectional.
- **Feed Type**: Double-ended antenna with unbalanced feed point, requires a BALUN for proper functioning (if used with an unbalanced source) and a balanced matching network (if present).
- **Polarisation**: Perhaps surprisingly given the shape, loop antennas are linearly polarised, regardless of the exact loop shape.

As for dipole antennas, given the frequencies at which the RABSII instrument will operate at, a full wave loop is likely unfeasible due to its large required size (roughly $3\,\mathrm{m}$ in diameter for the $28\,\mathrm{MHz}$ instrument). As the diameter of a loop antenna decreases, a significant reduction in radiation efficiency and bandwidth can be expected. [46, 49]

6.1.3. Other Antennas

A large number of other antennas can be considered. However, only the most commonly used and well-understood options are here presented.

Helical Antennas

Helical antennas, as the name suggests, are composed of a single helical-shaped conductor. With only one feed point, helical antennas are single ended, and hence require a ground plane to correctly function. The diameter of the coil determines the resonant frequency of the antenna in a similar manner to loop antennas where the diameter and transmission wavelength are directly linked. In terms of directivity, helical antennas are highly directional, with the number of coils in the helix determining how 'focussed' the transmission beam becomes. Lastly, helical antennas are circularly polarised. [46]

While they can be operated in a few different modes, helical antennas are intrinsically directional, and hence not a viable option for RABSII. Furthermore, given the small size of the Delfi-Twin platform, the satellite would not be able to fulfil the function of ground plane, hence requiring additional components and systems for correct functioning. Lastly, the large helix diameter required to achieve good radiation efficiencies at the required frequencies make helical antennas unfeasible.

Monopole Antennas

Monopole antennas can be considered as half of a dipole. Looking back at Figure 6.1, consider removing one of the two conductors coming from the feed point. The resulting antenna is a monopole. Being now single-ended, monopoles require a ground plane for correct functioning, just like helical antennas [46]. Furthermore, while technically being only half the size of an identical dipole, a monopole tuned for $28\,\mathrm{MHz}$ is still considerably large when compared to the Delfi-Twin satellite. As such, similarly to helical antennas, they are unfeasible for the RABSII payload.

6.1.4. Summary

Table 6.1 summarises the available options in terms of conductor shape together with their respective properties.

Table 6.1: Considered antenna types and relevant RF properties

Type	Directivity	Feed Type	Polarisation
Dipole	Omnidirectional	Double-ended (no ground plane)	Linear
Loop	Omnidirectional	Double-ended (no ground plane)	Linear
Helical	Directional	Single-ended (requires ground plane)	Circular
Monopole	Omnidirectional	Single-ended (requires ground plane)	Linear

While monopoles and helical antennas are not compatible with the RABSII instrument, both dipoles and loops could fulfil the system requirements. The properties of dipoles and loops are rather similar, with key differences requiring a more detailed analysis to be meaningfully discussed. Furthermore, given the frequencies requirements, it is expected that full-size resonant versions of either a dipole or a loop would be too big to be integrated onto the Delfi-Twin satellite platform.

6.2. Conductor Size

When it comes to antenna size, usually dimensions are entirely dictated by the frequency of the transmitted signals. To achieve resonance, the size of the conductor needs to be scaled to match some factor of the wavelength transmitted. As mentioned in section 6.1, this factor depends on the shape of the antenna. For dipoles, resonance is achieved when the total length L is equal to half the wavelength. For loops, the total conductor length needs to be equal to a whole wavelength. At 28 MHz, this translates to a dipole about 5 m in length, or a loop about 3 m in diameter. Given the size of Delfi-Twin (15x5x5 cm^3) and the available volume for the deployer itself (80x40x4 mm^3) a smaller antenna is required to make the RABSII instrument practical.

When considering reducing the size of the antenna conductor, the following trends can be expected [46, 49].

- **Bandwidth**: significant reduction
- **Radiation Efficiency**: moderate to significant reduction
- **Directivity**: depends on antenna type
- **Polarisation**: no change
- **Feed impedance**: moderate reduction in resistance, significant change in reactance

The extent to which each of these metrics may change requires more detailed analysis. It is however clear how a conductor smaller than a resonant one will always perform worse. The decision on the extent to which the chosen antenna can be down-scaled depends on the relation between each performance metric and size. To attempt to mitigate some of the performance losses, some approaches are available, presented back in subsection 3.2.4. To summarise, a shortened antenna can be electrically 'lengthened' by means of capacitive or inductive elements which alter the conductor impedance to more closely resemble that of a resonant conductor.

6.3. Conductor Cross-section

The cross-section of the conductor itself has a smaller effect on overall performance when compared to shape or size. It is nonetheless relevant when defining the geometry of the RABSII antenna beacon. Of primary concern is the relevant skin depth of the conductor, introduced in subsection 3.2.5. For both the 28 MHz and 50 MHz instruments, the skin depth ranges from around 10 µm to 15 µm depending on how conductive the chosen material is. It is relevant to note that once again, the 28 MHz instrument is the constraining one of the two, with a skin depth always higher than the 50 MHz. This means that regardless of the conductance of the conductor, a larger minimum cross-section is required to carry the same current. In terms of available choices, two options are considered.

Firstly, a simple round cross-section conductor in considered, such as a thin wire. This is the simplest option in terms of manufacturing and component acquisition. Given that currents are only carried over the top thin layer, this may however not be the most mass efficient option.

Secondly, a thin metallic strip with a rectangular cross-section is considered. Depending on the chosen deployment approach, this may be more mechanically effective than just a circular cross-section. While a regular rectangular cross-section is presented in Figure 6.3, some curvature along the long axis may be beneficial for deployment. To clarify, consider the behaviour of tape antennas, some curvature across the antenna strip is used to achieve a stable deployed configuration.

Figure 6.3 Presents a schematic of the two considered cross-section options.

6.4. Conductor Material

When it comes to materials, a lot of options are available. For clarity, materials considered are presented divided into two separate sections: uniform materials, and composite materials. The former refers to a single solid material, whereas the latter refers to combination of two or more materials making up the antenna conductor. Performance metrics which are relevant to consider are mechanical strength (stiffness and yield strength) and conductivity.

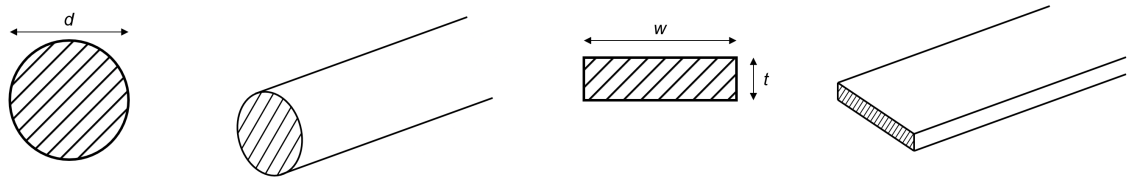

(a) Circular cross-section with diameter of d

(b) Rectangular cross-section with width and thickness of w and t respectively

Figure 6.3: Considered conductor cross-section schematics

6.4.1. Uniform Materials

When considering uniform materials, the key consideration is to find an option which is able to perform well both as an RF conductor, and as a structural material to support itself. The two functions are equally as important for the success of the RABSII payload. For this reason, materials which are very good conductors may very well not be a good option as often lacking the mechanical performance to remain stable and well-behaved once deployed. Table 6.2 presents the considered options for uniform solid materials together with the relevant mechanical properties.

Table 6.2: Uniform material options and relevant properties [39, 38]

Material	**Conductivity** σ [S m^{-1}]	**Density** ρ [g cm^{-3}]	**E-modulus** E [GPa]	**Yield strength** σ_y [MPa]
Aluminium 7075 (annealed)	19×10^6	2.8	70	96
Spring steel (1.4310)	1.4×10^6	7.9	190	1500

In practice, only steel and aluminium are viable options when considering uniform materials. Depending on whether mechanical or RF performance is more constraining, either may be the better option. Materials with better conductivity than aluminium have insufficient mechanical properties to be reliably deployed in space (consider pure copper, gold, and silver). In terms of mechanical properties, steel provides the best combination of stiffness and high yield strength although compromising on a lower conductivity. By mechanical properties alone, steel seems to be the metal with the best performance to make antenna which can be stowed, deployed, and operated in space.

6.4.2. Composite Materials

To fulfil the system requirements, a conductor made of a single uniform material may not be sufficient. Composite options are considered as they could allow having two sub-structures each performing one task: either mechanical support or RF conductor.

Given the very thin RF skin depth (see subsection 3.2.5) expected, currents will only flow through the material surface. As such, it is possible to use highly conductive coatings over a stiff and strong core and match the RF performance of an equivalently sized good uniform conductor. This approach allows for a large stiff core to support a thin conductive surface layer with potentially little performance drawbacks.

Steel alloys have one of the highest yield strength of any metal as well as a high stiffness [39]. They are an ideal candidate to be shaped into either a loop or dipole antenna and remain rigid after deployment. As such, steel alloys are the only option considered for the core of a composite conductor. Various compatible coating options are considered, and can be found in Table 6.3.

Looking at the coating materials, unsurprisingly, very good conductors are the only options presented. Copper and silver have very similar conductivities (58 vs $63\,\mathrm{S\,m^{-1}}$), but silver is a lot more expensive and hence less appealing. Nickel is also presented for the electroplated coating as often used as an extra layer to either improve adhesion to the substrate, or protect the copper and silver from the environment.

Table 6.3: Conductive coating options over a structural steel substrate [39, 38]

	Coating		
Description	**Material**	**Thickness Range** (µm)	**Conductivity** σ (S m^{-1})
Conductive cladding	Copper	$50 - 5000$	58×10^6
Electroplated coating	Nickel/Copper/Silver	$5 - 25$	$14 - 58 - 63 \times 10^6$
Spray-on coating	Copper/Silver	$5 - 100$	$58 \times 10^6 - 63 \times 10^6$

Looking at the achievable coating thicknesses, for reference, the expected skin depth for the transmitted RF signals ranges between 10-15 µm. While conductive coatings are usually 2-3 times the skin depth, both spray-on coatings and electroplated coatings should be sufficient to ensure RF performance similar to a pure conductor. Cladding may still be viable, but is usually used for much lower frequency signals where the skin depth measures in the range of millimetres.

6.5. Matching Network Topology

While not directly an antenna property, the design and implementation of matching networks is very much part of the antenna design. Introduced in subsection 3.3.1, the topology of a matching network simply refers to the arrangement of its internal components. With the basic goal of matching input to output impedance, they can also be tuned to allow for larger usable bandwidth at the expense of complexity and internal power dissipation.

Figure 6.4 presents some commonly used matching network topologies [9]. Do note that the topology only specifies the relative component configuration, not all permutations are shown to avoid needless repetition. Each capacitor may be swapped for an inductor, and vice versa, without changing the matching network topology.

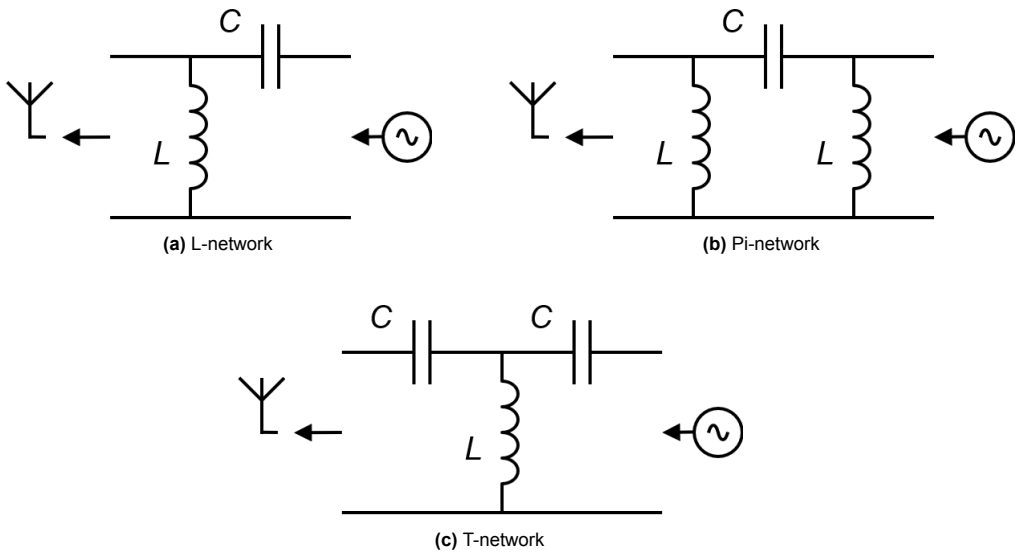

(a) L-network **(b)** Pi-network **(c)** T-network

Figure 6.4: Common **unbalanced** matching network topologies; capacitors with capacitance of C and inductors with inductance of L; source on the right, antenna on the left

All the matching networks presented are unbalanced. Since both the dipole and the loop antennas are double-ended, a balanced matching network configuration is required. The general unbalanced topologies in Figure 6.4 can be modified to produce identical behaviour, but in a balanced fashion. The configurations are altered to ensure that the forward path impedance towards the antenna is the same as the impedance of the return path to ground. These balanced options are presented in Figure 6.5

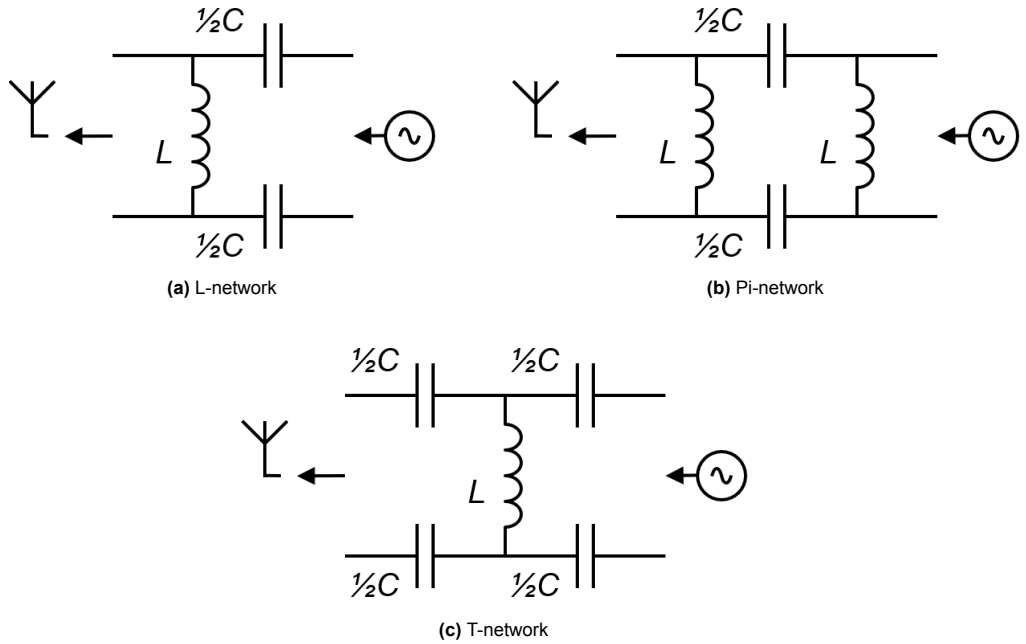

(a) L-network

(b) Pi-network

(c) T-network

Figure 6.5: Common **balanced** matching network topologies; capacitors with capacitance of C and inductors with inductance of L; sources on the right, antenna on the left

Which option is more suitable for RABSII will have to determined by simulating the antenna-and-matching-network system as one and comparing the obtained performance against the defined system requirements.

7

Antenna Performance Analysis Approach

This chapter presents a description of the simulation and analysis approach devised to identify a preferred design, as well as to characterise its performance with respect to the system requirements. Starting with the an overview of the analysis objectives presented in section 7.1, followed by a general description of the analysis approach presented in section 7.2, and lastly the simulation software used presented in section 7.3.

7.1. Objectives

The goal of the analysis to be performed is two fold: firstly, determine which type of antenna (conductor shape; loop or dipole) is most promising for the RABSII instrument. And secondly, characterise in detail the performance of the chosen design with respect to the various other design choices, such as conductor material, cross-section, etc. These objectives are summarised as follows.

Performance Characterisation Objectives

1. Identify the most promising antenna conductor shape: loop or dipole
2. Characterise the performance of such design with respect to the other design dimensions

Starting with the first objective, the performance of each considered design must be determined to a degree sufficient to make a choice on the most promising option. While many categories have been introduced in chapter 6 when it comes to the RABSII antenna design, one aspect is by far most influential on the system as a whole: the shape of the conductor. The choice between a dipole and a loop antenna is far more decisive to the outcomes of this project then the more detailed choices of conductor material and matching network type. It would be meaningless to optimise the conductor cross-section and composition before choosing whether such conductor should be in the shape of a loop or a dipole. As such, the first objective of the analysis is to identify whether a dipole or a loop antenna is a more suitable choice for RABSII.

Looking at the second objective, once an antenna shape has been identified, its performance is characterised for different variations of the other design dimensions presented in chapter 6. The results obtained are then checked against the defined system requirements. This is be used to determine whether a feasible design is possible, and to what extent the science case can be fulfilled. As outlined by the system requirements (see section 4.3), volume, and hence antenna size, is by far the most constraining aspect of the design. As such, size is considered a 'free parameter', or the independent variable in the analysis. When investigating a performance metric such as the radiation efficiency for example, data is presented as a function of antenna size. Various combinations of materials, cross-sections, and matching networks will yield different performance at different antenna dimensions. The choice hence becomes what combination of design choices yields sufficient performance to meet the requirements while minimising overall system size. Were the requirements to change as the maturity of the project increases, redesigning the system would come down to simply scaling the antenna up or down to match the new performance targets according to the data presented. As essentially all design choices (apart from conductor shape) are compatible with each other, each design dimension can be simulated mostly independently.

7.2. Approach

Based on the defined objectives, the analysis is approached in the following steps:

1. Choose between a dipole and a loop antenna (conductor shape)
2. Make informed choices on the remaining design dimensions (conductor material and cross-section, and matching network topology)
3. Characterise the final performance of the chosen design

Looking at step (***1***), the choice of using either a loop or a dipole is central to the rest of the conceptual design and must hence be tackled first. Once this choice is made, in step (***2***), the remaining design choices can be made. Lastly, in step (***3***), once the design has been identified, its performance can be more thoroughly characterised.

In order to make informed choices, the following performance metrics are considered:

1. Directivity
2. Radiated Power
3. Matching Network Efficiency
4. Available Bandwidth

These are all directly relevant to RABSII's system requirements. In addition to these metrics, to easily compare different design choices, radiation efficiency of the conductor is sometimes considered. Normally, looking at radiated power already incorporates changes and improvements in radiation efficiency. However, quantifying radiated power requires the full antenna system to be simulated (matching network plus conductor). When trying to investigate the effect of changing certain design aspects, such as conductor material or cross-section, looking at radiation efficiency is useful as it is a function of the conductor properties alone. Comparing radiation efficiency is useful as it does not require tuning or matching networks, and it is purely a function of the conductor.

7.3. Simulation Software Used

To meet the specified analysis objectives, numerical simulations are used as the primary tool. This allows for a great number of parameters to be changed and for the relation between them to be quickly investigated and quantified. For this very reason, practical testing of the antenna's RF performance would be impractical at this stage of the project. It may although be used as a tool in future work to validate the simulated antennas against real-world data.

Two pieces of software are used to perform the numerical simulations: Ansys Electronics and SimNEC. The reason for using two different simulation software packages is flexibility and data validation. Regarding the latter, while Ansys uses a mesh-based solver, SimNEC is based on the NEC engine, which uses the Method of Moments to simulate antennas. Comparing results between the two serves as a useful validation step on the simulation results. While Ansys may be more suited for complex high-precision simulations, SimNEC is more flexible for faster iterative design steps. Both workflows are needed to converge to a design quickly and then accurately characterise its performance. The capabilities and limitations of each software package as well as why they are relevant for this project are presented below.

Ansys Electronics

The electronics simulation suite from Ansys includes several discipline-specific tools. Relevant for this project are Ansys HFSS and Ansys Circuit. The former, HFSS, stands for High Frequency Structure Simulator. It uses a mesh-based approach to simulate 3D field equations for the design of any high-frequency electronic, in this case, antennas. The latter, Circuit, is used to simulate the behaviour and frequency response of electronic circuits. In this case, it will be used to simulate the matching networks. The two can be used together to simulate the antenna and matching network system as a whole. [36]

Being a mesh-based simulator, Ansys allows for very fine control over the geometry of the simulated conductors. This is required when investigating the effect of conductor cross-section on RF properties. However, this detail and precision comes at the expense of computation time and potential meshing issues. Extra care needs to be taken to ensure the meshing process does not alter the simulation results.

SimNEC

SimNEC is a software providing an interactive user interface for RF circuit design. It incorporates two key tools: a circuit analysis display, and a graphical user interface (GUI) for the NEC engine. The circuit analysis display provides tools to design and analyse ladder-circuits. Circuits can be defined and the frequency response can be characterised in terms of SWR, dissipated and transmitted power, and impedance. The GUI to the NEC engine instead provides a non-command-line-based approach to interact with various versions of the NEC engine. [3]

The NEC engine, standing for Numerical Electromagnetics Code, is a legacy solver written in Fortran to simulate near-field and far-field radiation patterns of antenna conductors. Several versions of the NEC engine have been released, some publicly, and some under licensing agreements. Most importantly, and differently from Ansys HFSS, the NEC engine is based on the Method of Moments, and not on a mesh-based approach. For the most commonly used versions of the NEC engine (up to NEC-4), this solving approach is restricted to solving the field integral equations for thin wires only. This limits the possible analysis to antennas which can be idealised as discrete segments of thin wires connected together. [12]

8

Design Choices

This chapter presents the process of making design choices across the identified design dimensions. Antenna performance is determined for various combinations of antenna shape, size, cross-section, material and matching network topology to identify which is most suitable to fulfil the RABSII science objectives. Based on the described analysis approach in section 7.2, section 8.1 first presents the choice between a loop and dipole antenna, followed by section 8.2 presenting the remaining design choices.

8.1. Conductor Shape Choice

The choice between dipole and loop antennas comes down to which can deliver better performance within the small volumetric constraints imposed by the satellite platform. In order, the following steps are taken to determine the most promising candidate.

1. Determine the maximum allowable antenna size
2. Compare available bandwidth
3. Compare directivity pattern
4. Compare radiated power
5. Choose most suitable design

Before any comparison can be performed, an upper bound must be placed on the allowable antenna size. Next, looking at bandwidth informs whether the bandwidth requirements can be met, while also providing information on the antenna's quality factor (useful to know how sensitive the system is to tuning/disturbances). Comparing the directivity pattern informs whether the antenna has 'sufficiently' omnidirectional properties for the link budget to be viable. Lastly, comparing the radiated power is directly relevant to determine whether the system requirements can be met.

8.1.1. Maximum Allowable Antenna Size

A range for the allowable size of the antennas is here defined. While it is hard to place an exact figure for this maximum size, existing missions and instruments can be used to provide a baseline estimate.

The maximum antenna size is determined based on the mechanical limitations of deploying RF antennas in space. As discussed in chapter 3, tape-springs-deployed dipoles are a very popular option for a large number of CubeSat and SmallSat missions. While other options are available for deployment, the constraining factor on the length of the dipole itself still remains how thin the conductor is with respect to its length. As the conductor becomes thinner and longer, its cross-section is not sufficient to remain rigid any more. This can cause the antenna to get tangled either during deployment or operations. Alternatively, the insufficient stiffness can cause a degree of bending/deformation significant enough to compromise the antenna's radiation performance.

Tape antennas usually tackle this problem by introducing curvature across the tape strip. While effective, this is still limited by how wide the strip is compared to its length. Were tape antennas not to be used in favour of a circular cross-section wire conductor, the same problem would still arise. In that case, the issue would be further emphasised by the fact that the wire diameter is now constrained by the internal stress distribution as the conductor is coiled for stowage before deployment.

Looking at existing missions and commercial systems, tape spring deployers have extensive flight heritage. Table 8.1 presents an overview of some relevant tape antennas and corresponding commercial manufacturers. In addition to length and width of the tape, an non-dimensional aspect ratio is presented for easier comparison. This ratio is defined as tape length divided by its width.

Table 8.1: Existing tape-deployed dipole antenna systems; aspect ratio is defined by the tape length divided by the tape width

Manufacturer	**Antenna System**	**Flight Proven**	**Dipole Arm Length** (cm)	**Tape Width** (mm)	**Aspect Ratio** ($-$)	
ISISpace	VHF/UHF Antenna for 1U-3U	Yes	55/20	3	180/65	[41]
MARMOTsat	HF antenna	No	260	30	85	[47]
MARMOTsat	VHF/UHF antenna	No	50/20	12.5	40/16	[47]
SpaceManic	Small Antenna Module (SAM)	Yes	55/20	3	180/65	[73]
EnduroSat	UHF Antenna	Yes	20	3	65	[21]
C3S	V-dipole Antenna System	Yes	20	3	65	[18]
Oxford Space Systems	Yagi Antenna (Dipole Element)	Yes	45	30	15	[76]
2NDSpace	CHORUS-01 Antenna	Yes	55	3	180	[1]

Most of the antennas found and presented are dipoles operating in the VHF/UHF frequency bands. Only one example of an antenna designed to operate in the HF band was found, currently still under development by a university team in Canada for a satellite called 'MARMOTsat'. Regardless, of the operating frequency band, most antenna tapes have an aspect ratio below 100. Some antennas in the VHF band have ratios up to about 180. While the length is fixed by the operating frequency, the width is purely a mechanical parameter constrained only by the deployment and operation dynamics. Hence these numbers are deemed relevant when looking at the RABSII instrument.

Were a resonant half-wave dipole to be used for the 28 MHz instrument, each arm would need to be roughly 2.5 m in length. Assuming an upper bound of 180 for the ratio between length and width, it would have to be about 1.4 cm wide. Based on the maximum RABSII deployer envelope of 80x40x4 mm^3, such tape would not be able to exceed 4 mm in width even when completely ignoring all the deployment hardware. Looking at the problem in reverse, given a maximum tape width of 4 mm, each dipole arm would not be able to be more than 72 cm in length, for a total maximum dipole length of about 1.5 m. It must be noted that this assumption of a 4 mm wide tape is very generous as it implies using 100 % of the available deployer thickness. Commercial deployers presented in Table 8.1 instead have a tape width of only about 30 % of the deployer thickness. Given these observations, going above a dipole length of 1.5 m posses a significant development and operational risk. Larger sizes would effectively trade antenna performance for engineering risk. Mitigating this risk would be non-trivial, given the large number of unknowns in the satellite-antenna system, as well as the complex and unpredictable dynamics of the deployment process.

Were a resonant loop to be used for the 28 MHz instrument instead, the antenna conductor would be about 10 m in length with a diameter of about 3 m. Just as for a resonant dipole, this is most likely unfeasible given the very small size of the satellite platform. The stiffness of such a deployed loop would depend on the material choice and cross-section geometry, but being a closed geometry, it would be much more stable than a dipole for the same dimensions. Given the lack of any relevant flight heritage the maximum allowable size is kept similar to an equivalent dipole. It is assumed that a loop with a dimeter larger than 1.5 m (equal to the identified max total dipole length) would not be feasible.

For a more visual reference of the sizes considered, both antenna shapes are presented with respect to the Delfi-Twin to scale for both the resonant variants (Figure 8.1), and the maximum allowed variants (Figure 8.2).

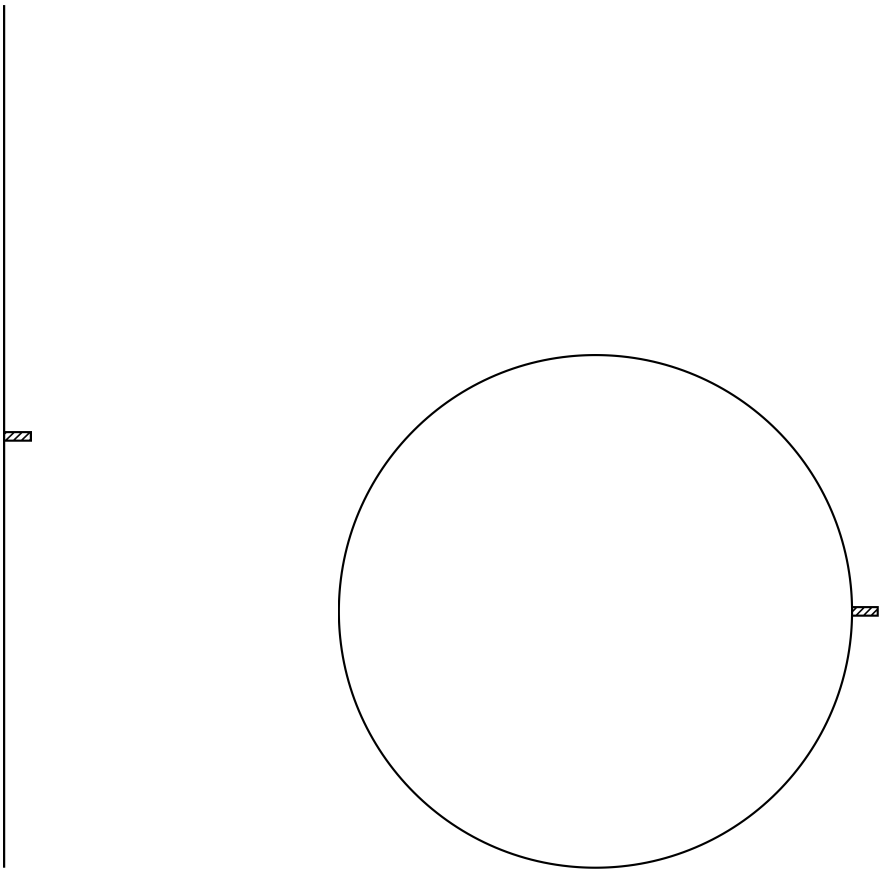

(a) Resonant Dipole **(b)** Resonant Loop

Figure 8.1: Resonant antenna sizes to scale next to Delfi-Twin (conductor thickness not to scale)

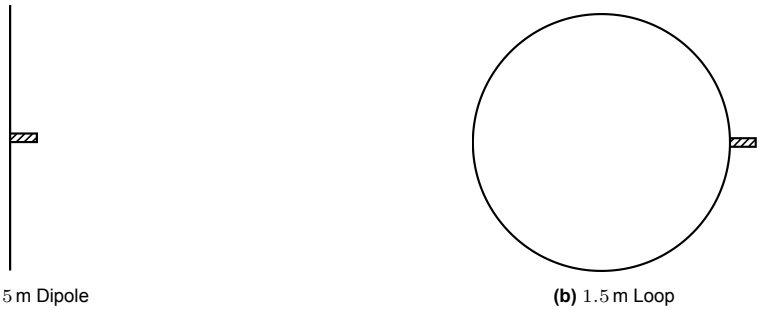

(a) 1.5 m Dipole **(b)** 1.5 m Loop

Figure 8.2: Maximum allowed antenna sizes to scale next to Delfi-Twin (conductor thickness not to scale)

When comparing RF performance, a 1.5 m long dipole and a 1.5 m in diameter loop are hence considered. This corresponds to a dipole about 30 % the size of a resonant dipole, and a loop about 50 % the size of a resonant loop. As only the conductor shape is relevant for now, all other antenna/system parameters are taken as either ideal (such as the conductivity), or equal between the two (such as cross-section or conductor wire diameter). The simulation parameters for both the dipole and loop test cases can be found in Table 8.2.

Table 8.2: Loop versus dipole parameters for comparative analysis

Parameter	Dipole	Loop
Length/Diameter (m)	1.5	1.5
Conductor cross-section	Circular	Circular
Conductor diameter (mm)	0.5	0.5
Matching network topology	L	L
Matching VSWR	1.00:1	1.00:1
Conductor material	PEC (ideal)	PEC (ideal)
Environment	Free space	Free space
Input RF power (mW)	500	500
Source impedance (Ω)	50	50
Capacitors Q	2000	2000
Inductors Q	200	200

It must be noted that for a fair comparison, performance is also investigated for variations in size down from the determined maximum value of 1.5 m.

8.1.2. Loop vs Dipole: Bandwidth

Recalling from the literature presented in chapter 3, bandwidth is generally defined as the range of frequencies over which the the return loss (RL) remains below -10 dB. This is the definition used from here on out when a specific return loss threshold is not explicitly mentioned.

Figure 8.3 presents the VSWR and return loss for both antennas plotted against frequencies just around 28 MHz. For reference, both systems are tuned to achieve a VSWR of exactly $1.00:1$ at 28 MHz.

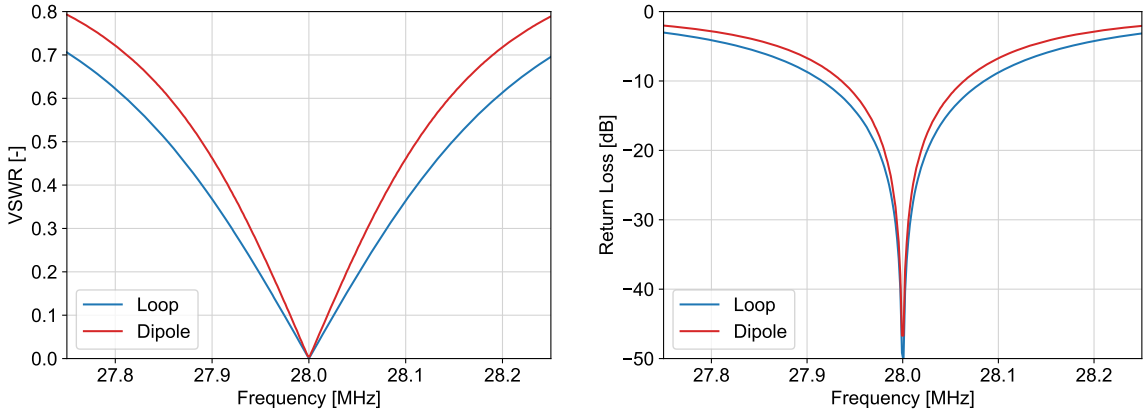

(a) VSWR

(b) Return loss

Figure 8.3: Antenna coupling within the range ± 250 kHz around the central transmitting frequency of 28 MHz; $VSWR = 1.00:1$ at 28 MHz

The two plots are very similar, indicating a close match in bandwidth between the two antennas. The exact bandwidth at various return loss intervals is presented in Table 8.3.

Table 8.3: Loop and Dipole antenna bandwidths

Antenna Type	Bandwidth (kHz) $RL < -10$dB	$RL < -20$dB	$RL < -30$dB
Loop	168.7	52.2	16.1
Dipole	128.5	40.2	12.1

While indeed the loop does have a larger bandwidth at 1.5 m in size, the difference is negligible when compared to the required bandwidth of 2.5 kHz (**REQ-SCI-04**; Table 4.6). The same bandwidth figures are also computed for a range of antenna sizes to see whether the relative difference changes meaningfully over the size range. Figure 8.4 presents the same bandwidth figures as Table 8.3, but now as a function of antenna size. Once again, all figures presented are for a perfectly matched system with $VSWR = 1.00 : 1$ at 28 MHz.

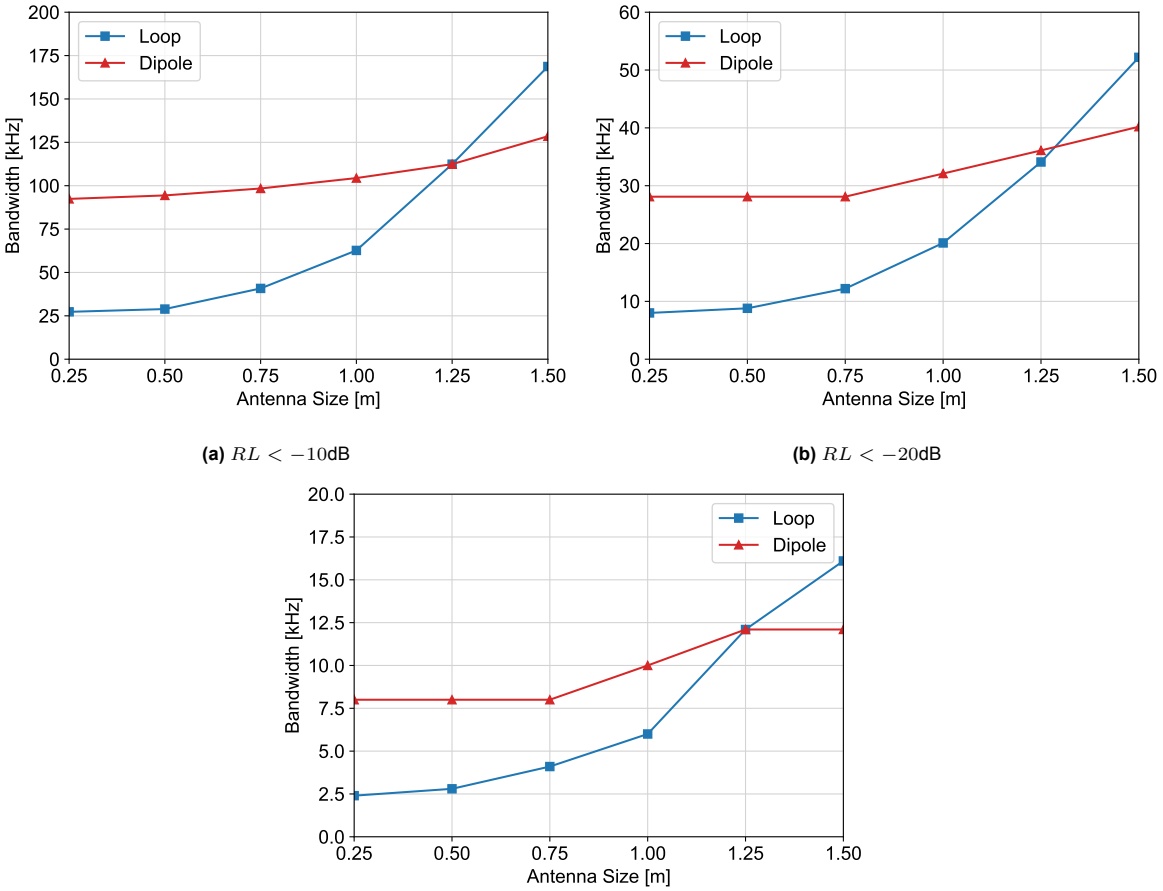

(a) $RL < -10$dB

(b) $RL < -20$dB

(c) $RL < -30$dB

Figure 8.4: Bandwidth in kHz vs antenna size for both a loop and a dipole

While there are some differences between the -10, -20, and -30 dB bandwidth, the trend is similar across them. Both antennas suffer from loss of bandwidth, but the loop has a more drastic decline as the dimensions are reduced when compared to the dipole. However, both antennas still have sufficient bandwidth to close the link budget even at the smallest considered size. At 0.25 m in size the loop and the dipole have a bandwidth of around 30 kHz and 90 kHz respectively.

8.1.3. Loop vs Dipole: Directivity

As the RABSII instrument requires omnidirectional transmission, the radiation pattern of both antennas is highly relevant. While both loops and dipoles are technically considered 'omnidirectional' antennas, the degree to which this is achieved is not clear when considering electrically short designs. For a qualitative comparison, the 3D radiation pattern for both 1.5 m antenna options is presented in Figure 8.5.

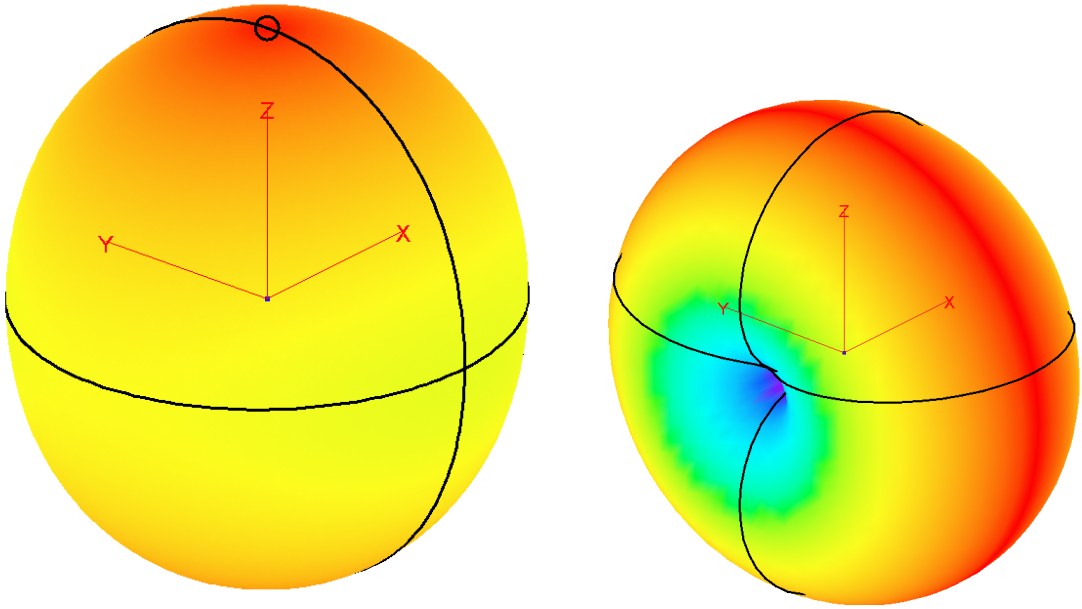

(a) Loop **(b)** Dipole

Figure 8.5: Radiation pattern shape at 28 MHz for the 1.5 m sized antennas

Numerically, the azimuth and elevation components of the antennas directivity gain are presented in Figure 8.6.

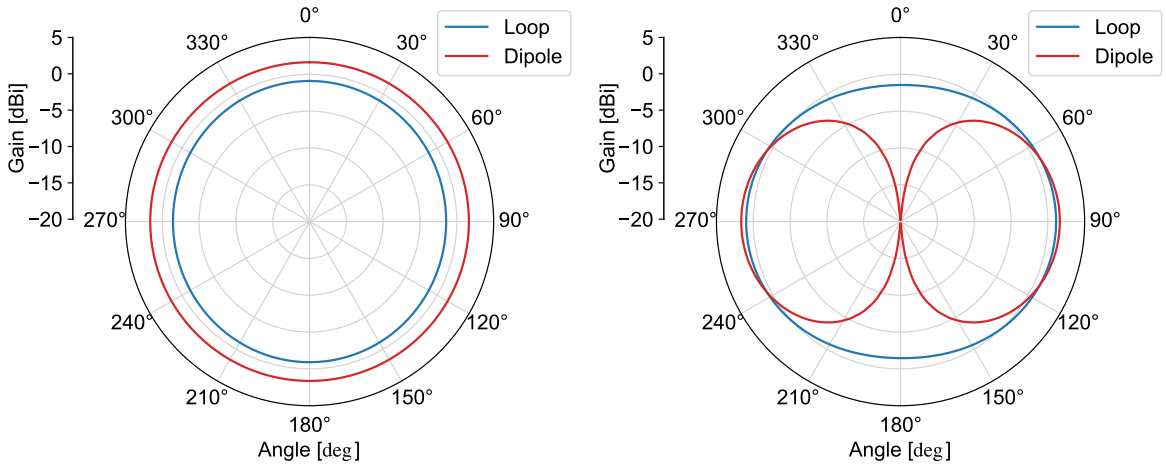

(a) Azimuth (elevation=0) **(b)** Elevation (azimuth=90)

Figure 8.6: Directivity gain across the azimuth and elevation planes

The data presented in Figure 8.5 and Figure 8.6 is equivalent, just visualised in a different way. The former presents a clearer graphical representation of the shape of the radiation pattern, while the latter is more useful for comparing the actual magnitudes of the directivity gain.

The 1.5 m loop has a much more omnidirectional pattern, with essentially no nulls at the poles. The shape is akin to that of an egg, with a slight elongation in both the azimuthal and elevation planes. The dipole instead displays the expected characteristic doughnut-shape pattern. The radiation is very constant across the azimuthal plane, but sharp nulls can be seen in the elevation plane, with nearly no radiation. The loop has a directivity gain about 1.5 dBi lower than the dipole in the azimuthal plane, but a higher directivity gain in most directions across the elevation plane. Overall, while some care needs to be taken on the mounting orientation on the satellite itself, both antennas would likely have sufficient omnidirectionality to meet the system requirements. However, given the uncontrolled attitude of Delfi-Twin, the absence of nulls for the loop is a considerable advantage.

Once again, the variation in directivity gain as a function of antenna size is also investigated. Figure 8.7 and Figure 8.8 present the elevation and azimuth directivity patterns for the loop and dipole antennas respectively considering multiple antenna sizes.

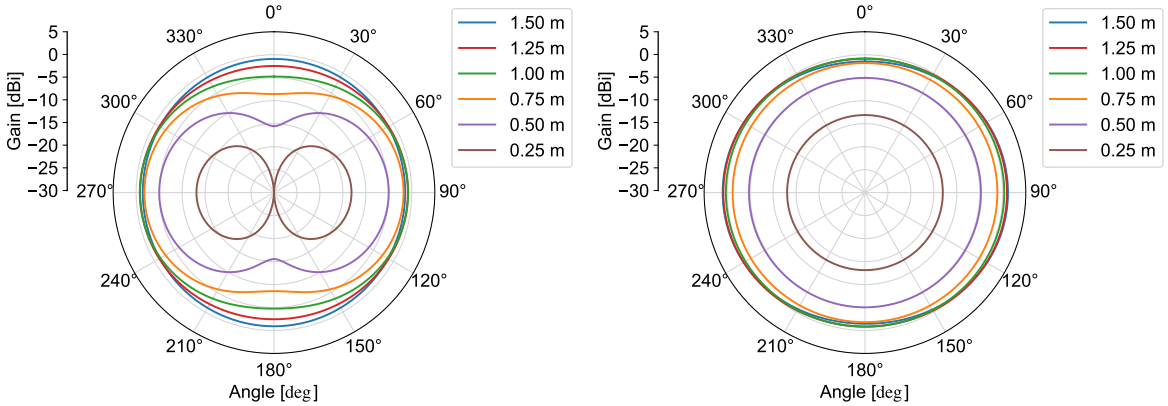

(a) Azimuth (elevation=0)

(b) Elevation (azimuth=90)

Figure 8.7: Loop antenna directivity gain as a function of antenna size

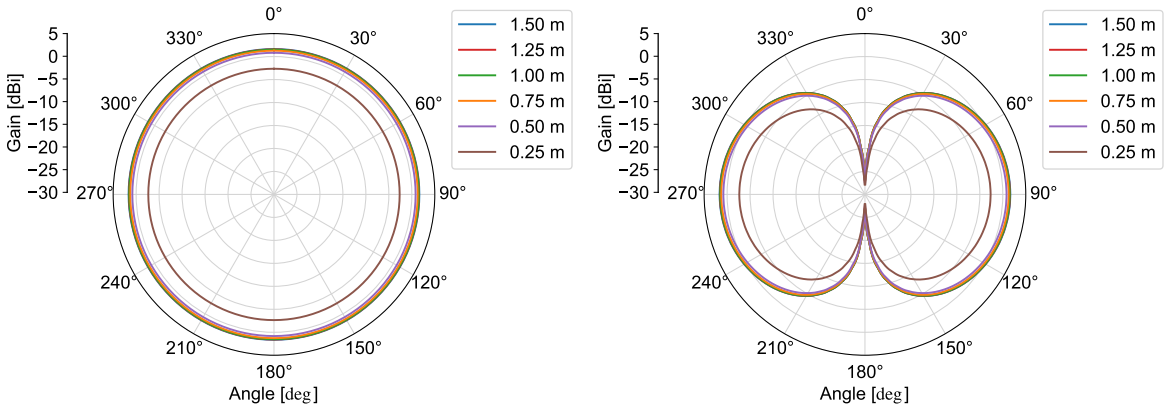

(a) Azimuth (elevation=0)

(b) Elevation (azimuth=90)

Figure 8.8: Dipole antenna directivity gain as a function of antenna size

Two key differences can be identified between the loop and the dipole. Firstly, the loop's radiation pattern is dependent on the conductor size, while the same is not true for the dipole. For the loop, the pattern in the elevation plane is rather constant across the size range. The pattern in the azimuth plane instead changes significantly as a function of antenna size, going from roughly uniform (circular) to doughnut-shaped.

Secondly, the loop displays a greater loss in directivity gain when compared to the dipole. This is not enough by itself to make a decision between the two antenna types just yet. What matters for closing the link budget is not directivity gain alone, but rather the actual radiated power. Power is a function of not just the directivity gain, but also the radiation efficiency and the sum of other system losses.

8.1.4. Loop vs Dipole: Radiated Power

In addition to directional gain (directivity), two other factors have been observed to be at play when looking at radiated power: the radiation efficiency of the conductor itself, and the efficiency of the required matching network.

The impedance of the loop and the dipole is considered first. While the pattern of resonance and anti-resonance described in subsection 3.2.2 is fairly comparable between the two antenna designs, the *type* of reactance measured is not. The loop, being more akin to an inductor, has a large amount of inductive reactance to be matched when coupled to a real source. The dipole has instead a large capacitive reactance to be matched when coupled to a real source. In practice, this means that electrically short loop antennas will require mostly capacitors in their matching network, while electrically short dipoles will require mostly inductors in their matching network. This is problematic for dipoles, as inductors have a significantly lower quality factor than capacitors, and hence dissipate a much larger amount of power as heat during normal operation.

Comparing the $1.5\,\mathrm{m}$ antennas, a reactance of around $5.8\,\mathrm{k\Omega}$ is measured for the loop compared to $-1.9\,\mathrm{k\Omega}$ measured for the dipole. The scale of the two values is similar but their sign is opposite (positive vs negative reactance). Figure 8.9 presents the reactance of both antennas at $28\,\mathrm{MHz}$ for sizes up to $1.5\,\mathrm{m}$. This is effectively the reactance which must be cancelled out by the matching network.

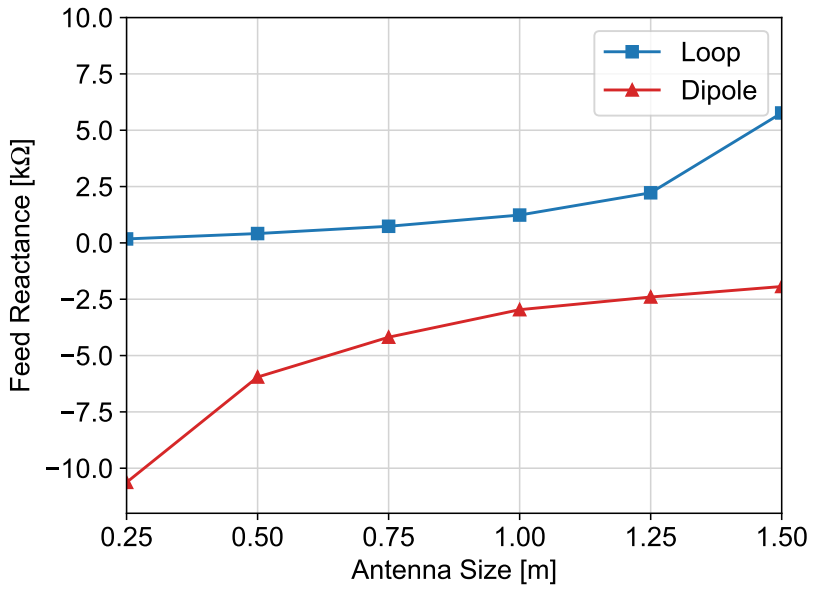

Figure 8.9: Feed reactance versus antenna size for both a loop and a dipole

As expected, the loop is purely inductive while the dipole is purely capacitive. Additionally, while as the loop grows smaller the magnitude of its reactance decreases, the opposite happens for the dipole. This means that making the loop smaller will also reduce the difference in reactance between the antenna feed and the source. Making the dipole smaller instead will increase the difference between feed and source reactance.

For both antenna types, Figure 8.10 now presents the resistive losses in the respective matching network as a percentage of the total supplied RF power ($500\,\text{mW}$) and as a function of the antenna size. A simple L-shaped matching network is used for both system with perfect coupling of $VSWR = 1.00 : 1$ at $28\,\text{MHz}$. When multiple matching paths were available, the one with the lowest dissipated power was chosen.

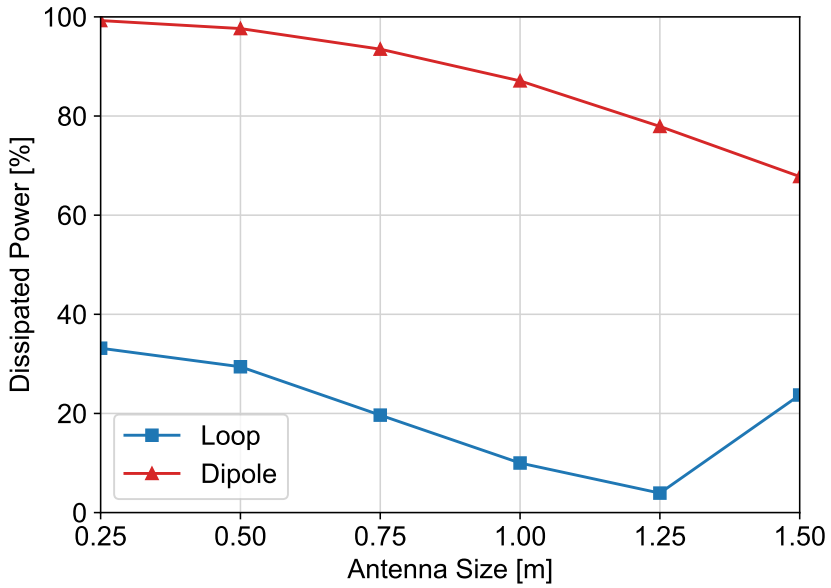

Figure 8.10: Matching network resistive losses as a fraction of the total supplied RF power

The difference is significant, with the loop's network dissipating between 3 to $30\,\%$ of the input RF power, and the dipole's network dissipating between 70 and $99\,\%$ of the input RF power. This data can be combined with the results obtained in subsection 8.1.3 to get a more complete picture of the radiative behaviour of both design options. Figure 8.11 and Figure 8.12 present the radiated power for the loop and dipole respectively for a few relevant conductor sizes.

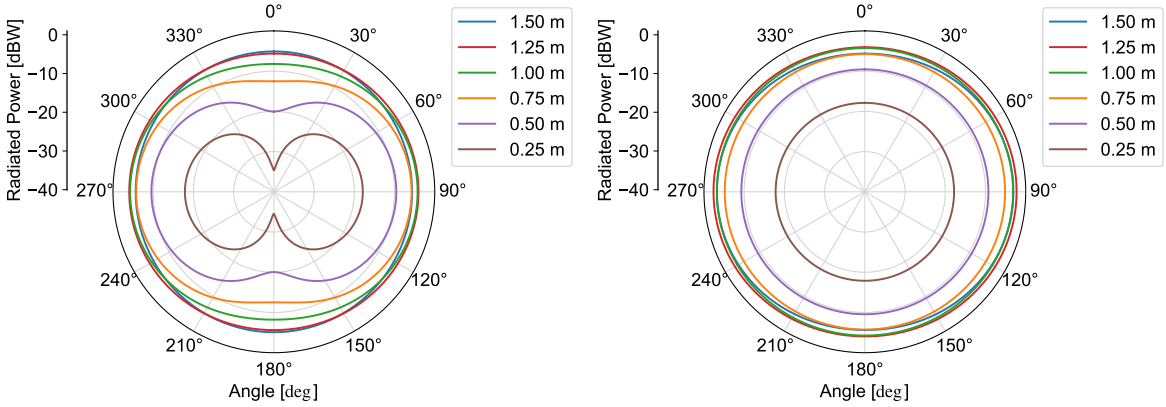

(a) Azimuth (elevation=0)

(b) Elevation (azimuth=90)

Figure 8.11: Loop antenna radiated power as a function of antenna size

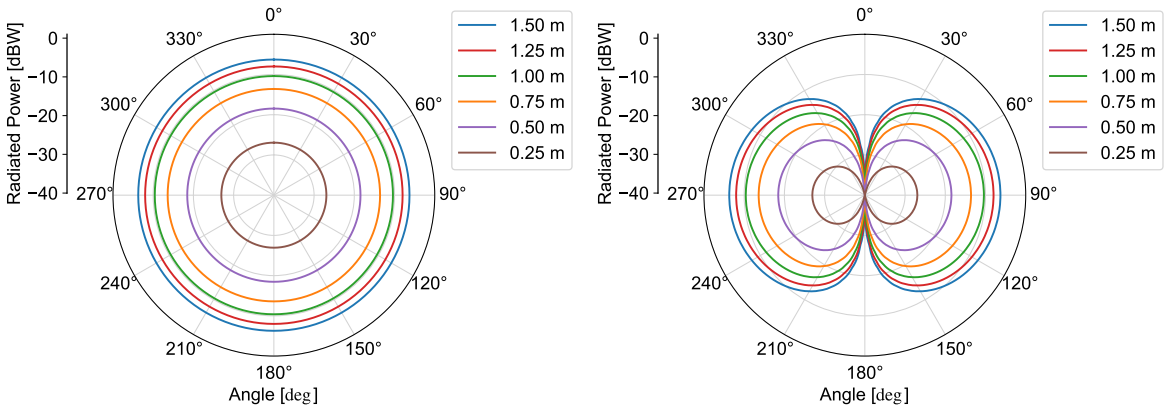

(a) Azimuth (elevation=0)

(b) Elevation (azimuth=90)

Figure 8.12: Dipole antenna radiated power as a function of antenna size

These results are now directly comparable to the outcomes of the link budget and the defined system requirements. For the 28 MHz instrument, a radiated power above -19.2 dB W (EIRP) is required to close the link budget (**REQ-LNK-10**; Table 4.6). The loop conductor is able to remain above this threshold across all directions for all sizes except for the 0.25 m diameter option. The dipole instead is not able to meet the -19.2 dB W requirement at all up to the 0.75 m long design. For the larger variants, dipoles still leave non-negligible gaps at the poles where the radiated power dips significantly below -20 dB W.

8.1.5. Final Choice

Based on the data presented, ***the loop is chosen as a more promising conductor shape to fulfil the RABSII system requirements***. The decision according to each relevant considered parameter can be summarised as follow.

1. **Bandwidth**
   Both conductor shapes have sufficient bandwidth regardless of size. As the size is decreased from the maximum allowed 1.5 m, the bandwidth of both antennas consistently decreases. While the loop initially has a larger bandwidth, its value also decreases more rapidly leaving the dipole with a bigger bandwidth at the smaller considered antenna sizes.
2. **Directivity**
   Both antennas can be considered omnidirectional, however, the dipole shows significant nulls at the opposing poles. The loop instead displays a more uniform directivity albeit with a slightly lower gain than an equivalent dipole.
3. **Radiated Power**
   Thanks to the inductive nature of loop conductors, the resistive losses incurred to match a loop antenna to a standard source are significantly lower than for a dipole. When combining the directivity and system (in)efficiencies, the loop is able to meet the required radiated power requirement for most of the considered sizes while retaining a relative uniform radiation pattern. The dipole instead in unable to meet the radiated power requirement for the majority of sizes across most of its radiation pattern rendering it effectively non-omnidirectional.

This decision is considered not only with respect to the technical performance of the two options, but also within the wider scope of the development of the RABSII instrument. As discussed in subsection 2.1.2, possible dipole deployment systems are already under investigation. Hence, regardless of the better performance, it is deemed more relevant to investigate this yet ignored design path to try to reduce the overall project development risk.

8.2. Remaining Design Choices

With the most promising antenna shape identified, the remaining aspects of the design can also be defined. To summarise, the following categories/options introduced in chapter 6 are still to be investigated.

1. **Conductor Size**
   The conductor size has been partially considered when looking at the antenna shape, it remains the 'independent variable' for the analysis. As such, no choice is made until the remaining parameters have been investigated.
2. **Conductor Cross-section**
   In order to make a choice for the conductor cross-section, RF performance is not the only relevant factor. The mechanical deployment approach is potentially much more constraining.
3. **Conductor Material**
   Similarly to the conductor cross-section, the few available options for conductor material are investigated, but a choice cannot be made until the deployment is considered.
4. **Matching Network Topology**
   A choice can be made based on the RF performance alone as the topology of the matching network does not affect the mechanical design of the system.

Excluding the conductor size, each other option is considered in detail below with respect to the relevant performance metrics.

8.2.1. Conductor Cross-section

While a final choice cannot be made, the difference in RF performance between the two options is investigated. Two loop antennas are analysed, one with a circular and one with a rectangular cross-section, see Figure 8.13 for a parametric definition of the sections.

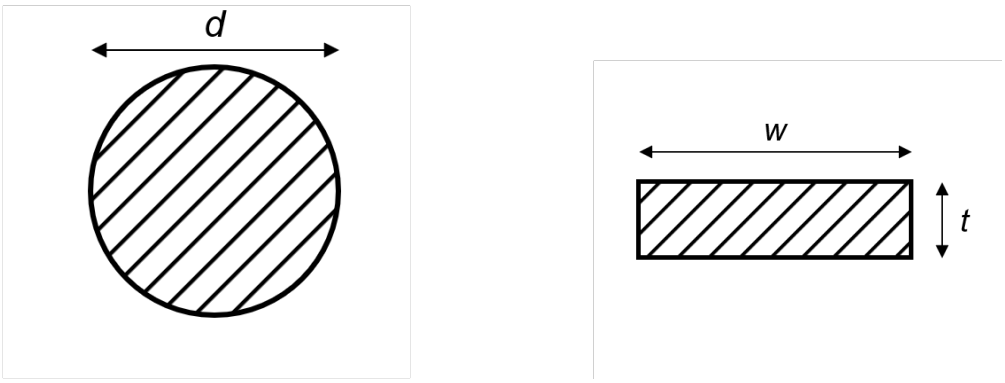

(a) Circular cross-section **(b)** Rectangular cross-section

Figure 8.13: Parametric cross-sections definitions

While the exact dimensions of both will depend on the deployment approach, an equal cross-sectional area is used for this initial comparison. A few additional variations are also analysed to understand how geometry affects radiation efficiency. Figure 8.14 presents the radiation efficiency of two conductors with identical cross-sectional area, one circular with diameter of 0.36 mm, and one rectangular with dimensions of 1x0.1 mm. A few additional cross-section dimensions are also presented to investigate the relation between cross-sectional area and radiation efficiency. PEC is used as a material for all test cases.

A few observations can be made about the results. First of all, all lines have a very similar S-shape across the domain, with a gradual initial increase followed by a sharp rise which then levels off as the efficiency approaches 1. Regarding the various cross-sections, some changes result in improvements, such as doubling the circular cross-section diameter, but some don't affect the results almost at all, such as doubling the rectangular cross-section thickness from 0.1 to 0.2 mm. To better understand what is happening, more geometrical parameters are presented in Table 8.4.

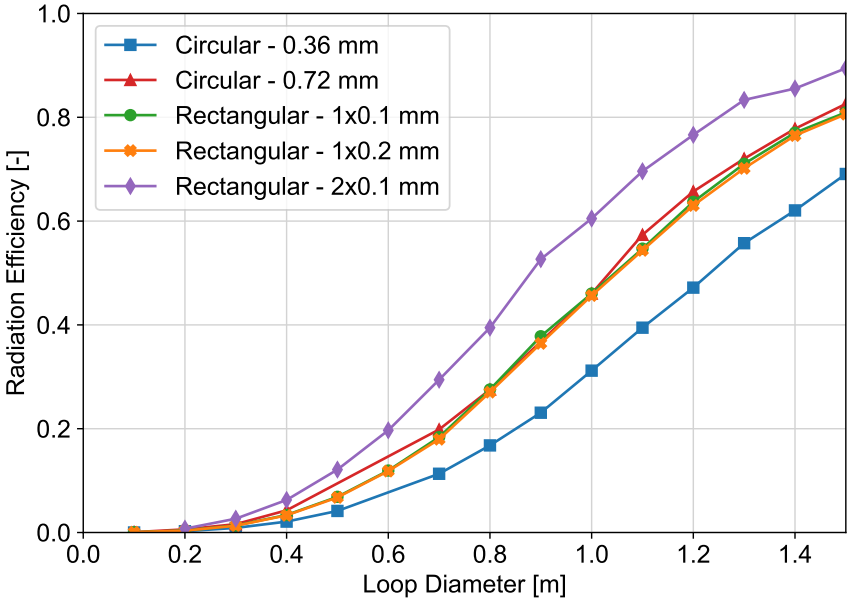

Figure 8.14: Radiation efficiency against loop diameter for various cross-sections

Table 8.4: Cross-sections geometrical parameters

Option	**Shape**	d mm	w mm	t mm	**Area** mm^2	**Perimeter** mm
1	Circle	0.36	N.A.	N.A.	0.1	1.12
2	Circle	0.72	N.A.	N.A.	0.4	2.24
3	Rectangle	N.A.	1	0.1	0.1	2.20
4	Rectangle	N.A.	1	0.2	0.2	2.40
5	Rectangle	N.A.	2	0.1	0.2	4.20

What can be noted, is that the radiation efficiency measured is directly proportional to the perimeter of the cross-section geometry, and not its area. Looking at options 2, 3 and 4, while having different shapes all have roughly the same outer perimeter. This is reflected by a nearly identical radiation efficiency throughout the entire measured domain. This behaviour can be explained by the nature of the RF currents themselves. As described in subsection 3.2.5, currents at these frequencies are not expected to travel further than a few microns to a few tens of microns deep. The current distribution is nearly fully constrained on the conductor's surface, hence why the perimeter is the determining factor in the observed performance.

With respect to the design of RABSII, the goal can be reframed to maximizing the conductor perimeter within the available volume and deployment constraints. If compatible with the deployment mechanism, thin wide strips are the preferable choice to maximise the radiation efficiency of the conductor. Within the available volume constraints, a strip no wider than 4 mm can be achieved. Realistically, 2-3 mm is as wide as a strip can be made while still allowing enough space for the rest of the mechanism components.

8.2.2. Conductor Material

The difference in RF performance between the various options is investigated. Materials are only simulated as uniform, including the conductive coatings. By ensuring sufficient coatings thickness (if coatings are used), their performance can be approximated as a uniform solid conductor anyway, so there is no need to simulate a complex composite structure. From Table 6.2 and Table 6.3, the following options are considered: spring steel, aluminium 7075, copper, and silver. Two additional materials are also considered: pure aluminium and nitinol. The former is done to investigate the performance gap between high strength aluminium alloys and pure aluminium. The latter instead is added for reference, being the material currently under investigation for the RABSII dipole deployment (see subsection 2.1.2). Radiation efficiency is presented as a function of loop diameter for all the options in Figure 8.15. A rectangular cross-section with dimensions of $1\text{x}0.1$ mm is used for all test cases.

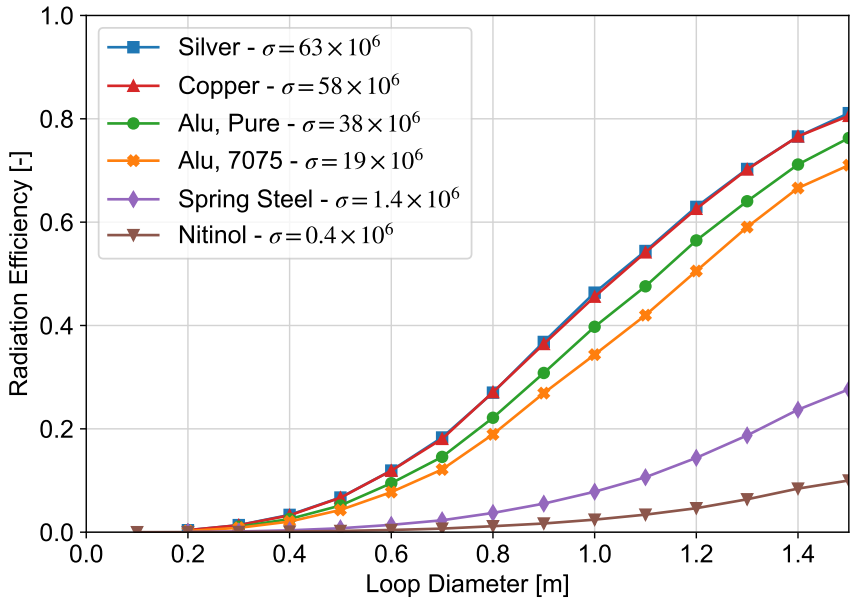

Figure 8.15: Radiation efficiency against loop diameter for various conductor materials

The efficiency of the various designs can be seen to be heavily dependent on the conductivity of the underlying material. However, as the conductivity rises, the returns are diminishing. Going from steel to aluminium 7075, there is a significant gap in efficiency, ranging from 4 dB up to 8 dB across the domain, while going from aluminium 7075 to silver, the gap is only about 0.6 dB. Thinking purely from an RF performance point of view, a good conductor like copper or silver would be preferable. When considering the deployment though, a more mechanical performant material such as aluminium 7075 or spring steel would be better. Aluminium 7075 seems to provide a good balance between good RF and good mechanical performance, but a final choice will need to be made based on the deployment approach and design. Being the mechanically most conservative option, steel is used as a baseline for performance characterisation for now. If the system requirements cannot be met with steel, upgrading to aluminium 7075 will be considered.

8.2.3. Matching Network Topology

Looking back at Figure 8.4, it is clear how the basic L-network topology is sufficient to meet the system's bandwidth requirements. Furthermore, from Figure 8.10, losses due to the matching network are non-negligible, even in the case of a loop antenna. Adding additional components would only increase those losses further reducing the RF power available for transmission. As such, the choice is made to keep an L-shaped matching network for the final design. More detailed circuit design is left as a future development path to further improve the design.

9

Design Characterisation

With a design now identified, its performance can be more precisely characterised. In order to identify at what size the design is able to fulfil the system requirements, the following performance metrics (introduced in section 7.2) are investigated as a function of antenna diameter.

1. Directivity
2. Radiated Power
3. Matching Network Efficiency
4. Available Bandwidth

Based on the design choices made in the previous chapter, the following antenna parameters are used. See Table 9.1.

Table 9.1: Chosen antenna properties summary

Parameter	**Choice**	**Justification**
Conductor Shape	Loop	See subsection 8.1.5.
Conductor Size	Undecided	Independent variable, full performance must be first characterised.
Conductor Cross-section	Rectangular; $w = 3$ mm; $t = 0.1$ mm	Better radiation efficiency than circular cross-sections for the same area. Width maxed out based on deployer volume envelope (allowing for some margins). Thickness subject to changes depending on deployment approach but has minimal effect on efficiency.
Conductor Material	Spring steel	Final choice to be made based on deployment approach, but for now steel provides the best mechanical performance at the expense of a RF performance loss. Pending investigating the deployer design, it is the most conservative option (mechanically).
Matching Network Topology	L-network	Least amount of components hence least resistive dissipation.

9.1. Directivity

Some results have already been presented in subsection 8.1.3 when it comes to the directivity of the loop antenna. This section provides a more in depth analysis of the omnidirectionality potential of a loop conductor.

An omnidirectional antenna is needed for RABSII to ensure stable signal strength at ground regardless of the relative orientation between the beacon and a ground station. This stability in the received signal however is a function of multiple system/mission aspects. Namely:

- The antenna's directivity pattern
- The satellite's attitude (and antenna mounting orientation)
- The relative position between the spacecraft and the ground station

In order, all three elements are investigated.

9.1.1. Antenna Directivity Pattern

The directivity gain for a loop antenna up to $1.5\,\text{m}$ in diameter is plotted in both the azimuth and the elevation plane in Figure 9.1.

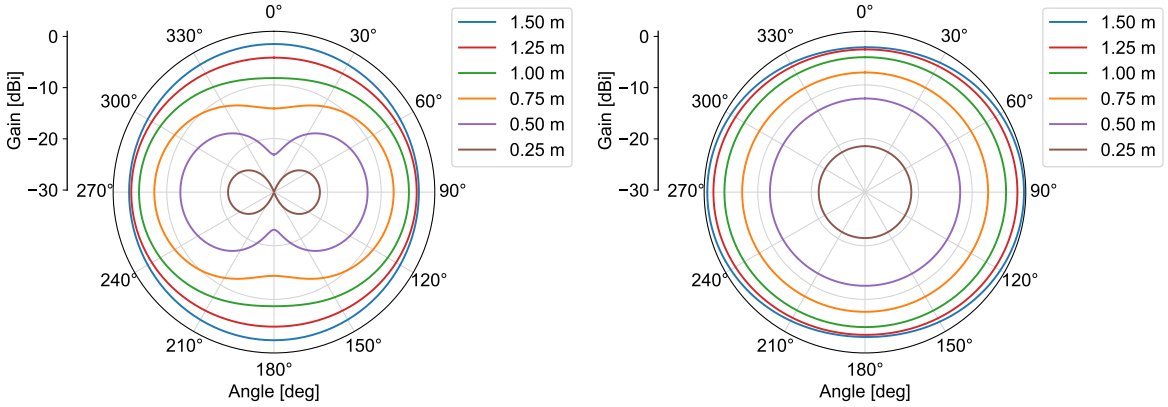

(a) Azimuth (elevation=0)

(b) Elevation (azimuth=90)

Figure 9.1: Loop antenna directivity on polar plots as a function of antenna size

As discussed in the comparison between the loop and the dipole, the pattern is observed to be very uniform for larger sizes, and progressively becomes more doughnut-shaped as the loop's diameter decreases. The same data can be plotted in a Cartesian graph to identify the signal strength variation range as a function of elevation and azimuth angle. Figure 9.2 presents the directivity gain as a function of radiation direction (angle) sweeping both the azimuth and elevation planes.

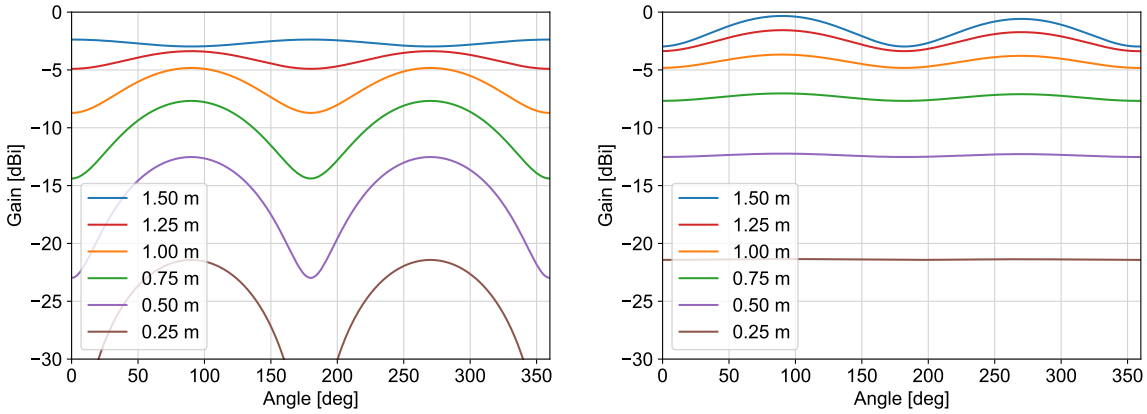

(a) Azimuth (elevation=0)

(b) Elevation (azimuth=90)

Figure 9.2: Loop antenna directivity on Cartesian plots as a function of antenna size

Much larger variations in directivity gain can be observed in the azimuth plane compared to the elevation plane. Furthermore, as the antenna size is reduced, this variation across radiation directions (angle) increases. For easier comparison, the maximum variation in gain across all angles is measured and reported as a function of antenna size for both the azimuth and elevation directions. This data is presented in Figure 9.3.

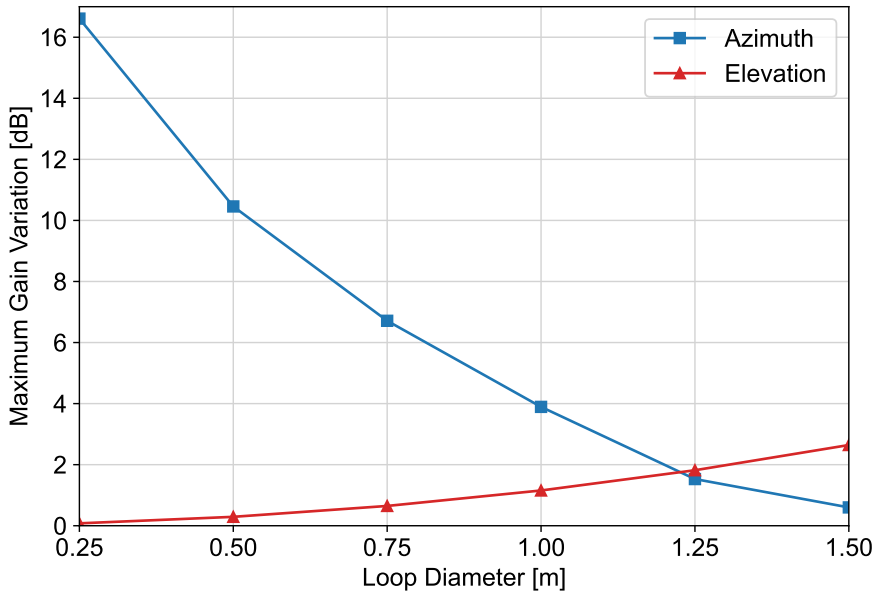

Figure 9.3: Maximum variation in directivity gain as a function of antenna size for both the azimuth and elevation directions

It is important to note that in this case, there is no need to look at the variation in radiated power separately as was done when comparing the loop and the dipole. While the absolute magnitudes of directivity or power gain may differ, the variation in radiated power gain is always equal to the variation in directivity gain across all angles.

Looking at Figure 9.3, while the maximum variation increases with smaller antenna sizes across the azimuth, the opposite is true in the elevation plane. At the cross-over point, at a loop diameter of about 1.25 m, the maximum variation in gain is equal across both the azimuth and elevation direction at a value of about 2 dB. Depending on the mounting location on Delfi-Twin, as well as the spacecraft's attitude and position, the signal strength measured at ground can be expected to vary with a magnitude equal to the numbers in Figure 9.3.

9.1.2. Satellite Attitude and Antenna Orientation

Two factors play a role when considering the physical orientation in space of the RABSII beacon: the attitude of the host satellite platform, and the relative mounting orientation of the antenna onto the satellite.

Looking at the attitude of Delfi-Twin first, while it is not actively controlled, its behaviour has been modelled and estimated. Delfi-Twin is expected to keep its long axis roughly aligned with the velocity vector with the angle between the two oscillating by around $\pm 20^{\circ}$. The satellite is also expected to rotate about its long axis at a rate between 5 and $10\,^{\circ}\,\mathrm{s}^{-1}$. Combining the two effects results in a procession of the satellite's long axis around the velocity vector at a rate of about $1\text{-}5\,^{\circ}\,\mathrm{s}^{-1}$. This behaviour can be seen in Figure 9.4, preliminary data courtesy of the Delfi-Twin team.

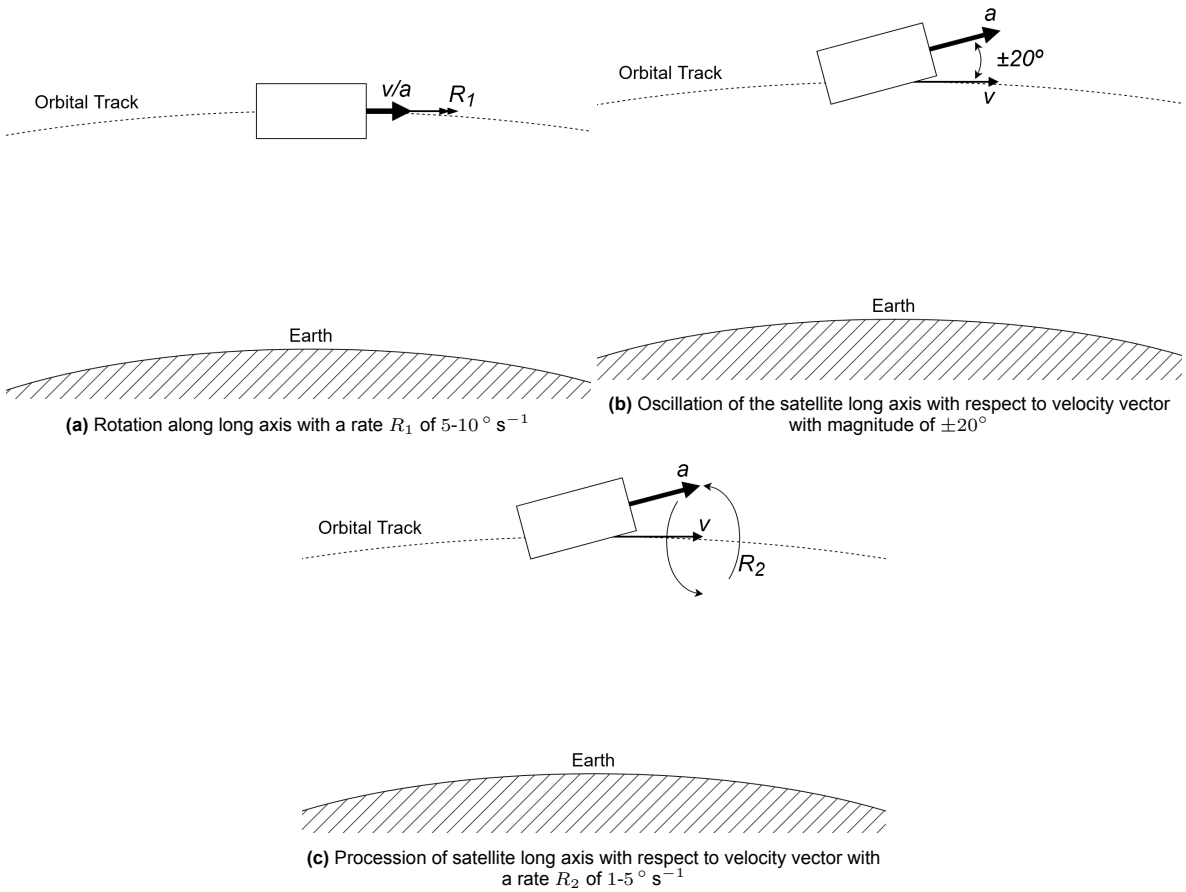

(a) Rotation along long axis with a rate R_1 of $5\text{-}10\,^{\circ}\,\mathrm{s}^{-1}$

(b) Oscillation of the satellite long axis with respect to velocity vector with magnitude of $\pm 20^{\circ}$

(c) Procession of satellite long axis with respect to velocity vector with a rate R_2 of $1\text{-}5\,^{\circ}\,\mathrm{s}^{-1}$

Figure 9.4: Attitude motion of the Delfi-Twin satellite; velocity vector v; Delfi-Twin long axis vector a

Based on the data in Figure 9.4, the antenna may experience a maximum oscillation of $\pm 20^{\circ}$ with respect to the satellite's nadir direction, and a full 360° rotation about the satellite's long axis.

In addition to the satellite orientation, the loop may be mounted at any orientation (allowing for mechanical and interface constraints) onto Delfi-Twin. The decision on how the RABSII instrument is mounted aboard the spacecraft needs to be considered with respect to the space availability on the bus itself. It will hence be discussed in more detail together with the deployment approach at a later point of this work.

9.1.3. Spacecraft-to-Ground-Station Relative Orientation

Identifying the relative orientation between a ground station and the spacecraft is straight forward. Based on the link budget assumptions presented in subsection 4.2.1, a minimum elevation angle of $10°$ above the horizon is expected. This is the lowest the satellite, and hence the radio beacon, will be above the horizon while transmitting to a ground station. At the highest point, in cases where the ground track passes exactly over the receiving ground station, the satellite will be exactly vertical above the receiving antenna. This results in a variation of $\pm 80°$ in observed satellite orientation when ignoring spacecraft attitude changes. Figure 9.5 presents the geometry of these two cases which set bounds on the relative orientation between the ground station and the passing spacecraft.

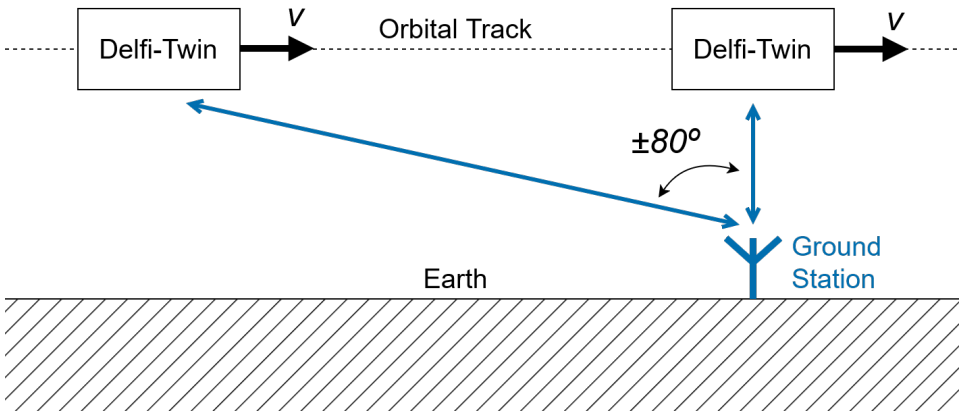

Figure 9.5: Angle range between the satellite and the ground station, link in blue

In the simplest case, the satellite is perfectly overhead and its long-axis vector is perfectly aligned to its velocity vector. Let's assume that in this case the angle between the beacon and the ground station is zero. From this baseline, considering the combined effects of changing satellite attitude and motion along the orbital track, over a single overhead pass this angle is expected to vary stochastically within the range $\pm 100°$ ($\pm 20°$ due to the changing satellite attitude and $\pm 80°$ due to the motion along the orbital track). This means that nuanced discussions about the mounting orientation of the antenna onto the satellite are meaningless, as pointing orientation with respect to a ground station is effectively randomised across multiple passes.

9.2. Radiated Power

Just as for the directivity, the radiated power is plotted in both the azimuth and elevation planes in Figure 9.6.

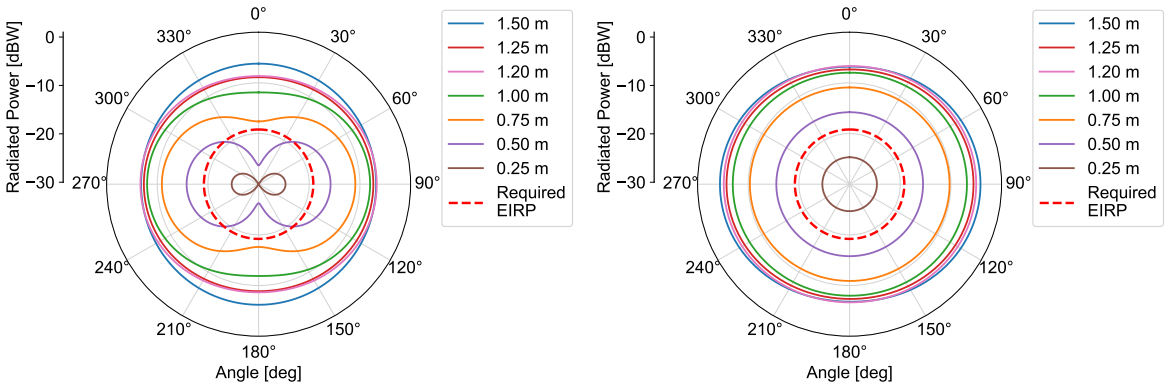

(a) Azimuth (elevation=0) **(b)** Elevation (azimuth=90)

Figure 9.6: Loop antenna radiated power on polar plots as a function of antenna size

The same data can be plotted on a Cartesian plot. This can be found in Figure 9.7.

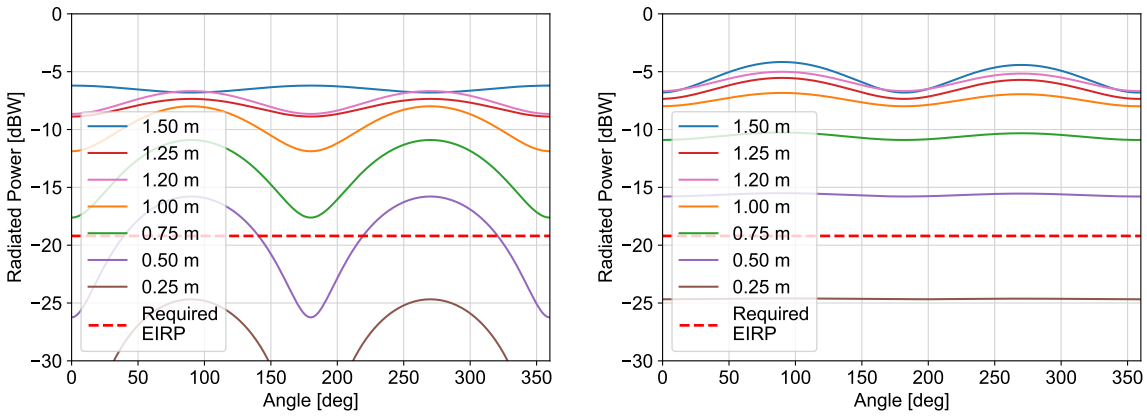

(a) Azimuth (elevation=0) **(b)** Elevation (azimuth=90)

Figure 9.7: Loop antenna radiated power on Cartesian plots as a function of antenna size

On both sets of figures, the minimum required EIRP is overlaid for context. By looking at the data, the considered spring steel conductor would be able to close the link budget in any direction starting from a diameter of around 0.75 m. Albeit at this size, maximum variations in signal strength between weakest and strongest points are expected to be around 6 dB across all planes.

In addition to the regular intervals of 0.25 m in the diameter variations, data is also presented for a loop with diameter of 1.2 m. Rather unexpectedly, even being smaller, the radiated power for this line is greater than that of a loop 1.25 m in diameter. This is due to an inflection point in the losses attributed to the matching network. The significance of this point is discussed in the next section.

9.3. Matching Network Efficiency

Resistive losses in the matching network are presented for various loop diameters in Figure 9.8.

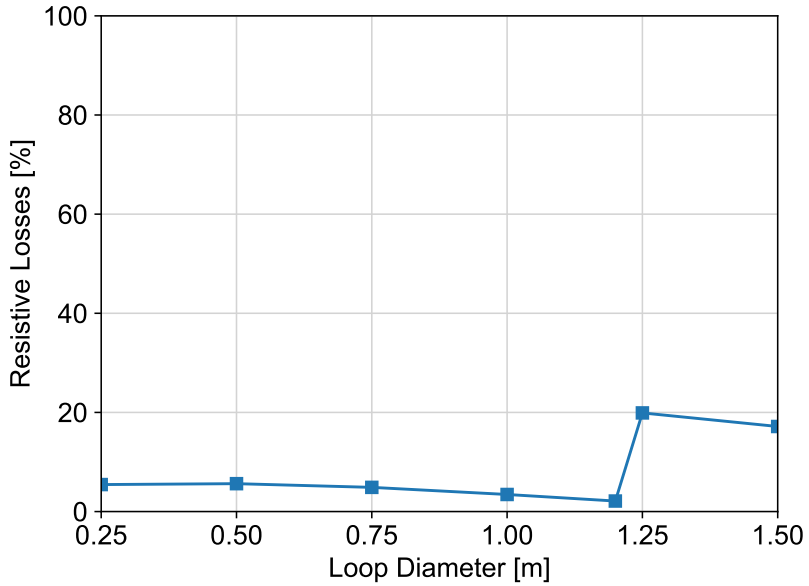

Figure 9.8: Matching network resistive losses as a fraction of the total supplied RF power

Of particular interest is the sharp increase in lost power going from $1.20\,\text{m}$ to $1.25\,\text{m}$ in diameter. As previously discussed, loop antennas are inductive, hence have an inductive reactance. This means that in general, they require primary capacitors to match the antenna feed impedance to a standard $50\,\Omega$ source. However, there is an exception to this 'rule'. If the resistance of the loop antenna to be matched is greater than that of the source, an inductor becomes necessary to impedance match. Figure 9.9 presents the impedance of the loop antenna as a function of diameter.

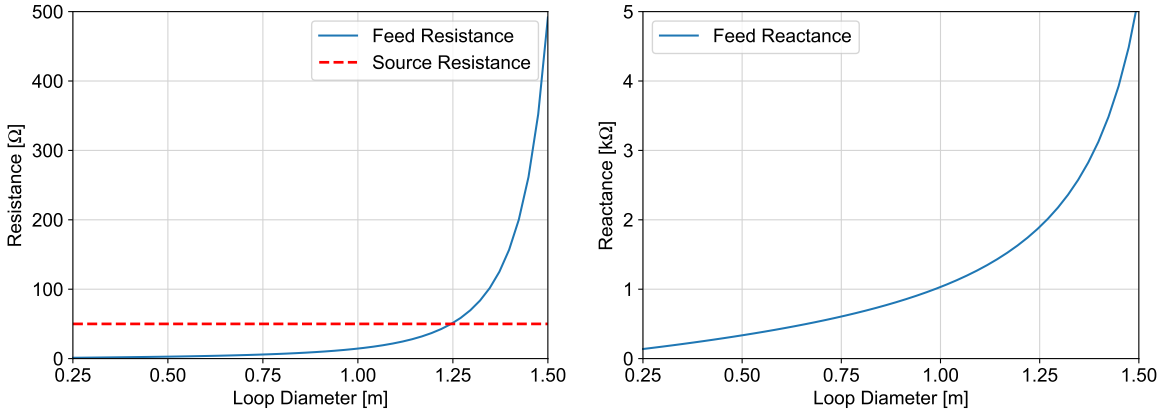

(a) Resistance of loop feed and source

(b) Reactance of loop feed

Figure 9.9: Feed impedance of the loop antenna as a function of diameter

As can be clearly seen from Figure 9.9, the loop feed resistance becomes larger than the source resistance for all diameters larger than $1.25\,\text{m}$. This coincides with the sharp increase in lost power in the matching network. For the final RABSII beacon design, it is hence advisable not to exceed a loop diameter of $1.25\,\text{m}$.

9.4. Available Bandwidth

Figure 9.10 presents the bandwidth for the loop antenna as a function of the loop diameter for return losses below -10 dB, -20 dB, and -30 dB. The required bandwidth of 2.5 kHz (**REQ-SCI-04**; Table 4.6) is overlaid for context.

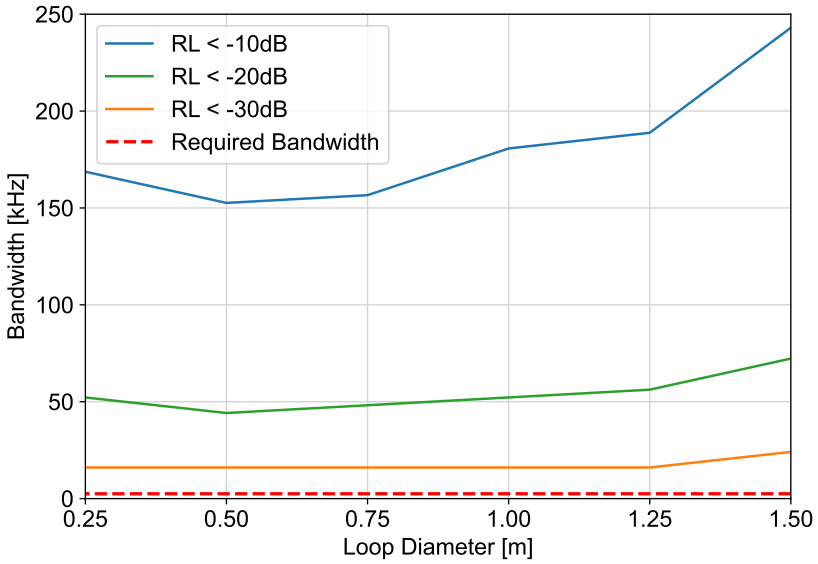

Figure 9.10: Bandwidth as a function of loop diameter for various return loss thresholds

While it would be simple to rule out bandwidth as a constraining factor and on with the design, the real picture is more complicated. When going from theoretical analysis to practical systems, the limitations and variability of real electronic components greatly affects the final performance. A few aspects must be considered and investigated when it comes to antenna bandwidth:

1. Real availability of capacitor/inductor values
2. Manufacturing and thermal tolerances of real capacitors/inductors

Number one refers to what is available for purchase. A perfect matching network may require a 10.274 pF capacitor, but in reality only standard values such as 10.2 and 10.3 pF may be available. The same goes for inductors. The second point instead refers to the unavoidable variability of the capacitance/inductance values of real components due to tolerance. Both must be taken into account given their non-negligible effects on performance.

These two aspects are investigated in the following sections before presenting a summary/mitigation strategy to get around these limitations.

9.4.1. Real Components Availability Limitations

The capacitors and inductors used up until now to match the loop antennas analysed have values in the following ranges. Capacitors values range between 4.5 pF and 750 pF, inductors values instead range between 8.5 µH and 10 µH. Both ranges are well covered by commercial suppliers. The component catalogue offered by **muRata**[1] is considered from here onwards due its large selection, but many other commercial suppliers exist with similar products offered.

MuRata offers ceramic capacitors with capacitance ranging from 0.1 pF up to 330 µF. This type of capacitors is most suited for RF applications due to their low manufacturing tolerances and good thermal stability. Inductors for RF applications and high frequency circuits are instead offered ranging from 0.1 nH up to 10 µH. This however is less relevant as the decision has been made in section 9.3 to avoid sizes requiring inductors for matching.

[1] https://www.murata.com/en-eu/products/capacitor/ceramiccapacitor

While single capacitors with the exact desired capacitance are likely not available, the ones available can easily be combined to obtain a new 'composite' component with a specific capacitance. This new component made by combining multiple individual capacitors is here referred to as a 'composite capacitor'. By combining capacitors in either series or parallel, a new composite capacitor can be created with the capacitance needed to match the antenna to the source. A simple python tool is created to achieve this task. The desired exact capacitance is provided as input. The script then recursively combines capacitors from the available catalogue to attempt to achieve a capacitance as close as possible to the desired input. The code can be found in Appendix A.

To illustrate the process, a loop with a diameter of 0.75 m is considered as an example. The same process can be repeated for any other antenna size, but only one example is here presented to demonstrate the process. The feed impedance of the 0.75 m diameter loop is measured at $Z_L = 5.905 + 606.3j\Omega$ at 28 MHz. A balanced matching network to feed the double-ended loop, this network is presented in Figure 9.11. Three capacitors, two with values C_1 =4.8185 pF and one with value C_2 =302 pF are required for a perfect match at $VSWR = 1.00 : 1$.

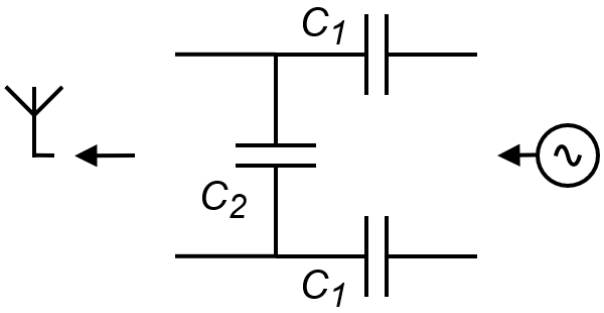

Figure 9.11: Ideal required matching network; C_1 =4.8185 pF; C_2 =302 pF

These are very specific capacitor values and are not directly available. Running the python tool on the muRata ceramic capacitor catalogue yields the following composite capacitors:

- C_1: Two capacitors in series of capacitance 9.3 pF and 10 pF with an effective combined capacitance of 4.8187 pF. Delta of 0.003% from the desired capacitance C_1.
- C_2: Two capacitors in series of capacitance 430 pF and 1000 pF with an effective combined capacitance of 300.7 pF. Delta of 0.4% from the desired capacitance C_2.

Swapping the capacitors in the ideal network for the composite ones just defined yields a new lowest $VSWR = 1.01 : 1$. The associated bandwidth suffers no measurable change, and the radiative matching network losses change by an entirely negligible 0.01 %.

Repeating the same process for other antenna sizes shows a similar pattern, with the composite capacitors often being less than 0.01 % away from the desired target and no significant changes in either bandwidth or matching network efficiency.

9.4.2. Real Components Manufacturing and Thermal Tolerances

Both manufacturing and thermal tolerances are directly specified in the components data sheet on the catalogue. For ceramic capacitors, the manufacturing tolerance ranges from ± 0.05 pF for capacitance values below 10 pF, to ± 1% for capacitance values between 10 pF and 1000 pF. Thermal tolerances are instead provided as maximum possible variation in capacitance as a function of temperature change, the unit used is change in parts per million per degree (ppm/ºC). For all capacitors considered in muRata's catalogue, this thermal stability value is equal to ± 30 ppm/ºC measured at 25°C. Based on estimates directly from the Delfi-Twin team for the expected space environment, the components' maximum temperature variation should not exceed $\pm 100^{\circ}$C from equilibrium. This corresponds to a thermal tolerance of only ± 0.3% from the rated value.

The components' manufacturing and thermal tolerances are integrated into the composite capacitor python tool. When requesting a composite capacitor of a certain value, the maximum variation from the reported composite capacitance is provided as a total cumulative tolerance.

Going back to the real matching example for the 0.75 m diameter loop introduced in subsection 9.4.1, the tolerances for the composite capacitors in the matching network are computed. This results in the following values:

- $C_{1,composite} = 4.8187 \pm 0.0511$pF
- $C_{2,composite} = 300.7 \pm 3.9091$pF

This corresponds to a range of ± 1.06% and ± 1.3% respectively. While not negligible, this is relatively small considering both temperature and manufacturing tolerances are accounted for. While small, given the narrow bandwidth of the antenna system, small variations in the matching network have large effects on the resonant frequency of the system. To investigate how severe this change is, the loop matched impedance is plotted on a smith chart for frequencies ± 250 kHz around the central transmitting frequency of 28 MHz. This can be seen plotted as a blue sweep in Figure 9.12. The matched impedance for the loop is also plotted for the minimum and maximum possible tolerance values which can be expected (for all matching network components combined). These two extremes can be seen plotted as red crosses in Figure 9.12. Lastly, for context, the impedance circle for a return loss below -10 dB is plotted as a red dashed line. All impedance values within this circle will result in an return loss below -10 dB.

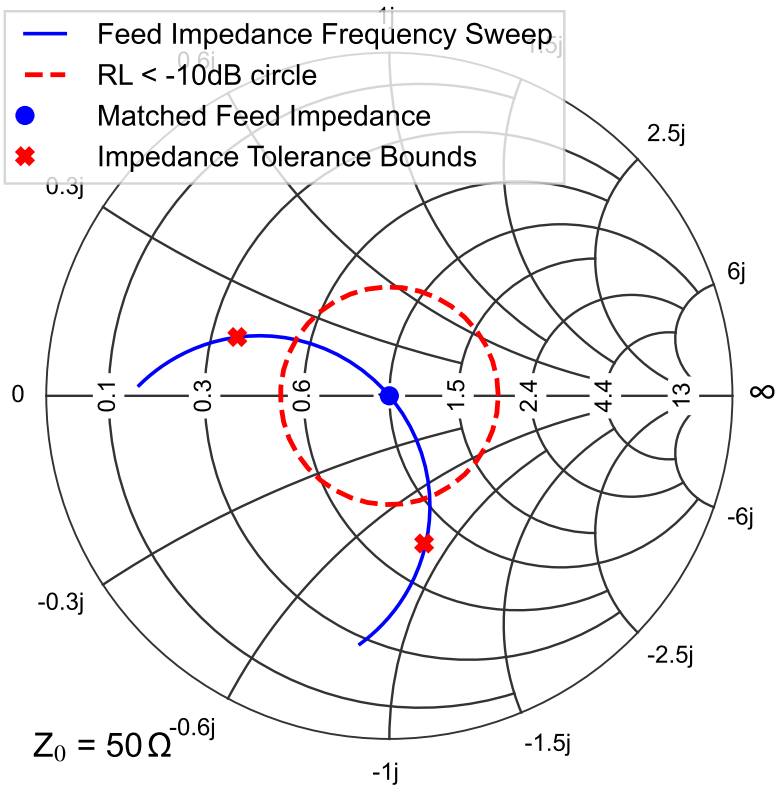

Figure 9.12: Matched impedance (blue) and expected impedance at the edged of the matching network capacitor tolerance range (red crosses)

As can be seen, in the case capacitor values change by most, or the entire, specified tolerance range, the system will no longer be able to effectively transmit on the 28 MHz frequency. This behaviour can be better understood by plotting the return loss as a function of frequency for both the matched case and the components' tolerance bounds. This can be seen in Figure 9.13.

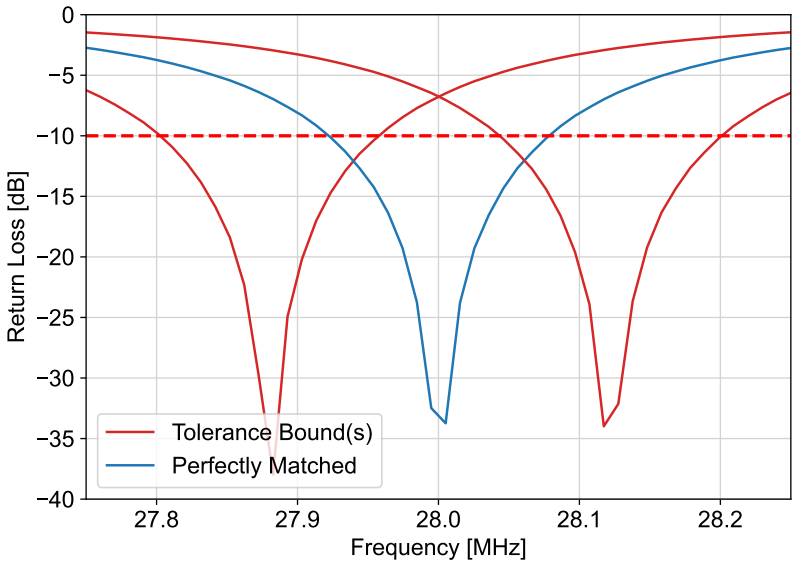

Figure 9.13: Return loss as a function of frequency for a perfectly matched system (blue), and for a system with matching network capacitance variation equal to the maximum tolerance range (red)

Based on the matching network capacitors manufacturing tolerances, the system may become unmatched at 28 MHz. However, shifting the transmitting frequency up or down slightly returns the system to a large usable bandwidth.

It must be noted that while the analysis is only presented for the 0.75 m diameter loop, the results are expected to be applicable to all other sizes too (between 0.75 and 1.5 m diameter loops). This is because increasing the loop diameter would translate into an increased available bandwidth, as was reported in Figure 9.10. With the same component tolerances but a wider bandwidth, the overlap between the tolerance bounds and the perfectly matched system (in Figure 9.13) is expected to increase. This makes tuning easier, if not potentially unnecessary.

9.4.3. Bandwidth Limitations Mitigation Strategies

As investigated, the bandwidth of the loop antenna is more than sufficient to meet the transmission demands. Furthermore, while very specific capacitor values are needed to achieve an efficient load-to-source matching, commercial components can be combined to effectively achieve a nearly perfect match. Regarding manufacturing and thermal tolerances, changes in capacitance close to the entire tolerance range would degrade the coupling efficiency between the antenna and the source to unusable levels. This is not acceptable.

The issue can be mitigated by looking back at Figure 9.13. While the extremes in impedance are above the required -10 dB return loss range, the frequency sweep shows that there is always a frequency at which an efficient coupling can be achieved. Knowing that the plotted sweep is only ± 250 kHz around the central frequency of 28 MHz, a frequency within this range exists at which sufficient bandwidth is available. Hence, the problem can be mitigated by periodically checking at which frequency the coupling is most effective, and adjusting the central transmitting frequency in response. Given that the majority of the tolerance range comes from the specified manufacturing tolerances (and is hence fixed through the payload's lifetime), this 'tuning' process can mostly be done during spacecraft commissioning or on ground before launch. If done in space, a tone can be transmitted sweeping across frequencies around 28 MHz repeatedly to identify at which frequency reception is strongest. To adjust for system changes, this process can be repeated periodically depending on operational constraints.

To summarise, while bandwidth is not a concern directly, the narrow bandwidth properties of electrically short antennas do add complications to the operations of the RABSII instrument. An initial (and potentially periodic) 'tuning' to identify the most effective transmission frequency is required to ensure efficiency coupling to the loop antenna. While data for the 0.75 m diameter loop has been presented as reference, the same concerns and considerations apply to all sizes up to 1.5 m in diameter.

9.5. Size Decision

Based on the presented RF performance, a decision on the size (or a range of sizes) of the loop antenna can be made. Constraints on size originating from all the considered performance metrics are summarised below.

- **Directivity**
  Antenna-to-ground orientation is effectively randomised regardless of instrument mounting angle (onto Delfi-Twin) due to a combination of the satellite's orbital motion and uncontrolled attitude variations. Picking a loop antenna with a dimeter of just below 1.25 m minimises the gain difference across all axes and achieves a maximum gain variation of 2 dB. To remain below 6 dB of gain difference between any two axes, the diameter of the loop must be greater than 0.75 m.

- **Radiated Power**
  Loops with a diameter greater than 0.75 m are sufficient to close the link budget while transmitting in any orientation.

- **Matching Network Efficiency**
  To avoid requiring inductors, and associated high resistive losses, the loop diameter should be smaller than 1.25 m.

- **Available Bandwidth**
  While the larger the better, all antenna sizes should have sufficient bandwidth to close the link budget. All loop diameters will require initial tuning (and potentially periodic) to achieve the presented performance. Having a smaller bandwidth to begin with, smaller loops are more sensitive to changes in the matching network capacitance and hence require more careful tuning.

In conclusion, a lower bound of 0.75 m and an upper bound of 1.25 m is identified for the loop diameter.

9.6. SimNEC and Ansys Electronics Validation

In order to have confidence in the results presented, there needs to be confidence in the simulation models used to generate the data itself. As mentioned, two software packages have been used for the presented analysis: SimNEC and Ansys Electronics.

Ansys electronics (and the Ansys software package in general) is one of the most commonly used software packages when it comes to fields and electronics simulation. It is a widely used commercial software package which has been thoroughly validated against real world data [37]. SimNEC instead, while not yet an established software package its far-fields and general analysis capabilities rely on the tried-and-tested NEC engine. More specifically, for the simulations presented, the NEC-2 engine. The NEC-2 engine has been thoroughly validated against real world data, and has been used for decades to simulate antenna behaviour with a high degree of fidelity [12].

Given the relatively simple configurations analysed, the results presented are expected to be valid with a degree of accuracy sufficient for this analysis. Simple conductor shapes, uniform conductor materials, the absence of imperfect grounds, and a free-space environment remove most of aspects which may raise concerns on the validity of the simulations. Regardless, a few key figures and results are obtained with both software packages to observe the similarities and the differences between the performance of the two. An identical 1 m diameter loop is used as input for all simulations. An ideal conductor (PEC) with a circular cross-section 10 mm in diameter is simulated in free space with the following results.

Firstly, looking at impedance, the values for resistance and reactance for a $1\,\mathrm{m}$ diameter loop are plotted in Figure 9.14. The differences between the Ansys and the SimNEC results are minimal. The behaviour of the curves is essentially identical, while the magnitudes differ by about $10\,\%$ or less across the entirety of the relevant domain.

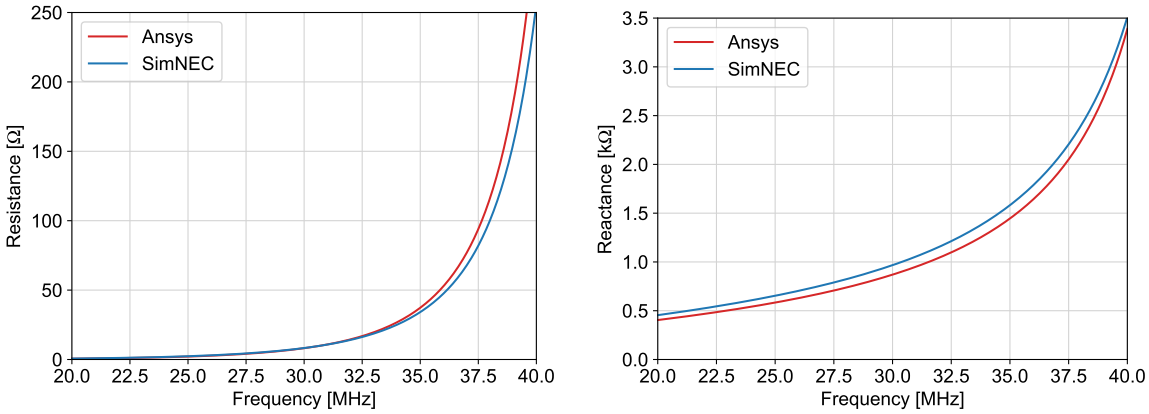

(a) Resistance **(b)** Reactance

Figure 9.14: Loop feed impedance comparison between Ansys and SimNEC

Secondly, the radiation efficiency of the two conductors is examined. Figure 9.15 presents the radiation efficiency obtained with both Ansys and SimNEC across a range of loop diameters. Note that the conductor material is switched from PEC to aluminium ($\sigma = 38 \times 10^6 \mathrm{S\,m^{-1}}$) when evaluating radiation efficiency. The difference between the figures obtained with SimNEC and Ansys is nearly negligible never exceeding about $5\,\%$ of the total value.

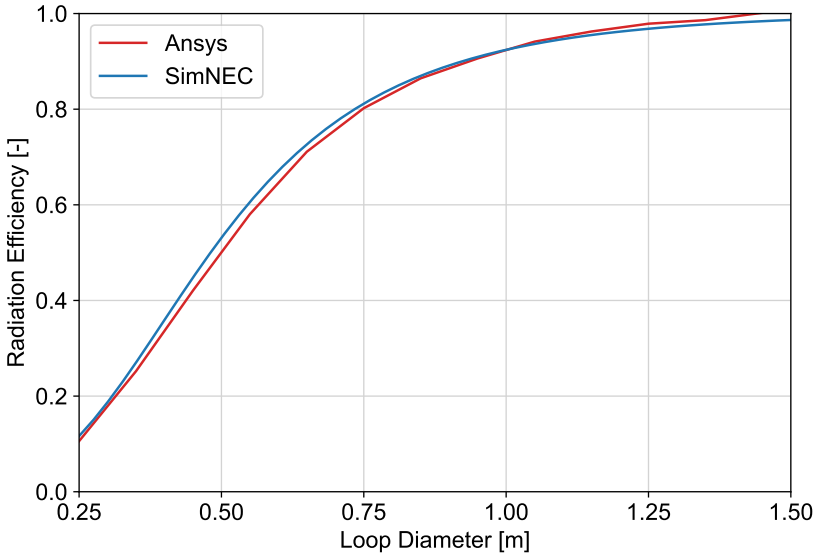

Figure 9.15: Radiation efficiency comparison between Ansys and SimNEC

Lastly, the radiation pattern is compared. More specifically, the directivity pattern obtained with both software packages is presented over a Cartesian plot as a function of the direction angle in Figure 9.16.

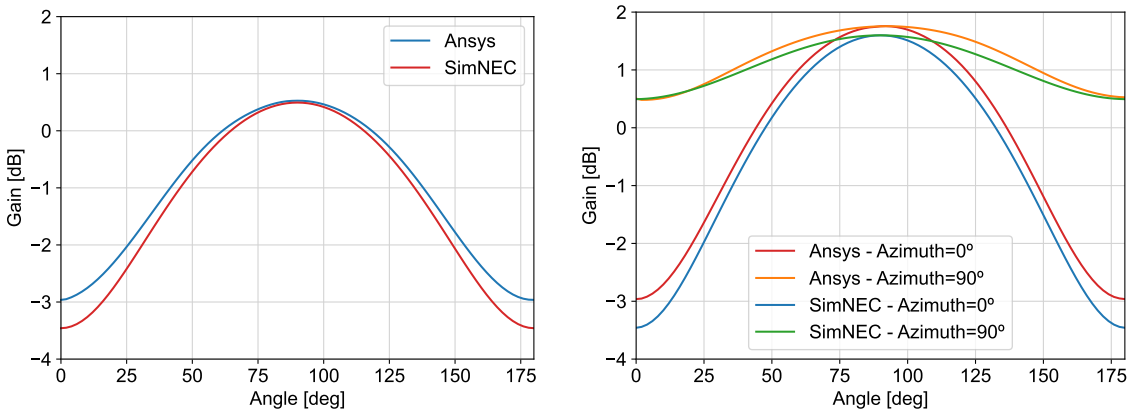

(a) Azimuth pattern; for elevation of 0°

(b) Elevation pattern; for elevations of 0° and 90°

Figure 9.16: Directivity gain comparison between Ansys and SimNEC

Three directions are considered: varying azimuth angles at an elevation of 0°, and varying elevation angles for azimuths equal to 0° and 90°. The maximum variation between the Ansys and SimNEC results never exceeds 0.5 dBi. The mean difference in gain across the two data sets (Ansys and SimNEC) ranges between 0.1 dBi and 0.3 dBi depending on the direction considered. While not zero, these differences are very small in magnitude and are not significant enough to change any of the outcomes presented in previous sections.

Overall, the two software packages used, Ansys and SimNEC (based on the NEC-2 engine), are capable of producing results comparable in both magnitude and shape. This is remarkable as they are based on completely different numerical methods: a mesh based approach for Ansys, and the method of moments for NEC-2. The findings in this sections are considered sufficient to validate the data presented covering the RF performance of the RABSII antenna.

10

Summary of Key Outcomes and Decisions

This second part of the report focusses on the second phase of the project and mainly delves into investigating answers to the second research question posed in section 2.3: ***To what extent can the antenna be downscaled compared to the currently proposed half-wave dipole while still meeting the RF requirements of the science case?***

The antenna design space has first been presented in chapter 6, where a few relevant design dimensions are identified. Secondly, the approach to making choices and characterising antenna RF performance was briefly discussed in chapter 7. Next, choices were made for all identified design dimensions in chapter 8. Lastly, the RF performance of the chosen design was characterised in chapter 9.

The following key choices were made.

- A loop antenna seems like the most promising option to fulfil the RABSII instrument science objectives.
- Spring steel should have sufficient RF performance to close the link budget, and is hence chosen as the prime candidate for the conductor material.
- A rectangular cross-section is preferred over a circular one due to the better radiation efficiency.
- An L-shaped balanced matching network should be able to fulfil the defined system requirements.
- The diameter of the loop antenna should be larger than 0.75 m but smaller than 1.25 m to meet the defined system requirements.
- Based on the results obtained for the 28 MHz instrument, the loop antenna for the 50 MHz instrument should have a diameter roughly between 0.42 m and 0.7 m to deliver similar RF performance. Do note that a lower radiated power is actually required for the 50 MHz instrument, so this size range is expected to be smaller.

Part III:

Demonstrator Construction and Testing

11

Antenna Deployment Conceptual Design

With a clear definition of the RABSII payload radio beacon antenna from Part II, the conceptual design of the deployer itself is defined here. The chapter begins with a description of the general deployer constraints in section 11.1. This is followed by an overview of the interface available aboard Delfi-Twin in section 11.2, a summary of the key design options in section 11.3, and the general design decisions in section 11.4. Lastly, a summary of the options and decisions made is presented in section 11.5

11.1. Deployment Constraints

In addition to the system requirements presented in section 4.3, a additional design constraints originate from the antenna design directly. These constraints can be formalised as follows.

1. The deployer design must be flexible enough to accommodate for loop antennas with a diameter ranging continuously from 0.75 m to 1.25 m.
2. A deployer design able to accommodate a loop antenna with a thin rectangular cross-section (a thin strip) is preferable.
3. A deployer design able to maximise the available width for the conductor strip is preferable (remaining within the overall payload envelope volume constraints; **REQ-SAT-07**, Table 4.6)

While these are not hard requirements, they do impact the performance and development risks associated with the project. The first constraint comes from the expected variability of the exact antenna dimension. When considering only the 28 MHz instrument, the final loop diameter may vary between the range defined in chapter 10, hence between 0.75 and 1.25 m. When instead considering both instruments, the 28 and 50 MHz variants, the latter is expected to be almost half the size of the former for the same performance, based solely on the difference in transmission frequency. It is hence important that the design presented can accommodate for these changes at a later stage of the instrument development without requiring a complete redesign of the system.

Regarding the second and third constraints, these are more performance specific. While a circular conductor would also meet the system requirements, a wide thin strip delivers better performance for the same diameter and cross-section. The design of the deployer is hence tailored around trying to deploy this antenna geometry.

11.2. Available Interface to Delfi-Twin

To begin the design of the deployer, the available interfaces to Delfi-Twin are defined. Figure 11.1 presents a simplified block CAD (Computer-Aided Design) model of Delfi-Twin. Two configurations are presented. Firstly, in Figure 11.1a the spacecraft in the stowed configuration is presented with the four wings folded flat against the main bus body. Figure 11.1c instead presents the spacecraft with wings in the fully deployed configuration, opened outwards by $180°$ when compared to the stowed configuration. As introduced in section 2.2, the angle of the wings is variable within a narrow range to allow for figure drag control. The angle of the wings is measured from the fully deployed state.

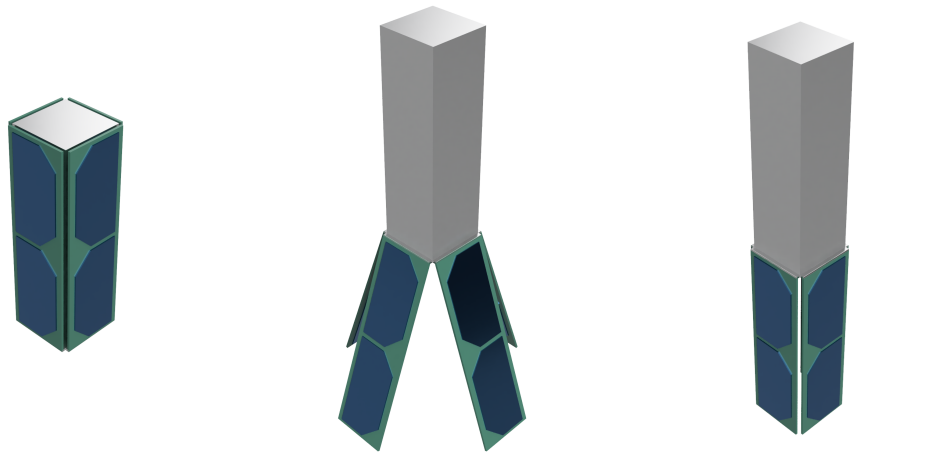

(a) Stowed configuration (wing angle: $180°$)

(b) Partially deployed configuration (wing angle: $20°$)

(c) Fully deployed configuration (wing angle: $0°$)

Figure 11.1: Delfi-Twin spacecraft various wing configurations

While the space within the bus is fully occupied by the primary mission hardware, some space on the wings is available for the RABSII deployer. Each wing houses solar cells both on the inner and outer surfaces (two per surface). Figure 11.2 shows an enlarged view of the solar cells on the inside and outside of one wing.

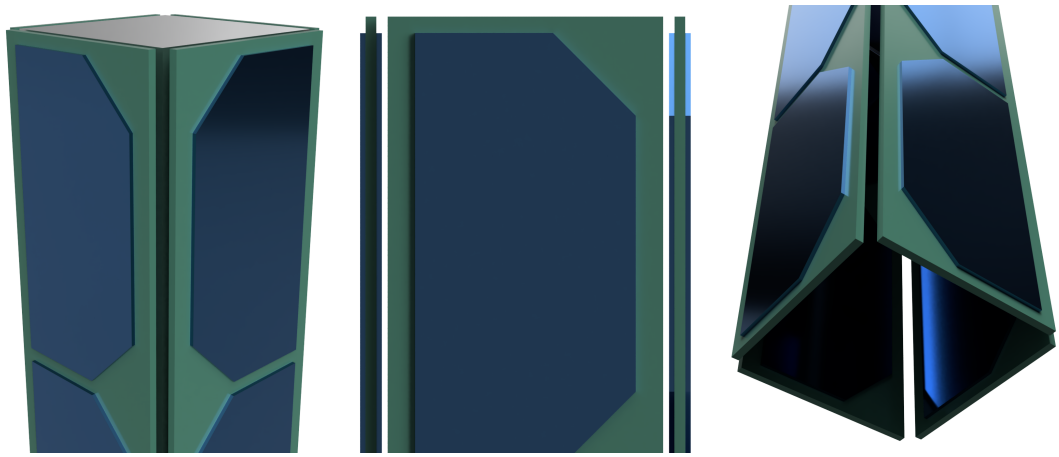

(a) Top view, stowed configuration (wing angle: $180°$)

(b) Orthographic view, stowed configuration (wing angle: $180°$)

(c) Bottom view, fully deployed configuration (wing angle: $0°$)

Figure 11.2: Delfi-Twin spacecraft solar cells placement

Looking at Figure 11.2b, the layered structure of the wings can be clearly seen. Made of a single PCB layer, with cells mounted on both surfaces.

The configurations shown in Figure 11.1 and Figure 11.2 do not have any free space on the wings. To make space for the RABSII deployer, a single solar cell is removed from one of the wings. The remaining volume is available for the payload to be integrated. This volume is highlighted with a red shaded box in both the stowed and deployed Delfi configurations in Figure 11.3. While some of the RF power electronics can fit inside the spacecraft bus, everything else is constrained within this available volume. Based on the dimensions of the Delfi-Twin spacecraft as well as the tolerances with the satellite deployer, this bounding box has a volume of 80x40x$4\,\text{mm}^3$ (**REQ-SAT-07**; see Table 4.6).

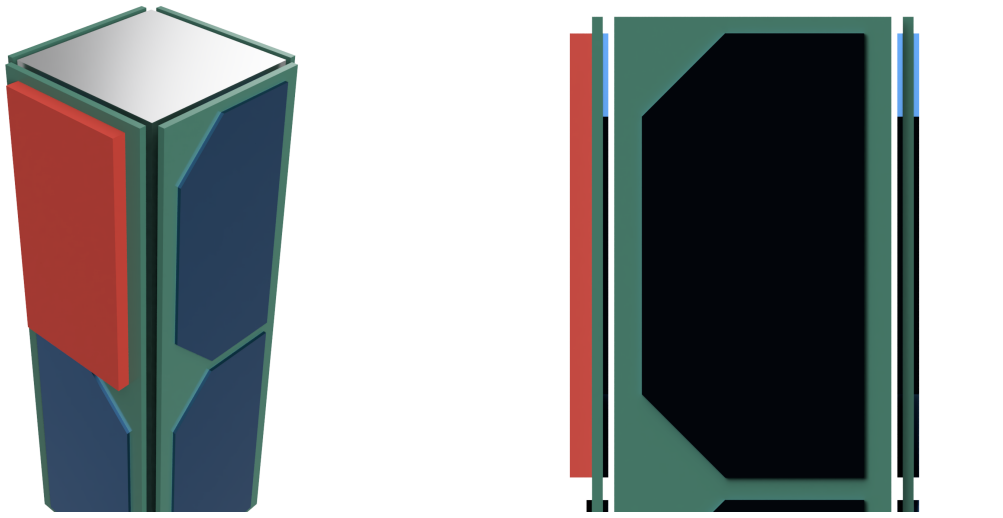

(a) Top view, stowed configuration (wing angle: 180°)

(b) Orthographic view, stowed configuration (wing angle: 180°)

Figure 11.3: RABSII payload available volume (red box) in relation to Delfi-Twin

11.3. Design Options

A few different options are considered when it comes to the deployment of the RABSII antenna. Two separate design dimensions are considered which are discussed in this section: the mounting approach onto Delfi-Twin, and the deployment approach of the antenna itself.

11.3.1. Delfi-Twin RABSII Mounting Interface

Two options are available to use the allocated volume (highlighted in red in Figure 11.4):

1. **Wing-mounted**: deployer mounted directly onto the spacecraft wing
2. **Bus-mounted**: hinged deployment anchored to the main bus

Option [**1**] is the simplest mounting configuration with the deployer mechanism directly and rigidly mounted onto the spacecraft wing. As the wing deploys, the stowed RABSII payload deploys with it. Once the wing reaches its final deployed state, the RABSII deployer is free to deploy the beacon antenna. This wing-mounted configuration onto the Delfi-Twin can be seen in Figure 11.4.

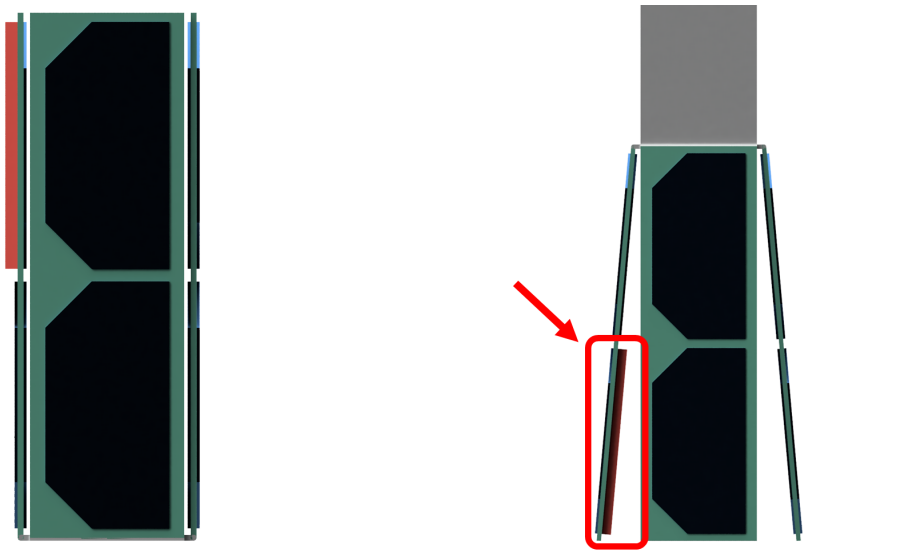

(a) Delfi in stowed configuration (wing angle: $180°$)

(b) Delfi in deployed configuration (wing angle: $5°$)

Figure 11.4: Mounting option 1: wing mounted; available deployer volume in red

Option [**2**] requires an additional mechanism, but may allow for more flexibility in terms of deployment configuration. The RABSII deployer is hinge mounted onto the Delfi-Twin main bus, simply laying on, but not connected to, the spacecraft wing during launch and satellite deployment. The configuration and its deployment steps can be seen in Figure 11.5.

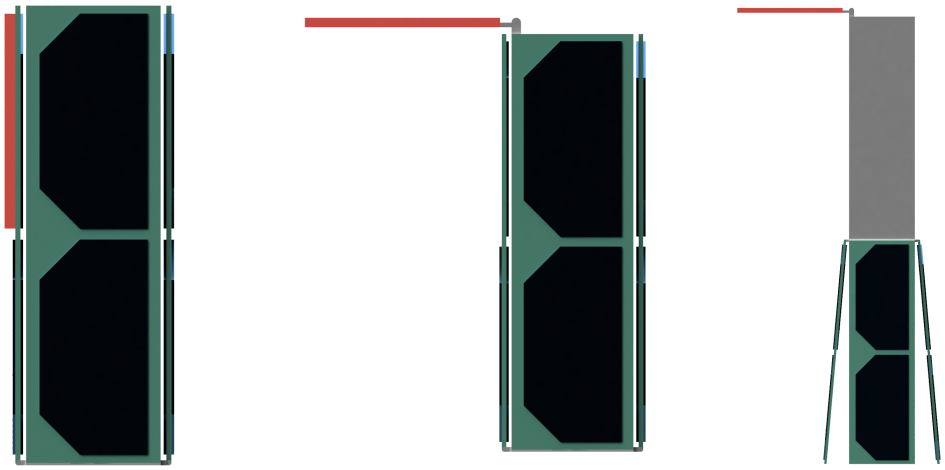

(a) Delfi in stowed configuration; stowed RABSII deployer (wing angle: $180°$)

(b) Delfi in stowed configuration; deployed RABSII antenna deployer (wing angle: $180°$)

(c) Delfi in deployed configuration; deployed RABSII antenna deployer (wing angle: $5°$)

Figure 11.5: Mounting option 2: bus mounted; available deployer volume in red

While not specifically for the loop antenna deployer, the exact hinge mechanism required for option [**2**] has already been designed by Aboubakr el Jouhri in a previous master thesis [43]. This work analyses and presents a design for a spring-actuated hinge to deploy the currently under-consideration dipole antenna system. However, it can just as easily be used to deploy the loop deployer presented by this analysis. The design of the hinge can be seen in Figure 11.6.

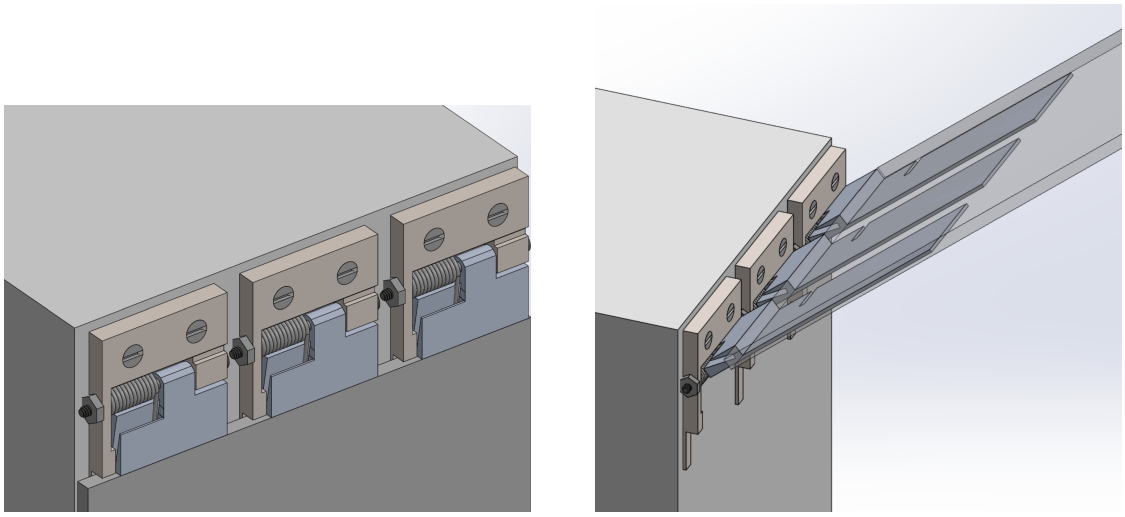

(a) Stowed; isometric view **(b)** Deployed; isometric view

Figure 11.6: Hinge deployer mounted on the top of the Delfi main bus, work from Aboubakr el Jouhri [43]

As per the analysis by Aboubakr el Jouhri, the added thickness from the hinge mechanism is contained below 0.5 mm. Accounting for the tolerances between the Delfi-Twin spacecraft and the satellite deployer, no changes have to be made to the RABSII antenna deployer design if choosing mounting interface option [**2**] over option [**1**].

11.3.2. Antenna Deployment Approach

For the deployment of the antenna itself, the following options are considered:

1. Pop-up tent coiled wire
2. Cassette wound-up tape

A brief overview of each idea is presented in the two sections below.

Pop-up Tent Coiled Wire

This concept revolves around using a single thin circular wire coiled around itself repeatedly to fit within the available payload volume. The conductor wire's lowest energy state is in the shape of the deployed loop. For stowage, it is pinched and twisted to form an '8-shape'. One of the two loops in the 8-shape is then bent over the other one effectively achieving a single loop half the diameter of the starting one. This process is repeated halving the diameter at every step until the final small loop has an area which can fit within the 80x40 mm^2 footprint of the deployer. This stowage process is illustrated in Figure 11.7.

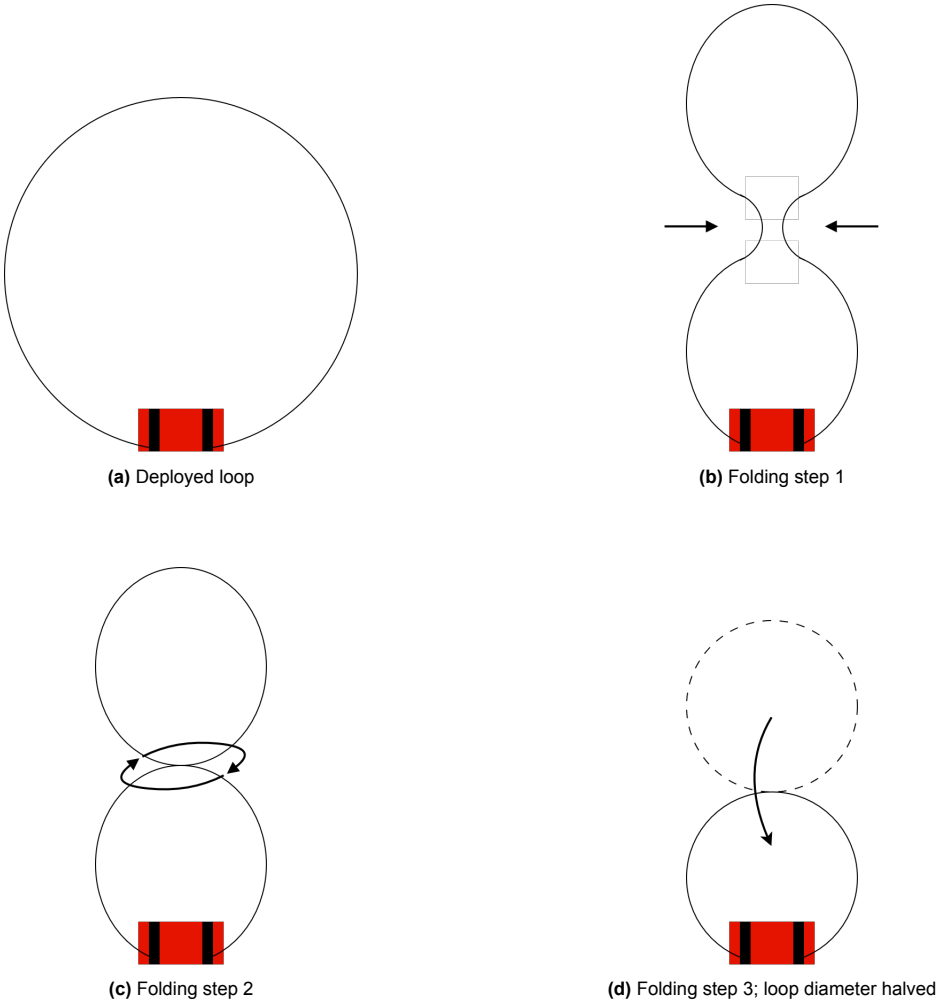

(a) Deployed loop

(b) Folding step 1

(c) Folding step 2

(d) Folding step 3; loop diameter halved

Figure 11.7: Pop-up tent loop antenna folding steps; deployer footprint in red (80x40 mm); antenna terminals in black

Once the desired loop diameter is achieved, the folded loop can be easily held down with either a burn wire, or a chord wrapped in a thermal knife. Severing the hold down wire/chord would result in the stored mechanical energy being released as the loop returns to its rest position: the fully deployed loop. This process is akin to a pop-up camping tent, hence the name of the concept.

Cassette Wound-Up Tape

The second option considered can visualised as a spring loaded tape cassette, where the tape is the antenna conductor. Consider the rectangular 80x$40\,\text{mm}^2$ footprint of the deployer, the 2:1 aspect ratio can accommodate two identical spools each housing half of the loop tape conductor. In the rest position, both spools are fully unwound, and the loop is deployed. To stow the antenna, both spools are wound up simultaneously, coiling the tape conductor around them. As the spools are wound, the torsion spring within them is also wound up. Once the entirety of the loop is wrapped within the spools, it can be held down with either burn wires or a chord and thermal knife. This stowage process can be seen in Figure 11.8. Upon release of the wire/chord, the two spools unwind releasing the mechanical energy stored in the two torsion springs. As the spools unwind, the loop is deployed.

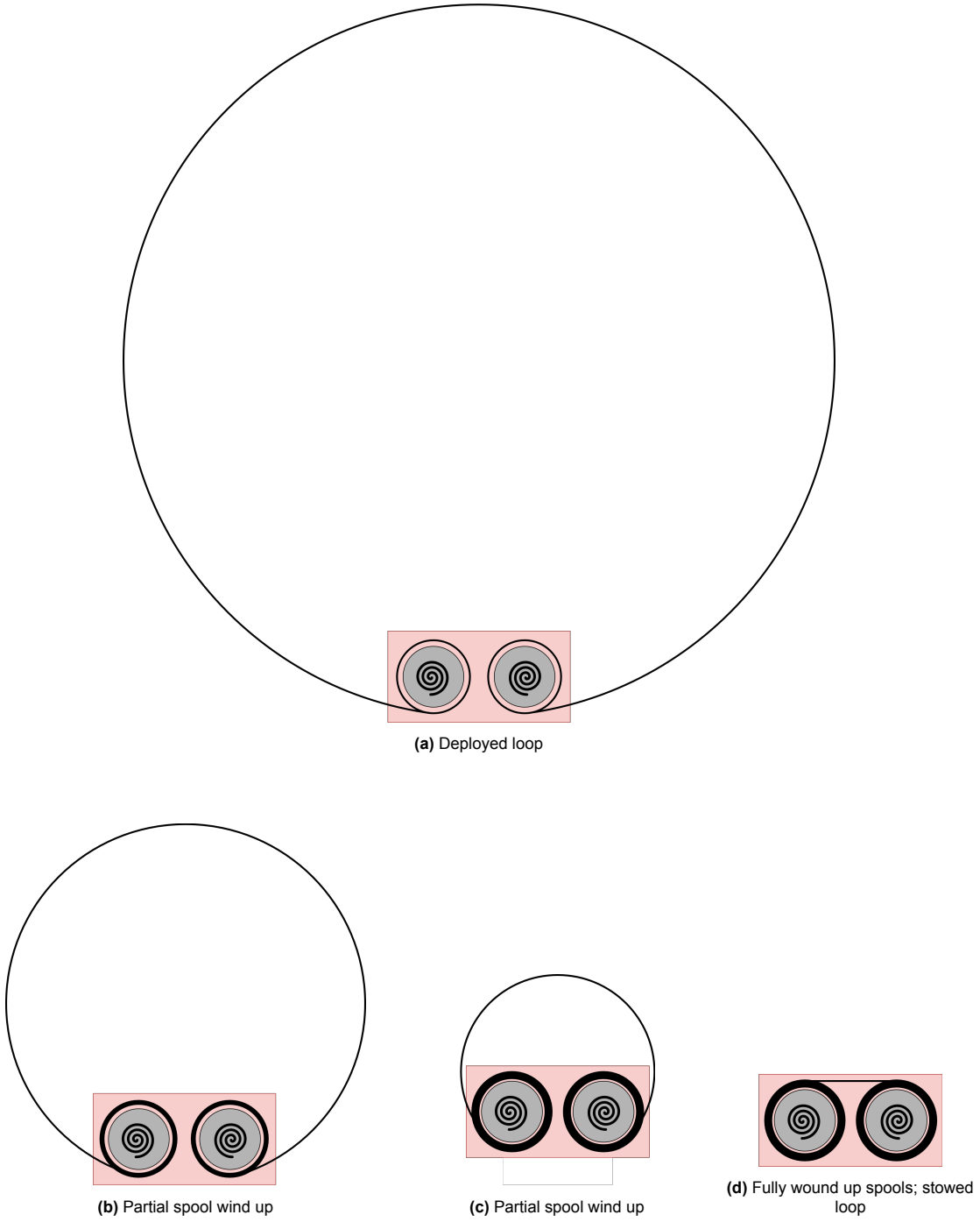

(a) Deployed loop

(b) Partial spool wind up

(c) Partial spool wind up

(d) Fully wound up spools; stowed loop

Figure 11.8: Cassette loop stowage approach; deployer footprint in red (80x40 mm); spools in gray; torsion springs as spirals

11.4. Design Choices

Two design choices must be made. The first choice is between mounting the RABSII deployer directly on the spacecraft wing, or onto a separate deployable hinge (bus-mounted versus wing-mounted). The second choice is instead between the pop-up tent and the cassette deployment approaches.

Looking at the first choice, both options are nearly identical in terms of deployer constraints. The only key difference is the orientation of the deployed antenna. Figure 11.9 and Figure 11.10 show the achieved antenna orientation for the bus and the wing mounted interface options respectively.

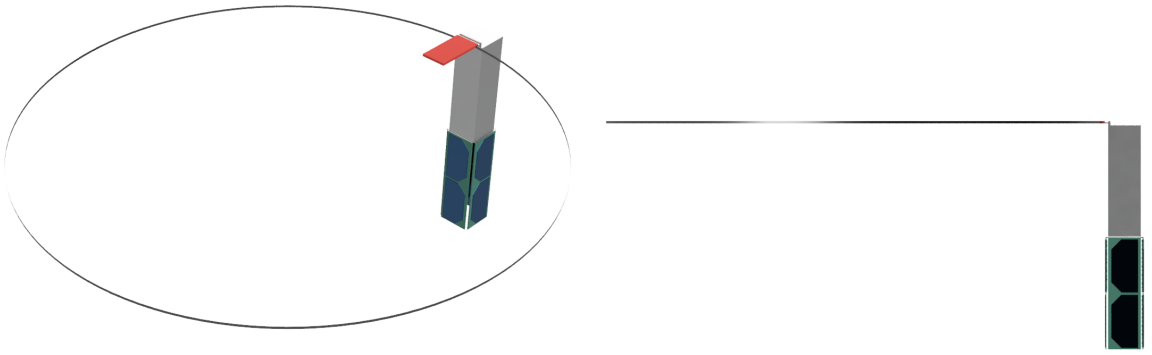

(a) Isometric view **(b)** Orthographic side view

Figure 11.9: Bus-mounted Delfi-Twin interface

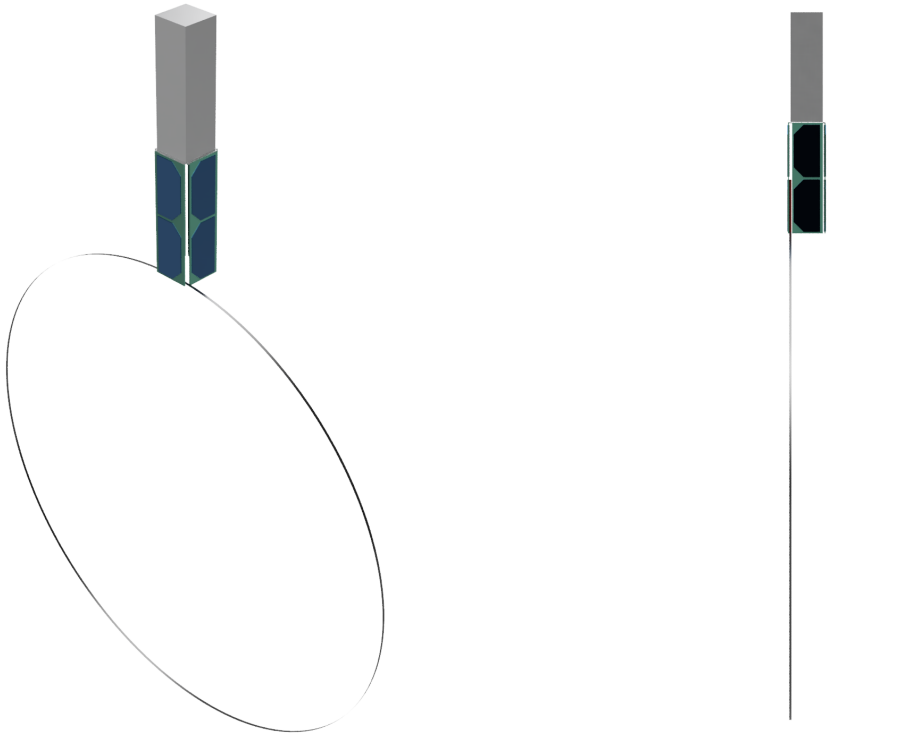

(a) Isometric view **(b)** Orthographic side view

Figure 11.10: Wing-mounted Delfi-Twin interface

Given the much more pronounced geometric asymmetry and added complexity of the bus-mounted option, the wing-mounted option is selected. Formation flying through drag control is the primary mission objective of Delfi-Twin. This could be compromised by adding a highly asymmetric appendage to the spacecraft. While the wings can be individually controlled to balance out the imbalanced torque due to the antenna, it is still considered less risky to go with the wing-mounted option. However, as there are negligible deployer modifications between the two options, this is not a consequential decision. Were the bus-mounted antenna orientation to be preferable for RF performance, or perhaps for easier operation of Delfi-Twin, this choice could be reversed with little consequence on the design.

Looking at the second choice, the decision is slightly more nuanced. While a few factors are considered to reach a decision, the main distinguishing aspect between the two deployment approaches is the expected reliability of the deployment.

The tent deployment approach is highly chaotic in nature. The loop coils wrap over each other repeatedly in the stowed configuration and the majority of the deployment force is in the bending and torsion of the wire itself. During stowage, the loop diameter needs to go from (up to) 1.25 m down to around 40 mm to fit within the deployer footprint. This corresponds to about five halving steps (one step presented in Figure 11.7), and a final coil with more than 30 turns of wire. This constrains the wire to a considerably thin diameter and does not allow for a strip to be used (which was one of the preferable deployer features presented in section 11.1). Small scale testing was done using a thin spring steel wire to investigate how this approach would perform. The deployment approach was confirmed to be quite unreliable with no clear path to fix the core issues stemming from the unpredictability of the system dynamics.

The cassette approach instead has the potential to be much more controlled and well-behaved. The deployment is actuated in a single dimension with the unwinding spools ejecting the loop strip conductor. Given the continuous nature of the unwinding process, the approach has the potential to be highly scalable, accommodating for a wide range of loop diameters. Furthermore, it is suitable to accommodate a wide strip conductor, ensuring better performance than the tent approach.

Based on these observations, and the preliminary practical testing, the cassette approach is chosen as more promising for deploying the RABSII antenna.

11.5. Conceptual Design Summary

Based on the available space aboard Delfi-Twin and the tolerances between the satellite and its deployer, a maximum payload envelope has been identified (Figure 11.3).

To place the RABSII payload in the available volume, two interface options are possible: a bus-mounted and a wing-mounted one. In the former, a hinge mechanism investigated and developed in a previous thesis project by Aboubakr el Jouhri [43] is used to attach the antenna deployed directly to the top of Delfi-Twin's bus. In the latter option, the antenna deployer is mounted directly onto one of the satellite wings. The wing-mounted option is chosen due to the lower complexity, however, a change in decision further in development would negligibly affect the antenna deployer design.

To deploy the loop antenna from the identified interface location, two approaches are defined. The first approach is akin to the principle behind the deployment of pop-up tents. The deployed loop is repeatedly pinched and folded in half to reduce the diameter until it fits within the deployer footprint. Stored mechanical energy provides the actuation force to return the loop to its full diameter once released. The second approach can be visualised as a tape cassette. The thin strip conductor is wound up on two spring loaded spools. As the spools are wound during packing, mechanical energy is stored in the torsional springs. Upon release, the energy in the springs unwinds the tape to deploy the loop antenna. The cassette approach is chosen over the pop-up tent after some small-scale testing with spring steel wire. As expected, the tent approach is too chaotic and unpredictable to reliably deploy. The wire often got tangled with itself, or the deployment jammed completely before getting started.

The chosen interface and deployment combination meets the constraints presented in section 11.1. A wing-mounted, cassette deployment approach should be able to accommodate a wide range of loop diameters while housing a strip antenna (rectangular cross-section).

12

Antenna Deployer Design

This chapter presents an overview of the deployer design. Starting from the cassette-style deployment approach defined in chapter 11, a number of iterations were conceptualised to reach the design presented hereafter. section 12.1 begins with an overview of the deployer CAD model. This is followed by three sections detailing the design of the three key deployer sub-assemblies: the rotor assembly, the case assembly, and the HDRM assembly. These are presented in section 12.2, section 12.3, and section 12.4, respectively. Lastly, an overview of the packing and deployment sequence is presented in section 12.5.

12.1. Design Overview

Following the general cassette-deployment approach defined in the previous chapter, an overview of the physical deployer design is presented here. The CAD of the deployer is illustrated in Figure 12.1. The design fits within a bounding box of exactly 80x40x$4\,\mathrm{mm}^3$, as per the system requirements.

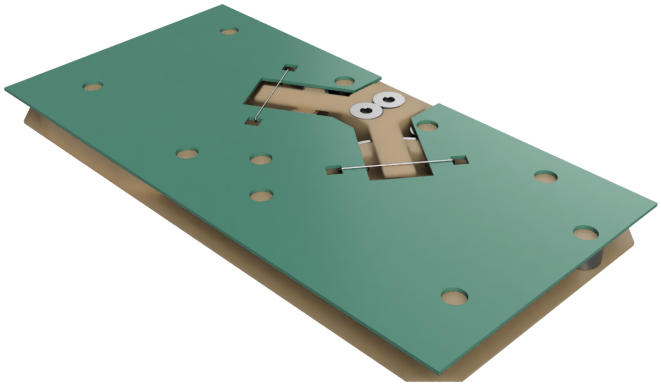

(a) Isometric view

(b) Side view (long side, $80\,\mathrm{mm}$)

(c) Side view (short side, $40\,\mathrm{mm}$)

Figure 12.1: Overview of the complete deployer design

The various parts are coloured according to the real material used. The large flat plate in green topping the deployer is a PCB. Figure 12.2 presents the same design with the top PCB removed in order to see the inner implementation of the cassette deployment.

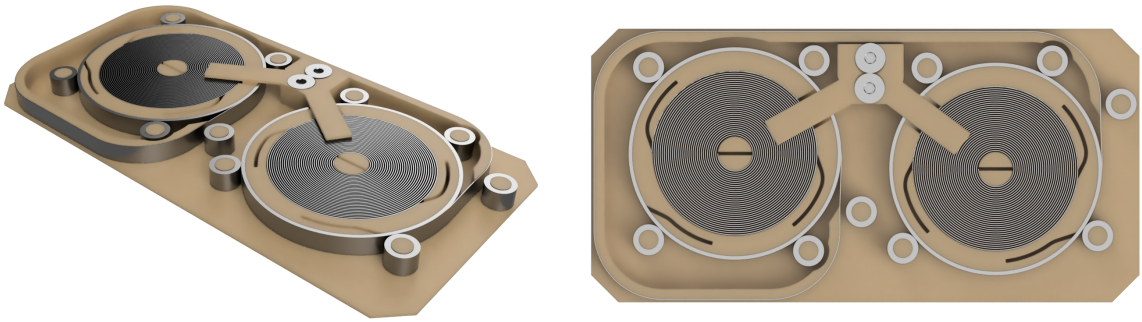

(a) Isometric view **(b)** Top orthographic view

Figure 12.2: Deployer design with the top PCB removed

The key systems can be clearly identified. Most notably are the two spools in brown (sometimes also referred to as rotors from now on), each taking up about half the available deployer footprint. Furthermore, the antenna strip can be seen coiled up on both spools and connected to both rotors by running on the outside of the deployer case. The hold down and release mechanism (HDRM) assembly instead takes up the space in between the two rotors. Two protrusion, or locking fingers, can be clearly seen overlapping with the rotors themselves. Lastly, all the small metallic cylinder are bushings. Their primary function is to guide the antenna strip as it deploys and reduce internal friction.

The following key functional assemblies can be identified:

1. **Rotor assembly (x2)**: each comprised of the rigid spool and the torsion spring
2. **Deployer case**: comprised of the bottom and top case halves, as well as the bushings and vertical connecting columns
3. **HDRM mechanism**: comprised of the locking fingers, and burn wires for actuation

The remainder of the chapter is divided according to the assemblies defined. The high level design choices are presented for each section.

12.2. Rotor Assembly

The rotor assembly is defined as the combination of the solid rotor, the torsional spring at its core, and the antenna strip coiled over it. As the antenna is coiled up onto two individual rotors, the assembly is essentially duplicated, with one in each half of the deployer. The components comprising the two rotor assemblies are coloured in Figure 12.3.

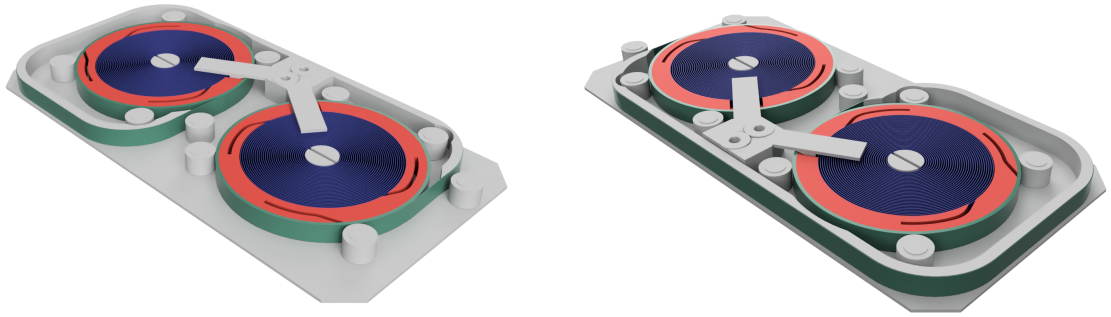

(a) Front view **(b)** Back view

Figure 12.3: Rotor assembly components coloured; rigid rotors in red; torsion springs in blue; antenna conductor strip in green

Starting with the antenna itself, the chosen configuration may seem odd, but the design is tailored specifically to be able to deploy the loop in the correct orientation with respect to Delfi-Twin. Looking back at Figure 11.10 and Figure 11.9, for the loop to correctly deploy it must do so in the direction of the deployer long axis. Figure 12.4 graphically shows this with respect to the deployer footprint and the Delfi-Twin wing panel onto which the deployer is mounted. Deploying in the wrong direction results with the loop in a highly asymmetrical configuration, protruding sideways from the satellite's body.

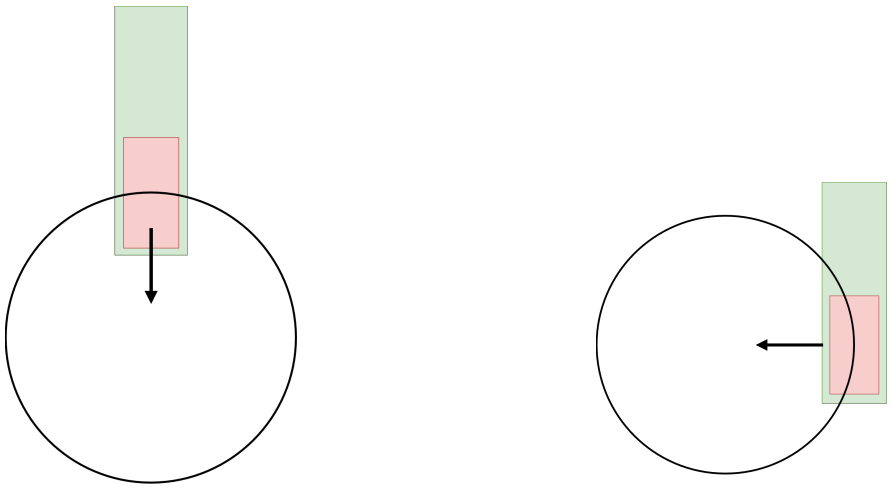

(a) Correct **(b)** Wrong

Figure 12.4: Required loop deployment orientations; deployer footprint in red; Delfi-Twin wing panel in green

The approach in which the deployer design achieves this correct deployment direction can be seen in Figure 12.5 in the next page.

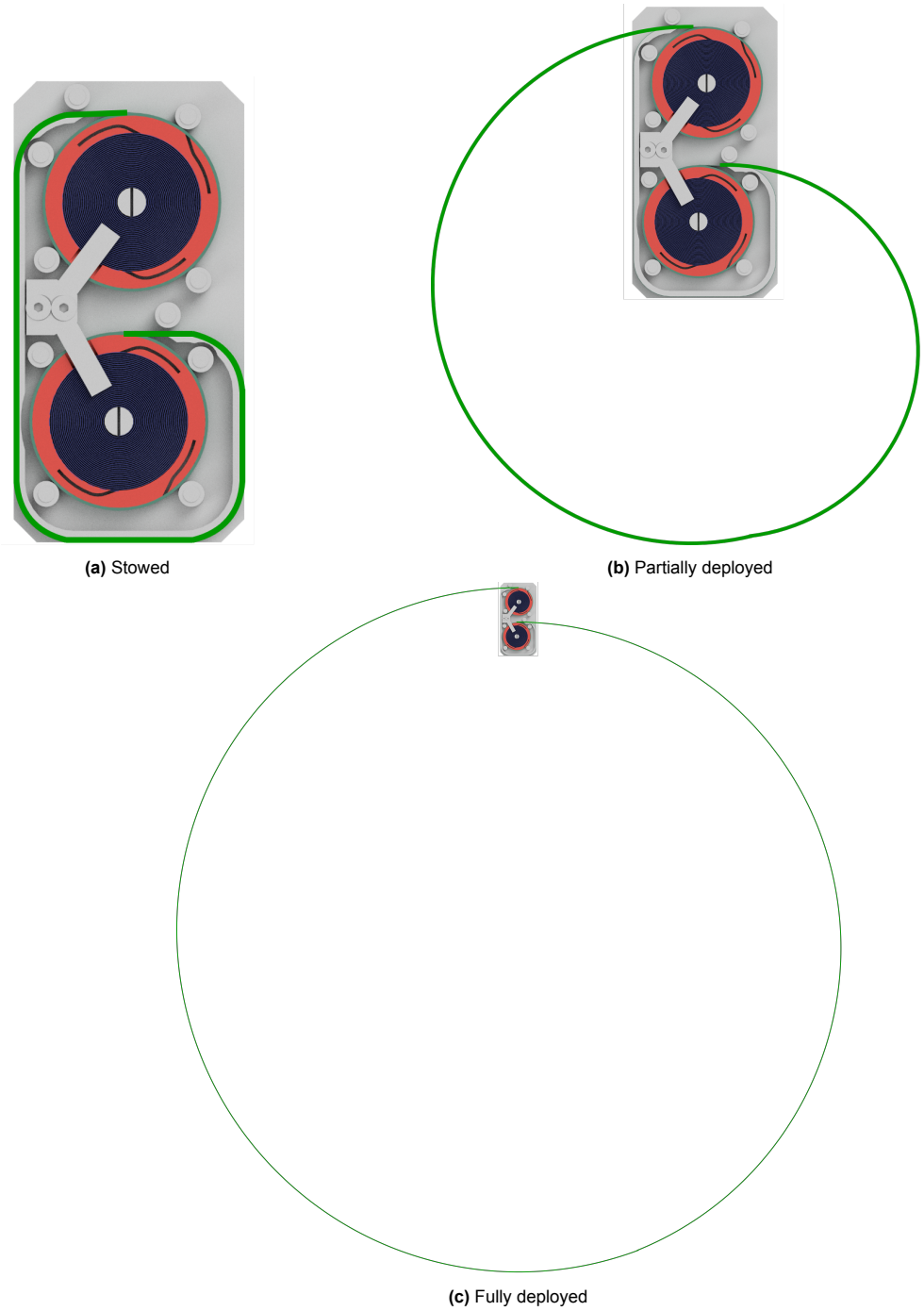

(a) Stowed

(b) Partially deployed

(c) Fully deployed

Figure 12.5: Loop conductor deployment steps; antenna conductor (green) thickness exaggerated for clarity

Lastly, about the antenna conductor strip, the rectangular cross-section dimensions compatible with the deployer are 3 mm by 0.1 mm. The width of 3 mm is achieved by minimising the thickness of the top and bottom plates making up the deployer case. The strip thickness of 0.1 mm instead is chosen to ensure that no plastic deformation occurs during storage and deployment of the loop antenna. Using the material properties for spring steel defined in Table 6.2, the peak internal stress in the strip can be computed as a function of bending radius with the following equation [6].

$$\sigma = \frac{Et}{2R} \tag{12.1}$$

Where σ is the peak internal stress, E is the material E-modulus, t is the strip thickness, and R is the bend radius. Using the known properties of spring steel, the tightest bending radius achievable with $t = 0.1$ mm is $R = 6.3$ mm. The deployer design presented requires bends as tight as 10 mm in radius to be able to fit within the available volume, so going above $t = 0.1$ mm would bring the internal stress too close to the yield point of the material for the extended storage period before deployment.

With a rotor diameter of 30 mm, about 10 cm of antenna length can be stored by each spool for each turn. For a loop diameter ranging between 75 and 125 cm, this translates to 12 to 20 rotor turns to store the entire antenna. Accounting for the strip thickness, 12 to 20 turns means a total spool thickness on the rotors of 1.2 to 2 mm. This is easily achievable. Were the number of turns too many, the spool diameter can be increased up to about 34 mm by making the whole assembly tighter. This would reduce the number of rotor turns required down to a range between 11 and 18 depending on the loop's length. Considering the 50 MHz instrument deployer, the required number of turns drops down to a range of 7 to 11.

The last relevant element of the rotor assembly is the torsional spring. Having the antenna conductor made of spring steel means that essentially the same material can also be used for the spring. The torsion spring is made of a pair of thin, coiled spring steel strips spiralling inwards towards the central shaft (fixed to the deployer case).

Of primary interest for the successful deployment of the antenna is the torque curve of the spring. This torque curve can be tuned based on the following geometrical parameters.

- Thickness of the spring strip
- Width of the spring strip (fixed to a maximum 3 mm)
- Number of turns of the spring strip
- Rest curvature of the spring strip

Based on these parameters, the equation defining the spring's torque can be derived as follows. It is assumed that the spring can be idealised as a thin cantilever beam, self collisions are ignored.

$$T(\theta) = \frac{E}{L} \cdot \frac{wt^3}{12} \cdot (\theta + \theta_0) \tag{12.2}$$

Where T is the spring's output torque as a function of the rotation angle θ, E is the E-modulus of the material, w is the spring strip width (in this case 3 mm), t is the spring strip thickness, and θ_0 is the number of pre-stress turns applied to the spring before reaching the working range. Using this simple model, the relation between free parameters and torque can be identified. Thickness of the spring strip has the greatest effect on torque, given the cubed relation between the two. Spring width instead is only linearly related to torque. The same is true for the number of pre-stress turns.

Given the large space available between the central shaft (with a diameter of 5 mm) and the inside of the rotors (diameter of 24 mm), there should not be any issues fitting a spring with sufficient torque to actuate the deployer.

While both the antenna strip and spring are required to be made of spring steel, the choice in material for the solid rotors is more open. They could be machined out of aluminium/steel/titanium with little performance difference other than their weight. Or potentially, if mass becomes a concern, printed polymers would also suffice. At this stage, PEEK is used for the rotors given its ability to be printed and hence easily achieve precise complex geometries. What must be considered during testing is whether a heavier rotor with a larger inertia may be beneficial for deployment reliability. A heavy rotor would be less likely to get jammed mid-deployment once it gets moving.

12.3. Deployer Case Assembly

The deployer case assembly is comprised of the bottom half, the top PCB, and the bushings. These elements can be seen coloured in Figure 12.6.

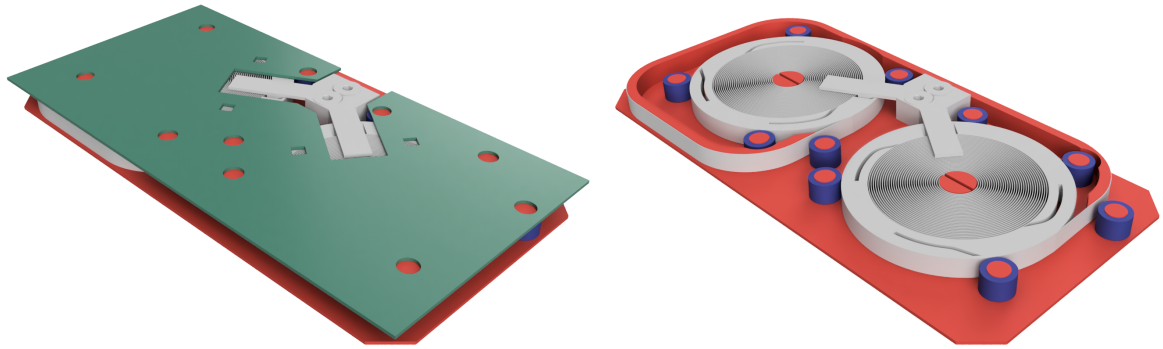

(a) Complete deployer **(b)** Top PCB removed

Figure 12.6: Deployer case assembly components coloured; case bottom in red; case top PCB in green; bushings in blue

Three components are presented, the top PCB, the bushings, and monolithic part which makes up the bottom half of the deployer case.

Starting from the case bottom (red), this component serves as a mounting point for the rest of the deployer. It is a monolithic part printed in high strength PEEK, but carbon infused PEEK variants may be used if higher rigidity is required. Its geometry is shown isolated from the rest of the deployer in Figure 12.7.

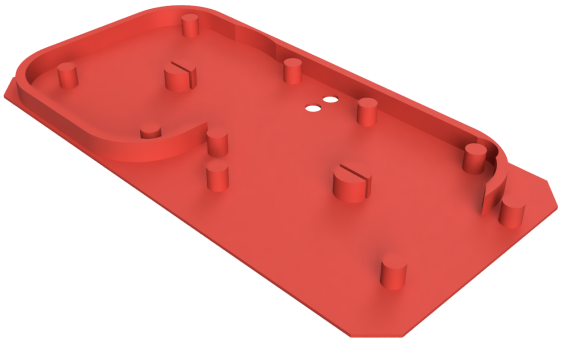

Figure 12.7: Deployer case bottom part

A few features can be identified. Firstly, the two slotted shafts positioned at the centre of each rotor are used as a central anchor for the torsional springs. Next, the other thinner solid shafts are used for mounting the bushings. They also serve as mounting points for the top PCB to join the two halves of the case. Lastly, the curved wall running around most of the part perimeter is used as a guide to retain the antenna conductor strip while the system is in the stowed configuration.

Looking at the bushings, their purpose is to guide the deployment of the antenna strip and to ensure a low friction interface between the moving antenna (during deployment) and the stationary case. While many options are available, the lowest friction alternative is PTFE bushings, with a friction coefficient around 0.1 [82]. However, as virgin PTFE has a relatively high thermal expansion coefficient when compared to other polymers or metals, steel wrapped PTFE bushings are chosen. They are easily acquired commercially in a variety of sizes, and should deliver low friction while remaining dimensionally stable.

The last component in the assembly is the top PCB (in green). This part has two functions: structural strength, and providing connection points for the various electronic components. In terms of strength, the PCB completes what is essentially a sandwich structure ensuring the deployer is stiff even before mounting on the Delfi-Twin wing plate. In terms of electronics, the PCB is responsible for linking the antenna feed points, mounting the matching network capacitors, and providing conductive pads and traces to mount and actuate the burn wires to initiate deployment. Combining all these functions in one structural element greatly simplifies the manufacturing and integration of an already small-scale mechanical system.

Overall, the entire case is able to remain within the 4 mm deployer thickness requirement. The top and bottom plates measure about 0.5 mm in thickness each, with a usable thickness of 3 mm allocated for the rotors, springs, and antenna tape.

12.4. HDRM Assembly

The last assembly of the deployer is the HDRM. Its components can be seen coloured in Figure 12.8.

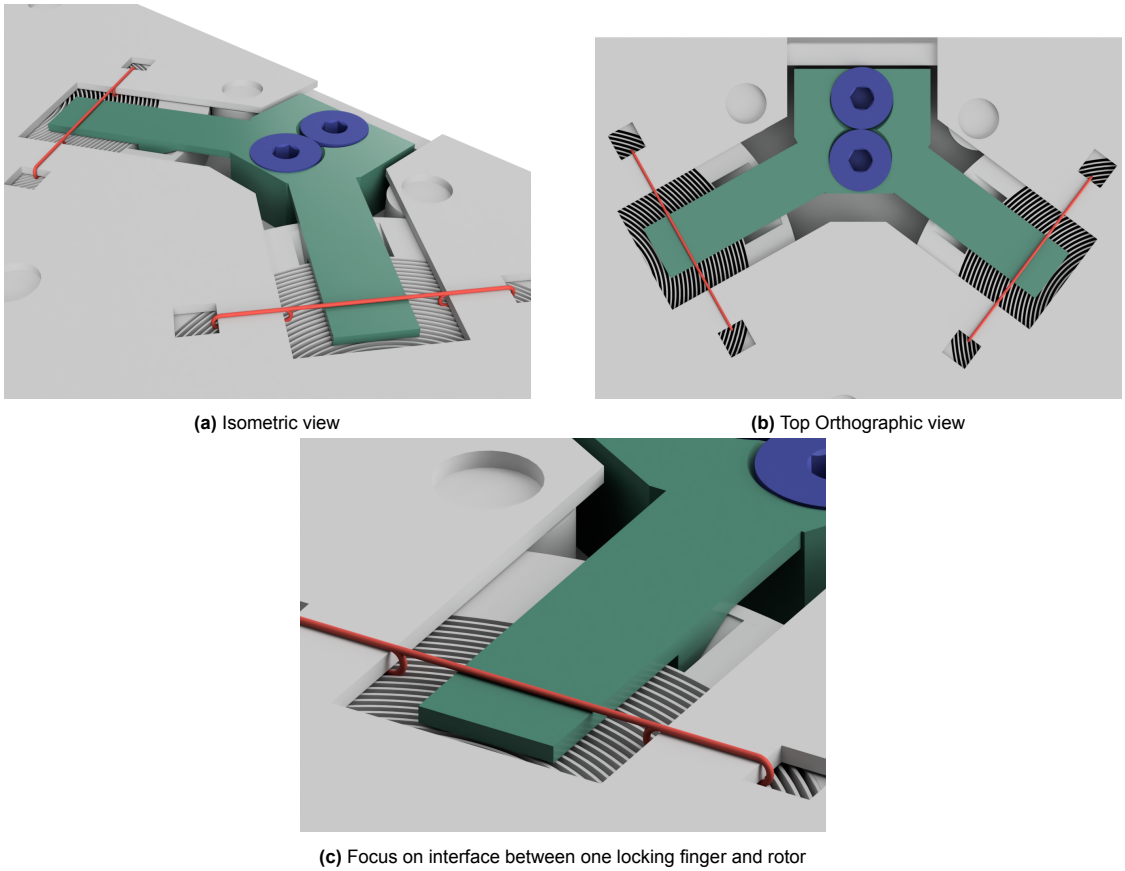

(a) Isometric view

(b) Top Orthographic view

(c) Focus on interface between one locking finger and rotor

Figure 12.8: HDRM assembly components coloured; burn wire(s) in red; locking fingers in green; retaining M2.5 bolts in blue

The following key parts can be identified. First, the locking fingers, in green, are responsible for physically locking the rotors from rotating before antenna deployment. Second, the burn wires, in red, are responsible for holding the locking fingers in place until deployment. The two M2.5x4 bolts in blue are used to fix the locking fingers, in green, to the bottom of the deployer case.

While the locking fingers are depicted as straight in all previous figures, their rest position is actually curved upwards, well out of the way of the rotors, antenna, and springs. The locking finger component is presented integrated into the deployer in rest position (the way it is manufactured) in Figure 12.9. The burn wires are omitted.

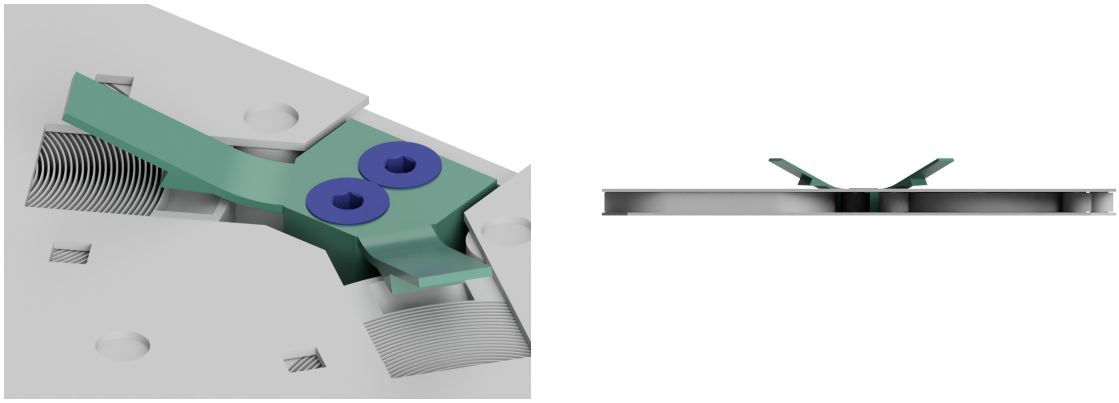

(a) Isometric view **(b)** Orthographic side view

Figure 12.9: Locking fingers in their rest position

As can be seen, in their rest position the locking fingers are well out of the way of the rotors allowing them to spin freely. The burn wires, each strung between two holes in the top PCB, elastically deform the locking fingers pushing them down into the path of the rotors. Power to break the burn wires is provided directly by the PCB, through conductive pads around the holes they are mounted in. Alternative burn wire configurations are possible depending on whether the risk of premature deployment or the risk of no deployment is considered more critical. In the former case, two or more burn wires can be strung across each finger requiring all of them to break before the deployer can actuate. In the latter case, a single continuous burn wire can be strung across both gaps so that its actuation can trigger the release of both spring-loaded rotors.

The locking fingers component is printed out of PEEK. The design of this component benefits from using a material with high yield strength but low elastic modulus to avoid plastic deformation when bent downwards. Were PEEK deemed insufficient for the design, the fingers themselves could be swapped for a bent spring steel strip with no change to the HDRM conceptual approach.

The design of the HDRM has been conceptualised to ensure that no parts of the mechanism get pushed in the path of the springs or rotors once the deployment is actuated. Once severed, the burn wires get pushed outwards away from the inner moving elements.

12.5. Packing and Deployment Sequence

To summarise the key design choices, the functions of the deployers are presented in order from packing the antenna, all the way to final deployment.

1. **Assembling the deployer base and rotors**
   The deployer assembly starts from the bottom case part (Figure 12.7). The bushings are then inserted from above, with five bushings per rotor. The two rotors are added in place (potentially held down with clamps temporarily). The torsion springs are then added around the two slotted shafts, and their ends are connected to the rotors. The locking fingers component is bolted down onto the deployer bottom case. The rotors are still free to move until the fingers are bent downwards in the path of the rotors.

2. **Packing the antenna in the deployer**
   The antenna strip is connected to both rotors in the deployed configuration with the case top still open. The two rotors are then wound up (either individually or simultaneously) until the antenna strip tightly hugs the outside of the deployer case. Until the locking fingers can be locked down, the rotors are temporarily clamped to stop them from deploying the antenna.

3. **Closing the deployer case**
   The PCB is assembled: the matching network components are added to the PCB, together with the burn wires and the antenna feed terminals. The completed PCB is added to the top of the deployer from above. This forces the locking fingers down, locking the rotors in place. This marks the conclusion of the antenna packing.

4. **Integrating the deployer onto Delfi-Twin**
   The completed deployer is mounted onto Delfi-Twin's wing. This is done by adhesively bonding the bottom of the deployer case (Figure 12.7) to the wing panel. Alternatively, bolts can be used depending on the preference of the Delfi team. Since only the bottom of the case is secured to the wing panel, the deployer can still be actuated, tested, and repacked. Depending on the preferences of the Delfi team, the antenna may also be packed after integration into Delfi with no change to the highlighted procedure.

5. **In-Space Deployment**
   Once the actuation command is sent, a small current is passed through the burn wires. As the wire get cut, the mechanical energy stored in the locking fingers pushes them up and away from the rotors. Now free to move, the rotors are actuated by the large coil springs which accelerate them. As they unspool, the antenna strip is pushed outwards from both rotors until the loop reaches the full design size. At full deployment, the springs aren't completely unwound. This ensures that the antenna feed points are pressed onto the designated contacts leading to the top PCB.

6. **In-Space Operations**
   With the antenna fully deployed, each end of the conductive strip is securely in contact with the respective PCB trace. The antenna can be operated like any other antenna through the interface provided on the PCB.

13

Deployer Functional Demonstration

While a detailed design for the antenna deployer has been defined and presented, it is difficult to have confidence in its performance without either extensive analysis or a full test campaign. Both options are beyond the scope of this project, however, a physical demonstrator is still constructed to validate the deployment approach and investigate the potential of the design. This chapter documents how the physical demonstrator deployer model was created, and how it performed in terms of storing and deploying the RABSII loop antenna. From here onwards, the test article is referred to as '*(deployer/-physical) demonstrator*'.

The goals behind the construction of the demonstrator deployer are first presented in section 13.1. Next, the assumptions and simplifications made from the full design (presented in chapter 12) are presented in section 13.2. The suppliers and acquisition of the components is then presented in section 13.3, followed by an overview of the physical assembly in section 13.4. Lastly, the observed performance, deployment characteristics, and lessons learned are presented in section 13.5, followed by recommendations for further testing in section 13.6.

13.1. Demonstrator Objectives

The goal of constructing a physical demonstrator can be summarised as follows.

Demonstrator Construction Objective

To demonstrate that the cassette-style deployment approach is a viable option to deploy the RABSII payload loop antenna.

Creating a representative physical model of the antenna deployer allows to directly investigate the feasibility of the design without getting lost in hard-to-validate complex physical simulations. While simulating the antenna's RF performance is a ideal task for numerical models, the same cannot be said about the deployment dynamics. The deployment involves complex interactions between the fixed case, rotating bushing and rotors; elastic energy release from both the torsion springs, the antenna strip, and the locking fingers; dynamic oscillations of the accelerating rotating rotor assemblies; and friction between moving and stationary parts. Simulating all of this and having confidence in the results would be non-trivial. However, by using a representative physical demonstrator, it can be directly identified whether the design is promising or not.

13.2. Assumptions and Design Simplifications

In order for the demonstrator to be a useful tool, it must be representative of the real deployer, at least in the ways that matter. The easiest option would be to just build the exact design presented in chapter 12. However, due to the limited resources available in this work, such as time, money, and access to equipment, this is not a feasible option. The goal still remains to build a prototype able to demonstrate the functionality of the deployer by changing as little as possible to the original design.

The following assumptions are made:

1. Deployer operation in atmosphere instead of vacuum does not significantly affect the deployment behaviour.
2. Deployer operation under gravity loads, instead of microgravity, does not aid deployment.
3. Deployer operation under gravity loads, instead of microgravity, increases friction forces between components, making deployment more difficult.

It is relevant to mention that it is expected that gravity loads will result in increased friction between components. Most notably, this is expected between the rotor assemblies and the deployer case as their weight (together with that of the antenna strip) will sit on the interface between the two. This friction force will not be present when deploying in space under microgravity conditions. If the demonstrator can deploy successfully under gravity loads, it should be able to do so in microgravity as well.

As mentioned, some simplifications are made to the original design to make building a prototype feasible. For each design simplification/change, four aspects are presented: the **change** itself, the **justification** (why?), the **design implications** (how this affects the demonstrator design compared to the original design), and the **functional implications** (how this affects the expected performance of the demonstrator compared to the original design). The following changes/simplifications are made:

1. → **Change**: Antenna strip conductor capped at 0.3 meter in total length.
   → **Justification**: Not possible to source a spring steel strip with the required dimensions for large antenna diameters. The only available option is a 300 mm spring steel strip. Multiple were acquired to be joined together, but feasibility of extending conductor length in this manner is still uncertain.
   → **Design Implications**: Total deployed conductor length equal to about 0.3 m. Up to a length of 1 m may be possible depending on whether multiple strips can be joined successfully, which would translate to a loop diameter of just above 30 cm.
   → **Functional Implications**: Deployed loop is smaller than the required size. However, the deployment process and associated functions remain unchanged. The deployment dynamics are still representative of the original design. Once the rotors and antenna spools start moving, they have a non-negligible inertia making them unlikely to get stuck mid-deployment. Critical phase is the initial actuation, which remains unchanged with a shorter conductor length.

2. → **Change**: Top PCB replaced with a plain PEEK plate.
   → **Justification**: Implementation of the antenna electronics is beyond the scope this project and does not effect the deployment dynamics.
   → **Design Implications**: PCB not manufactured, matching network not physically implemented, top PCB replaced with a plate with identical geometry but made out of the same material as the bottom deployer case.
   → **Functional Implications**: Mechanically, none, except for a slight change in stiffness in the top plate.

3. → **Change**: UV curing resin (FormLabs® Clear resin) used instead of PEEK.

   → **Justification**: PEEK and carbon infused PEEK were not available for manufacturing the components.

   → **Design Implications**: Parts designed to be made with PEEK were printed in clear resin: the rotors, the bottom case, the locking fingers, and the top plate. Thickness of deployer top/bottom plate was scaled according to the old/new flexural modulus of the materials to preserve the same bending stiffness. Do note that the here-mentioned resin-printed parts were always printed on a SLA (stereolithography) machine.

   → **Functional Implications**: Overall deployer case is slightly thicker than the required 4 mm, overall deployer demonstrator case is less strong than a PEEK equivalent.

4. → **Change**: Height of the rotor assembly (rotors, springs, and antenna strip) is increased from 3 mm to 3.175 mm.

   → **Justification**: The best found commercially available option for the springs and antenna strip has a width of 3.175 mm instead of the desired 3 mm.

   → **Design Implications**: Overall deployer thickness is increased by 175 µm, no other changes are made to the geometry.

   → **Functional Implications**: Deployer case is slightly thicker than the required 4 mm, but no meaningful performance differences are expected.

None of the changes made are expected to alter the deployment dynamics significantly. It is hence assumed that the physical demonstrator will be representative enough to validate the feasibility of the deployment approach.

13.3. Components Acquisition

Table 13.1 presents a list of all the components in the deployer demonstrator. A few components were acquired but not used in the final deployer demonstrator: namely, larger plain bush bearings (with dimensions of 4.5x5x3 mm), PTFE tubing 5 mm in diameter, a 4 mm wide 0.1 mm thick aluminium strip, and PLA (PolyLactic Acid) for FDM (Fused Deposition Modelling) 3D printing.

Table 13.1: Deployer demonstrator components

Component	Quantity	Supplier	Description	Image
Constant Force Spring [SCF 0.076X3.175X252]	7	LESJÖFORS	Usually used to provide a nearly constant linear force, these springs are made of a single 1.4310 steel strip coiled onto itself. The strip measures 305 mm in length, 3.175 mm in width, and 0.076 mm in thickness. Two springs are used at the core of each rotor, and the remaining three are used for the antenna strip conductor.	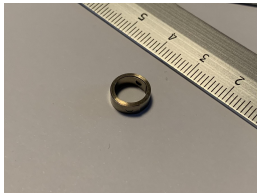
Plain Bush Bearings [SKF PCM030403E/VB055]	10	SKF	PTFE composite bush bearings with a steel sheet backing made to be operated with no additional lubrication. The inner bush bearing diameter is 3 mm, the outer diameter is 4.5 mm, and the cylindrical height is 3 mm.	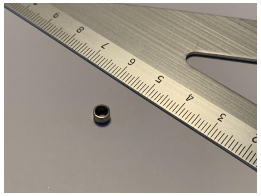
Formlabs Clear Resin V5	N.A.	Formlabs/TU Delft	This clear resin is used to manufacture all printed components. Relevant to the deployer design, it has a tensile modulus of 2.75 GPa, and a flexural strength of 105 MPa	
Graphite Powder	N.A.	Local hardware store	Pure graphite powder is used to further reduce friction within the demonstrator; if needed, it can be used for the final flight hardware too, as it is compatible with the space environment.	
M2.5 Bolts	2	Local hardware store	Used to secure the locking fingers component to the deployer base.	

13.4. Demonstrator Assembly

The deployer demonstrator is assembled using the same procedure described in section 12.5. The process is presented with photos taken during assembly, starting with the resin-printed bottom plate in Figure 13.1.

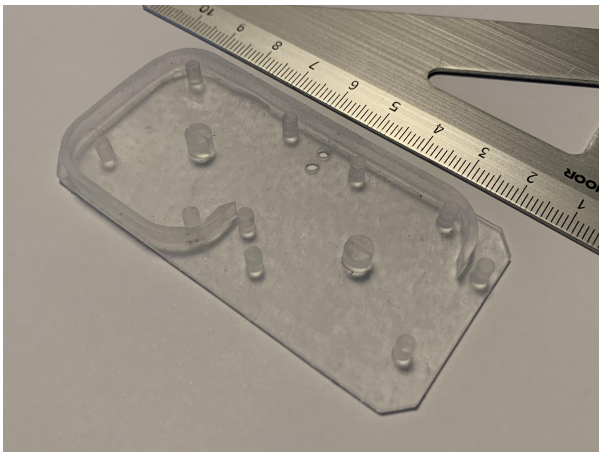

Figure 13.1: Case bottom

The bushings are then added in Figure 13.2

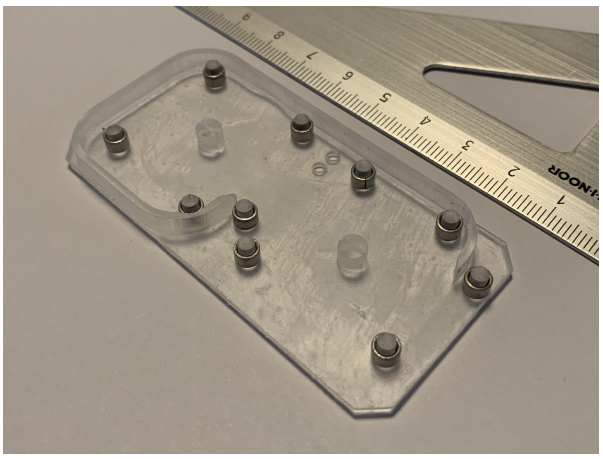

Figure 13.2: Bushings integrated into the case bottom

The two rotors are slotted in place within the bottom case together with the springs in Figure 13.3.

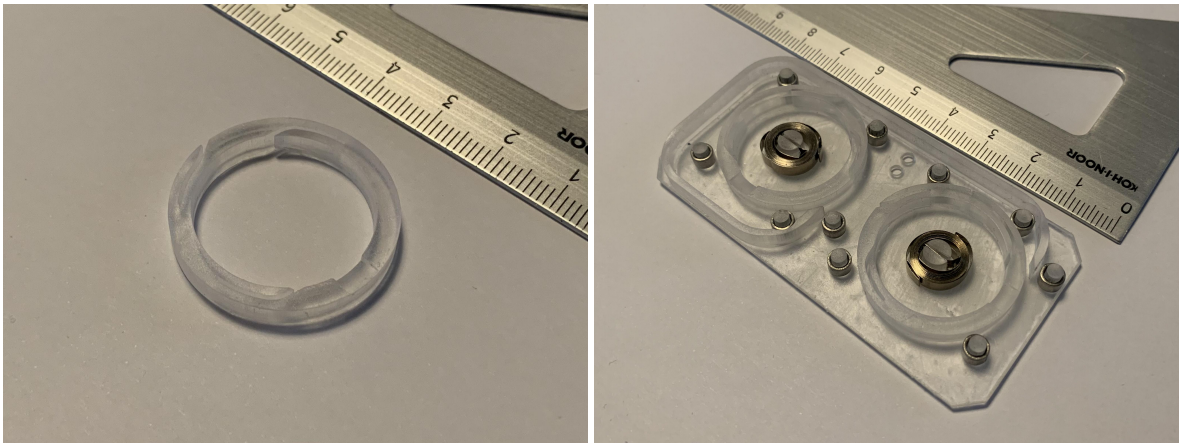

(a) Single rotor part **(b)** Springs and rotors

Figure 13.3: Rotors and springs added to the case bottom

The springs are then connected to the rotors themselves. See Figure 13.4.

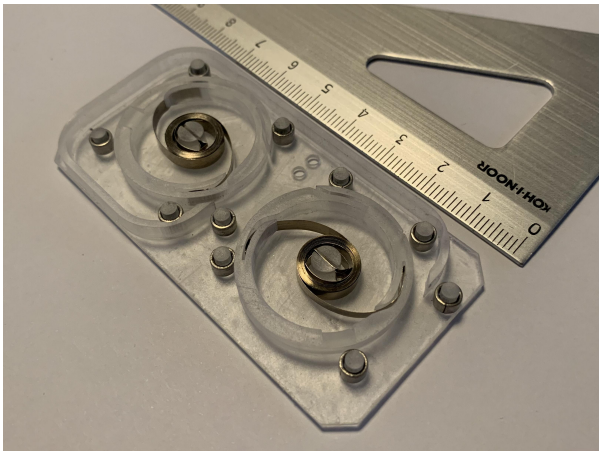

Figure 13.4: Springs connected to the inner surface of the rotors

The locking fingers component is then added, see Figure 13.5.

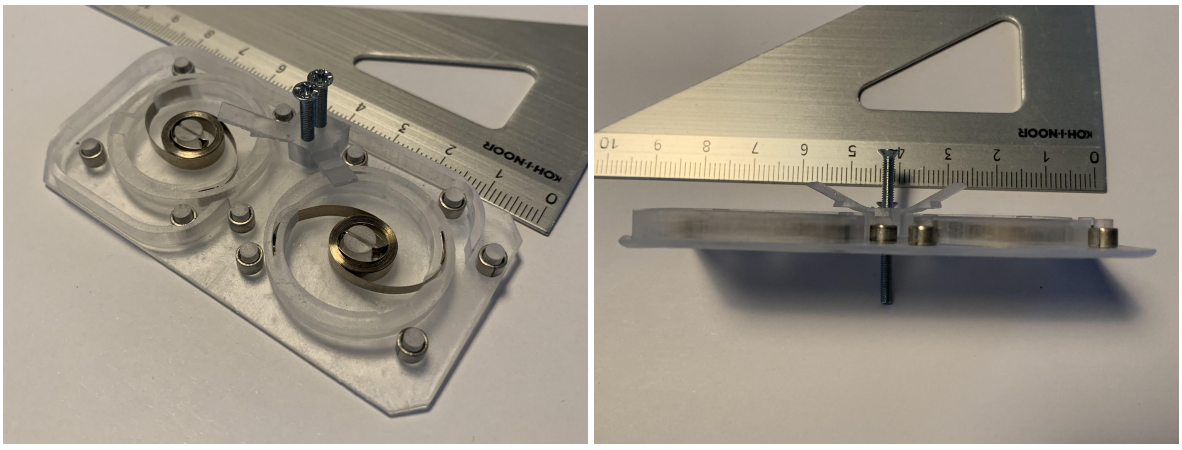

(a) Isometric view **(b)** Side profile view

Figure 13.5: Locking fingers component added to the assembly

The antenna conductor can finally be attached to both rotors, see Figure 13.6

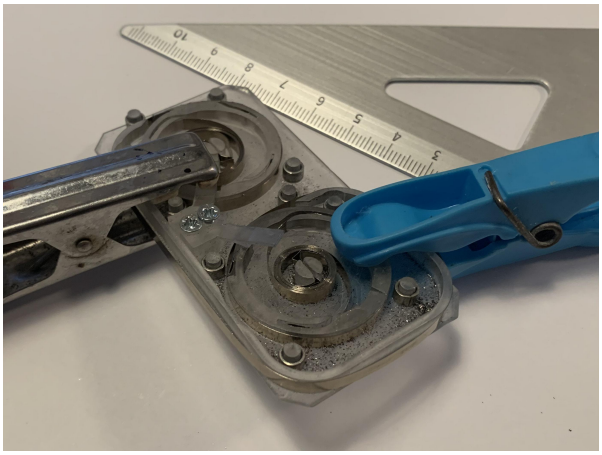

Figure 13.6: Antenna conductor added to the assembly; clamps used to prevent the rotors from deploying prematurely

Lastly, the top plate is added, completing the assembly, see Figure 13.7.

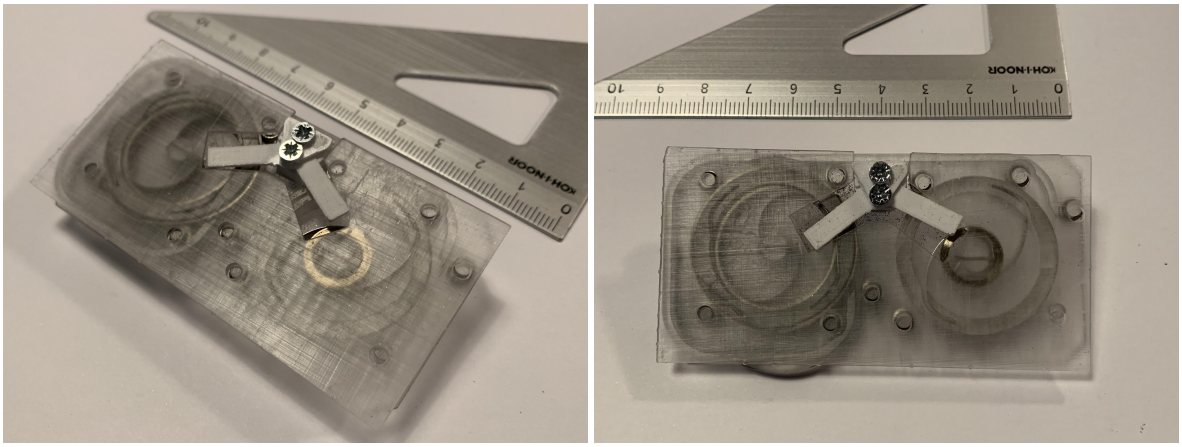

(a) Isometric view **(b)** Top view

Figure 13.7: Transparent top plate added to complete the assembly

This marks the completion of the assembly process for the deployer demonstrator. Before moving on to a description of the observed performance, a few relevant aspects must be mentioned.

Firstly, as can been seen from the assembly images, some components initially manufactured in transparent resin were later switched for identical versions printed in white plastic. This was done purely for practical reasons. A FDM printer was available at home. For faster prototyping and for replacing broken parts, this printer was often more easily accessible. Except for the lower printing resolution, this did not noticeably affect performance.

Secondly, the locking fingers were sometimes printed directly in their 'locked' configuration. Meaning, they were printed straight, and not bent upwards. This ensured that, at rest, they engaged with the rotor keeping it passively locked. The only functional change was that for mechanism actuation, the fingers had to be manually lifted away from the rotors instead of simply being released. This feature greatly simplified the testing process by avoiding premature mechanism actuation.

13.5. Performance and Lessons Learned

This section presents a mostly qualitative overview of the observed performance of the deployer demonstrator. While only the final version has been presented so far, many iterations have been worked on to achieve sufficient functionality.

Ultimately, the performance of the demonstrator is promising, with many of the systems designed working as intended. The following observations about the deployment behaviour have been made. These observations cover all relevant systems and deployment functions, being: the springs, the HDRM/locking, the bushings, the antenna conductor, and other miscellaneous design aspects.

1. **HDRM Actuation**
   The actuation of the hold down and release mechanism was perhaps the aspect of the design that worked the best. The locking fingers, regardless of the exact geometry, material, or design were almost always more than sufficient to retain the rotors stationary before deployment. Even significant shaking or tapping on the assembly was not sufficient to release the rotors. As briefly mentioned at the end of the previous section, two variants of the locking fingers were used: one resting in the locked position and one resting in the deployed position. While the latter is the intended configuration, the former was used to ensure the system remained locked unless a force was applied (instead of the other way around). An image of both locking fingers design can be found in Figure 13.8.

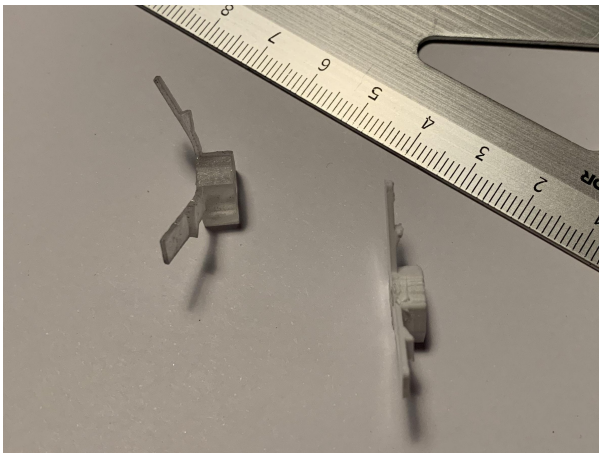

Figure 13.8: Bent (left) and straight (right) locking fingers

   The geometry of the interface between the locking fingers and the rotors was proven to be successful in achieving the goal of locking the deployment. While only plastic/resin fingers were tested, further development and testing of spring steel fingers would be recommended for long term actuation reliability. Repeated bending of the fingers was observed to permanently deform them beyond the usable range. While the mechanism would only have to actuate once, and not repeatedly, seeing how fragile and important this aspect of the mechanism is, alternatives to plastics/resins should be further investigated. Beyond material choices, the burn wire actuation has also not been directly tested. However, given the simplicity of the design, it is the opinion of the author, as well as consulted experts, that actuation should not be a significant hurdle.

2. **Deployment End-stop and Locking**
   The end-stop at the end of antenna deployment is crucial to ensure that the antenna conductor makes sufficient contact with the feed points. This contact point can be seen marked in Figure 13.9.

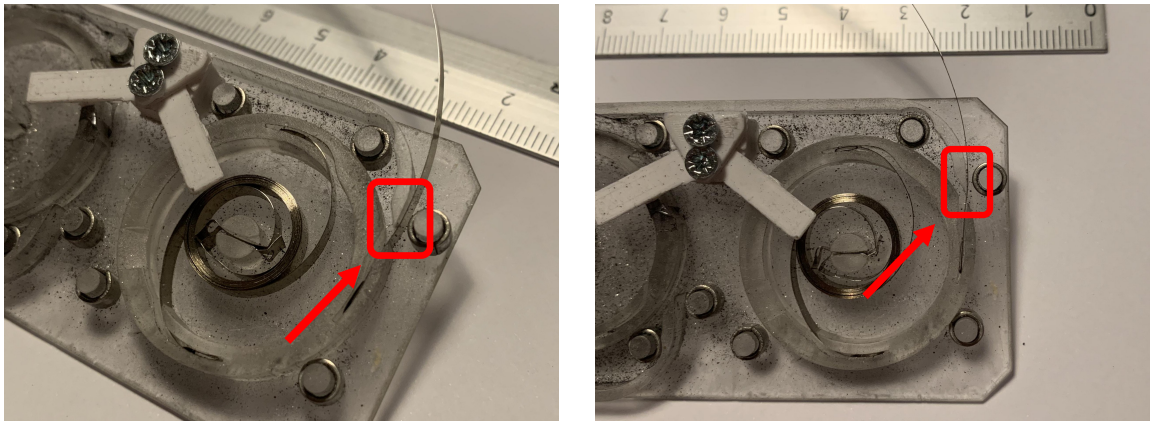

(a) Isometric view **(b)** Top view

Figure 13.9: Contact point between deployed antenna conductor and deployer case bottom marked in red

In the figure presented, the antenna conductor can be seen physically touching the case at the marked point. Regardless of the demonstrator configuration, this contact point was achieved reliably and consistently. While no conductive trace is present in the demonstrator, this is the location from where the antenna feed points would be connected to. A few options are available to achieve this goal. The contact surface could be covered with a conductive coating linking up to the top PCB; or, a wide conductive patch component could be directly surface-mounted to the top PCB sticking out into the path of the contact point. Otherwise, a flexible copper/aluminium conductive insert could be added at the marked location both absorbing some of the deployment impact, and making a secure electrical connection to the antenna. Either way, as the springs were not allowed to fully unwind at deployment end, a consistent force keeping the antenna in the fully deployed position was observed. This is promising. While not shown in Figure 13.9, the other spool displays identical behaviour being an exact mirror copy. For further development, it is recommended to test the electrical connection thoroughly and investigate whether the geometry of the interface has to be refined to ensure a good conduction path.

3. **Bushings Tolerances**
   The bushings used in the design worked well to guide the deployment of the antenna conductor. The interface between the PTFE in the inner surface of the bushings and the shaft has low friction, ensuring smooth motion. The presented design has shafts for the bushing manufactured as one with the bottom case of the deployer. To investigate whether a different shaft material improved the performance, steel bolts were also tried to house the bushings. This seemed to provide a marginal improvement in the smoothness of the motion, but not significant. Figure 13.10 shows examples of both the resin and steel shafts for comparison.

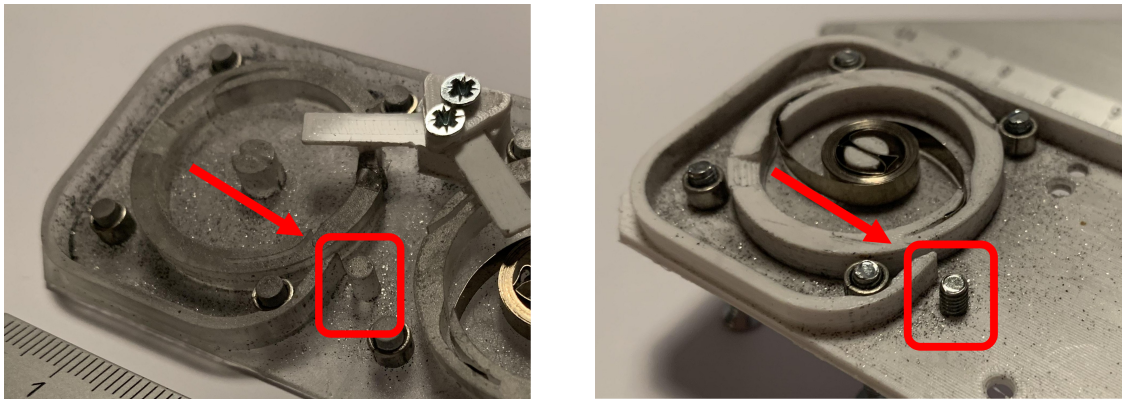

(a) Resin **(b)** Steel (M3 bolt)

Figure 13.10: Various material options for the bushings shafts

In addition to material choices, the tolerances between the bushings and the shafts was also investigated. Per specification, an f7 tolerance is recommended for the bushing's shaft. For the nominal diameter of 3 mm, this translates to a shaft diameter ranging between 2.984 and 2.994 mm [72]. A calibration block was printed in resin with various shaft diameters to test the precision of the available resin printer. This calibration block can be seen in Figure 13.11. Do note that only the resin printer was used when bushing shafts were 3D printed, the FDM printer did not have sufficient precision for the task.

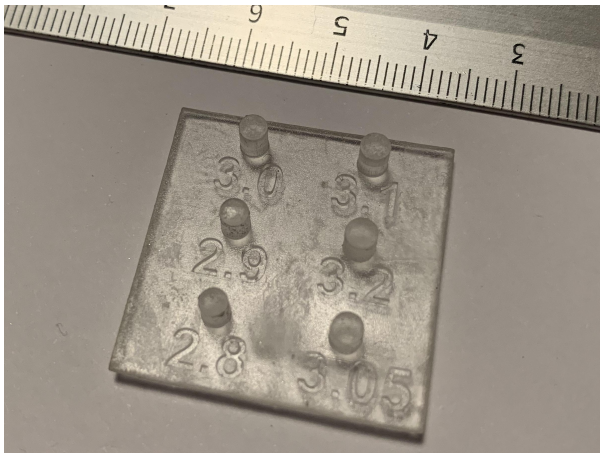

Figure 13.11: Shaft diameter resin calibration block

Using the calibration block, bushing shafts were regularly manufactured within the specified tolerance (or better). However, issues still arose with some of the purchased bushings with some of them gripping on the shafts too tightly and being unable to spin freely. Overall, it is recommended to err on the side of caution (at least for testing), and remain below the specified shaft tolerance range.

4. **Aluminium versus Steel Antenna Strip**
   An aluminium strip was also purchased to investigate practically whether its material properties would be sufficient to replace the steel. Referring back to Figure 8.15, aluminium 7075 had been identified as a potentially viable replacement for spring steel given its good mechanical performance and much better conductance. However, given the uncertainty surrounding the deployment, steel had been chosen as a baseline. Due to resource constraints, the aluminium strip acquired was not 7075 aluminium, but a more pure alloy. This resulted in a much lower yield strength when compared to the high strength aluminium proposed for the design. The tested strip was not able to remain in the elastic regime when integrated into the demonstrator showing significant plastic deformation when spooled up around the rotors. See Figure 13.12.

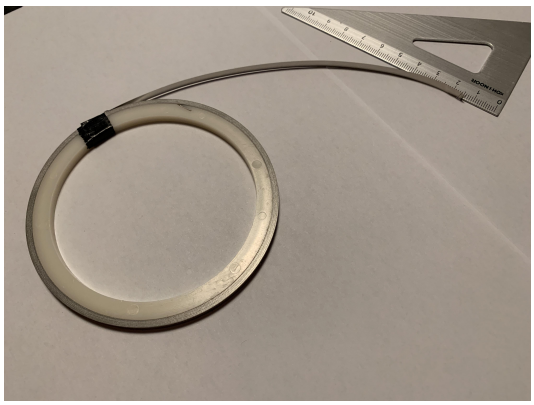

(a) Source material coil

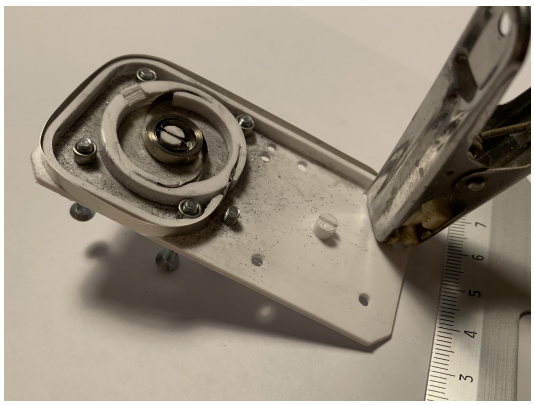

(b) Short strip integrated outo the outside of the deployer

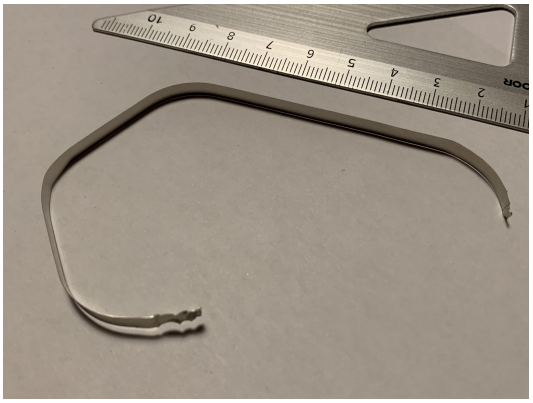

(c) Plastically deformed strip once removed from the deployer

Figure 13.12: Aluminium antenna strip plastically deformed after being integrated into the deployer

While still potentially viable, due to resource constraints, initial testing was not sufficient to determine whether the switch from steel to aluminium would be viable. While not directly commercially available, an aluminium 7075 strip should be either custom made or manufactured to specifications to investigate whether it could be an alternative to steel.

5. **Extending Conductor Length**
   As presented in Table 13.1, the spring steel strips acquired were limited to a length of about 300 mm. While this was enough to investigate the release and initial deployment of a thin strip, it was not sufficient to replicate the expected antenna conductor length. Multiple 300 mm sections were acquired and attempted to be joined using different methods to make a longer single antenna conductor. While adhesive was sufficient to join the sections together, significant thickness was added at the location of the joint. See Figure 13.13.

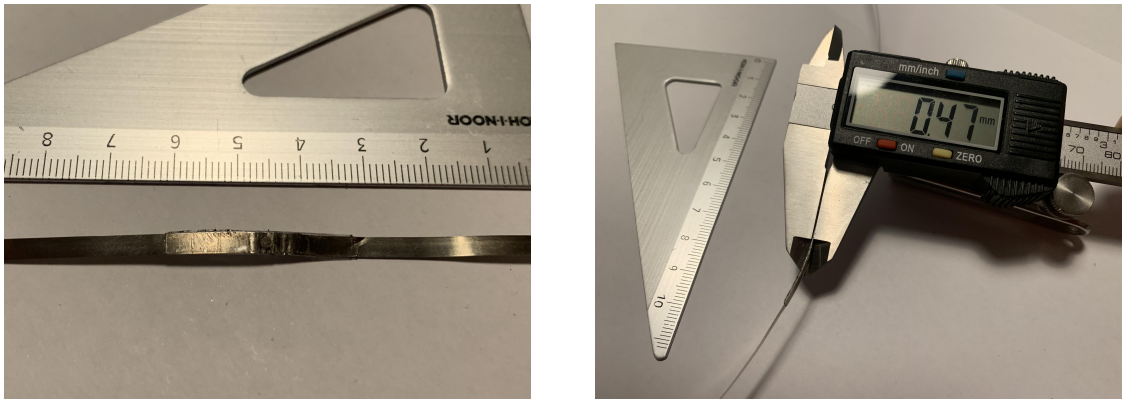

(a) Top view of the joined strips

(b) Joint thickness

Figure 13.13: Joint location of two antenna steel strips; Join thickness: 0.47 mm; Nominal strip thickness: 0.07 mm

This made testing unreliable, as the added thickness bulging out at the joints regularly caused the strip to catch on the inside of the deployer. Results for the extended conductor length were hence dismissed, as deemed non-representative of the real system. In any case, the acquisition of the steel strips used in this work was rather challenging, custom manufactured parts should be considered as an option for further testing. As discussed in the previous point, switching to aluminium could perhaps simplify the component acquisition process. Overall, while the full conductor length was not tested, the results obtained are still considered relevant. The more challenging aspect of deployment seems to be reliable initial rotation of the spools. However, once they are moving their inertia is sufficient to overcome friction. This behaviour is not expected to significantly change were the spools to store a longer conductive strip.

6. **Internal Friction**
   Through repeated testing, internal friction was identified as the primary risk factor to deployment failure. Identifying the sources of friction and reducing their effect has been the primary task when working on the design of the deployer. From observation, friction has been identified as critical primarily at the beginning of deployment actuation. While the locking fingers reliably released the rotors, it often occurred that the deployment did not fully initiate due to friction between the antenna spools and the inside of the deployer case. Graphite is later discussed as a way to potentially mitigate these issues, but other aspects are relevant to mitigating the problem.

   When held stationary or deploying, the antenna spool only has a few designated points of contact with the stationary components, namely, the bushings. While these offer low friction (when toleranced correctly), the antenna spool was sometimes observed 'bowing' outwards where unsupported, making direct contact with the deployer case itself. This behaviour can be seen in Figure 13.14.

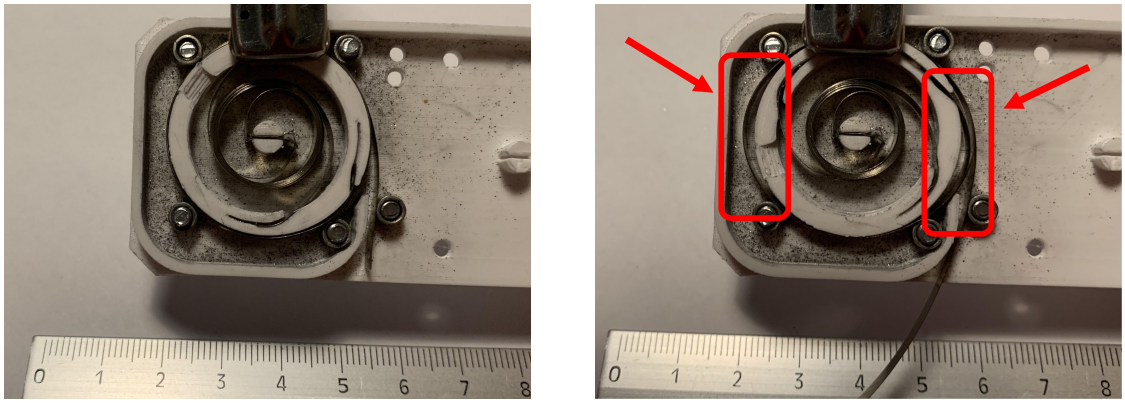

(a) Tightly packed around rotor

(b) Bowing outwards at locations marked in red

Figure 13.14: Antenna strip configuration around one of the rotors

This unwanted behaviour, when present, resulted in an increased static friction between the antenna spools and the stationary case. While this was observed not to be particularly problematic once the spools started spinning, it did often prevent initial deployment actuation when present. Some workarounds and mitigation strategies were devised to minimise the impact of this phenomena. Round PTFE tubing was used to fill the unsupported gaps between bushings. While helpful, the added material often had the wrong geometry to properly support the antenna spool without becoming a detriment to the deployment. An example of a section of PTFE tubing added to one of the spools can be seen in Figure 13.15.

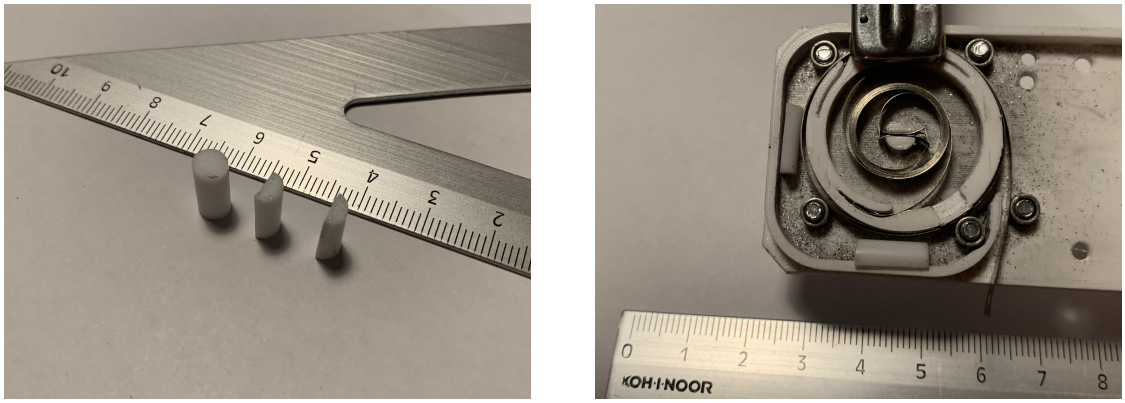

(a) PTFE sections

(b) PTFE sections added within the deployer

Figure 13.15: PTFE tubing used to reduce potential contact between antenna strip and

With access to more materials and manufacturing capabilities, one could consider the addition of a whole ring of smooth PTFE around the spools with small gaps for the bushings. This would ensure that the spool cannot deviate from its circular geometry by much while keeping friction down. Alternatively (or in combination), more bushings could be added around the spools to reduce the length of the unsupported stretches. Given the small size of the bushings, and the space still available within the assembly (see for example Figure 13.5), it would not be unreasonable to add 3-4 more bushings per rotor. These mitigation strategies and design changes should be further investigated and tested to assess the eventual final feasibility of the deployer design.

7. **Antenna Conductor Stability**
   The antenna conductor was made out of the same material as the springs. As such, when acquired, it was significantly curved and coiled over itself considerably tightly (with a permanent bend radius of less than 5 mm). To remove this curvature, each antenna conductor strip was repeatedly bent backwards over corners with various sharpness to deform the spring steel back to a straight strip. 3D printed curved edges were used as jigs during this process. While very tedious, this method did yield good results, usable to investigate the deployment process. The problem with the manual nature of the process however comes from the difficulty in tightly controlling the end product. While straightening the strips, it was challenging not to introduce some out-of-plane curvature. What is meant by this, is that it was not possible to avoid some degree of twist along the strip. The results of this issue can be seen in Figure 13.16.

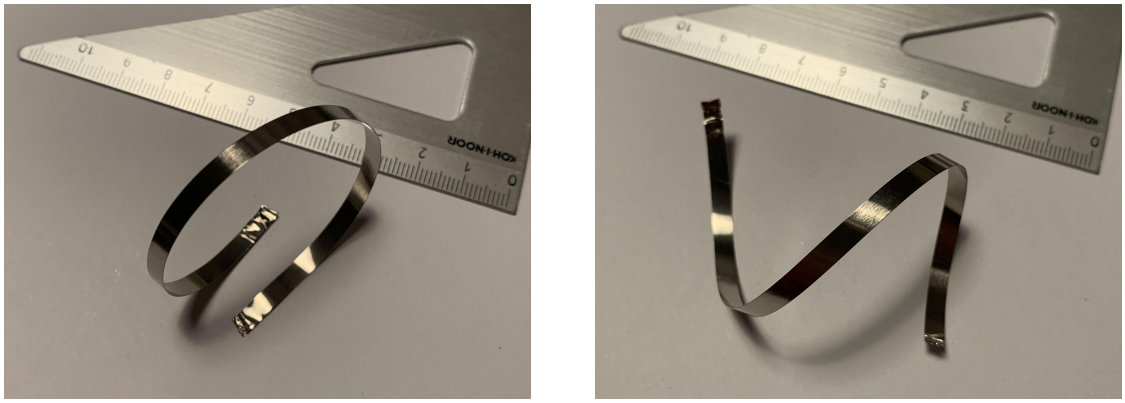

(a) Slight twisting **(b)** Significant twisting

Figure 13.16: Various degrees of twisting in the coiled antenna strips

This inherent twist in the antenna strips resulted in the tendency of the antenna to want to coil up onto and over itself, sometimes bending out of plane unpredictably. To verify that this was solely a consequence of the unwanted twist, the (untwisted) aluminium strip was used to construct a 1.25 m diameter loop. While not self-supporting under gravity, this loop showed no tendency to coil onto itself regardless of the orientation it was supported in. A small version of this loop can be seen laying flat in Figure 13.17, it remained stable regardless of disturbances.

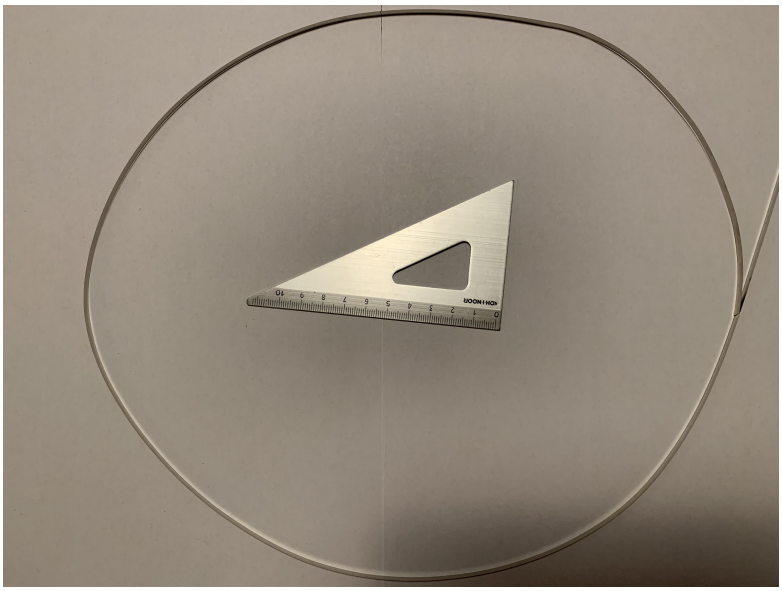

Figure 13.17: Stable scaled loop made with a perfectly straight (untwisted) aluminium strip

While making testing more challenging, this twisting behaviour is not inherent to the deployer design or deployment approach. Instead, it is a consequence of being unable to source the exact components required. Fixing the issues would have necessitated ordering components custom made for this application: this was not feasible within the resource and time constraints of this project. In spite of these limitations, the antenna conductors used still provided sufficient performance to investigate the deployment behaviour.

8. **Spring Configurations**
A two-spring-per-rotor configuration is depicted in most of the figures and design descriptions, however, other options were considered and investigated. Initially, a single coil spring per rotor was employed. While technically working, this setup introduced significant unwanted asymmetric loads into the rotor in addition to the desired pure torque. This asymmetry can be seen in Figure 13.18.

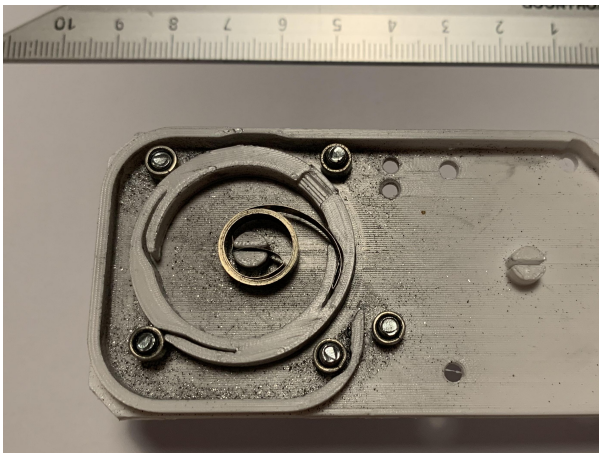

Figure 13.18: Single spring per rotor configuration

The asymmetry of the loads caused by the single spring caused the antenna spool to be pinched against either the bushings or the case itself adding a lot of unwanted friction. The configuration was hence discarded as not compatible with the design.

A double-spring configuration for each rotor was then devised, where two springs are coiled onto each other to interface with each rotor at two opposing points. This not only eliminated the problematic asymmetric loads, but also doubled the torque delivered to the rotors. The configuration can be seen in Figure 13.19 below.

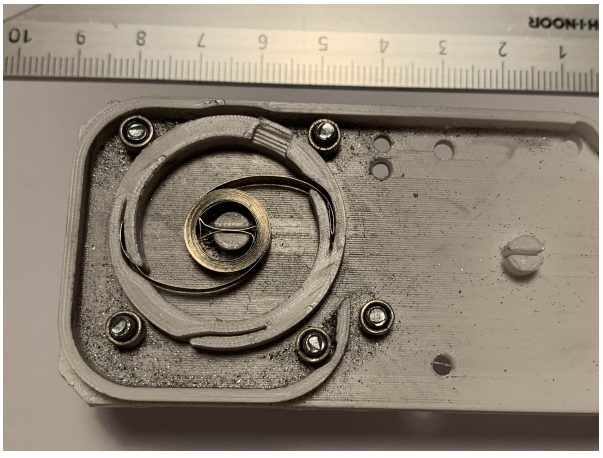

Figure 13.19: Double spring per rotor configuration

While functional, this configuration is not the most effective use of space. As described by Equation 12.2, the most effective way to increase torque is to increase the spring strip thickness. Adding a second spring doubles the torque, while doubling the spring thickness results in a times eight torque increase (2^3), with essentially the same footprint. Put differently, eight identical springs would deliver the same torque as one with the same geometry but its thickness doubled. Other more complex options, such as stacking four springs per rotor were tried. However, for the reasons just described, these are not effective methods to increase torque when limited by available volume. Figure 13.20 below shows a quad-spring configuration.

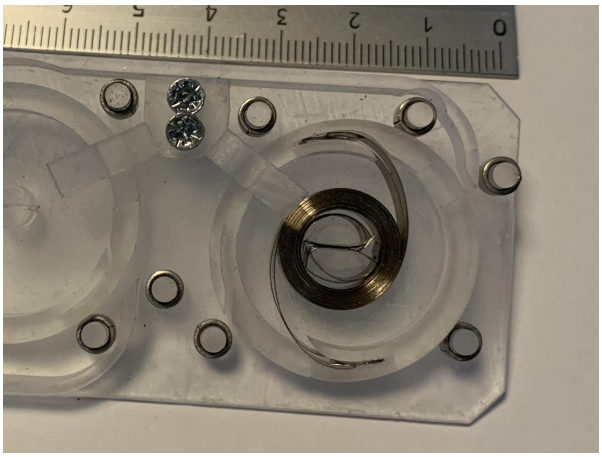

Figure 13.20: Quad spring per rotor configuration

While reducing friction is a valid option to increase reliability of actuation and deployment, increasing spring torque is another potentially viable alternative. Although thicker springs were not available for testing, it is recommended to acquire springs with twice or more the current thickness and investigate their effect on deployment actuation.

Lastly, about range of motion, while the springs used were only about 300 mm in length, space is available for springs twice the length or more (see Figure 13.3, there is still lots of available space within the rotors). In the double-spring configuration, the rotors were capable of delivering about seven usable turns before bottoming out the springs. Based on the available space, achieving the required 12-20 turns (as described in section 12.2) is likely achievable, especially when considering the even less restrictive requirements of the 50 MHz instrument. Testing with longer springs is recommended to investigate the maximum loop diameter which can be reliably deployed. If space were to be an issue, there is still some margin to either increase the diameter of the rotors, or decrease their thickness to make more space for the springs at their core.

9. **Graphite versus No Graphite**
   Graphite powder has been used throughout testing to see whether dry lubricants could be an effective method to reduce friction between moving components. Figure 13.21 below shows a zoomed in view under the microscope of a printed part both covered in graphite, and left untreated.

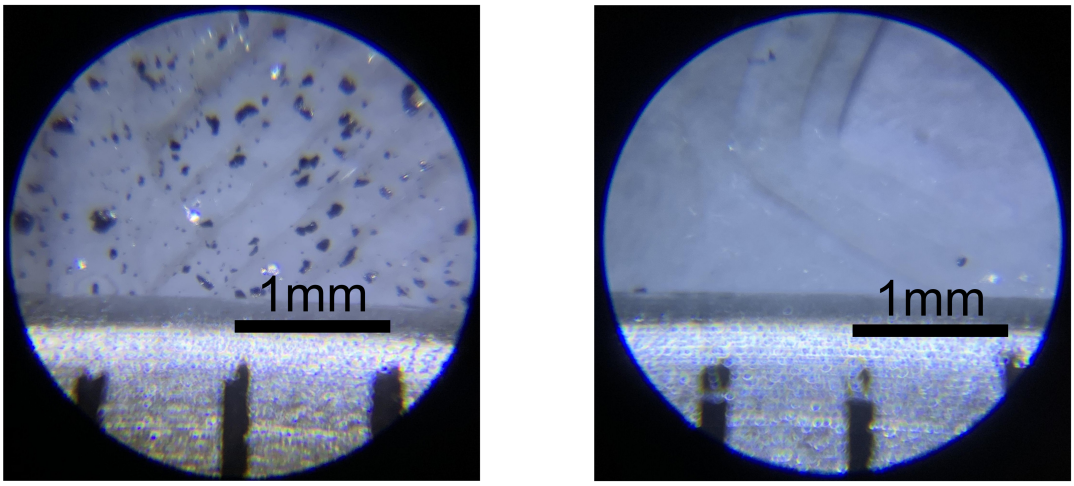

(a) With graphite **(b)** Without graphite

Figure 13.21: 3D printed demonstrator bottom case under the microscope

Graphite was observed to be an effective tool to reduce friction at the interface both between plastic and plastic, as well as between plastic and steel. The layered structure of the 3D printed components (especially the ones produced with an FDM printer) made it easier for the graphite to stick to the surfaces after initial application. While effective, being conductive, there are concerns that excess graphite may interfere with the RF behaviour of the antenna conductor. Furthermore, while untested in the demonstrator, the matching network or other exposed electrical components on the top PCB may also be adversely affected by loose graphite powder in the space environment. Lastly, while effective on Earth, graphite may not be the best dry lubricant option when it comes to in-space operations [50]. Another perhaps more viable lubricant option would be PTFE powder, which is non-conductive. For now, dry lubricants have been identified as being an effective option to reduce internal friction.

13.6. Mechanical Testing Recommendations

Based on the lessons learned from the deployer demonstrator, a list of follow-up testing recommendations is here presented. These are aspects of the design which should be further investigated to gain confidence in the mechanical effectiveness of the design. The testing recommendations are presented roughly in order of importance from 'most critical' to 'least critical. Critical recommendations should be tackled first as concerning challenges which must be solved before the deployer can be actually flown. Less critical recommendations instead refer to aspects which may be further investigated, time and resources allowing, but are not an obstacle to design functionality.

Most critical

↓

↓

↓

↓

↓

1. Test the following options to reduce static friction at deployment initiation: add more bushings to reduce unsupported antenna spool sections, and/or add PTFE rings around antenna spools to retain circular shape.
2. Acquire longer individual spring steel strips to test deployment of larger loops.
3. Acquire longer torsion springs and test their behaviour to determine the maximum conductor length which can be stored and deployed within the available space.
4. Acquire thicker torsion springs and test their deployment behaviour. Investigate whether the increase in torque can increase deployment reliability and to what extent.
5. Acquire a straight (untwisted) spring steel strip. Alternatively, develop better methods to straighten coiled springs while not introducing unwanted twist.
6. Manufacture a prototype of the top PCB and integrate it into the deployer. Investigate its mechanical performance as a structural PCB.

↓
↓
↓
↓
↓
↓

Least critical

7. Test repeatability and consistency of the created electrical connection between the antenna and feed point at deployment completion.
8. Acquire burn wires samples. Test deployment actuation by means of severing the burn wires instead of manual deployment
9. Manufacture resin parts out of PEEK and evaluate the functional differences, especially with respect to the frequency response of the deployer.
10. Replace the plastic/resin locking fingers with metal ones and test their relative performance.
11. Acquire PTFE powder dry lubricant and compare its effectiveness to graphite powder.
12. Acquire and test an aluminium 7075 strip for the antenna conductor to investigate whether it is a viable replacement for spring steel.
13. Manufacture the solid rotors out of a denser material to investigate whether a higher inertia can smooth out the deployment sequence.

As outside the scope of this project, there are a few aspects that were not here considered, but that must be further investigated following up on the initial testing just presented. In no particular order, the following aspects should be further investigated.

- The effects of the launch environment and exposure to vacuum should be simulated or tested however possible. While not considered for the deployment itself, they must be considered to evaluate success of the deployer across all mission phases. This includes UV radiation and exposure to atomic oxygen which could degrade performance of certain components over time.
- Cold welding is a potential issue for the antenna steel strip and spring before deployment. Severity of the issues and potential mitigation strategies should be investigated. For example, one side of the strip could be coated with an inert material/polymer, or thin Kapton sheets could be wound in between steel layers to physically separate the steel. Alternatively, it should be investigated whether the graphite used as a dry lubricant could be enough to prevent cold welding if properly distributed within and between all metallic components.
- The frequency response of the deployer should be simulated and/or tested, especially for the top PCB and bottom case both having relatively large, thin, unsupported sections. Additional stiffening may be needed, or perhaps adhesively bonding the deployer to Delfi-Twin's wing panel may be sufficient to thwart low frequency modes.

14

Summary of Key Outcomes and Decisions

This third part of the report focusses on the third project phase. It mainly deals with investigating answers to the third research question posed in section 2.3: ***How can the RABSII antenna be effectively packaged to be compatible with integration aboard Delfi-Twin satellite platform?***

Firstly, a conceptual design for the deployment of the RABSII loop antenna was presented in chapter 11. Next, based on this concept, a complete design was defined in CAD and presented in chapter 12. Lastly, to gain more confidence in the feasibility of the design presented, a simplified demonstrator was built and tested. The findings were presented in chapter 13.

Based on the deployer concept, design, and prototype, the following key findings can be identified.

- The deployment approach identified is compatible with the mounting interface options available on the host satellite platform: Delfi-Twin.
- The deployment approach identified is scalable enough to accommodate loop diameters spanning all the considered dimensions of the both the 28 and 50 MHz instruments with little to no changes in the design.
- Manufacturing the demonstrator prototype has given enough confidence to confirm that the proposed deployer design can be successfully produced and assembled.
- While overall promising, investigating the performance of the demonstrator has helped identify a few areas which require further work before the proposed deployer can be considered fully functional. Namely, the prototype has issues with reliably initiating the motion and deployment of the antenna spools. Further development and testing focussed on this aspect is required.

Part IV:

Project Outcomes

15

Results Overview

Before having a look at how the project faired with respect to the main objective and research questions defined in chapter 2, a summary of the key results is presented here. Just as the structure of this report, the work carried out was divided into three key parts: the project background and link budget, the RF design of the payload antenna, and the mechanical design of the deployer. Key results and outcomes are presented in this chapter, divided into their respective sections. For a more detailed view on specific results and figures, the last chapter of each section can be used as a reference. This 'Results Overview' chapter only serves to tie everything together into a single coherent picture to draw conclusions on the outcomes of this project as a whole.

15.1. Link Budget Results

The analysis started with an overview of the science case for the Radio Amateur Beacons aboard a NanoSatellite for the Investigation of the Ionosphere (RABSII) payload. Based on the science objectives of the mission, the need for two radio beacons was identified, transmitting on two distinct frequencies: 28 and 50 MHz respectively.

To inform the design of each antenna system, the first step was to carry out a link budget analysis to obtain key figures of the radio link. A few differences were observed in the analysis of the two instruments. The most significant difference being the magnitude of the free-space loss, which was by far the most dominant loss source. The free-space loss is proportional to signal frequency, hence being larger for the 50 MHz instrument when compared to the 28 MHz one. Additionally, based on the noise models presented, the noise power at ground is inversely proportional to signal frequency. A much higher noise temperature, and hence noise power is observed for the 28 MHz instrument. The free space loss and noise power figures for both instruments are presented in Table 15.1.

Table 15.1: Frequency-dependent link budget figures

Transmission Frequency [MHz]	**Free-Space Loss** [dB]	**Noise Power at Ground** [dB W]
28	-126.6	-139.8
50	-131.6	-146.7

While free-space loss and noise power show opposite trends, noise is dominant on the link budget. Based on these figures, two parameters were of particular interest for informing the design process: the required Effective Isotropic Radiated Power (EIRP) and the required minimum transmitter gain. The obtained values for these two parameters for both instruments (28 and 50 MHz) are presented in Table 15.2.

Table 15.2: Minimum required characteristics of the two transmitting antennas

Transmission Frequency [MHz]	**EIRP** [dB W]	**Transmitter gain** [dB]
28	-19.2	-13.2
50	-21.1	-15.1

In terms of performance requirements alone, the 28 MHz instrument is observed to be more constraining than the 50 MHz one. Furthermore, based on the literature presented in chapter 3, the 28 MHz instrument has to be larger than the 50 MHz one to achieve the same performance, solely because of the longer signal wavelength.

Based on these insights, the choice is made to proceed with designing the 28 MHz instrument. If a feasible configuration can be identified for this instrument, the 50 MHz instrument would consequently also be feasible given its more relaxed performance requirements.

15.2. RF Design Results

Two key aspects are presented when it comes to the results of the antenna's RF design: the design choices, and the characterisation of the performance of the final antenna design.

15.2.1. Design Choices

The RF design of the 28 MHz instrument began with an overview of the various design dimensions to be considered. These are:

- Antenna Conductor Shape
- Antenna Conductor Size
- Antenna Conductor Cross-section
- Antenna Conductor Material
- Antenna Matching Network Topology

All choices were identified as mostly independent from one another, and can hence be interchanged and matched freely to one another. However, most critical to design of the antenna, is the shape of the conductor, the antenna type. As omnidirectional transmission is required, two viable options were identified: a loop antenna and a dipole antenna. A choice first had to be made between these two options. Through looking at what has been achieved by commercial antenna deployers, using a full resonant sized version of either was deemed unfeasible, or at the very least a significant technical risk. This would have translated into a 5 m long dipole, or a loop 3 m in diameter to be integrated into a satellite only 5x5x15 cm in size. Based on commercial antenna deployers, an upper bound of 1.5 m was placed for maximum antenna size. This translates to an upper bound of 1.5 m long for the dipole, and 1.5 m in diameter for the loop.

To characterise RF performance, the following performance metrics were considered:

- Bandwidth
- Directivity
- Matching Network Efficiency
- Radiated Power / Radiation Efficiency

All design dimensions were considered as a function of antenna size, which became the independent variable for the analysis. The performance of a loop and a dipole with comparable properties was first investigated.

1. **Loop vs Dipole: Bandwidth**
   Depending on antenna size, bandwidth ranges between 170 kHz and 30 kHz for the loop, and between 130 kHz and 90 kHz for the dipole (see Figure 15.1). As the required system bandwidth is 2.5 kHz, both antennas have more than sufficient performance to meet bandwidth requirements.

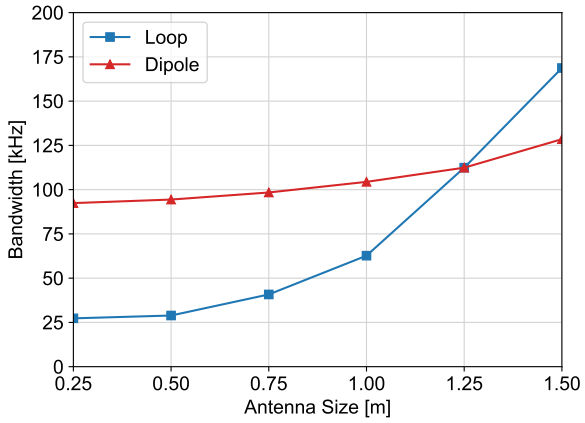

Figure 15.1: Bandwidth as a function of antenna size for both a loop and a dipole

2. **Loop vs Dipole: Directivity**
   Both antennas are technically omnidirectional. However, the dipole shows pronounced nulls at the poles where no power is radiated, this pattern remains constant regardless of antenna size. The loop instead displays an almost spherical radiation pattern at larger sizes, nulls at the poles (like for the dipole) are slowly introduced as the loop diameter is shrunk.
3. **Loop vs Dipole: Matching Network Efficiency**
   While loop antennas are inductive, dipoles are capacitive. This translates to opposite matching network designs, where loops rely primarily on capacitors and dipoles on inductors to match feed to source impedance. Given the much higher quality factors expected from capacitors, this leads to significantly higher resistive power losses for a dipole compared to a loop, see Figure 15.2.

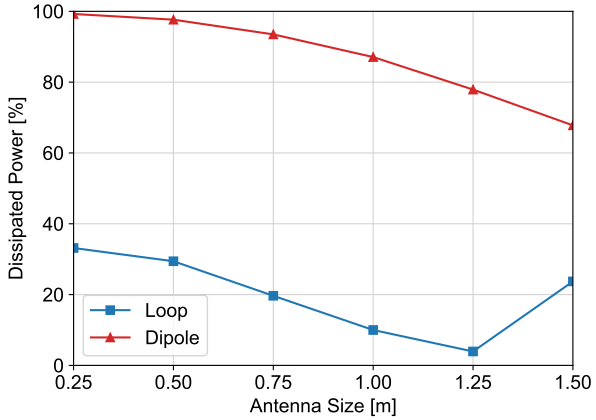

Figure 15.2: Resistive power losses in the matching network as a fraction of total supplied RF power, and as a function of antenna size for both a loop and a dipole

4. **Loop vs Dipole: Radiated Power**
   Combining the radiation patterns and the system losses, the radiated power for both a loop and a dipole antenna was computed. Figure 15.3 and Figure 15.4 present the radiated power across the azimuth and elevation planes for both antennas as a function of size.

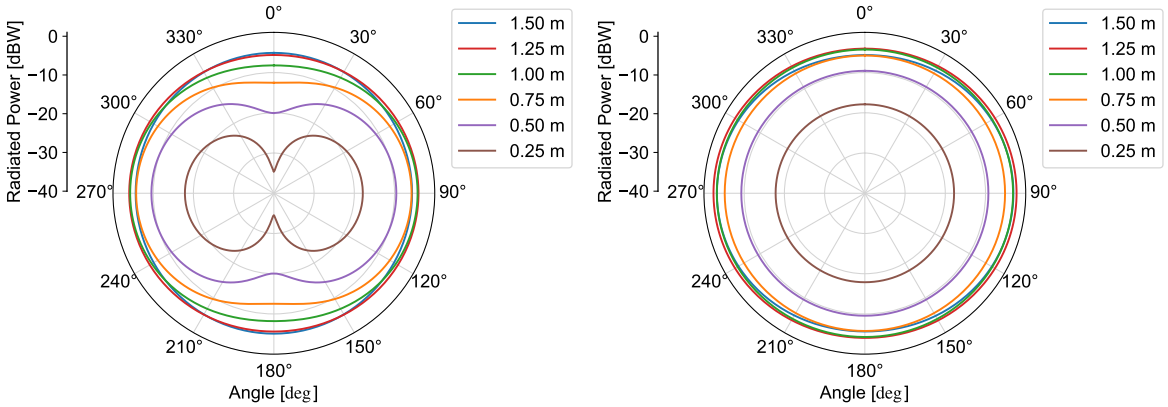

(a) Azimuth (elevation=0) **(b)** Elevation (azimuth=90)

Figure 15.3: Loop antenna radiated power as a function of antenna size

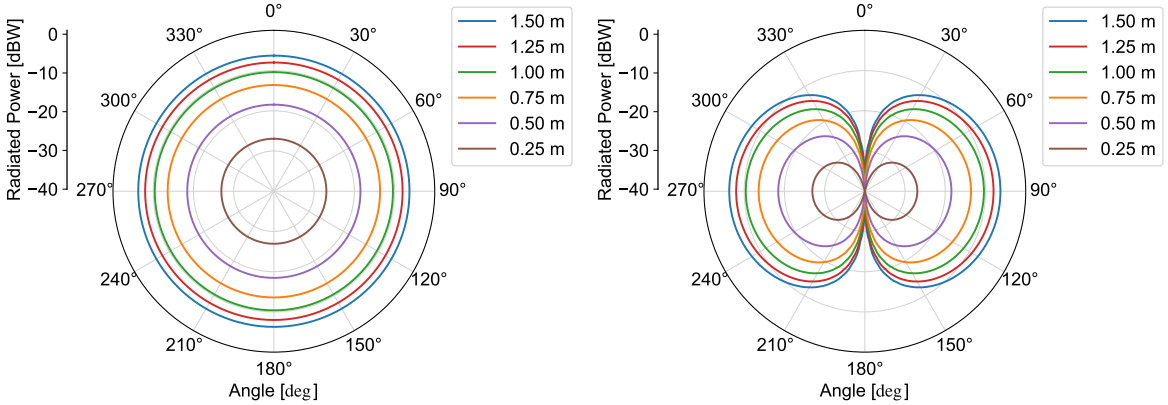

(a) Azimuth (elevation=0) **(b)** Elevation (azimuth=90)

Figure 15.4: Dipole antenna radiated power as a function of antenna size

Based on these figures, the loop antenna was identified as more promising than the dipole for the RABSII payload. The loop displayed a more uniform directivity and higher radiated power across all transmission angles.

The remaining design dimensions were then investigated yielding the following results.

1. **Conductor Cross-Section**
   Due to the tendency of AC power to travel across the surface of a conductor (skin effect), longer cross-section perimeters performed better for the same cross-sectional area. This favoured rectangular cross-sections over circular ones. A final choice was however not made solely on RF performance pending investigating the deployer mechanical design.

2. **Conductor Material**
   Predictably, higher material conductivity led to better radiation efficiency. Spring steel was chosen for the antenna conductor. While not a great conductor, it displays the best mechanical properties of any material considered. Aluminium 7075 delivered significantly higher radiation efficiency at the cost of lower strength, is was hence kept as a second option pending investigation on the deployer mechanical design.
3. **Matching Network Topology**
   The most basic L-network topology was observed to already be sufficient to meet the bandwidth requirements. Increasing the number of components in the matching network inevitably leads to higher resistive losses. Within the scope of this analysis, no more complex options were considered.

15.2.2. Final Design Characterisation

Based on the design choices made, the performance of the antenna was then characterised across the considered performance metrics. The following results were obtained.

1. **Directivity**
   The loop conductor has a nearly spherical radiation pattern when considering an antenna with diameter of about $1.25\,\mathrm{m}$. Reducing the loop diameter effectively 'pinches' the radiation pattern at the poles to obtain a doughnut-shaped emission. Measuring the maximum variation in gain across the azimuth and elevation directions shows opposing trends for the two. Reducing the loop diameter increases this maximum variation in the azimuth direction, but decreases it across the elevation direction. Considering both directions, the maximum variation in gain across all axes is minimised at a loop diameter of about $1.25\,\mathrm{m}$. This can be seen in Figure 15.5.

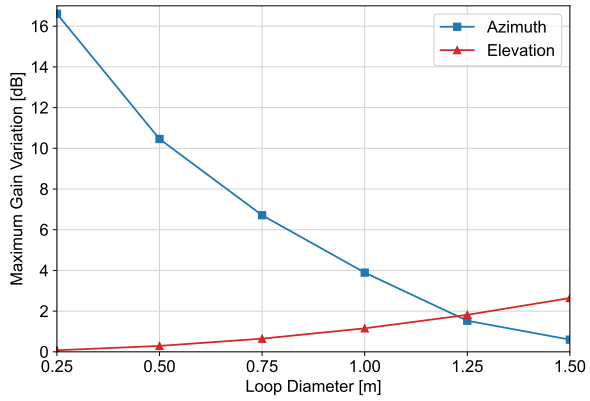

Figure 15.5: Maximum variation in directivity gain as a function of antenna size for for both the azimuth and elevation directions

This is relevant given the foreseen relative orientation between the antenna and ground station. Combining the (uncontrolled) attitude variations of the satellite with its motion along the orbital track, antenna pointing is expected to vary by $\pm^\circ 100$ in one plane, and by a complete revolution (a whole $^\circ 360$) in the other (azimuth or elevation depending on mounting orientation aboard Delfi-Twin). These changes are mainly stochastic, rendering the observed antenna pointing orientation from ground essentially random.

2. **Radiated Power**
   Based on the requirements originating from the link budget, the loop diameter must be greater than 0.75 m to ensure sufficient power is delivered to ground to close the link budget. Taking into account the behaviour of the matching network, it would be preferred to keep the loop diameter below 1.25 m. Going above this introduces an inductor in the matching network (instead of only capacitors) which significantly drives up resistive losses. Going above a diameter of 1.25 m is technically possible but results in little to no improvement in radiated power. The radiated power across both the azimuth and elevation planes for a loop of various diameters can be seen plotted in Figure 15.6.

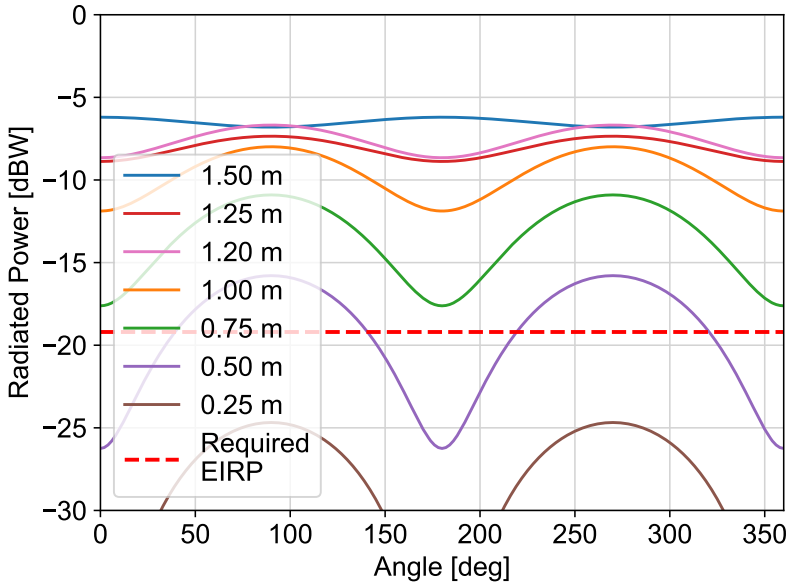

(a) Azimuth (elevation=0)

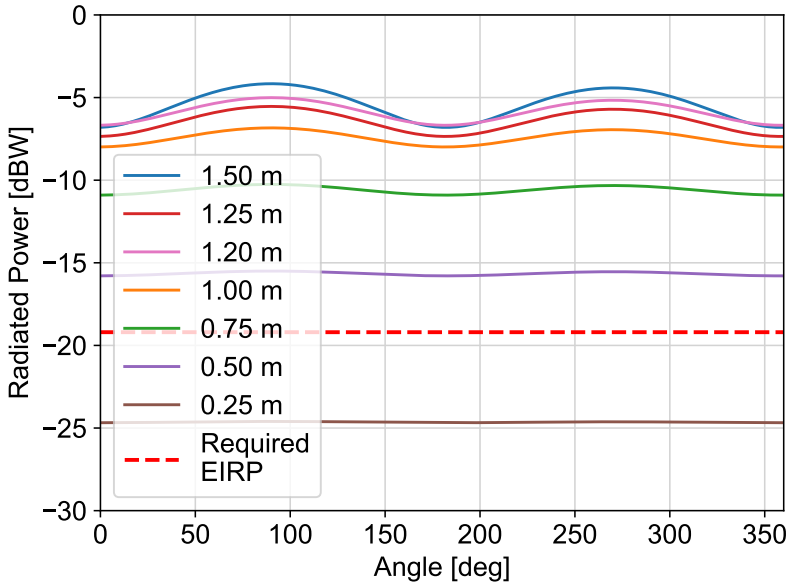

(b) Elevation (azimuth=90)

Figure 15.6: Loop antenna radiated power on Cartesian plots as a function of antenna size

3. **Bandwidth**
   While available bandwidth is technically sufficient for all loop diameters above 0.25 m, the behaviour of real electrical components imposes additional performance limitations. Two aspects were considered when investigating the influence of real matching network components on bandwidth: the availability of specific capacitors values, and their thermal and manufacturing tolerances.

   Regarding real capacitance, while exact values cannot be directly obtained, multiple commercially available capacitors can easily be combined in series/parallel to obtain 'composite capacitors' with the required capacitance. Through this process, ideal capacitors were replaced with composite capacitors made of components from commercial manufacturers. The effective change in capacitance observed going from ideal to composite capacitors amounted to less then 0.5 % of the desired value. A negligible drop in bandwidth was observed as a result.

   Regarding thermal and manufacturing tolerances, while no affect was observed to the available bandwidth, a non-negligible change in central matched frequency was observed. Considering the extreme cases at the outer bounds of the capacitance tolerance range, led to a maximum change in central matched frequency of about ± 120 kHz, see Figure 15.7 below. On-ground or in-space tuning can be used to correct for these variations by adjusting the central frequency over which transmissions are broadcasted.

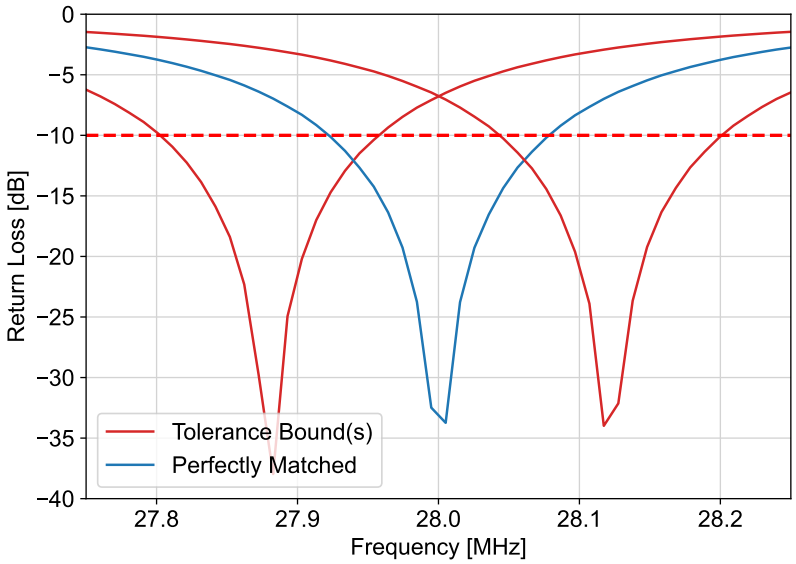

Figure 15.7: Return loss as a function of frequency for a perfectly matched system (blue), and for a system with matching network capacitance variation equal to the maximum tolerance range (red)

Based on the analysis presented, the loop diameter must be between 0.75 and 1.25 m for the system to meet the performance requirements.

15.3. Mechanical Design Results

The goals of the mechanical design were to identify a possible deployment approach compatible with the loop antenna and assess its feasibility. After considering various deployment concepts, one was selected as 'most promising' for the RABSII instrument. The chosen approach can be compared to a VHS (Video Home System) tape, or a tape cassette. The antenna strip (with a thin rectangular cross-section) is coiled around two rotors, half of the antenna on each. The rotors are spring loaded to deploy the antenna (once released) by ejecting the strip outwards to its neutral rest configuration: a loop. CAD models of the design were made, with several iteration needed to get to a design which could be manufactured, see Figure 15.8.

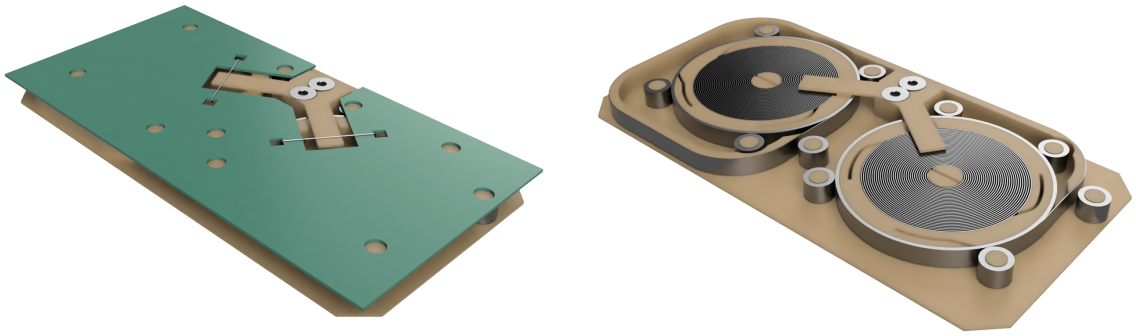

(a) Full model **(b)** Inner mechanism, top plate removed

Figure 15.8: Overview of the deployer design

Considering the limited resources of this project, as well as the overall scope of the research, a simplified demonstrator was constructed to attempt to provide some confidence that the deployment approach has potential to fulfil the requirements of the RABSII instrument. The following key observations were made by investigating the functionality of this demonstrator.

- HDRM actuation worked as intended. The primary component (locking fingers) used to secure and release the deployment securely engages with the rotors, and releases them reliably. Its plastic/resin construction could however fail under repetitive strain, switching to metal should be considered.
- Spring steel was mechanically sufficient for the antenna conductor strip. Aluminium 7075 was not tested as a replacement, but could still be a feasible option.
- Physical tolerances between components were not as problematic as anticipated given the small size of the system, with the exception of the bushings. Their rotation was easily impeded or completely blocked by an oversized shaft, increasing the internal friction considerably.
- Testing of a full-scale antenna conductor (0.75-1.25 m diameter loop) was attempted but was ultimately not possible. Commercially available options limited the total antenna conductor to a length of about 300 mm.
- The loop antenna shape was observed to remain stable in the deployed configuration. However, stability was observed to be compromised by unwanted twist in the conductor strip. Starting from coiled strips for the antenna, it was not possible to entirely eliminate unwanted twist in the spring steel antenna conductor during testing.
- The torsional springs that were used to provide the actuation force behaved as expected, with a relatively wide range of free parameters available for tuning to 'tune' the springs' torque profile. Namely, the thickness of the spring strips, the number of springs used, and the number of pre-stress turns can be used to change the output torque. Furthermore, the length of the spring strips can be used to change the available range of motion.
- Graphite powder was observed to aid in reducing the internal mechanism friction. This points to dry lubricants being a viable options to mitigate friction failures.

While promising, one critical aspect must be tackled if the deployer is to be integrated into Delfi-Twin for flight. The rotors were often unreliable in commencing rotation (and hence deployment) due to unmitigated internal friction sources. Bulging of the antenna strip coil, and the relatively wide gaps between bushings resulted in unpredictable internal friction which made deployment initiation unreliable. Once deployment successfully initiated, the inertia of the spinning rotors was sufficient to prevent seizing mid-deployment.

16

Conclusion

This thesis project set out with the goal to investigate, analyse, and propose design solutions capable of fulfilling the RABSII payload science objectives. The research objective of the work here presented was been defined as follows.

Research Objective

To design an HF antenna beacon compatible with the Delfi-Twin satellite platform and demonstrate its stowage and deployment.

The analysis presented tackled three key research questions attempting to meet the defined research objective. Based on the work presented in this thesis, the answers to those research questions are hereby presented.

Research Question 1

RQ-1: What antenna gain and radiated power is required to close the science case's link budget with sufficient margin?

RQ-1.1: What are the relevant noise sources to consider in the instrument link budget?

RQ-1.2: What are the relevant attenuation sources to consider in the instrument link budget?

The first research question focusses on the radio link between the RABSII beacon and ground. Answers to this question were investigated and can be found in section 4.2. Looking at the individual sub-questions first:

RQ-1.1: *What are the relevant noise sources to consider in the instrument link budget?*

Two noise sources were found to be relevant for the RABSII link budget:

- **Terrestrial Noise**: is dominated by man-made noise. Using ITU recommendation, estimates vary mainly depending on considered frequency and ground station location. The increase in man-made noise is substantial going from rural areas to densely populated areas.
- **Extra-Terrestrial Noise**: is dominated by galactic noise. while exact values are hard to determine, a lower and an upper bound for galactic noise power can be determined based on galactic temperature maps adjusted to the considered frequency.

RQ-1.2: *What are the relevant attenuation sources to consider in the instrument link budget?*

Two attenuation sources were identified to be relevant for the RABSII link budget:

- **Free-Space Loss**: is responsible for the vast majority of the signal attenuation. The exact figure for free-space loss is directly proportional to signal frequency, where higher losses are expected at higher frequencies.
- **Polarisation Mismatch Loss**: is much smaller than free-space loss, but harder to quantify. For signals in the HF/VHF bands, it has to be modelled stochastically as the ionosphere and Earth's magnetic field effectively randomise the polarisation of incoming signals.

Returning back to **RQ-1**, the answers from **RQ-1.1** and **RQ-1.2** are used to determine an answer.

RQ-1: *What antenna gain and radiated power is required to close the science case's link budget with sufficient margin?*

The outcomes of the link budget were described in subsection 4.2.4, see Table 16.1 below for the required antenna gain and radiated power for the two instruments (28 and 50 MHz).

Table 16.1: Minimum required antenna gain and radiated power for the two RABSII instruments

Transmission Frequency [MHz]	**Transmitter gain** [dB]	**EIRP** [dB W]
28	-13.2	-19.2
50	-15.1	-21.1

Research Question 2

RQ-2: To what extent can the antenna be downscaled compared to the currently proposed half-wave dipole while still meeting the RF requirements of the science case?

RQ-2.1: What key antenna design parameters effect its RF performance?

RQ-2.2: How sensitive is the antenna RF performance to the identified design parameters?

RQ-2.3: What combination of materials/geometry/drive electronics is sufficient to meet the identified requirements?

The second research question focusses on the antenna RF design and performance, the majority of Part II of this report works towards answering this question. Given the size limitations imposed by the very small satellite platform, it is important to understand how far the RABSII payload antenna can be reduced in size. Looking at the individual sub-questions first:

RQ-2.1: *What key antenna design parameters effect its RF performance?*

The following design parameters were identified as relevant to antenna RF performance:

- The antenna conductor shape
- The antenna conductor size
- The antenna conductor cross-section
- The antenna conductor material
- The driving matching network topology

These are the design dimensions identified and described in chapter 6. Each one has a direct measurable impact on the RF performance of the final antenna.

RQ-2.2: *How sensitive is the antenna RF performance to the identified design parameters?*

While direct relations cannot be determined analytically, the effect of each parameter on the final RF performance has been thoroughly investigated in chapter 8. The sensitivity of the performance across relevant metrics to each design parameter is summarised qualitatively in Table 16.2. Do note that while discussed and investigated in chapter 9, matching network efficiency is not a metric describing antenna performance directly, and is hence left out here.

Table 16.2: Qualitative sensitivity of various antenna RF performance metrics with respect to changes in design parameters; Ranging from *Significant* (black), *Moderate* (gray), and *Negligible* (white)

		Performance Metrics		
		Directivity	***Radiated Power***	***Bandwidth***
Design Parameters	***Conductor Shape***	Significant	Moderate	Moderate
	Conductor Size	Moderate	Significant	Significant
	Conductor Cross-section	Negligible	Moderate	Negligible
	Conductor Material	Negligible	Significant	Negligible
	Matching Network Topology	*Unknown*	*Unknown*	*Unknown*

RQ-2.3: *What combination of materials/geometry/drive electronics is sufficient to meet the identified requirements?*

The following combination of design choices was shown sufficient to meet the identified system requirements:

- Conductor shape: loop
- Conductor size: loop diameter between 0.75 m and 1.25 m
- Conductor cross-section: rectangular, 3x0.1 mm in size
- Conductor material: 1.4310 spring steel, with Aluminium 7075 as a potential alternative
- Matching network topology: L-network

Returning back to **RQ-2**, the answers from **RQ-2.1**, **RQ-2.2**, and **RQ-2.3** are used to determine an answer.

RQ-2: *To what extent can the antenna be downscaled compared to the currently proposed half-wave dipole while still meeting the RF requirements of the science case?*

Compared to the originally proposed 5-meter half-wave dipole, the loop antenna proposed is capable of meeting the identified requirements with a possible diameter ranging between 0.75 and 1.25 m. A specific choice within this size range must be made after further refining the deployer design and science case requirements.

Research Question 3

RQ-3: How can the RABSII antenna be effectively packaged to be compatible with integration aboard thr Delfi-Twin satellite platform?

- **RQ-3.1:** What system requirements are driving when it comes to the mechanical design of the antenna deployer?
- **RQ-3.2:** How can the designed RABSII antenna be stored and deployed?
- **RQ-3.3:** How can the devised deployment approach be demonstrated within the resource and time constraints of this project?
- **RQ-3.4:** What aspects of the deployment are critical and must be further investigated?

The third research question focusses on the mechanical design of the deployer for the RABSII instrument, the majority of Part III of this report works towards answering this question. Looking at the individual sub-questions first:

RQ-3.1: *What system requirements are driving when it comes to the mechanical design of the antenna deployer?*

Volume, **REQ-SAT-07**, is by far the most constraining requirement when it comes to the design of the deployer. The very small allocated deployer volume (80x40x$4\,\text{mm}^3$) rules out 'traditional' commercially tested deployment approaches forcing a novel solution to be investigated. Furthermore, the very thin profile of the available volume ($4\,\text{mm}$) results in an essentially 2-dimensional design space, with layered structures hardly possible.

RQ-3.2: *How can the designed RABSII antenna be stored and deployed?*

The RABSII loop antenna can be stored and deployed by being wound up on spring loaded rotors. This cassette-style approach, illustrated back in Figure 11.8, shows promise in fulfilling the system requirements.

RQ-3.3: *How can the devised deployment approach be demonstrated within the resource and time constraints of this project?*

The cassette-style deployment approach defined can be demonstrated through the construction of a physical demonstrator. Constructing a physical prototype is useful to directly observe and investigate the feasibility of the deployer design, assuming it can be made in a representative manner.

RQ-3.4: *What aspects of the deployment are critical and must be further investigated?*

Deployment initiation has been identified as the most critical aspect of the design. Internal friction and unwanted deformation of the antenna spool often prevent the initiation of deployment, with the tested springs sometimes unable to overcome the static friction in the system. Better supporting the stowed antenna spool, use of dry lubricants, or better tuning of the springs' torque can be considered to resolve this issue.

Returning back to **RQ-3**, the answers from **RQ-3.1**, **RQ-3.2**, **RQ-3.3**, and **RQ-3.4** are used to determine an answer.

RQ-3: *How can the RABSII antenna be effectively packaged to be compatible with integration aboard the Delfi-Twin satellite platform?*

A novel deployment approach has been conceptualised, and a deployer design has been proposed. Following initial testing of a representative physical demonstrator, a cassette-style deployer seems capable to deploy the RABSII loop antenna while integrating with the available interface aboard the Delfi-Twin spacecraft. A few open issues have been identified, and subsequent testing steps have been proposed to mitigate these issues to refine the design and work towards usable flight hardware.

16.1. Closing Remarks

Investigating and measuring the structure of the ionosphere is a challenge given its spatial and temporal variability. Understanding its composition is highly relevant to radio communication, given its significant impact on transmissions on the HF/VHF bands. The RABSII payload, proposed by Vanhamel [79], provides a potential solution by using a space-based radio beacon to indirectly measure the sporadic E ionospheric phenomena. While a 5-meter halfwave dipole is currently being considered for RABSII, the antenna's very large size compared to the very small host satellite platform, the 3P PocketQube Delfi-Twin, raises concerns on its practical feasibility.

This thesis attempts to reduce the project's technical risk by investigating ways in which the payload's antenna can be downscaled while still meeting the requirements dictated by the science case. A loop antenna, with diameter ranging between 0.75 and 1.25 meters has been proposed, and its performance has been characterised with respect to relevant design dimensions. A deployer for this antenna was then conceptualised, prototyped, and tested to investigate its preliminary feasibility. Initial results suggest it may be capable of meeting the RABSII payload's system requirements while integrating into the Delfi-Twin satellite platform.

Besides, direct applicability to the RABSII instrument, this thesis also provides relevant data on the performance of electrically short antennas. These types of antennas are rarely used for space applications, and the relation between their performance and size is often unclear and undefined in literature. The data presented provides some relevant insights in how electrically short antennas may be used to reduce the footprint of telecommunication systems aboard modern small satellites. Furthermore, the novel deployer design could also serve as a useful starting point for other antenna systems by providing preliminary insights into the operations of a new antenna deployment approach.

17

Recommendation and Future Work

While most of the project objectives were met, throughout the report, a few areas were identified as requiring further work in order to bring the RABSII instrument to flight. Covering both design, analysis, and testing aspects, the following are recommendations for areas which should be further investigated.

- **Perform the additional testing proposed for the deployer demonstrator.**
  While relevant results were obtained from the construction of the deployer demonstrator, due to time/resources limitations it was not possible to conduct a thorough test campaign. As such, general recommendations for further testing have been presented in section 13.6, they can be here summarised with the following key points:
  - Test adding more bushings or PTFE supports to reduce friction at deployment actuation.
  - Test a more representative demonstrator: longer and untwisted antenna strips, longer/custom torsion springs, add burn wires for actuation.
  - Manufacture and test the PCB, demonstrate feed connection points.
  - Test aluminium 7075 as a steel replacement for the antenna.

- **Further investigate loop antenna bandwidth limitations.**
  Manufacturing tolerances were observed to be dominant over thermal tolerances. While outside the scope of this work, the antenna's response should be further investigated (and possibly simulated) to observe what would happen were the antenna to be tuned on ground already. Being constant, it is expected that manufacturing tolerances can be accounted for during the manufacturing and integration of the proposed instrument. It would be highly relevant to understand how wide the frequency change would be were the thermal tolerances to be the only factor introducing variability in the matching network system during in-space operations.

- **Simulate spacecraft motion along orbital track, determine antenna-to-ground angle distribution.**
  As outside the scope of this work, the spacecraft motion was not simulated, rather, figures were obtained directly from the Delfi-Twin team. To better characterise the radio link, it would be relevant to simulate the distribution of expected angles between the instrument and a ground station. This would help better inform the true required omnidirectionality of the antenna.

- **Analyse other matching network topologies.**
  While only L-networks were used throughout the presented analysis, other options were identified as potentially viable. As beyond the scope of the analysis, those options were not further investigate. Pi, T, or other topologies should be investigated to see whether they can be used to further extend the instrument's bandwidth.

- **Antenna drag analysis.**
  Given the relatively large size of the antenna compared to Delfi-Twin, its form drag contribution to the spacecraft should be investigated. This would include modelling the antenna together with the spacecraft, and simulate its collective drag as the spacecraft's attitude oscillates. As part of another student's ongoing thesis project, Delfi-Twin's attitude dynamics is currently being further investigated. This will provide the data and models needed to investigate how the instrument would change Delfi-Twin's flight.

- **Refine link budget analysis once the instrument is more defined.**
  The link budget analysis was performed to a degree sufficient to inform the system requirements for the RABSII instrument. Given the very early stage status of the project, many data points were still missing, and key aspects had to be estimated as best as possible. As the RABSII project matures, the assumptions detailed in section 3.1 should be revised and the potential changes should be investigated.

- **Further investigate the bus-mounted Delfi-Twin interface configuration.**
  As shown in Figure 11.5, an alternative interface option for the deployer was considered. The hinge mechanism required to accommodate for this interface option was referenced from a previous Master thesis work, but no further analysis was carried out as outside the scope of this project. As the Delfi-Twin design matures, it should be further investigated how the proposed deployer would interface with this already designed hinge mechanism.

References

[1] 2NDSpace. *Chorus-01 Deployable Cubesat antenna*. URL: https://www.2ndspace.eu/copy-of-drop-03.

[2] Suhila Abulgasem et al. “Antenna designs for CubeSats: A review”. In: *IEEE access* 9 (2021), pp. 45289–45324.

[3] AE6TY. *SimNEC for Interactive RF Circuit Analysis*. URL: https://www.ae6ty.com/smith_charts/.

[4] Alessandra Babuscia et al. “Inflatable antenna for cubesats: Motivation for development and antenna design”. In: *Acta Astronautica* 91 (2013), pp. 322–332.

[5] Constantine A. Balanis. *Antenna theory: analysis and design*. John wiley & sons, 2016.

[6] Ferdinand P. Beer et al. *Mechanics of materials*. McGraw Hill, 2006.

[7] Joachim Block, Marco Straubel, and Martin Wiedemann. “Ultralight deployable booms for solar sails and other large gossamer structures in space”. In: *Acta astronautica* 68.7-8 (2011), pp. 984–992.

[8] J. Bouwmeester, G.T. Aalbers, and W.J. Ubbels. “Preliminary mission results and project evaluation of the delfi-c3 nano-satellite”. In: *4S Symposium Small Satellites Systems and Services*. Vol. 660. 2008, p. 25.

[9] Christopher Bowick. *RF circuit design*. Elsevier, 2011. ISBN: 978-0-7506-85184.

[10] Francesco Branz et al. *Next Generation CubeSats and SmallSats: Enabling Technologies, Missions, and Markets*. Elsevier, 2023.

[11] Gary Breed et al. “Basic principles of electrically small antennas”. In: *High frequency electronics* 6.2 (2007), pp. 50–53.

[12] Gerald J. Burke, Edmund K. Miller, and Andrew J. Poggio. “The numerical electromagnetics code (NEC)-A brief history”. In: *IEEE Antennas and Propagation Society Symposium, 2004.* Vol. 3. IEEE. 2004, pp. 2871–2874.

[13] Constantine G. Cassapakis, Allan W. Love, and Arthur L. Palisoc. “Inflatable space antennas-a brief overview”. In: *1998 IEEE Aerospace Conference Proceedings (Cat. No. 98TH8339)*. Vol. 3. IEEE. 1998, pp. 453–459.

[14] Nacer Chahat. *CubeSat antenna design*. John Wiley & Sons, 2020.

[15] Nacer Chahat et al. “Advanced CubeSat Antennas for Deep Space and Earth Science Missions: A review”. In: *IEEE Antennas and Propagation Magazine* 61.5 (2019), pp. 37–46. DOI: 10.1109/MAP.2019.2932608.

[16] Frederik Michel Dekking. *A Modern Introduction to Probability and Statistics: Understanding why and how*. Springer Science & Business Media, 2005.

[17] TU Delft. *Delfi-n3Xt*. https://www.tudelft.nl/en/ae/delfi-space/delfi-n3xt. Accessed: 15-05-2025.

[18] C3S Electronics Development. *Antenna System*. URL: https://c3s.hu/wp-content/uploads/2022/01/C3S_ANTENNA_datasheet.pdf.

[19] Thomas W. Duerig, K.N. Melton, and D.W.C.M. Stockel. *Engineering aspects of shape memory alloys*. Butterworth-heinemann, 2013.

[20] Walid M.G. Dyab et al. “The resonant electrical length of helical antennas placed between metallic parallel plates”. In: *2022 16th European Conference on Antennas and Propagation (EuCAP)*. IEEE. 2022, pp. 1–3.

[21] EnduroSat. *UHF Antenna 1U*. URL: https://www.endurosat.com/products/uhf-antenna-iii/.

[22] Yulin Fang and Yue Ping Zhang. “Theory and analysis of the loop antenna and Ω-shaped loop-dipole antenna”. In: *IEEE Open Journal of Antennas and Propagation* 3 (2022), pp. 1161–1171.

[23] Akos Farago, Peter Kantor, and Janos Zoltan Bito. “Rain effects on 5G millimeter wave ad-hoc mesh networks investigated with different rain models”. In: *Periodica Polytechnica Electrical Engineering and Computer Science* 60.1 (2016), pp. 44–50.

[24] Charles A. Gross and Thaddeus A. Roppel. *Fundamentals of electrical engineering*. CRC press, 2012.
[25] Jian Guo, Jasper Bouwmeester, and Eberhard Gill. “In-orbit results of Delfi-n3Xt: Lessons learned and move forward”. In: *Acta Astronautica* 121 (2016), pp. 39–50.
[26] Mats Gustafsson and Sven Nordebo. *Bandwidth, Q factor, and resonance models of antennas*. Tech. rep. Lund University, 2005.
[27] Robbert Hamann, Jasper Bouwmeester, and Geert Brouwer. “Delfi-C3 Preliminary mission results”. In: *Small Satellite Conference* (2009).
[28] D. Hartl and D. Lagoudas. *Shape memory alloys: modeling and engineering applications*. 2008.
[29] Alain Herique et al. “Direct observations of asteroid interior and regolith structure: Science measurement requirements”. In: *Advances in Space Research* 62.8 (2018), pp. 2141–2162.
[30] Yue Honghao et al. “Research progress of space non-pyrotechnic low-shock connection and separation technology (SNLT): A review”. In: *Chinese Journal of Aeronautics* 35.11 (2022), pp. 113–154.
[31] Ted Hopper, Markus Anders, and Christoph Stuckmann. “Building electric motors for space, with redundancy and high reliability”. In: *Proc. 14th European Space Mechanics and Tribology Symposium, ESMATS2011. Constance, Germany*. 2011, pp. 373–378.
[32] D. Howe. “Magnetic actuators”. In: *Sensors and Actuators A: Physical* 81.1-3 (2000), pp. 268–274.
[33] John Huang. “The development of inflatable array antennas”. In: *IEEE Antennas and Propagation Magazine* 43.4 (2002), pp. 44–50.
[34] W. Huang and W. Toh. “Training two-way shape memory alloy by reheat treatment”. In: *Journal of materials science letters* 19.17 (2000), pp. 1549–1550.
[35] Austin Hughes and Bill Drury. *Electric motors and drives: fundamentals, types and applications*. Newnes, 2019.
[36] Ansys Inc. *Ansys HFSS: Best-In-Class 3D High Frequency Structure Simulation Software*. URL: https://www.ansys.com/products/electronics/ansys-hfss.
[37] Ansys Inc. *Quality Assurance*. URL: https://www.ansys.com/company-information/quality-assurance.
[38] ASM International. *ASM Handbook Volume 2: Properties and Selection: Nonferrous Alloys and Special-Purpose Materials*. ASM International, 1990. ISBN: 978-0-87170-378-1.
[39] ASM International. *ASM Handbook, Volume 1: Properties and Selection: Irons, Steels, and High-Performance Alloys*. ASM International, 1990. ISBN: 978-0-87170-377-4.
[40] Louis J. Ippolito. *Radiowave propagation in satellite communications*. Springer Science & Business Media, 2012.
[41] ISISPACE. *VHF/UHF Antenna for 1U-3U*. URL: https://www.isispace.nl/product/vhf-uhf-antenna-for-1u-3u/.
[42] Jaronie Mohd Jani et al. “A review of shape memory alloy research, applications and opportunities”. In: *Materials & Design* 56 (2014), pp. 1078–1113.
[43] Aboubakr el Jouhri. “Deployment System for the RABSII Antenna”. MA thesis. Delfi University of Technology, 2025.
[44] Reto B Keller. *Design for electromagnetic compatibility–in a nutshell: theory and practice*. Springer Nature, 2023.
[45] Jan King. *AMSAT-IARU Link Model Rev2.5.3*. URL: https://www.amsat.org/tools-for-calculating-spacecraft-communications-link-budgets-and-other-design-issues/.
[46] Alois Krischke. *Rothammel’s Antenna Book*. DARC Verlag GmbH, 2019.
[47] UVic Propagation Lab. *MARMOTSat - Satellite*. URL: https://www.propagationlab.ca/satellite/.
[48] Clay Laster. *THE BEGINNER’S HANDBOOK OF AMATEUR RADIO*. McGraw-Hill, 2001.
[49] American Radio Relay League. *The ARRL antenna book*. 15. The League, 1949.
[50] Jeffrey R. Lince. “Effective application of solid lubricants in spacecraft mechanisms”. In: *Lubricants* 8.7 (2020), p. 74.
[51] Douglas A Litteken. “Inflatable technology: using flexible materials to make large structures”. In: *Electroactive polymer actuators and devices (EAPAD) XXI*. Vol. 10966. SPIE. 2019.
[52] Abdul Halim Lokman et al. “A review of antennas for picosatellite applications”. In: *International Journal of Antennas and Propagation* 2017.1 (2017), p. 4940656.

[53] J.S. Mandeep and Hafizah Mustapha. “Design, and analysis of dipole and monopole antenna for CubeSat application”. In: *Research Journal of Applied Sciences, Engineering and Technology* 6.17 (2013), pp. 3094–3097.
[54] A.F. McKinley et al. “The analytical basis for the resonances and anti-resonances of loop antennas and meta-material ring resonators”. In: *Journal of Applied Physics* 112.9 (2012).
[55] Eugene Morgan. *Setting the Record Straight: SWR*. Ogden Amateur Radio Club.
[56] National Institute of Standards and Technology. *Reference Tables*. https://www.nist.gov/ncnr/sample-environment/sample-mounting/reference-tables. Retrieved October 12, 2025, from NIST. 2025.
[57] Kevin Nolan. “Spirit and Opportunity”. In: *MARS A Cosmic Stepping Stone: Uncovering Humanity’s Cosmic Context*. Springer, 2008, pp. 241–268.
[58] James Charles Novaco. *Galactic background maps at 3.93 and 6.55 MHz*. Tech. rep. NASA, 1973.
[59] Angelica de Oliveira-Costa et al. “A model of diffuse Galactic radio emission from 10 MHz to 100 GHz”. In: *Monthly Notices of the Royal Astronomical Society* 388.1 (2008), pp. 247–260.
[60] Harshkumar Patel et al. “Development of Shape Memory Alloy (SMA) Based Hold-Down and Release Mechanism for Space Applications”. In: *Advances in Industrial Machines and Mechanisms: Select Proceedings of IPROMM 2020*. Springer, 2021, pp. 393–403.
[61] Peyton Z. Peebles Jr. *Probability, random variables, and random signal principles*. McGraw-Hill, 2001.
[62] EE Power. *Q factor: Chapter 1 - Fundamentals*. URL: https://eepower.com/capacitor-guide/fundamentals/q-factor/.
[63] Silvana Radu et al. “Delfi-pq: The first pocketqube of delft university of technology”. In: *69th International Astronautical Congress, Bremen, Germany, IAC*. 2018, pp. 1–10.
[64] N. Razavi-Ghods et al. “Analysis of sky contributions to system temperature for low frequency SKA aperture array geometries”. In: *Experimental Astronomy* 33 (2012), pp. 141–155.
[65] Giles Read. *HF Antennas for Everyone*. Radio Society of Great Britain, 2012.
[66] *Recommendation ITU-R P.372-15*. International Telecommunication Union. Geneva, Sept. 2021.
[67] *Recommendation ITU-R P.531-16*. International Telecommunication Union. Geneva, Sept. 2025.
[68] M. Sakovsky, S. Pellegrino, and J. Costantine. “Rapid Design of Deployable Antennas for CubeSats”. In: *IEEE Antennas & Propagation Magazine* (2017). DOI: 10.1109/MAP.2017.2655531.
[69] Kamal Sarabandi and Menglou Rao. “Bandwidth and SNR of small receiving antennas: To match or not to match”. In: *IEEE Transactions on Antennas and Propagation* 71.1 (2022), pp. 99–104.
[70] Mark Schenk et al. “Review of inflatable booms for deployable space structures: packing and rigidization”. In: *Journal of Spacecraft and Rockets* 51.3 (2014), pp. 762–778.
[71] K.A. Seffen. “On the behavior of folded tape-springs”. In: *Journal of Applied Mechanics* 68.3 (2001), pp. 369–375.
[72] Simply Bearings Ltd. *Technical Specifications SKF PCM030403E/VB055 Metric Plain Bush 3x4.5x3mm*. https://simplybearings.co.uk/shop/p20259001/SKF-PCM030403E/VB055-Metric-Plain-Bush-Bearing-3x4.5x3mm/product_info.html. Retrieved December 13, 2025. 2025.
[73] SPACEMANIC. *Small Antenna Module (SAM)*. URL: https://spacemanic.com/products/sam-antenna/.
[74] Stefano Speretta. *Satellite Communication Systems*. TU Delft, MSc Space, Slide for Course AE4SIO Microsat Engineering. Nov. 2022.
[75] Stefano Speretta, Rens van der Zwaard, and Mehmet Sevket Uludag. “Autonomous formation flying in the traffic”. In: *15th IAA Symposium on Small Satellites for Earth Observation*. DLR. 2025, pp. 1–8.
[76] Oxford Space Systems. *Yagi Antenna*. URL: https://oxford.space/yagi/.
[77] Adam Thurn et al. “A nichrome burn wire release mechanism for CubeSats”. In: *The 41st Aerospace Mechanisms Symposium, Jet Propulsion Laboratory*. 2012, pp. 479–488.
[78] Mehmet Sevket Uludag and Stefano Speretta. “Delfi-PQ: In-Orbit Performance and Lessons Learned in Developing a 3P PocketQube”. In: *International Astronautical Congress* (2025).
[79] Jurgen Vanhamel, Walter Machiels, and Herve Lamy. “Using the WSPR Mode for Antenna Performance Evaluation and Propagation Assessment on the 160-m Band”. In: *International Journal of Antennas and Propagation* 2022.1 (2022).

[80] Jurgen Vanhamel et al. “Concept of Sporadic E Monitoring Using Space-Based Low Power Multiple Beacon-Systems”. In: *Atmosphere* 15.11 (2024), p. 1306.
[81] Ningning Wang et al. “Thin-film-integrated power inductor on Si and its performance in an 8-MHz buck converter”. In: *IEEE Transactions on Magnetics* 44.11 (2008), pp. 4096–4099.
[82] Wojciech Wieleba. “The statistical correlation of the coefficient of friction and wear rate of PTFE composites with steel counterface roughness and hardness”. In: *Wear* 252.9-10 (2002), pp. 719–729.

A

Composite Capacitors Code

```
import numpy as np
import matplotlib.pyplot as plt
from alive_progress import alive_bar

# defining helper functions
def add_C(C1, C2):
    return (C1 * C2) / (C1 + C2)

def variance(C1_data, C2_data):
    C1, var1 = C1_data
    C2, var2 = C2_data

    C1_list = [C1 + var1, C1 - var1]
    C2_list = [C2 + var2, C2 - var2]

    C_distribution = []
    for C1_temp in C1_list:
        for C2_temp in C2_list:
            C_distribution.append(add_C(C1_temp, C2_temp))

    deltas = [abs(add_C(C1, C2) - C) for C in C_distribution]

    return max(deltas)


# using pF as a unit for capacitance throughout the whole script

# ----------------------------------------------------
desired_C = 302    # pF            # TODO: input the desired capacitor value
# ----------------------------------------------------

search_depth = 2        # how many series capacitors to check

# ceramic capacitors available at MuRata Electronics: https://www.murata.com/en-eu/products/capacitor/ceramiccapacitor
database = np.append(np.arange(1, 10, 0.1), [10, 11, 12, 13, 15, 16, 18, 19, 20, 22, 24, 25, 27, 30, 33, 36, 39, 43, 47, 51, 56, 62, 68, 75, 82, 91, 100, 110, 120, 130, 150, 160, 180, 200, 220, 240, 270, 300, 330, 360, 390, 430, 470, 510, 560, 620, 680, 750, 820, 910, 1000])

# value provided @25ºC: range between +25ºC and +125ºC
max_temp_change = 100           # K     # max +- range from reference temperature of 25ºC
thermal_stability = 30/1e6      # +-ppm/ºC

# assigning tolerances to available capacitors
available_C = []
for i, C in enumerate(database):
    if C < 10:
```

```
        available_C.append([C, 0.05 + C*thermal_stability*max_temp_change])   # +- 0.05pF for capacitors below 10pF + 30ppm/ºC * max_temp_range

    else:
        available_C.append([C, 0.01 * C + C*thermal_stability*max_temp_change]) # +- 1% pF for capacitors above 10pF + 30ppm/ºC * max_temp_range


# available_C: for each entry: [capacitance (pF), tolerance (+- XpF)]
available_C = np.array(available_C)


all_combinations = []

with alive_bar(len(available_C)) as bar:
    for C1_data in available_C:
        # print(C1_data[0])
        # add single capacitor configurations
        data_temp = [C1_data[0], C1_data[1], sorted([C1_data[0]])]
        if data_temp not in all_combinations:
            all_combinations.append(data_temp)

        for C2_data in available_C:
            # print(C1_data[0], C2_data[0])
            # add two capacitor configurations
            data_temp = [add_C(C1_data[0], C2_data[0]), variance(C1_data, C2_data), sorted([C1_data[0], C2_data[0]])]
            if data_temp not in all_combinations:
                all_combinations.append(data_temp)

            # for C3_data in available_C:
            #     # add three capacitor configurations
            #     data_temp = [add_C(add_C(C1_data[0], C2_data[0]), C3_data[0]), variance([add_C(C1_data[0], C2_data[0]),
            #                  variance(C1_data, C2_data)], C3_data), sorted([C1_data[0], C2_data[0], C3_data[0]])]
            #     if data_temp not in all_combinations:
            #         all_combinations.append(data_temp)

        bar()

# sort by variance first
all_combinations.sort(key=lambda x: x[1])

# then sort by difference from desired value
all_combinations.sort(key=lambda data: abs(data[0]-desired_C))


# ---------------------------------------------------------------------
# printing top 10 best choices to let the user choose
print(f"\n\nDesired capacitance: {desired_C}pF\nOptions sorted by capacitance error, check tolerance value!")
print(f"{'_'*84}")
print(f"| Delta [pF]  | C [pF]  | Tolerance [+-pF] | C1 [pF]  | C2 [pF]  | C3 [pF]  |")
for i in range(10):
    C, var, components = all_combinations[i]

    if len(components) == 1:
        C1 = components[0]
        C2 = 0
        C3 = 0
    elif len(components) == 2:
        [C1, C2] = components
        C3 = 0
    elif len(components) == 3:
        [C1, C2, C3] = components

    print(f"|   {round(abs(C-desired_C), 4):7}   | {round(C, 4):8}  |      +-{round(var, 4):7}     |  {round(C1, 1):6}  |  {round(C2, 1):6}  |  {round(C3, 1):6}  |")
print(f"{'-'*84}")
```